Enhanced stiffness modeling of serial and parallel manipulators for robotic-based processing of high performance materials

Alexandr Klimchik

Ecole Centrale de Nantes

ÉCOLE DOCTORALE

Ecole Doctorale SPIGA

Année 2011. N° B.U. :

Thèse de DOCTORAT

Spécialité : GENIE MECANIQUE

Présentée et soutenue publiquement par :

ALEXANDR KLIMCHIK

le 27 Octobre 2011
à Nantes

TITRE

ENHANCED STIFFNESS MODELLING OF SERIAL AND PARALLEL MANIPULATORS FOR ROBOTIC-BASED PROCESSING OF HIGH PERFORMANCE MATERIALS

JURY

Président :	Jean-Pierre MERLET	Directeur de Recherche, INRIA, Sophia Antipolis
Rapporteurs :	Gabriel ABBA	Professeur, Ecole nationale d'ingénieurs de Metz, Metz
	Grigore GOGU	Professeur, Institut Français de Mécanique Avancée, Clermont-Ferrand
Examinateurs :	Anatol PASHKEVICH	Professeur, Ecole des Mines de Nantes, Nantes
	Damien CHABLAT	Directeur de Recherche, CNRS, IRCCyN, Nantes
	Jean-Pierre MERLET	Directeur de Recherche, INRIA, Sophia Antipolis
	Geir Hovland	Professeur, University of Agder, Kristiansand, Norway
	Christelle BOUTOLLEAU	Docteur, Ingénieur, Europe Technologies

---

Directeur de thèse : Damien CHABLAT
Laboratoire : Institut de Recherche en Communications et Cybernétique de Nantes
Co-Directeur : Anatol PASHKEVICH
Laboratoire : Institut de Recherche en Communications et Cybernétique de Nantes

N° ED …

ACKNOWLEDGMENTS

Before beginning this manuscript, I would like to express my gratitude to people who have helped and guided me in my research and who have provided all possible assistance throughout the time of working on the thesis. It is a pleasure for me to thank those who made this thesis possible.

First and foremost I am heartily thankful to my supervisor, Professor Anatol Pashkevich, for his continuous aid in my research and everyday life, who has proposed me to make my PhD in France. It is difficult to assess his contribution in my background and in my researches, he always directed my research in a right way, gave invaluable advices, spent a lot of time to make my thesis better and research significant, he taught me to write high-quality scientific works and carry out independent research. It is an honor for me to thank another supervisor Damien Chablat, who has introduced and trained me to CATIA software, which was very useful while my research, and who has acquaint me with researchers from all over the world.

I am grateful for all conversations and discussions with Stephane Caro, Sébastien Briot, Dmitry Bondarenko, Claire Dumas, they always gave well-reasoned answers or high-quality advices on the existing problem, discover important questions in my research which needed further investigations, and generate interesting ideas, that aided to further my research and made a significant contribution to my background and thesis. I also pleased grateful to Benoit Furet for the opportunity to understand and observe some physical aspects of my research on a real robot. In addition, I want to thank Isabelle Laine, Anita Niebroj-Kaelbel for their administrative support.

I would like to thank all colleagues from Ecole des Mines de Nantes (people from DAP and all persons with whom I had the opportunity to cross) and IRCCyN (people from MCM, ROBOTIQUE and MO2P) who provided any aid, support or assist during last three years. I am pleased to the friends who share time with me during lunches, coffee breaks and week-ends.

The last and most important thanks goes to my family, who always supported me in all my pursuits. I would like to thank them for all their love and encouragement.

This work is founded by the project of region “Pays de la Loire” RoboComposite.

CONTENTS

LIST OF FIGURES

LIST OF TABLES

LIST OF SYMBOLS

A	cross-section area
b	chip width, [mm]
d_0	initial distance between the end-point and the singularity-plane, [mm]
E	Young's Modulus, [N/mm^2]
f_t	feed rate, [m/min]
$\mathbf{F}$	vector of the external loading applied to the end-effector, 6×1
$\mathbf{F} = f(\mathbf{t}\,|\,\mathbf{t}_0)$	non-linear force-deflection relations corresponding to the target point $\mathbf{t}_0$
F_{cr}	critical force, [N]
F_{max}	maximal cutting force, [N]
$\mathbf{g}(\mathbf{q},\boldsymbol{\theta})$	geometrical function that defines end-point location
$\mathbf{g}_j(\mathbf{q},\boldsymbol{\theta})$	geometrical function that defines j-th node-point locatio
$\mathbf{G}$	matrix of auxiliary forces applied to intermediate node of kinematic chain, $6n\times1$
$\mathbf{G}_i$	auxiliary forces applied to i-th intermediate node, 6×1
$\mathbf{H}_{\theta\theta},\mathbf{H}_{\theta q},\mathbf{H}_{q\theta},\mathbf{H}_{qq}$	aggregated Hessian matrices, $n_q\times n_q$, $n_\theta\times n_\theta$, $n_q\times n_\theta$ and $n_\theta\times n_q$ respectively
$\mathbf{H}^{(F)}_{qq},\mathbf{H}^{(F)}_{\theta\theta},\mathbf{H}^{(F)}_{q\theta},\mathbf{H}^{(F)}_{\theta q}$	Hessians of the scalar function $\Psi=\mathbf{g}(\mathbf{q},\boldsymbol{\theta})^{\mathrm{T}}\cdot\mathbf{F}$ with respect passive and virtual joint coordinates, $n_q\times n_q$, $n_\theta\times n_\theta$, $n_q\times n_\theta$ and $n_\theta\times n_q$ respectively
$\mathbf{H}^{(G)}_{\theta\theta},\mathbf{H}^{(G)}_{qq},\mathbf{H}^{(G)}_{\theta q},\mathbf{H}^{(G)}_{q\theta}$	Hessians of the scalar function $\sum_{j=1}^{n}\left(\mathbf{g}_j{}^T(\mathbf{q},\boldsymbol{\theta})\cdot\mathbf{G}_j\right)$ with respect passive and virtual joint coordinates, $n_q\times n_q$, $n_\theta\times n_\theta$, $n_q\times n_\theta$ and $n_\theta\times n_q$ respectively
I_y, I_z	second moments, [mm^4]
J	cross-section property, [N/mm^2]
$\mathbf{J}^{(i)}_{\mathrm{v}}$	transformation Jacobians, which define geometrical mapping between end-points of i-th serial chains and reference point frame (end-effector).
$\mathbf{J}_{\mathrm{q}}$ and $\mathbf{J}^{(F)}_{\mathrm{q}}$	Jacobian matrix related to the passive joints for the end-point , $6\times n_q$
$\mathbf{J}^{(j)}_{\mathrm{q}}$	Jacobian matrix related to the passive joints for the intermediate point j , $6\times n_q$
$\mathbf{J}^{(G)}_{\mathrm{q}}$	aggregated Jacobian matrix related to virtual springs of the intermediate points, $6n\times n_q$
$\mathbf{J}_{\theta}$ and $\mathbf{J}^{(\mathrm{F})}_{\theta}$	Jacobian matrix related to the virtual springs for the end-point , $6\times n_\theta$
$\mathbf{J}^{(j)}_{\theta}$	Jacobian matrix related to the virtual springs for the intermediate point j, $6\times n_\theta$
$\mathbf{J}^{(\mathrm{G})}_{\theta}$	aggregated Jacobian matrix related to virtual springs of the intermediate points, $6n\times n_\theta$
h	chip thickness, [mm]
$\mathbf{k}$	compliance matrix, 6×6
$\mathbf{k}^{\mathrm{F}}_{\theta}$	modified joint compliance matrix, $n_\theta\times n_\theta$
$\mathbf{K}_{6\times6}$	Cartesian stiffness matrix of cantilever beam, 6×6
$\mathbf{K}_{12\times12}$	Cartesian stiffness matrix of double-side loaded link, 12×12
$\mathbf{K}$	stiffness matrix, 6×6
$\mathbf{K}_{\mathrm{C}}$	Cartesian Stiffness Matrix, 6×6
$\mathbf{K}_{\mathrm{C}}(\mathbf{t}\,|\,\mathbf{t}_0)$	Cartesian stiffness matrix computed in the point $\mathbf{t}$, $\mathbf{t}_0$ denotes the unloaded location of the end-platform, 6×6
$\mathbf{K}_{\mathrm{t.p.}}(\mathbf{t}_0\,|\,\mathbf{t}^{(\mathrm{F})}_0)$	Cartesian stiffness matrix computed with respect to the second argument of the stiffness model, 6×6
$\mathbf{K}^{0}_{\mathrm{C}}$ and $\mathbf{K}^{0(F)}_{C}$	stiffness matrix of serial chain without passive joints in the unloaded/loaded mode, 6×6

$\mathbf{K}_{Cq}$	stiffness matrices defining linear mappings of end-point displacement to passive joint coordinates $\Delta\mathbf{q}$, $6\times n_\theta$
$\mathbf{K}_{C\theta}$	stiffness matrices defining linear mappings of end-point displacement to virtual joint coordinates $\boldsymbol{\theta}$, $6\times n_\theta$
$\mathbf{K}_F$	part of joint stiffness matrix that is induced by external loading , $n_\theta \times n_\theta$
$\mathbf{K}_I$	part of joint stiffness matrix that is induced by the geometrical constraints, $n_\theta \times n_\theta$
$\mathbf{K}_u$	joint stiffness matrix that is a solution of a non-linear matrix equation, $n_\theta \times n_\theta$
$\mathbf{K}_\theta$	Joint-Space Stiffness Matrix, $n_\theta \times n_\theta$
k_c	specific cutting force, [N/mm^3]
$k_{i1.1}$	main value of the specific cutting force, [N/mm^2]
K_{PRO}, K_V, K_γ, K_{CM}, K_{TW}, K_{CL}, K_{WS}	correction factor for cutting forces due to manufacturing process, cutting speed, rake angle, cutting material, tool wear, cutting fluid and workpiece shape respectively
$\mathbf{L}$	vector of link geometry, 3×1
m_c	exponent of specific cutting force
n_q	number of passive joints $\mathbf{q}$ in a serial chain
n_θ	number of virtual joints $\boldsymbol{\theta}$ in a serial chain
N	spindle speed, [rpm]
$\mathbf{p}$ and $\delta\mathbf{p}$	spatial position of the point and it displacement caused by loading, 3×1
$\{\mathbf{p}_i, \Delta\mathbf{p}_i \mid i=\overline{1,n}\}$	displacement field, where $\mathbf{p}_i$ define the node initial location and $\Delta\mathbf{p}_i$ refers to the node displacement due to the applied force/torque, and n is the number of considered nodes
$\mathbf{P}_i$	skew-symmetric matrix corresponding to the vector $\mathbf{p}_i$, 3×3
P_{sp}	spindle power, [kW]
$\mathbf{q}$ and $\delta\mathbf{q}$	passive joint coordinates and their deflections caused by loading, $n_q \times 1$
$\mathbf{R}$	orthogonal rotational matrix, 3×3
$\mathbf{t}$ and $\delta\mathbf{t}$	end-effector (end-point) location and it displacement caused by loading, 6×1
$\mathbf{t}_0$	end-point location for the unloaded mode, 6×1
$\mathbf{t}_0^{(F)}$	modified target location, 6×1
$\mathbf{t}_j$	location of j-th node-point, 6×1
$\mathbf{t} = f^{-1}(\mathbf{F} \mid \mathbf{t}_0)$	non-linear deflection-force relations corresponding to the target point $\mathbf{t}_0$
$\mathbf{T}$, $\mathbf{T}_{Base}$, $\mathbf{T}_{3D}(...)$, $\mathbf{T}_{Link}^i$, $\mathbf{T}_{Tool}$	homogenous transformation matrices, 4×4
v_c	cutting speed, [m/min]
$\mathbf{W}$, $\mathbf{W}_1$, $\mathbf{W}_2$	wrenches applied to the link ends, 6×1
α	scalar parameter insuring convergence, $\alpha \in (0,1)$
Δ_{cr}	critical deflection, [mm]
$\boldsymbol{\varepsilon}_i$	accumulates influences of all geometrical errors on the end-point location of i-th kinematic chain, 6×1
$\boldsymbol{\theta}$ and $\delta\boldsymbol{\theta}$	virtual joint coordinates and their deflections caused by loading, $n_\theta \times 1$
$\boldsymbol{\theta}_0$	preloading in virtual joints, $n_\theta \times 1$
ν	Poisson's Ratio
σ	standard deviation
$\boldsymbol{\tau}_q$	vector of the passive joint reactions on the loading, $n_q \times 1$
$\boldsymbol{\tau}_\theta$	vector of the virtual joint reactions on the loading, $n_\theta \times 1$
$\boldsymbol{\varphi}$ and $\delta\boldsymbol{\varphi}$	orientation of the element and it displacement caused by loading, 3×1

INTRODUCTION

Motivation. At present, aerospace and ship building industries progressively replace conventional materials by new ones that provide essential advantages from the point of view of mechanical properties of the final products, but at the same time introduce some complexity in the manufacturing process. In particular, machining of modern high-performance materials requires revision of some approaches in design and programming of manufacturing cells that must provide high accuracy and high productivity simultaneously.

In machining of such materials, currently there are two main trends. The first of these is based on conventional CNC-machines that are provided by dedicated cutting tools, which are able to achieve desired quality and productivity. However, this classical approach has essential limitations and can be hardly applied when a workpiece geometry is complicated and its dimensions are rather large. In this case, the second trend, which is based on industrial robotic manipulators, looks very attractive. This type of machining cells can be implemented using either serial or parallel manipulators. Both approaches have their advantages and disadvantages. In particular, serial robots provide large workspace but usually are quite heavy and the influence of gravity forces is significant. In contrast, in parallel manipulators the gravity influence is essentially smaller (but not negligible), while the work envelop is limited by particularities of this architecture. Aside these, in both cases the cutting forces produce essential compliance errors that influence the quality of the final product. For this reason, *stiffness analysis of robotic manipulators under essential external forces* becomes a critical issue in design of robotic-based manufacturing cells for machining of modern high-performance materials.

In literature, the main results in manipulator stiffness analysis are obtained assuming that the compliance errors are small enough and may be evaluated by linear models. However, for the considered application area this assumption should be revised, which requires development of relevant non-linear stiffness modeling techniques that are able to evaluate the compliance errors caused by different types of external and internal loadings (cutting and gravity forces, internal preloading in joints introduced in order to eliminate backlash, forces generated by gravity compensators, internal stresses caused by assembling of non-perfect over-constrained closed-loops in parallel manipulators, etc.). Another difficulty is related to taking into account the influence of passive joints that are numerous in parallel manipulators. Hence, the manipulator stiffness modeling for these industry-motivated conditions is a challenge in robotic science.

In this work, to develop the desired stiffness model and corresponding compliance error compensation technique, the Virtual Joint Modeling (VJM) concept is used. This choice is motivated by its essential advantages for the considered application areas, such as high computational efficiency and acceptable accuracy. Compared to other alternative approaches (Finite Element Analysis, Matrix Structural Analysis), the VJM technique is more suitable for both on-line and off-line modes, but it should be essentially enhanced to ensure stiffness modeling in the cases of significant external/internal forces for manipulators with passive joints. In addition, the models to be developed should be able to detect some certain non-linear effects in the stiffness behavior of the manipulator under high loading (buckling for instance). Another promising research direction is related to accuracy improvement of the VJM model parameters using FEA-based virtual experiments for manipulator elements, because current approaches still use crude approximations of manipulator links that are not able to take into account real shape of links and contact surfaces. In addition, existing approaches implicitly assume that all robot components are perfect and there are no internal stresses caused by assembling of over-constrained structure. So, in spite of the fact that the problem of stiffness modeling of serial and parallel manipulators was in the focus of numerous researches ([Salisbury 1980], [Gosselin 1990], [Yi 1992], [Pigoski 1998], [Ciblak 1999], [Chen 2000a], [Zhang 2002], [Alici 2005], [Quennouelle 2008a], [Pashkevich 2010] and others), the main results are in the area of linear stiffness analysis and there are still a number of open theoretical questions, some of which will be considered in this work.

The industrial importance of these problems is confirmed by application of the obtained results in the frame of the research projects "Integrated design of parallel mechanisms and industrial robotic systems for automated processing of composite materials" (RoboComposite) founded by a project of the “Pays de la Loire” region of France and "Imageur Robotisé pour les Intervention Mini-Invasives" (IRIMI) FUI project and "Modelling and control of robots for machining operations of large composite parts and friction stir welding." (COROSOO) ANR project.

Thesis goal and research problems. This thesis focuses on *enhancement of stiffness modeling techniques for serial and parallel manipulators in order to increase the accuracy and efficiency of robotic-based machining of high performance materials by means of compensation of the compliance errors (in on-line or/and off-line mode).* To achieve this goal, several problems have to be solved:

Problem 1:

Accuracy improvement of stiffness matrices used in the VJM model (taking into account complex shape of manipulator links, coupling between rotational/translational deflections and joint particularities).

Problem 2:

Enhancement of VJM-based stiffness modeling technique for serial and parallel manipulators with arbitrary location of passive joints in the case of small deflections (unloaded mode).

Problem 3:

Extension of the proposed VJM-based technique for the case of large deflections caused by internal and external loadings, taking into account related changes in Jacobians and equilibrium coordinates.

Problem 4:

Application of the developed technique to the analysis of non-linear effects in manipulator stiffness behavior under loadings and determining the potentially dangerous configurations and critical forces that may provoke undesired buckling phenomena, i.e. sudden change of current configuration of the loaded manipulator.

Thesis structure. To address the above defined problems, the thesis is organized as follows. *Chapter* 1 is devoted to the state of art and literature review on the robotic based processing of high performance materials and stiffness modeling of robotic manipulators. It includes a review of robot applications for machining of high performance materials, determination of potential demands, limitations and advantages, specification of robots errors in machining application and review of error compensation methods. The main focus of this chapter is on the stiffness modeling methods and stiffness modeling approaches for unloaded and loaded modes. Finally, this allows us to define the goal and the problems statement of the thesis

Chapter 2 is devoted to the accuracy improvement of the elastostatic model for manipulator links. It proposes a computationally efficient identification procedure which is based on the FEA-modeling and allows us to obtain the stiffness matrix taking into account complex shape of the link, couplings between rotational and translational deflections and joints particularities. Simulation study shows that it is able to evaluate the stiffness matrix elements with accuracy about 0.1% and also to detect non-significant ones. The developed identification procedure is illustrated by several examples that will be used in the following chapters for the VJM-based modeling of the entire manipulator.

Chapter 3 is devoted to the enhancement of VJM-based stiffness modeling technique for serial and parallel manipulators with arbitrary location of passive joints in the case of small deflections (unloaded mode). It proposes a computationally efficient procedure which is able to produce singular and non-singular Cartesian stiffness matrix for the kinematic chain both in numerical and an analytical form. This allows us to extend the classical stiffness mapping equation for the case of manipulators with passive joints and to evaluate stiffness matrix properties analytically. It also proposes a new aggregation technique, which is able to take into account geometry of the mobile platform and to compute internal deflections and forces/torques as well as the displacement of mobile-platform caused by geometrical errors in the kinematic chains. The developed stiffness analysis technique is illustrated by several examples which deal with parallel manipulators.

Chapter 4 is devoted to the extension of the VJM-based stiffness modeling technique developed in the previous Section for the case of large deflections (loaded mode). It proposes a computationally efficient procedure, which is able to take into account the internal and external loadings and to obtain a non-linear force-deflection relation. It also produces Cartesian stiffness matrix both in numerical and analytical form. This allows us to extend the classical stiffness mapping equation for the case of manipulators with passive joints in the loaded mode. The stiffness model aggregation technique is also extended for the case of the loaded parallel manipulator. It is able to produce non-linear force-deflection and deflection-force relations as well as to compute internal deflections and forces/torques caused by different types of loadings and geometrical errors in kinematic chains. In addition, a non-linear compliance errors compensation technique is proposed based on the developed stiffness model. These results are illustrated by several examples.

Chapter 5 is devoted to the application of the developed modeling technique for the non-linear stiffness analysis of the manipulators with passive joints in the loaded mode. It focuses on detecting non-linear effects in the manipulator stiffness behavior under loading and determining potentially dangerous configurations and critical forces that may provoke undesired buckling phenomena (i.e. sudden change of current configuration of the loaded manipulator). The stiffness analysis is carried out for serial and parallel manipulators with different assumptions on their flexibility and the type of loading. Particular attention is paid to multiple equilibriums, stability of the kinematic chain configuration and kinetostatic singularities in loaded manipulators. Finally, *Conclusion* summarizes the main results and defines future research directions.

Main contributions. Theoretical results presented in this work are in the area of the VJM-based non-linear stiffness modeling of robotic manipulators with passive joints under external and internal loadings. Among them, there are four contributions that can be treated as the most essential ones. Their brief summary is presented below.

(i) *FEA-based methodology for stiffness matrix identification of the manipulator links with the complex shape, which takes into account coupling between rotational/translational deflections and joint particularities that are related to the contact surfaces of the adjacent links*.

This result contributes to the area of virtual experiments planning in CAD-based environment and algorithmic data processing that produces the desired stiffness matrix with required accuracy. In contrast to other works, the developed technique operates with the deflection field in the neighborhood of the reference point, which provides higher identification accuracy (about 0.1% for stiffness matrix element). Proposed analytical expressions for accuracy evaluation of the developed identification technique provides the ability to determine the optimal settings for the FEA-based experiments and to improve the identification accuracy. In addition, statistical processing of the experimental data allows us to minimise the identification errors by eliminating outliers, to determine the confidence intervals for the matrix elements and to set to zero non-significant ones. This methodology provides good integration with existing CAD-based systems and results of the identification technique can be used both for the VJM and the MSA methods, which operates with 6×6 and 12×12 stiffness matrices respectively.

(ii) *Stiffness modeling of serial and parallel manipulators with passive joints in the unloaded mode* (*i.e. under assumption of small deformations*).

This contribution is in the area of the VJM modeling approach that was enhanced for serial and parallel manipulators with arbitrary location of passive joints. In contrast to other works, the developed technique starts from stiffness modeling of all kinematic chains *separately* and then *aggregates* them in a unique model. For the serial chains is proposed an analytical expression for stiffness matrix modification induced by passive joints, which extends the classical stiffness mapping notion, and related recursive procedure for stiffness matrix elements computing, which allows to treat passive joints sequentially (one-by-one). The developed technique is more computationally efficient, includes low-order matrix inversion, and is able to obtain *both non-singular and singular stiffness matrices* that take intoaccount the influence of passive joints or the kinematic singularities. Relevant assembling procedure allows to compute the *aggregated Cartesian stiffness matrix* of the parallel manipulator and also to evaluate the *internal forces/torques* and *end-platform deflections* caused by geometrical errors in the kinematic chains of over-constrained mechanism. This issue has never been studied before and has essential practical significance for evaluating desired tolerances in links/joints geometry and corresponding internal stresses in over-constrained mechanisms. The developed method combines advantages of the FEA and the VJM modeling approaches (accuracy and computational efficiency respectively) and allows to obtain stiffness matrices either in numerical or in analytical form.

(iii) *Non-linear stiffness modeling of serial and parallel manipulators with passive joints in the loaded mode* (*i.e. under assumption of large deformations*).

This result contributes to generalization of the VJM modeling approach for the case of large deflections caused by internal and external loadings applied to the end-point or/and to the intermediate nodes of the kinematic chains. In contrast to other works, the developed technique includes computing of the static equilibrium configuration corresponding to the given loading. In addition, it allows us to check the "internal stability" of relevant chain configuration. Similar to the unloaded mode, the stiffness modeling of parallel manipulators starts from kinematic chains, but it yields a non-linear function describing force-deflection relation. Besides, for each kinematic chain, this technique is also able to obtain *both non-singular and singular stiffness matrices*. Relevant aggregation procedure allows us to obtain a non-linear force-deflection (or deflection-force) relation for the parallel manipulator and to compute the *aggregated Cartesian stiffness matrix*, as well as to evaluate the *internal forces/torques* and *end-platform deflections* caused by loadings and geometrical errors in the kinematic chains. Further, this model is used for compensation of the compliance errors caused by the internal and external loadings. The developed method also combines advantages of the FEA and the VJM modeling approaches (accuracy and computational efficiency respectively).

(iv) *Application of the developed stiffness modeling technique for the non-linear stiffness analysis of serial and parallel industrial manipulators used in machining of high-performance materials.*

This contribution deals with detecting non-linear effects in the manipulator stiffness behavior and determining the potentially dangerous configurations and critical forces that may provoke undesired buckling phenomena in typical robotic architectures. In contrast to other works, it was firstly showed that in externally/internally loaded manipulators some kinematic chains may be unstable and/or there may exist elastostatic singularities (in addition to ordinary geometrical ones), for which even small disturbances may lead to sudden change of current configuration. From practical point of view, these results are useful for pre-design stage. They allow the designer to evaluate admissible range of the loading that does not create undesirable effects in the manipulator behavior during machining.

Publications and conference presentations. The main results obtained in this thesis are have been published in 9 works and have been presented at 7 conferences. Among them, there are two papers in international journals (Mechanism and Machine Theory, Mobile Robotics & Intelligent Systems), a book chapter (In: Advances in Robot Manipulators), proceedings of six international conferences (IEEE/RSJ International Conference on Intelligent Robots and Systems, IFTOMM European Conference on Mechanism Science, International Symposium Advances in Robot Kinematics, International Conference on Computer and Automation Technology, CIRP Conference on Manufacturing Systems, CIRP Design Conference).

CHAPTER 1

ROBOTIC-BASED PROCESSING OF HIGH-PERFORMANCE MATERIALS AND STIFFNESS MODELING OF ROBOTIC MANIPULATORS

This chapter is devoted to the state of art and related literature review on the robotic based processing of high performance materials and stiffness modeling of robotic manipulators. It proposes a review of robot applications for machining of high performance materials, determination of potential demands, limitations and advantages, specification of robots errors in machining application and review of error compensation methods. The main focus of this chapter is to review existing literature on stiffness modeling methods and stiffness modeling approaches for unloaded and loaded modes. Finally, this allows us to define the goal and problems for the thesis

1.1 ROBOT APPLICATION FOR MACHINING OF HIGH PERFORMANCE MATERIALS

High performance materials provide greater strength, resistance, durability and ductility and significantly increase the longevity of structures. For these reasons they are widely used in the aerospace and ship building industries and in other fields. But their processing introduces additional complexity compared to conventional materials and often requires special equipment, so a manufacturing process has to be revised. Moreover, since aerospace and ship building usually employ limited production systems and operate with rather large workpieces, application of industrial robots in machining of high-performance materials is very reasonable. However, it creates a number of engineering problems, that are in the focus of this Chapter.

1.1.1 Modern trends in machining

General trends in machining. Generally, modern trends in machining are aimed at improving machining efficiency while reducing the product price. These trends are contradictive, so all related research focus on a compromise that ensures high manufacturing accuracy and acceptable cost. In the frame of formal models used in this area, most of the design objectives are usually converted into the constrains that define acceptable (but obviously not strictly optimal) values of corresponding performance measures. This approach

allows us to reduce complexity of the related optimization problem, but does not eliminate the need for development of specific mathematical models for assessing of each particular performance.

The most useful ways of reducing the price and improving the product quality are related to the enhancement of cutting technology and optimization of tool path. In particular, reducing the total amount of material removal and using optimal cutting parameters for the maximization of metal removal rate yield an essential reduction of the manufacturing time. While the first improvement can be achieved rather easily (by proper dimensioning of raw primary part), the second one requires optimization of the machining process by increasing of the depth of cut and feed rate as well as the spindle speed to the maximum allowed levels. The later is obviously accompanied by an increase of cutting forces that still are not very essential for the conventional CNC-machines with rather rigid mechanical structure. However, in robotic-based processing, these forces may cause essential deformations of the manipulator and consequent impact on the processing accuracy. Therefore, this issue needs detailed analysis which will be in the focus of this work.

The tool path optimization is aimed at the reduction of non-cutting time as well as the minimisation of efforts in actuator drives by proper selection of the tool moving direction. The first of them is also called 'airtime' [Castelino 2003] in order to distinguish from the machining time when the tool is actually cutting material. As it follows from related research [Veeramani 1998], [Oysu 2009], the airtime can be quite significant when multiple tools are used or a number of small regions are being machined. Mathematically, this problem is formulated as a specific version of the traveling salesman problem with rather hard precedence constraints [Ozgur 1995]. The second issue, minimisation of actuator efforts, is equivalent to optimization of tool path in the manipulator workspace. It was previously studied mainly using kinematic criterion [Nektarios 2010], but machining application (especially for hard materials) requires direct computing of forces/torques in actuated joints that are also considered in this work.

Other issues that are important for manufacturing but are beyond of the scope of this work are related to minimization of setup time, using multi-operation machine tools and quick-change systems for tooling, automation of loading/unloading operations, improving accuracy of traditional roughing process, reduction of manufacturing lead time, applying of just-in-time production strategy, minimization of inventory cost, etc. [Lin 2011]. Besides, on the product development stage, the concurrent engineering methodology is also attractive. Integration of all these approaches yields maximal utilization of expensive equipment and significantly reduces the product price.

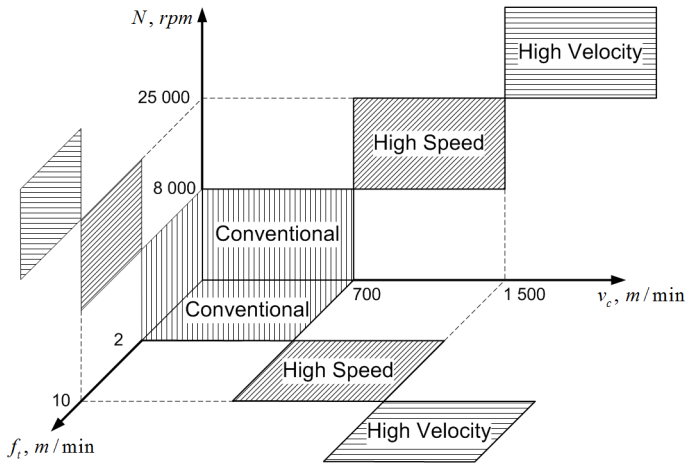

Figure 1.1 General limits for High Speed Machining [Garant 2010]

It is worth mentioning that, in spite of obviously positive impact, some advances in modern machining technology adversely affect the processing accuracy. For instance, increasing depth of cut generates high forces/torques which may cause significant (and inadmissible) compliance deformations of the machining tool or robot. To reduce related machining errors there exist two main approaches. The first these is aimed at increasing of the machine tool or robot stiffness as well as optimal part placement in the workspace. However, increasing of the mechanism stiffness obviously leads to decreasing of the dynamic properties (due to higher mass and inertia of the links). The second approach is based on *compliance errors compensation*

via proper off-line modification of control program describing desired tool trajectory or by using the force feedback in the online mode. To implement this approach, a suitable stiffness model of the CNC-machine or manipulator is required, which is proposed in the following chapters.

High Speed Machining (HSM). The most essential current trends in machining of high performance materials are integrated in HSM-concept, which has been already successfully implemented in several projects for the aerospace and ship building industries [Terrier 2004] that are known by their strong requirements for accuracy and high demands for efficiency. But simultaneously with obvious advantages, these applications demonstrated rather strong constrains on the specifications of the manufacturing equipment. This is caused by high spindle speed, high feed rate and by other factors. Typically, HSM-based manufacturing conditions are associated with the following parameters [Garant 2010]:

- spindle speed N from 8000-10000 revolutions per minute (rpm) for widely used wares and up to 40000 rpm and higher for aerospace and medical industry, high accuracy wares and machining with small tools;
- cutting speed v_c from 700 m/min for milling with small tools;
- feed rate f_t has to be at least 2-2.5 m/min and amount up to 40 m/min and more for high velocity machining;
- spindle power P_{sp} from 10-15 kW for tools with low feed rate and traverse 50 kW for high velocity machining of stiff materials.

It should be stressed that all these specifications of the machining process are not strict and can vary, but they essentially differ from the conventional ones. Approximate manufacturing conditions limits for HSM are summarized in Figure 1.1. Main advantages of HSM are summarized in Figure 1.2, which shows the influence of cutting speed on cutting forces, surface quality, time-cutting volume, thermal workpiece load and tool life travel [Garant 2010].

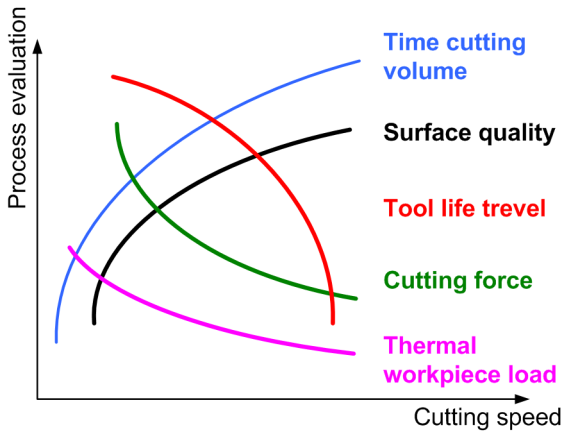

Figure 1.2 Influence of cutting speed on the process evaluation [Garant 2010]

Special requirements of HSM. To obtain potential advantages of HSM, a number of special demands for the manufacturing process have to be satisfied [Garant 2010], [Sharma 2001]. All these requirements can be classified into the following groups with respect to their origins:

(a) Spindle drive requirements:

- High speed rpm takes significant amounts of power just to rotate the spindle, besides the additional power required to cut the material, which increases with feed rate. Hence, a powerful spindle motor to machining with high feed rates is required.
- Static and dynamic stiffness of the spindle must have the bending compliance.
- High performance spindles must have short run uptime and high stiffness.
- Size and type (angular contact, roller), number of bearings, bearing preload (stiffness), type of lubricants, and bearing material (steel, ceramic) require to be critically examined for high speed machine tools.

(b) Machining process requirements:
- Working method with low backlash and low vibration,
- High rigidity,
- Light-construction moving parts,
- High speed and concentricity of spindles,
- Implementation of high feed rates (linear drives),

(c) Requirements for the tool:
- Appropriate cutting tool system: longer tool-life and better surface qualities can only be achieved with the corresponding tool materials,
- High concentricity,
- High balancing speed (geometry, shank design),
- Long tool-life (with special cutter geometries and coatings),
- High rigidity.

(d) Tool holder requirements:
- High concentricity,
- Hydroexpanding, high-precision or shrink-fit chuck.

(e) Requirements for workpiece:
- Stable and low-vibration fixing,

Hence, to achieve potential advantages of HSM, the machining process and its components should satisfy very strict requirements. One of promising direction in this area is using parallel kinematic machines (or parallel robots) instead of traditional CNC-machines with Cartesian architecture. Hypothetically, the parallel architectures offer a number of advantages due to lower moving masses but their stiffness models are not trivial [Yi 1992], [Deblaise 2006a], [Quennouelle 2008a], [Wei 2010]. Besides, to evaluate possible compliance errors, it is required to estimate the forces and torques caused by interaction between the cutting tool and the workpiece. This issue is conspired in the following subsection.

1.1.2 Machining of high performance materials

Machining of high performance materials generates significant loading on the processing mechanism caused by interaction of machining tool and workpiece (Figure 1.3). It is evident that, this loading is essentially higher compared to conventional materials and it leads to the compliance errors which can be significant and deteriorate surface property. Generally, the compliant errors depend on two independent factors: the loading value and the resistance of the machining mechanism to the loading. Let us concentrate first on the *computation of the force/torque* associated with the machining process, while the issue of the machining mechanism resistance to the loading will be considered further.

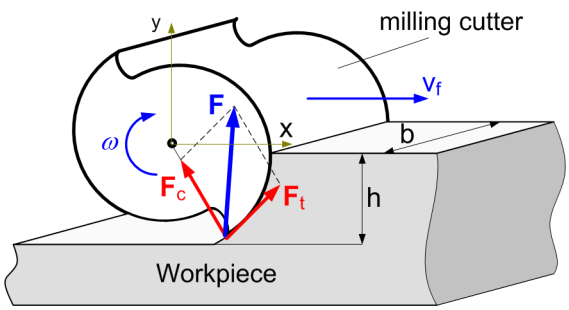

Figure 1.3 Cutting forces in machining process

In general, cutting forces depend on a number of factors. Among the most important ones are the materials of the machining tool and workpiece, the feed rate and the spindle rotation speed, the degree of tool

wear, the tool temperature, the cutting geometry, the cutting width and thickness and other factors [Tsai 2001], [Lamikiz 2004], [Xu 2007], [Wan 2009]. Moreover, the cutting forces are not constant and vary with the feed rate. Since in practice it is difficult to find the exact value of the cutting force, it is reasonable to estimate it for the worst case. For this reason, in engineering practice, usually simplified expressions are used where the impact of each factor is taken into account via a relevant correction coefficient [Garant 2010], [Grote 2009], [Beitz 1994]:

$$F = b \cdot h \cdot k_{\mathrm{c}} \cdot K_{\mathrm{PRO}} \cdot K_{\mathrm{V}} \cdot K_{\gamma} \cdot K_{\mathrm{CM}} \cdot K_{\mathrm{TW}} \cdot K_{\mathrm{CL}} \cdot K_{\mathrm{WS}} \tag{1.1}$$

Here b, h are the chip width and thickness respectively, k_{c} is 'the specific cutting force', K_{PRO} is a correction factor for the manufacturing process, K_{V} is the cutting speed correction factor, K_{γ} is the rake angle correction factor, K_{CM} is the cutting material correction factor, K_{TW} is the tool wear correction factor, K_{CL} is the cutting fluid correction factors, K_{WS} is the workpiece shape correction factor. Typical values of the correction factors are presented in Table 1.1.

Table 1.1 Correction factors for the cutting force computing [Grote 2009]

Correction factor	Notation	Value
Manufacturing process	K_{PRO}	$K_{PRO} = 1.2 - 1.4$ (the factor takes into account that the machining indices obtained from turning tests)
Cutting speed	K_V	$K_V = \frac{2.023}{v_c^{0.153}}$ for $v_c < 100\ m/\min$ $K_V = \frac{1.380}{v_c^{0.07}}$ for $v_c > 100\ m/\min$
Rake angle	K_γ	$K_\gamma = 1.09 - 0.012\angle^\circ$ (steel) $K_\gamma = 1.03 - 0.012\angle^\circ$ (cast iron)
Cutting material	K_{CM}	$K_{CM} = 1.05$ (HSS) $K_{CM} = 1.0$ (cemented carbide) $K_{CM} = 0.9 - 0.95$ (ceramic)
Tool wear	K_{TW}	$K_{TW} = 1.3 - 1.5$ $K_{TW} = 1.0$ for sharp cutting edge
Cutting fluid	K_{CL}	$K_{CL} = 1$ (dry) $K_{CL} = 0.85$ (non-water soluble coolant) $K_{CL} = 0.9$ (emulsion-type coolant)
Workpiece shape	K_{WS}	$K_{WS} = 1.0$ (outer diameter turning) $K_{WS} = 1.2$ (inner diameter turning)

The remaining coefficient k_c (so called 'the specific cutting force') that is not included in the above table, depends on the chip thickness h nonlinearly and is usually computed as [Garant 2010]:

$$k_c = \frac{k_{c1.1}}{h^{m_c}} \tag{1.2}$$

where $k_{i1.1}$ is the main value of the specific cutting force (which depends on the material properties), m_c is its exponent. Table 1.2 contains typical values of $k_{c1.1}$ and m_c for several high performance materials.

Table 1.2 Mechanical properties of typical high performance materials [Garant 2010]

Material	Main value of specific cutting power $k_{t1.1}$, [N / mm^2]	Rise of the tangent m_c	Typical use
Monel 400 (NiCu30Fe)	2600	0.19	Aerospace material with favourable mechanical and chemical-corrosion properties, pressure tank construction, centrifuges, ship's valves
Inconell 718 (NiCr19NbMo)	2088	0.29	Aerospace material, excellent properties in the extremely low temperature range, very good corrosion resistance, rocket propulsion units, gas turbines, pumps
Ti Al 6 V 4	1370	0.21	Aircraft and spacecraft construction, fittings, mechanical engineering
Al Mg 4.5 Mn	780	0.23	Vehicle construction, shipbuilding, pressure tanks

There also exist nonlinear expressions for the cutting force which take into account some other specific factors. For instance, [Paris 2007] has proposed the fractal model for cutting force

$$F = \frac{a_1 \cdot h + a_2 \cdot h^2}{1 + a_3 \cdot h} \tag{1.3}$$

where h is the cut depth and a_1, a_2, a_3 are the model coefficients that depend on material properties, specific chip thickness and cutting stiffness.

For the *worst-case analysis*, expressions (1.1) and (1.3) can be reduced to the linear relation

$$F_{max} = 2 \cdot k_c \cdot b \cdot h \tag{1.4}$$

which includes only factor k_c depending on the cutting tool and material properties as well as the cutting cross-section $b \times h$. Numerical values of the maximum cutting forces computed using this expression are presented in (1.4) which includes results for two high performance materials with different cutting settings. They allow us to compare F_{max} for two materials with essentially different cutting stiffness. In particular, for the same cutting depth $h = 0.2\ mm$, cutting width $b = 8\ mm$ and cutting speed from 1000 to 2000 m/min, the cutting force is about 2 kN for the aluminum alloy (Al Mg 4.5 Mn) and close to 7 kN for Monel 400. It is evident that both of these values are high enough to cause significant deformations of the CNC-machine or robotic manipulator. For instance, for robot manipulator KUKA-240 [Dumas 2010] such loading may generate linear deflections 0.1..5.0 mm and angular deflections 0.1..0.2° depending on the cutting force direction.

It is worth mentioning that, for the constant feed rate, the cutting force reduces with increasing of the spindle speed. This effect is in good agreement with equation (1.4): increasing of the spindle speed for the same feed rate does not change the cutting speed, while the chip thickness h reduces. This effect is widely used in practice. But to save the processing time, usually the feed rate increases with the spindle speed. This does not allow us to reduce relevant compliance errors.

Another issue that should be taken into account while evaluating reactions associated with machining of high performance materials is related to the *spindle axial torque*. Usually this value is obtained from experiments [Kaya 2011], but it is also possible to estimate its range from nominal values of spindle power and rotation rate. For instance, the values 20 kW and 10000 rpm correspond to the torque of about 10 N·m (for the efficiency factor 50%). For typical industrial application based on robot KUKA-240, this torque may cause linear/angular deflections of 0.001..0.008 mm and 0.1..1.6° respectively (depending on the feed direction). Besides, the cutting forces may exert essential *lateral torque* with respect to the robot-mounting flange. For example, for the tool reference point offset of 100 mm, the cutting force 2-7 kN (see Table 1.3) produces the torque 20-140 N·m that makes non-negligible linear and angular deflections.

Table 1.3 Cutting forces for high performance materials

Material	Depth of cutting h, mm	Width of cutting b, mm	Cutting speed v_c m/min		
			1000	1500	2000
Monel 400 (NiCu30Fe)	0.2	8	6.97 kN	6.77 kN	6.64 kN
		16	13.94 kN	13.54 kN	13.28 kN
	1	8	25.65 kN	24.93 kN	24.44 kN
		16	51.30 kN	49.86 kN	48.88 kN
Al Mg 4.5 Mn	0.2	8	2.23 kN	2.17 kN	2.12 kN
		16	4.46 kN	4.34 kN	4.24 kN
	1	8	7.70 kN	7.48 kN	7.33 kN
		16	15.40 kN	14.96 kN	14.66 kN

Hence, the cutting forces and torques associated with milling of high performance materials are essentially higher compared to conventional ones. They may cause significant linear and angular deflections of the machining tool that lead to essential reduction of the accuracy and quality of the final product. This issue justifies the goal of this research work.

1.1.3 Machining with robots versus traditional machining tools

At present, there are two main approaches in designing of machining workcells: (i) utilization of classical CNC-machines with Cartesian architecture and (ii) using industrial robots of either serial or parallel architecture. Both of them have their own advantages and disadvantages that are briefly discussed below from the point of view of applicability to machining of high performance materials.

CNC-machines. Computer Numerical Control (CNC) machines refer to the automatic machine tools, which use abstractly programmed commands to specify the tool path and relative location of the workpiece while machining [Lo 2000]. The earliest CNC equipment was based on existing traditional machine tools that were supplemented by motors that control the cutter feed rate. Further, all control execution functions were given to computers and the control program preparation was carried out in CAD/CAM environment [Newmana 2008], [Werner 2000], [Xu 2006]. The latter advances have essentially changed the machining process and provided fundamental benefits, which can be summarized as follows:

(i) full automation of the machining and programming processes, which requires the final dimensions of the product only; this reduces human errors to minimum;

(ii) ability to produce both simple trajectories and the surfaces of high complexity, which extend their application from conventional milling to drilling, lathing, laser cutting, etc.;

(iii) high accuracy and good surface quality that is insured by high rigidity of the tool manipulation mechanism and accurate control of the tool motions;

(iv) flexibility of machining which allows us to process different types of products and combine several operations (milling, drilling, grinding) by changing control program only; this essentially reduces the manufacturing time and the product cost;

There are also some other benefits that are offered by the CNC machines and promote their wide application in industry (advanced machine control, more precise production planning due to high reputability of the machining, etc.) [Newmana 2008]. However, relatively high cost and limited workspace are usually treated as their main disadvantages [Krause 1984]. Typical examples of CNC-machines are presented in Figure 1.4.

Variety of existing CNC-machines is usually classified with respect to the type of motion control system, implemented control algorithm and the number of actuated axes. With respect to the *motion control system*, the CNC-machines may be classified as point-to-point and contouring ones. The first of them, also

called a positioning system, moves the tool to the given location without control of the path and speed (they are not important for some applications, such as drilling). Continuous path systems ensure the path and speed control of the tool while machining, they implement simultaneous control of all driven axes. Typical application areas of continuous motion control are milling and turning.

(a) CNC milling machine (b) CNC grinding machine (c) CNC machining center

Figure 1.4 Examples of CNC-machines

Based on the *control algorithm,* the CNC-machines are divided into open-loop and closed-loop ones. In the open-loop systems, the actuator input is entirely defined by the programmed instructions and there is no feedback to check whether the desired goal (position, velocity) has been achieved. They are obviously rather sensitive to external disturbances, so their application area is limited by the cases where the accuracy requirements are not critical. In contrast, closed-loop systems have a feedback, which allows us to compensate any differences between the desired position/velocity and its actual value. This feedback may be implemented using both analogous and digital technique, the close-loop systems are usually considered to be very precise and attractive for accurate machining.

With respect to the third classification factor, the *number of axes,* the CNC-machines with 2, 3, 4 and 5 axes are distinguished. The first of these usually have only two translational driven axes that ensure control of the tool in the plane. The 3-axis machines are able to process more complex 3-dimentional surfaces, they usually employ three translational drives with mutually orthogonal axes. The more sophisticated are 4- and 5-axis CNC machines that are able to change the tool orientation, in addition to translational motions. This allows to produce more complex tool path movements and to process very complicated products. In general, increasing of the number of axes provides numerous advantages such as better surface quality, reduction of the machining time, improved access to under cuts and deep pockets, etc. It is worth also mentioning that the axes may be actuated either sequentially or simultaneously, but present systems usually implement the simultaneous control.

In modern CNC systems, the machining trajectory design is highly automated and is performed in a CAD/CAM environment. It is used for creating spatial representation of a part; planning and optimization of the tool paths and cutting parameters in creating CNC code; loading, initialization, and operating the CNC-machine; etc. So, CAD/CAM technologies introduce essential benefits to machining such as higher productivity, reduced design time, more accurate designs, less time required for modifications, repeatability.

Hence, the CNC-machines ensure a number of benefits for machining of high performance materials. However, for some aeronautic applications that are closely related to this research, they have rather limited workspace and are not applicable for machining of large dimensional parts. In this case, industrial robots are more attractive, so their suitability for the milling of high performance materials is considered below.

Industrial robots. For the considered application area, robots could gain all functionalities of the CNC-machines and are reasonable alternative for them. Also, they provide *larger workspace* and more *flexibility* [Fassi 2000], [Larsson 2006], [Brogardh 2007]. Besides, emerging technologies allow robots to perform diverse manufacturing processes such as complex cutting and material removal, tapping and drilling, surface finishing and others. All these functions can be realized by the same robot, that makes it universal,

while CNC-machines can execute only one or a group of similar operations. In addition, robot-based machining cells are applicable for secondary operations and have a relatively large working envelope, which is extremely important for large components. Such machining cells are more flexible and allow us to produce different products at the same time, they can be also easily adopted to manufacturing of other products. They usually provide two alternative solutions to modify the tool path: (i) to change it in the CAD/CAM system, or (ii) to teach a robot in some key points. Robots are more intelligent and ensure more sophisticated motion control, and users can map their inaccuracies and compensate for them off-line using a dedicated model (the stiffness model for instance, as in this work) [Rocco 1997] .

In machining applications, robots often use force and torque sensors that allow online estimation of the deflections in the tool locations with respect to the desired ones. The force and torque sensors are usually integrated into a robot's wrist, and the robot controller are able to compensate these deflections via relevant calculations. However, to achieve good quality of machining process and to eliminate robots errors caused by different factors, some additional research is required [Sulzer 2010]. This is the main issue that resists to robot applications in some areas.

With respect to their architecture, all industrial robots can be classified into two groups. First group includes robots with strictly serial architecture, which are currently the most common industrial ones. The second group put together manipulators with strictly parallel architecture and cross-linkages [Merlet 2006], [Merlet 2008]. Typical examples of robots from both groups are presented in Figure 1.5. In order to indicate advantages of both architectures let us focus on their principal features.

(a) serial industrial robot (b) parallel industrial robot

Figure 1.5 A serial Kuka robot (a) and an Adept parallel robots (b)

Serial robots. This type of robots is based on serial kinematic chains composed of rather rigid links connected by actuated joints. The joints may be either rotational or translational. The main advantage of serial robots is large workspace with respect to their own volume and occupied floor space. But, since serial manipulators have open kinematic structure, all errors are accumulated and amplified from link to link. Besides, it is impossible (or rather difficult) to get high stiffness and high dynamic properties simultaneously. For instance, robots with high stiffness usually are heavy and cannot provide high speed. Moreover, their own weight induces undesirable significant stresses in actuated joints that reduces allowed payload. On the other hand, serial robots with small link mass have low stiffness and cannot provide high payload because of significant compliance errors. These issues essentially decrease efficiency and application areas of such manipulators. However, some limitations related to manufacturing errors can be withdrawn by advanced control.

According to its kinematic architecture, serial manipulators can be classified into three main groups: (a) SCARA robots, (b) Articulated robots and (c) Cartesian/Gantry robots [www robotmatrix]. It is worth mentioning that sometimes the robot classification includes some other types of manipulators (cylindrical, spherical, etc.) but here they are included in articulated ones.

The *SCARA* acronym stands for "Selective Compliant Assembly Robot", it is also often referred to as: "Selective Compliant Articulated Robot Arm". This type of robots is based on a 4-axis manipulator (Figure 1.6a) [Das 2005]that ensures motion to any point within its workspace (X-Y-Z translation) and the end-effector rotation around the vertical axis (theta-Z). For this architecture, the vertical Z-motion is independent and is provided by a dedicated linear actuator, while three remaining rotational joints (with parallel axes)

ensure full range of translations and rotations in XY-plane. Because of this specific architecture (with three parallel rotational joints), SCARA is slightly compliant in the XY-plane but is rather rigid in the Z-direction (so called selective compliance). The selective compliant feature makes this robot highly suitable for many types of assembly operations. Due to low mass in moving parts, it provides very good dynamic properties. This promote SCARA to be ideal for pick-and-place, palletizing and de-palletizing, machine loading/unloading and packaging applications, which require fast, repeatable and articulate point-to-point movements.

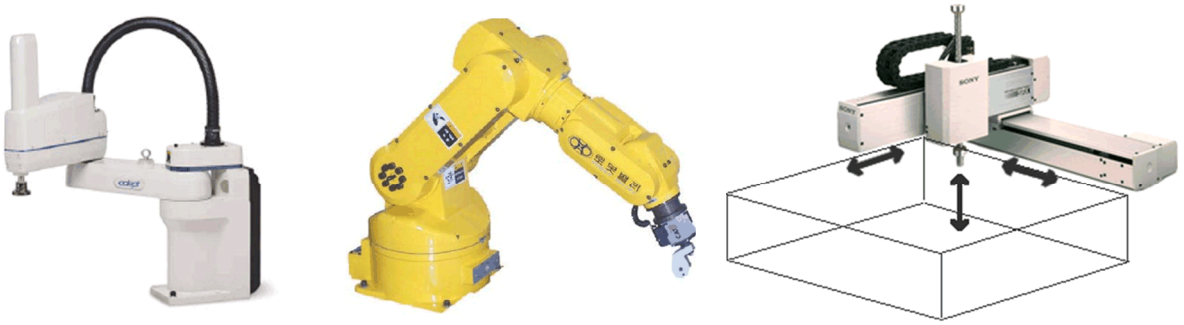

(a) SCARA robot (b) articulated robot (c) Cartesian/Gantry robot

Figure 1.6 Typical architectures of serial robots

The second group includes *articulated robots* (Figure 1.6b) [Matsuoka 1999], [Benamar 2010], which are also called "anthropomorphic arms". Their mechanical structure is based on rotational joints and the links are arranged in a chain. Usually the articulated robots have five or six controlled axes, while robots with seven and more actuated joints also exist. This structure provides very good kinematic dexterity, so the robots have an ability to reach the target location over obstacles and ensure almost any position and orientation of the tool within the workspace. Essential advantage of the articulated robots is that they are very compact and provide the largest workspace relative to their size. However, because of complexity of direct/inverse kinematics, their control is not trivial: when driving an articulated robot in its natural coordinate system (joint space), it is difficult to obtain a straight-line-motion of the end-effector in Cartesian space. So, intensive computations are required to transform the Cartesian location into the actuated joint angles (and vice versa), but this problem is not already significant because of essential computing capacity of modern microprocessors. The capabilities of the articulated robots make them well suit for a wide variety of industrial application, including machining [Olabi 2010], [Abele 2007].

The third group includes *Cartesian robots* (Figure 1.6c) [Dadfarnia 2004], which have almost the same kinematic architecture as conventional CNC-machines. The main differences are in the areas of control principle, programming language and mechanical design of the end-effector connector, which for the robots is rather universal. The mechanical structure of such robots is based on three translational actuated joints whose axes are mutually orthogonal. Such arrangement ensures very simple control when any motion in X-Y-Z space is achieved by straightforward actuation of relevant joints. Cartesian robots have a rectangular workspace whose volume can be increased easily. Extremely large work envelope is ensured by Gantry robots (also belonging to the Cartesian family), where one of the horizontal translational axes is supported at both ends. Due to their mechanical structure, Cartesian robots provide high rigidity and good accuracy but their kinematic dexterity is rather limited; sometimes they cannot reach around objects. Besides, to satisfy the large workspace requirement, they need large volumes to operate and occupy essential floor space. Because of its rigidity, such robots are very attractive for machining applications, but only if the tool orientation may remain the same during processing.

Parallel robots. This type of robots, which are also often referred to as parallel kinematic machines (PKM), is a closed-loop mechanism whose end-effector is linked to the base by several independent kinematic chains [Merlet 2006]. The kinematic chains are composed of several links that are connected to each other by both passive joints and actuated joints (rotational or translational). Such kinematics claim to offer several essential *advantages*, like high structural rigidity, high dynamic capacities and high accuracy [Tlusty 1999], [Wenger 1999, 2001]. Another important advantage of parallel robots is better accuracy,

because here the position and orientation errors of separate kinematic chains are averaged by the end-platform (instead of straightforward accumulation, as in serial robots). Besides, using special arrangement of kinematic chains, it is possible to ensure high stiffness and high dynamic properties simultaneously. These capabilities make the parallel robots well suitable for high-speed machining and they are often used in the manufacturing cells (Figure 1.7), for instance in HexaM 5-axis milling machine, Hexapod OKUMA machine, the VERNE machine, Hexapod-Machine Mikromat 6X, Urane SX, and others [Pierrot 1999], [Goto 1985], [Kanaan 2009], [Neugebauer 1998], [Renault 1999], [Son 2009].

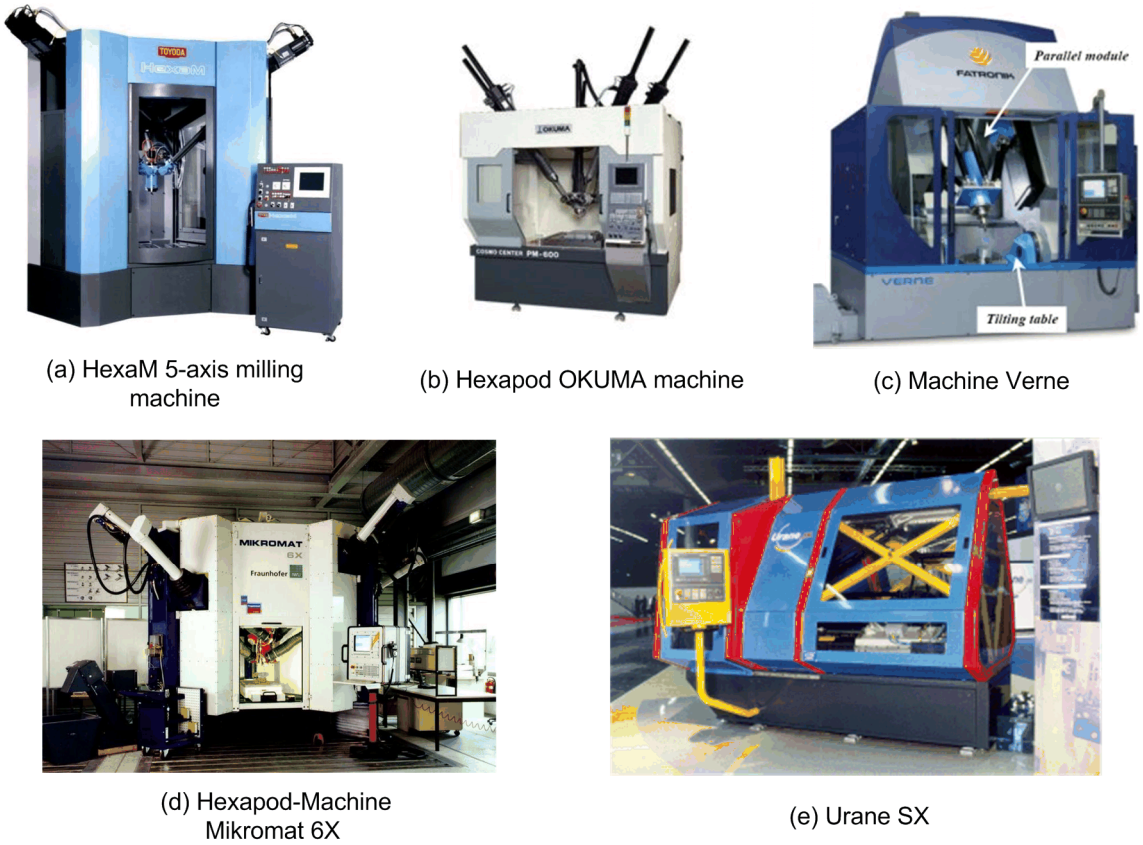

(a) HexaM 5-axis milling machine

(b) Hexapod OKUMA machine

(c) Machine Verne

(d) Hexapod-Machine Mikromat 6X

(e) Urane SX

Figure 1.7 Examples of parallel robots integrated in the machining cells

However, parallel robots have very complex workspace and highly non-linear relation between natural coordinates (actuated joints) and Cartesian ones. Consequently, their performances (maximum speeds, accuracy and rigidity) essentially differ from point to point and also depend on the moving directions. Other *disadvantages* of parallel manipulators are their large footprint-to-workspace ratio (except the Tricept robot which requires less space) and small range of motion because of parallel configuration. These are the main obstacles for the machine application of parallel robots [Kim 1997], [Wenger 1999], [Rehsteiner 1999].

At present, there exists a large variety of parallel manipulators, several examples are presented in Figure 1.8. Depending on the architecture, they may be divided into two groups that differ by the type of connection between the base-platform and the serial chains [Chablat 2003].

The first group contains manipulators with fixed foot points and variable length struts. Most robots of this group implement the Stewart-Gough architecture, have 6 degrees of freedom and are called Hexapods (Figure 1.9) [Merlet 2006]. They provide high precision and accuracy, good stiffness and high load/weight ratio. Due to these essential advantages, Hexapods are often used in flight simulators, precision machining, surgical robots, and other areas. By variation of the link lengths, Hexapods may satisfy both small and large workspace, but increasing of the link length has a direct effects on the accuracy. The main technical problem of Hexapod is high friction in the ball joints. Typical examples of parallel manipulators belonging to the first group are presented in (Figure 1.8 a-g), they include VARIAX, HEXA, TRICEPT, TRIPOD, Delta and others [Geldart 2003], [Pierrot 1991], [Pierrot 2009], [Neumann 1988], [Zhang 2005], [Clavel 1988], [Tsai 2000].

(a) TRICEPT
from Neos-Robotics

(b) the Quattro from Adept

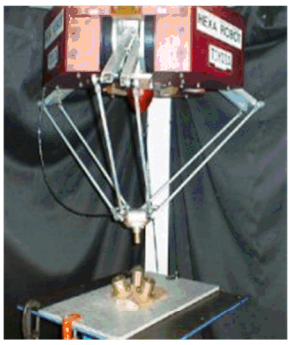

(c) High-Speed Parallel
Robot HEXA

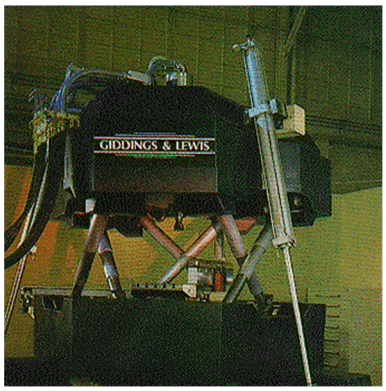

(d) VARIAX (Gidding&Lewis)

(e) Tripod - Parallel
Kinematic Microrobot

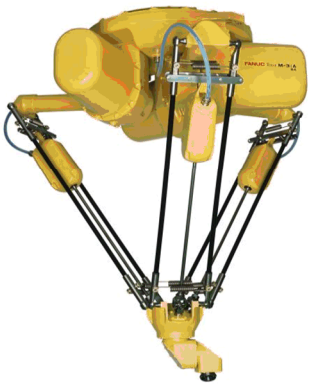

(i) Fanuc M-3iA Series

(g) ABB IRB 340
Flexpicker

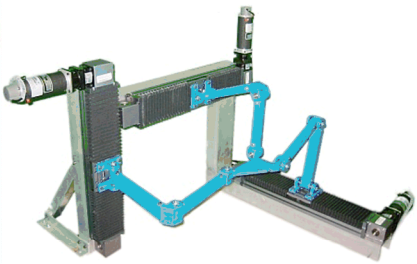

(h) Tripteron Parallel
Manipulator

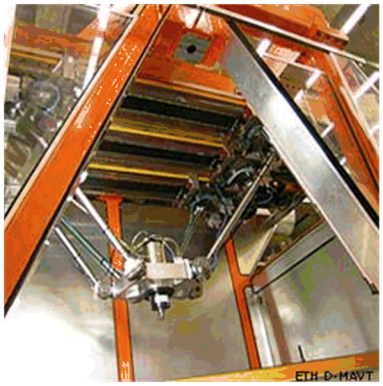

(i) HEXAGLIDE (ETH Zurich)

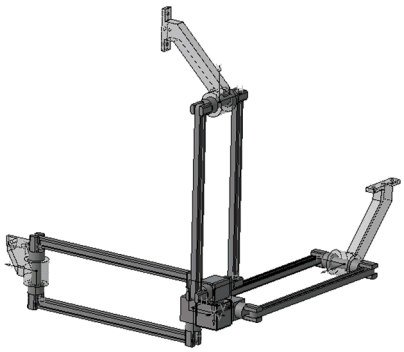

(j) Orthoglide manipulator

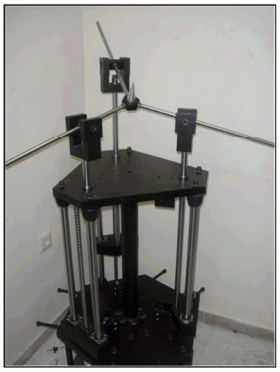

(k) 3-PSP Parallel
Manipulator

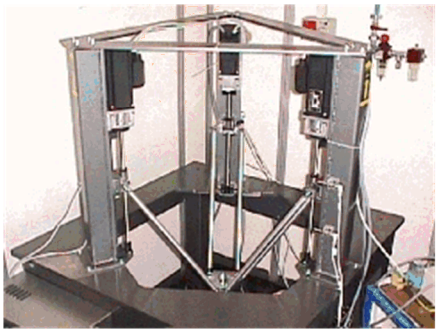

(l) the 'SLOTH' robot

Figure 1.8 Typical architectures of parallel robots

(a) Fanuc F-200i Robot

(b) M-840 HexaLight 6-Axis Positioning System

(c) M-850K Ultra-High Load Hexapod

(d) M-850K Large-Aperture High-Load Hexapod

Figure 1.9 Examples of Hexapod parallel kinematic machines

The second group includes manipulators with foot points gliding on fixed linear joints. Robots of this group differ by the number of actuated translational axes and their location with respect to each other, as well as by the type of links connecting the base and moving platforms. Typically, they have 5 or 6 degrees of freedom (HEXAGLIDE, HexaM) but there are also 3 degrees of freedom translational manipulators of this family (Orthoglide) that employ parallelogram-based links similar to Delta robots [Wiegand 1996], [Toyama 1998]. [Chablat 2003]. The robots of the second group (see Figure 1.8 h-l) are attractive for machining application because of lower moving mass compared to the hexapods and tripods. However, to ensure large workspace, such robots require large volumes to operate and occupy essential floor space.

Hence, parallel robots provide essential benefits compared to the serial ones, which promote them to high speed and high precision machining applications considered in this work. For this reason, they have already been employed in commercial machining centers (see Figure 1.7) that progressively replace conventional CNC machines based on serial Cartesian architecture. A short summary of a dedicated comparison study is given below.

Résumé. Integrated results of the above analysis are summarized in Table 1.4. They show that the CNC-machines are quite suitable for majority of machining operations provided that a large workspace and high dynamics are not required. However, for high speed machining of relatively large parts that are widely used in the aerospace and shipbuilding industries, conventional CNC-machines can be hardly used. In contrast, robotic manipulators are able to execute such tasks and simultaneously ensure higher flexibility of automated machining cells. The only problem with robots application is their rather low stiffness that leads to non-negligible position errors under the forces/torques of the technological process. Thus, the next section focuses on the robot accuracy issue.

Table 1.4 Comparison of CNC and robotic-based machining

Performance factor	Conventional XYZ CNC-machines	Robotic-based machining	
		Serial robots	Parallel robots
Workspace	Limited (by foot print)	Large (limited by link lengths)	Limited (by parallel architecture)
Flexibility	Limited number of operations	Any operation in the workspace	
Dynamics	Low	Limited	High
Accuracy	High	Depends on the stiffness, link weights and payload	
Stiffness	High	Moderate, compliance is accumulated along the chain	High, separate chain stiffness is aggregated

1.2 ROBOTS ERRORS IN MACHINING APPLICATION

In machining applications, robot accuracy depends on a numbers of factors. The most essential of them are related to manufacturing tolerances leading to geometrical parameters deviation with respect to their nominal values (geometrical errors) as well as to the end-effector deflections caused by the cutting forces and torques (compliance errors). This section gives detailed analysis of different error sources and their compensation techniques.

1.2.1 Classification of robots errors

In literature [Kevin 2000], precision of the robotic manipulator is usually described by three different performance measures: the resolution, repeatability and accuracy. The first of them, *resolution*, determines the smallest incremental move that the robot can produce. *Repeatability* is a measure of the robot's ability to move back to the same position and orientation. And finally, robot *accuracy* (that is also referred to as absolute accuracy) is defined as its ability to precisely move to a desired location in Cartesian space. For machining applications, the dynamic accuracy that describes the robot ability to follow a desired trajectory is also important. However, in the frame of this work, the main attention will be paid to the absolute accuracy that can be essentially improved using the kinetostatic models developed in the following chapters.

Following [Khalil 2002] and [Paziani 2009], the main sources of robot positioning errors can be divided in two principal groups: geometrical and non-geometrical ones. A more detailed classification is presented in Figure 1.10. It is worth mentioning that these sources may be both independent and correlated but in practice they are usually treated sequentially, assuming that they are statistically independent.

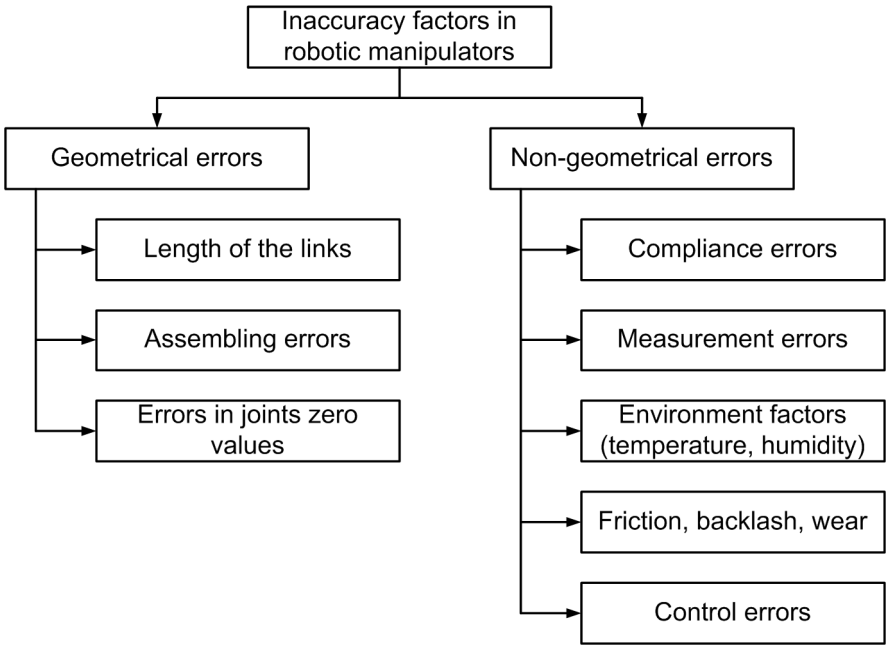

Figure 1.10 Sources of errors in robotic manipulator

Usually, in applications where the external forces/torques applied to the end-effector are relatively small, the prime source of manipulator inaccuracy are the *geometrical errors*. As reported by the number of authors [Elatta 2004], [Rolland 2003], they are responsible for about 90% of total position error. These errors are associated with differences between nominal and actual values of the link/joint parameters. Typical examples of them are the differences between the nominal and the actual lengths of links, differences between zero values of actuator coordinates in real robot and mathematical model embedded in comptroller (joint offsets); they can also be induced by non-perfect assembling of different elements and arise in shifting and/or rotation of the frames associated with different components, which normally are assumed to be matched and aligned. It is clear that the geometrical errors do not depend on the manipulator configuration, while their effect on the position accuracy depends on last one. At present, there exists a number of sophisticated calibration techniques that are able to identify differences between actual and nominal

geometrical parameters [Veitchegger 1986], [Roth 1987], [Bennett 1991], [Mirman 1992], [Khalil 2004], [Daney 2006], [Dolinsky 2007], [Hollerbach 2008]. Consequently, this type of errors can be efficiently compensated for either by adjusting the controller input (i.e. the target point coordinates) or by straightforward modification of geometrical model parameters used in the robot controller.

In some other cases, the geometrical errors may be dominated by *non-geometrical* ones that are caused by influence of a number of factors [Gong 2000], [Cui 2006], [Bogdan 2009]. For instance, the forces/torques associated with the tool-workpiece interaction in the technological process may cause essential deformations of the manipulator components (compliance errors) [Meggiolaro 2005]. Also, the environmental conditions (temperature, atmospheric pressure and others) may affect physical properties of manipulator components and lead to undesirable changes in link dimensions. It is worth mentioning that, in the regular service conditions, the *compliance errors* are the most significant ones. Their influence is particularly important for heavy robots and for manipulators with low stiffness. For example, the cutting forces/torques from the technological process may induce significant deformations, which are not negligible in the precise machining. In this case, influence of the compliance errors on the robot position accuracy can be even higher than the geometrical ones. This issue is very important for the designers of parallel manipulators, who often are looking for a compromise between the manipulator stiffness and its dynamic capabilities [Cheboxarov 2000].

Generally, the compliance errors depend on two main factors: (i) the stiffness of the robotic manipulator and (ii) loading applied to it. In additional to conventional external loading (cutting forces and torques), in some cases it is necessary to take into account influence of the link weights, the effect of the gravity compensation mechanisms, as well as preloadings in the joints introduced in order to eliminate backlash. Similar to the geometrical ones, the compliance errors highly depend on the manipulator configuration and essentially differ throughout the workspace. However, relevant modeling and compensation techniques are still under development. There are only some results which will be presented in the following sub-section [Ramesh 2000], [Dow 2004], [Bera 2011].

1.2.2 Compensation of robot errors

To increase robot accuracy, the above described errors should be compensated. The straightforward approach in robot error compensation is based on the *absolute position feedback*, which is provided by additional sensors that are able to measure the position and orientation of the end-effector with respect to the robot base coordinate frame. Its essential advantage is an ability to compensate all types of the robot errors (caused by various factors), independent of their physical nature. However, in practice, industrial robots are equipped with joint encoders only, so the end-effector absolute location is estimated via the direct kinematic transformation. The absolute measurement systems are usually considered as too expensive and non-suitable for industrial application, they are mostly used for robot calibration or laboratory experiments [Watanabe 2006]. Typically, such measurement equipment is based on stereo vision systems or laser scanners [Daney 2006] that can hardly provide desired data in common industrial environment with numerous obstacles in the neighborhood of the end-effector. Hence, for the considered application area that deals with robot-based machining of high performance materials, a dedicated error compensation technique should take into account real-life industrial constraints. In particular, it should utilize the feedback from the joint encoders only and, perhaps, from the force/torque sensors that may be integrated in the end-effector.

Under such constraints, the problem of the robot error compensation can be solved in two ways that differ in degree of modification of the robot control software:

(a) by *modification of the manipulator model* (Figure 1.11a) which better suits the real manipulator and is used by the robot controller (in a simple case, it can be limited by tuning of the nominal model, but may also involve essential model enhancement by introducing additional parameters, if it is allowed by a robot manufacturer);

(b) by *modification of the robot control program* (Figure 1.11b) that defines the prescribed trajectory in Cartesian space (here, using relevant error model, the input trajectory is generated in such way that the output trajectory coincides with the desired one).

(a) Modification of the manipulator model

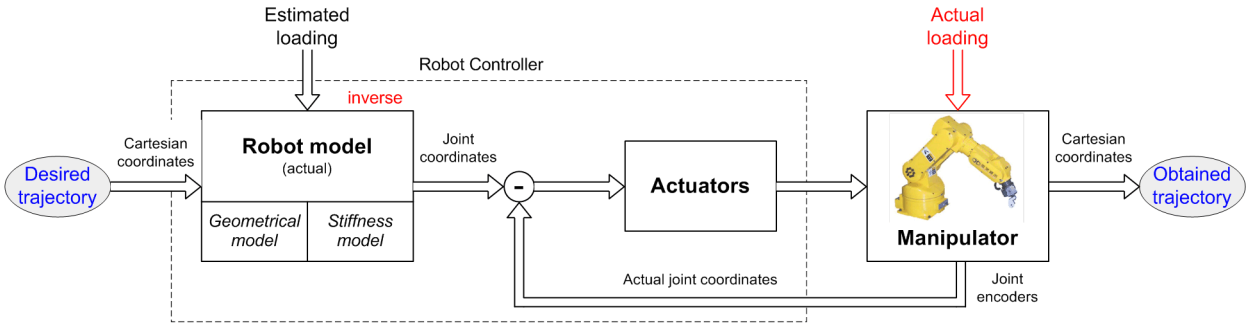

(b) Modification of the target trajectory

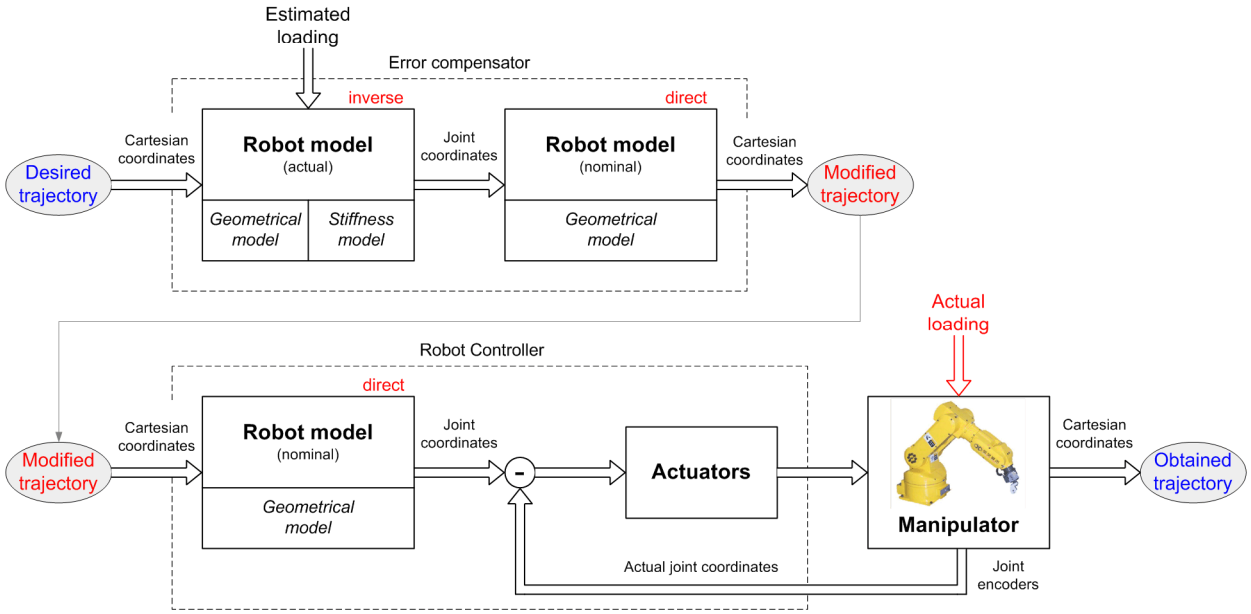

Figure 1.11 Robot error compensation methods

It is clear that the first approach can be implemented in on-line mode, while the second one requires preliminary off-line computations. It is worth mentioning that the stiffness models being developed in this work are suitable for both of these approaches. But in practice it is rather unrealistic to include the stiffness model in a commercial industrial controller where all transformations between the joint and Cartesian coordinates are based on the manipulator geometrical model. In contrast, the off-line error compensation, based on the second approach, is attractive for industrial applications.

For the *geometrical errors*, relevant compensation techniques are already well developed. Comprehensive review of related works is given in [Bernhardt 1994], [Elatta 2004], [Hollerbach 2008]. Here, if the main error sources are concentrated in the link length or in the joint offsets, the compensation is reduced to straightforward modification of the manipulator parameters in the robot controller. Otherwise, if there are any geometrical error sources that are not presented in the nominal inverse/direct kinematics, relevant modification of the controller input is required. In this case, it is possible to use (in off-line mode) either extended geometrical model with additional parameters or simply a non-linear function that describes the error distribution throughout the workspace. Examples of such a function are given in [Zhong 1996], [Lu 1997] where the neural network technique is employed. In the frame of this work, it is assumed that the geometrical errors are less essential compared to the non-geometrical ones caused by the force/torque interaction between the machining tool and workpiece. So, the main attention will be paid to the compliance errors and their compensation techniques.

For the *compliance errors*, the compensation technique must rely on two components. The first of them describes distribution of the stiffness properties throughout the workspace and is defined by the stiffness matrix as a function of the joint coordinates or the Cartesian location. The second component describes the forces/torques acting on the end-effector while the manipulator is performing its manufacturing task (it will also be referred to further as a manipulator *loading*). In this work, it is assumed that the second component is given and can be obtained either from the dedicated technological process model or by direct measurements using the force/torque sensor integrated into the end-effector. However it is necessary to take into account that the force sensors introduce additional undesirable compliance which has direct affect on the position accuracy. More detailed information concerning the force/torque computing and measurement for high speed milling of high performance materials is given in [Budak 2006], [Grote 2009], [Garant 2010].

The *stiffness matrix* required for the compliance errors compensation highly depends on the robot configuration and essentially varies throughout the workspace. Hypothetically, it can be also approximated by a neural network, similar to the geometrical error compensation mentioned above. However, this approach is not practically attractive, so it is more convenient to compute the stiffness matrix using specially developed expressions and algorithms that are described in more details in Section 1.3. This work also contributes to the stiffness matrix computation algorithms (for some particular cases, when external loading is essential and/or manipulator includes numerous passive joints).

From general point of view, full-scale compensation of the compliance errors requires essential revision of the manipulator model embedded in the robot controller. In fact, instead of a conventional geometrical model that provides inverse/direct coordinate transformations from the joint to Cartesian spaces and vice versa, here it is necessary to employ the so-called *kinetostatic model* [Su 2006]. The later defines the mapping between the joint and Cartesian spaces taking into account deflections caused by external forces/torques applied to the manipulator end-effector. It is essentially more complicated than the geometrical model and requires rather intensive computations that are discussed in Chapter 4.

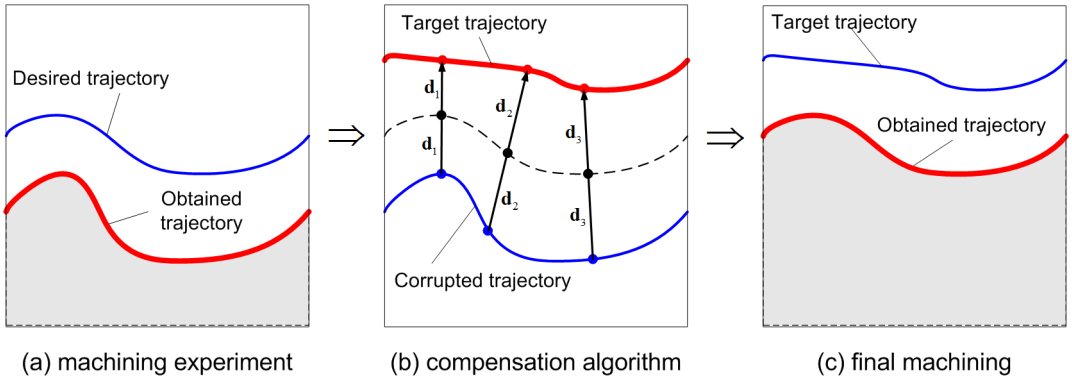

Figure 1.12 Method of symmetrical trajectory for compensation of the compliance errors

If the compliance errors are relatively small, composition of conventional geometrical model and the stiffness matrix give rather accurate approximation of the modified mapping from the joint to Cartesian space. In this case, for the first compensation scheme (see Figure 1.11a) the kinetostatic model can be easily implemented online if there is access to the control software modification. Otherwise, the second scheme (see Figure 1.11b) can be easily applied. However with regard to the robot-based machining, there is a very elegant solution that does not require force/torque measurements or computations [Seo 1998], [Depince 2006]. Its basic idea is presented in Figure 1.12, where at the first stage it is performed, the machining experiment gives a trajectory corrupted by the compliance errors. Then, the difference between the desired and the obtained trajectories is evaluated via appropriate measurements, which give the compliance errors along the path. Using this data and assuming that the stiffness model is linear, the target trajectory for the robot controller is modified by applying the "mirror" technique (where corresponding points of the corrupted and target trajectories are symmetrical with respect to the relevant points of the desired trajectory). An evident advantage of this technique is its applicability to the compensation of all types of the robot errors, including geometrical and compliance ones. However, this approach is only suitable for the large-scale production where the manufacturing task and the workpiece location remains the same. There

are also some other publications [Drouet 1998], [Meggiolaro 1998], [Meggiolaro 2004], where the problems of geometrical and compliance errors compensation are considered simultaneously but these techniques cannot be applied to robot-based machining directly.

Summarizing this section, it should be noted that, to be applied to the considered application area, the existing compliance errors compensation techniques should be essentially revised to take into account essential forces and torques associated with high speed machining of high performance materials. The next section presents the state of the art in the manipulator stiffness modeling, which is a fundamental issue for the compliance errors compensation.

1.3 STIFFNESS MODELING OF ROBOTIC MANIPULATOR

To ensure efficient compensation of the compliance errors in the robot-based machining, an appropriate stiffness model which is able to take into account both changes in manipulator configuration and influence of the external forces/torques is required. This section presents an analytical review of existing approaches in the stiffness modeling of robotic manipulators both serial and parallel architectures, with special attention to the virtual joint method providing a reasonable compromise between the model accuracy and computational efficiency. In addition, a special emphasis is given to the stiffness modeling in the loaded mode, which is essential for the considered application area.

1.3.1 Problem of stiffness modeling and existing approaches

Common approaches. Similar to general structural mechanics, the robot stiffness characterizes the manipulator resistance to the deformations caused by an external force or torque applied to the end-effector [Duffy 1996], [Angeles 2007]. Numerically, this property is usually defined through the stiffness matrix $\mathbf{K}$, which is incorporated in a linear relation between the translational/rotational displacement and static forces/torques causing this transition (assuming that all of them are small enough). The inverse of $\mathbf{K}$ is usually called the compliance matrix and is denoted as $\mathbf{k}$. As it follows from related works, for conservative systems $\mathbf{K}$ is a 6×6 semi-definite non-negative symmetrical matrix but its structure may be non-diagonal to represent the coupling between the translation and rotation [Kövecses 2007]. However, in general, for non-conservative systems and/or some special parameterizations of end-effector location, in the loaded mode the stiffness matrix may be asymmetrical[1].

In stiffness modeling of robotic manipulator, because of some specificity, there are some peculiarities in terminology. In particular, the matrix $\mathbf{K}$ is usually referred to as the "Cartesian Stiffness Matrix" $\mathbf{K}_C$ and it is distinguished from the "Joint-Space Stiffness Matrix" $\mathbf{K}_\theta$ that describes the relationship between the static forces/torques and corresponding deflections in the joints [Ciblak 1999]. Both of these stiffness matrices can be mapped to each other using the Conservative Congruency Transformation [Kao 1999], [Chen 1999], [Huang 2002], which is trivial if the external (or internal) loading is negligible. In this case, the transformation is entirely defined by the corresponding Jacobian matrix. However, if the loading is essential, it is described by a more complicated equation that includes both the Jacobian as well as the Jacobian derivatives and the loading vector [Yi 1993], [Chen 2002]. Other specific cases, where the above transformation is non-trivial (non-linear or even singular), are related to manipulators with passive joints and over-constrained parallel architectures [Pashkevich 2010]. Since this work contributes to both problems, these issues will be considered in more detail below.

In the most general sense, existing approaches to the manipulator stiffness modeling may be roughly divided into three main groups: (i) the *Finite Elements Analysis* (FEA), (ii) the *Matrix Structural Analysis* (MSA), and (iii) the *Virtual Joint Modeling method* (VJM). Their advantages and disadvantages are briefly presented below, with special emphasis to the computational complexity and accuracy.

Finite Element Analysis method (FEA). Its basic idea is to decompose the physical model of the mechanical structure on a number of rather small (finite) elements and to introduce compliant relations between adjacent nods described by relevant stiffness matrices. These finite elements have a standard shape

[1] In robotic literature, there is rather intensive discussions concerning the symmetry of the stiffness matrix in the loaded mode [Ciblak 1994], [Zafran 1996], [Pigoski 1998], [Howard 1998] [Ciblak 1998], [Chen 1999], [Chen 2000a,b], [Zafran 2002]. But in this work, due to the adopted assumptions, the stiffness matrix is certainly symmetrical.

(pyramids, cubes, etc.) for which the stiffness matrix can be computed analytically. Using this discretization, the static equilibrium equations for each node are derived, and they are aggregated in a global matrix expression defining relations between the applied force/torque and node deflections. Then, the obtained matrix of rather large size is inverted and is used to obtain the desired stiffness matrix by simple extraction of proper elements. In the modern CAD-environment, the above process is highly automated and is integrated with 3D-modeling of mechanical structures and mechanisms. In particular, the decomposition into a set of finite elements (so called meshing) usually needs definition of the discretization step and the mesh type only. The latter can be either linear or parabolic, which correspond to pyramids with 4 and 10 nodes respectively (with either 6 or 12 compliance relations). Then (for this finite element model), the CAD-based tools provides both numerical data and convenient visualization defining the deflections vectors for each nodes and potential dangerous areas with high stresses.

An evident advantage of the FEA-modeling is its high accuracy that is limited by the discretization step only. For robotic application it is very attractive, since the links/joints are modeled with its true dimension and shape [Corradini 2004] [Bouzgarrou 2004], [Akin 2005]. However, while increasing of the number of finite elements, the problem of limited computer memory and the difficulty of the high-dimension matrix inversion become more and more critical. Besides the high computational efforts, this matrix inversion generates numerous accumulative round-off errors, which reduce accuracy. In robotics, this causes rather high computational expenses for the repeated re-meshing and re-computing, so in this area the FEA method is usually applied at the final design stage only [El-Khasawneh 1999], [Long 2003], [Corradini 2004], [Rizk 2006]. Nevertheless, in this work this method is applied for the links stiffness matrix identification that is further used in the frame of the VJM technique. Such combination allows us to use the advantages of the FEA while avoiding intensive computations for different manipulator configurations.

Matrix Structural Analysis method (MSA). This method incorporates the main ideas of the FEA but operates with rather large compliant elements such as beams, arcs, cables, etc. [Martin 1996]. This obviously leads to the reduction of the computational expenses and, in some cases, allows us to obtain an analytical stiffness matrix for the specific task. Similar to the FEA-modeling the MSA method gives forces/torques and displacements for each node, but here it has a clear physical interpretation (manipulator active or passive joint), which can be useful for some tasks [Nagai 2008]. For parallel robots, this method has been developed in works [Deblaise 2006a], [Deblaise 2006b], where a general technique for stiffness modeling of the manipulator with rigid/flexible links and passive joints was proposed. It has been illustrated by stiffness analysis of parallel manipulator of Delta architecture where the links were approximated by regular beams. The latter causes some doubts in the model accuracy compared to the combination of the FEA and VJM techniques that are being developed here. Besides, this result was obtained under the assumption that the external forces/torques are relatively small (i.e. for the unloaded mode), and it is unlikely that such approach can be enhanced to take into account particularities of manipulator behavior in loaded mode. In addition, here there exists a problem of the stiffness matrix computation for the manipulator singular configurations.

From a computational point of view, the MSA method is less complicated than the FEA-based one. In spite of the fact that the MSA still involves matrix operations of rather high-dimension, it gives a reasonable trade-off between the accuracy and computational time, provided that links approximations by the beam elements are realistic. It should be also noted that, in their general formulations, the FEA and MSA methods are closed: both of them interpret physical system as a set of nodes with mutual flexible connections. The main difference is that the MSA operates with true physical objects (like beams, arcs and others), while the FEA decomposes them into small finite elements. So, the MSA can be treated as a special case of the FEA that has already found its application in robotics.

From the other side, if each link is applied to the FEA-based stiffness matrix identification technique developed below (see Chapter 2), an advanced combination of the MSA and FEA that is suitable for the stiffness modeling of arbitrary parallel manipulators (with numerous internal loops) can be obtained. However, it is out of the scope of this work because of the above mentioned critical limitation, which makes the method applicable to the case of the unloaded mode only.

Virtual Joint Modeling method (VJM). The core of this method is an extension of the conventional rigid-body model of the robotic manipulator, where the links are treated as rigid but the joints are assumed to

be compliant (in order to accumulate all types of existing flexibilities in the joints only). Geometrically, such approximation is equivalent to adding to the joints some auxiliary virtual joints (with embedded virtual springs). It is obvious that such lumped presentation of the manipulator stiffness (that in reality is distributed) essentially simplifies the model. So, at present it is the most popular stiffness analysis method in robotics. This method was first introduced by Salisbury [Salisbury 1980] and Gosselin [Gosselin 1990], who assumed that the main flexibility sources were concentrated in the actuator joints. The derived expression defining relation between the joint and Cartesian stiffness matrices (Conservative Congruency Transformation) became a basis for the manipulator stiffness analysis in many research works. Later, these results have been further developed in order to take into account some specific geometrical constrains [Yi 1993], [Quennouelle 2009a] and external loading [Alici 2005], [Chen 2002]. Nevertheless, external loading is assumed small enough to detect any non-linear effects discovered in this work. Due to its computational simplicity, the VJM method has also been successfully applied to the analytical stiffness analysis of a translational parallel manipulator [Majou 2007].

A key issue of this method is how to define the virtual spring parameters. At the beginning, it was assumed that each actuated joint is presented by a single one-dimensional virtual spring [Pigoski 1998], [Zhang 2000], [Gosselin 2002]. Further, to take into account the links flexibilities, the number of virtual joints was increased and in each actual actuated or passive joint several translational and rotational virtual springs were included [Majou 2004]. The latest developments in this area operate with 6-dimensinal virtual springs identified using the FEA-based method [Pashkevich 2010]. This leads to essential increasing of the VJM method accuracy that becomes comparable with the accuracy of the FEA-based techniques, but with much lower computational expenses.

The only essential disadvantage of the VJM method is related to some difficulty in stiffness modeling of parallel manipulators. While for strictly parallel architectures, where there are only serial chains between the base and moving platforms, for architectures with internal loops (or with parallelogram-based links) the VJM-base stiffness analysis is rather complicated. Nevertheless, taking into account all advantages and disadvantages of the FEA, the MSA and the VJM techniques, this work give preference to the VJM method that is presented in more details in the next sub-section.

Computational complexity. The main benchmark that allows us to evaluate the computational complexity of the above described methods is related to the computational efforts required for the matrix inversions inside of the corresponding algorithms. Generally, for the matrix inversion of size $n \times n$, it can be defined as $O(n^3)$ [Lin 2009].

For the FEA method n depends on the discretization step and the type of finite elements used. As it follows from a relevant study, in the case of the parabolic mesh (10 nodes and 12 connections per a finite element) the value of n can be approximately computed as $n = 30\nu n_L$, where n_L is the number of manipulator links, ν is the number of finite elements per link (it should be about 10^3 to ensure desired precision). For the MSA method, the upper bound of the above matrix size $n = 12n_d$ can be computed via the node number n_d. Finally, for the VJM method, the size of the matrix to be inverted is $n = 6 + n_q$, where n_q is total number of the degrees of freedom in the passive joints.

Using these formulas, it was estimated the stiffness model complexity for three types of manipulators (Stewart platform, Delta, Orthoglide). Relevant results are presented in Table 1.5. As it follows from them, the VJM method essentially overcomes FEA and MSA, so it will be used in this work as a preferable one. It is presented in more details below.

Table 1.5 Computational complexity of existing stiffness modeling methods

Stiffness modeling method	Manipulator architecture		
	Stewart Platform	Delta	Orthoglide
FEA	$\sim 10^{16}$	$\sim 10^{17}$	$\sim 10^{17}$
MSA	$\sim 10^{6}$	$\sim 10^{8}$	$\sim 10^{7}$
VJM	$\sim 10^{3}$	$\sim 10^{3}$	$\sim 10^{3}$

1.3.2 Virtual Joint Method in stiffness modeling of robots

Since the VJM-based method is proved to be more computationally efficient while providing acceptable accuracy, let us consider it in more details. Taking into account some specificities of the considered application area, the main attention will be paid to the VJM applicability to the stiffness modeling of parallel manipulators (both under-constrained and over-constrained), considering the impact of the passive joint, evaluating the influence of the external and internal forces/torques as well as accuracy improvement of the stiffness model.

VJM method background. In the frame of this method, all types of compliance existing in a real manipulator (both distributed and lumped) are replaced by localized virtual springs located in its joints. Then, for this mechanism consisting of rigid links and compliance joints, the static equilibrium equations is derived and linearized in order to obtain Cartesian stiffness matrix, which in a general case depends on the manipulator posture (configuration). Usually it is assumed that the elastic deflections in virtual springs are relatively small and linearization is performed in the neighborhood of the equilibrium configuration corresponding to zero forces and torques (unloaded mode).

This technique originates from the work of Salisbury [Salisbury 1980] who derived a closed-form expression for the Cartesian stiffness matrix of a serial manipulator assuming that the mechanical elasticity is concentrated in the actuated joints. The basic equations have been written as it follows

$$\delta\mathbf{t} = \mathbf{J}_\theta \cdot \delta\boldsymbol{\theta}; \qquad \boldsymbol{\tau} = \mathbf{J}_\theta^{\mathrm{T}} \cdot \mathbf{F}; \qquad \boldsymbol{\tau} = \mathbf{K}_\theta \cdot \delta\boldsymbol{\theta}; \tag{1.5}$$

where $\delta\mathbf{t}$ denotes the end-effector displacement in Cartesian space (both positional and orientational), $\mathbf{F}$ is the vector of the external loading applied to the end-effector (that includes both the force and the torque components), $\delta\boldsymbol{\theta}$ is the deflection in the virtual joint coordinates $\boldsymbol{\theta}$ caused by this loading, $\boldsymbol{\tau}$ is the vector of reactions in the elastic joints, $\mathbf{K}_\theta$ is the corresponding joint stiffness matrix, $\mathbf{J}_\theta$ is the Jacobian matrix computed with respect to the elastic joints. Here, the first equation is derived from the manipulator geometrical model, the second one describes the static equilibrium condition (assuming that the load is not essential), and the third equation presents the linear elasticity relation (Hooke's law).

After relevant transformations of (1.5), the desired linear relation between the external loading $\mathbf{F}$ and the end-effector displacement $\delta\mathbf{t}$ is presented as

$$\delta\mathbf{t} = \left(\mathbf{J}_\theta \cdot \mathbf{K}_\theta^{-1} \cdot \mathbf{J}_\theta^{\mathrm{T}}\right) \cdot \mathbf{F}, \tag{1.6}$$

which gives Cartesian stiffness matrix

$$\mathbf{K}_\mathrm{C} = \mathbf{J}_\theta^{-\mathrm{T}} \cdot \mathbf{K}_\theta \cdot \mathbf{J}_\theta^{-1} \tag{1.7}$$

In literature [Li 2001], [Chen 2000a,b], the latter may be also presented in a slightly different form

$$\mathbf{K}_\theta = \mathbf{J}_\theta \cdot \mathbf{K}_\mathrm{C} \cdot \mathbf{J}_\theta^{\mathrm{T}} \tag{1.8}$$

which sometimes is referred to as Conservative Congruency Transformation (CCT), to emphasize that it describes mapping from the joint stiffness to Cartesian one, and vice versa.

In further works, similar equations were obtained for parallel manipulators assuming that they are not over-constrained and the elasticity is concentrated in the actuator joints while the passive joints are perfect [Gosselin 1990]. Other contributions to this area include [Ciblak 1994, 1999], [Ciblak 1998], [Pigoski 1998], [Zhang 2004], [Xi 2004], [Zhang 2002], [Company 2005], [Pashkevich 2010], where the VJM method was partially extended. It is also worth mentioning the works where the VJM technique was applied to particular manipulators, in particular to the CaPAMan, Orthoglide and H4 robots, Stewart–Gough platforms, etc. [Corradini 2002], [Company 2002], [Arumugan 2004], [Abele 2007], [Majou 2007], [Vertechy 2007], [Tyapin 2009].

VJM model parameters. In the first works, it was explicitly assumed that the main sources of elasticity are concentrated in actuated joints. Correspondingly, the links were assumed to be rigid and the VJM model included one-dimensional springs only. In other recent works, compliance of the links has been taken into account by introducing additional virtual joints describing their longitudinal elasticity

[Gosselin 2002] or stiffness properties in several directions [Mayou 2007]. Recent development in this area use 6-dimensional virtual joints to describe elasticity of each link [Li 2008].

At the beginning, the *stiffness parameters* of the virtual joints describing the link elasticity (and incorporated in the matrix $\mathbf{K}_\theta$) were evaluated rather roughly, using a simplified representation of the link shape by regular beams. Besides, it was assumed that all linear and angular deflections (compression/tension, bending, torsion) are decoupled and are presented by independent one-dimensional springs that produce a diagonal stiffness matrix of size 6×6 for each link. Afterwards, this elasticity model was enhanced by using complete 6×6 non-diagonal stiffness matrix of the cantilever beam [Li 2008]. This allowed taking into account all types of the translational/rotational compliance and relevant coupling between different deflections. Other enhancements include the link approximation by several beams, but it gives rather modest improvement in accuracy.

Further advance in this direction (applicable to the links of complicated shape) led to the *FEA-based identification technique* that involves virtual loading experiments in CAD environment and stiffness matrix estimation using dedicated numerical routines [Pashkevich 2010]. The latter essentially increased accuracy of the VJM-modeling while preserving its high computational efficiency. It is worth mentioning that usual high computational expenses of the FEA is not a critical issue here, because it is applied only once for each link (in contrast to the straightforward the FEA-modeling for the entire manipulator, which requires complete re-computing for each manipulator posture). As a result, this approach allowed the authors to integrate accuracy of the FEA-modeling into the VJM-modeling technique that provides high computational efficiency. General methodology of this hybrid approach is presented in Figure 1.13.

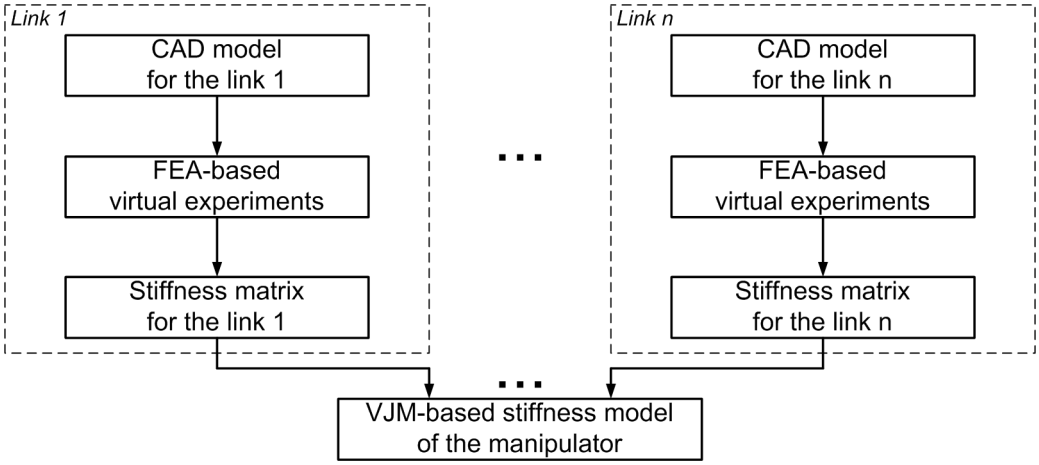

Figure 1.13 Integration of VJM modeling approach with FEA-based identification technique of the stiffness model parameters

However, in spite of good results obtained for some case studies, there are still a number of open questions in the FEA-based identification technique. They include optimal setting of the virtual experiment (i.e. definition of the mesh parameters, the joint contact surfaces to apply forces, etc.) and enhancement of numerical algorithms used for computation of the stiffness matrix elements (increasing robustness with respect to FEA-modeling errors, distinguishing zero elements from small ones, etc.). These issues have never been given proper attention in previous works and will be in the focus of Chapter 2.

VJM model for manipulators with passive joints. Another important issue is related to taking into account influence of the *passive joints,* which are widely used in parallel manipulators. In the simplest case, when the geometrical constraints imposed by the manipulator assembly are not redundant, the passive joint coordinates may be just eliminated from the kinematic model, allowing us direct application of the Salisbury formula. However, in the case of over-constrained or under-constrained manipulators, the elimination technique cannot be used directly.

For *serial kinematic chains* with passive joints, the problem has been solved for the general case [Pashkevich 2008]. In particular, it was proposed an algorithmic solution that extends the Salisbury formula and is able to produce the rank-deficient stiffness matrices describing “zero-resistance” of the end-effector to

certain types of displacements, which do not require deflections in the virtual springs (due to presence of passive joints and/or kinematic singularity of the examined posture). The relevant technique involves inversion of dedicated square matrix of size $(n_\theta + 6)\times(n_\theta + 6)$, which is composed of the links stiffness matrices, and kinematic Jacobians of both virtual springs and passive joints (here n_θ is the number of passive joints). Then, the desired Cartesian stiffness matrix is obtained by simple extraction of an appropriate 6×6 sub-matrix from the computed inverse. Corresponding expression for stiffness matrix computation can be presented as

$$\begin{bmatrix} \mathbf{K}_\mathrm{C} & * \\ * & * \end{bmatrix} = \begin{bmatrix} \mathbf{J}_\theta \mathbf{K}_\theta^{-1} \mathbf{J}_\theta^\mathrm{T} & \mathbf{J}_\mathrm{q} \\ \mathbf{J}_\mathrm{q}^\mathrm{T} & \mathbf{0} \end{bmatrix}^{-1} \tag{1.9}$$

where $\mathbf{J}_\theta$ is Jacobian related to the virtual springs ($6\times n_\theta$), $\mathbf{J}_\mathrm{q}$ is Jacobian related to the passive joints ($6\times n_\mathrm{q}$). The main advantage of this method is its computational simplicity, since the number of the virtual springs do not influence on the size of the matrix to be inverted. Besides, the method does not require manual elimination of the redundant spring corresponding to the passive joints, since this operation is inherently included in the numerical algorithm.

However, for *parallel manipulators* with passive joints, solutions were obtained for less general cases. They include "pure" parallel architectures where the base and the end platform are connected by strictly serial kinematic chains. Here, the total stiffness matrix can be presented as the sum of partial matrices corresponding to separate chains (computed using the above described technique)

$$\mathbf{K}_C = \sum_i \mathbf{K}_\mathrm{C}^{(i)}; \qquad \begin{bmatrix} \mathbf{K}_\mathrm{C}^{(i)} & * \\ * & * \end{bmatrix} = \begin{bmatrix} \mathbf{J}_{\theta i} \mathbf{K}_{\theta i}^{-1} \mathbf{J}_{\theta i}^T & \mathbf{J}_{\mathrm{q}i} \\ \mathbf{J}_{\mathrm{q}i}^\mathrm{T} & \mathbf{0} \end{bmatrix}^{-1} \tag{1.10}$$

so the passive joints are taken into account easily. Besides, in this case the over-constraining of the mechanism does not create additional difficulties. For instance, for the *over-constrained* manipulator of Orthoglide family [Chablat 2003], each of the parallel chains yields the stiffness matrix of rank 4 while their aggregation gives the matrix of full rank 6. But if there exists a cross-linking between the parallel chains (like in kinematic parallelograms, for instance), this method can not be applied directly. For this case, some interesting results are presented in [Quennouelle 2008b, 2008c, 2009a] where the geometrical constraints were treated in a general way but detailed computational techniques were not developed.

VJM modeling of parallel manipulators. In spite of the fact that the VJM technique has been originally developed for serial manipulators, it can be efficiently applied to parallel robots. The basic idea here is to obtain first the stiffness models of each kinematic chain separately, and after, to integrate them in a united model corresponding to the parallel manipulator. This idea was partially implemented in [Xi 2004], [Pashkevich 2010], where the manipulator structure was assumed to be strictly parallel (i.e. without internal loops) and the kinematic chains where assembled in the same end-point.

Under such assumptions, the stiffness matrix of the parallel manipulator can be computed via straightforward summation of the chain stiffness matrices

$$\mathbf{K}_\mathrm{C} = \sum_{i=1}^{n} \mathbf{K}_\mathrm{C}^{(i)} \tag{1.11}$$

where the index *i* defines the kinematic chains and *n* is the total number of chains. However, in more general (and practically important) cases where the kinematic chains are connected to different points of the end-platform, this formula cannot be applied directly. Besides, for parallel manipulators with parallelogram-based links, some essential modifications are required.

Other limitation of the existing results devoted to the parallel manipulators is related to the assumption that the assembling does not produce any internal stresses. But in practice, numerous errors are accumulated in serial chains [Rizk 2007] and they cause non-negligible internal forces in manipulator joints (even if the external force applied to the end-effector is equal to zero). The internal forces may essentially change the manipulator behavior (modify the stiffness matrix, change the end-effector location, etc.) and should be obviously taken into account in the stiffness model. However, existing works ignore this issue. Another

research issue is associated with stiffness modeling of parallel manipulators under loading, which has not received proper attention yet.

1.3.3 Stiffness modeling under external and internal loadings

Manipulator stiffness modeling in the loaded mode is a relatively new research area, which is worth to be considered separately. This subsection presents analysis of related works and defines some important research problems that will be in the focus of this work. Some of them are based on the analogy that can be established between robotics and structural mechanics (it concerns buckling phenomena, for instance).

Types of loadings. Manipulator loading may be of different nature. For the stiffness modeling, it is reasonable to distinguish two main types of loading, external and internal ones. The *external loading* is caused mainly by an interaction between the robot end-effector and the workpiece, which is processed or transported in the considered technological process [Alici 2005], [Chen 2000a]. Another type of external loading exists due to the gravity influence on the manipulator links, for many heavy manipulators employed in machining the link weight is not negligible [Yi 1992], [Yi 1993]. Besides, to compensate in a certain degree the gravity influence, some manipulators include special mechanisms generating external forces/torques in the opposite direction. It is worth mentioning that the external loading generated by a technological process is always applied to the manipulator end-effector while others may be applied at intermediate points (at joints, for instance). Besides, the external loadings caused by gravity have obvious distributed nature.

In addition to the above mentioned forces/torques, *internal loading* in some joints may exists. For instance, to eliminate backlash, the joints may include preloaded springs, which generate the force or torque even in standard "mechanical zero" configuration [Wei 2010]. Though the internal forces/torques do not influence on the global equilibrium equations, they may change the equilibrium configuration and have influence on the manipulator stiffness properties. For this reason, internal preloading is used sometimes to improve the manipulator stiffness, especially in the neighborhood of kinematic singularities. Another case where the internal loading exists by default, is related to over-constrained manipulators that are subject of the so-called antagonistic actuating [Chakarov 1999], [Chakarov 2004]. Here, redundant actuators generate internal forces and torques that are equilibrated in the frame of close loops.

It is obvious that the both external and internal loadings influence on the manipulator equilibrium configuration and, consequently, may modify the stiffness properties. So, they must undoubtedly be taken into account while developing the stiffness model.

VJM model for the loaded mode. At present, in most of related works the stiffness is evaluated in a quasi-static configuration with no external or internal loading. There is a very limited number of publications that directly address the loaded mode case (or so-called case of “large deflections”), where in addition to the conventional “*elastic stiffness*” in the joints it is necessary to take into account the “*geometrical stiffness*” arising due to the change in the manipulator configuration under the load. Although the existence of this additional stiffness component for elastic structures has been known for a long time [Przemieniecki 1968], the importance of this problem for robotic manipulators has been highlighted rather recently. The most essential results in this area were obtained in [Alici 2005], [Chen 2002], [Li 2002a] where there are presented both some theoretical issues and several case studies for serial and parallel manipulators. Several authors [Chakarov 1999], [Chakarov 2004], [Wei 2010] addressed the problem of stiffness analysis for the manipulators with internal preloading or antagonistic actuating, but in relevant equations some of the second order kinematic derivates were neglected. Using notation adopted in this work and summarizing existing results [Alici 2005], [Chen 2002], [Merlet 2008], the manipulator stiffness matrix for the loaded can be expressed as follows

$$\mathbf{K}_{\mathrm{C}} = \mathbf{J}_{\theta}^{-\mathrm{T}} \left(\mathbf{K}_{\theta} - \mathbf{K}_{\mathrm{F}} \right) \mathbf{J}_{\theta}^{-1} \tag{1.12}$$

where $\mathbf{K}_{\mathrm{F}}$ is $n_{\theta} \times n_{\theta}$ stiffness matrix that is induced by external loading and is not presented in previous equation (1.7). This matrix depends on both the derivatives of the Jacobian $\mathbf{J}_{\theta}$ and the loading vector $\mathbf{F}$. Required details concerning computing of $\mathbf{K}_{\mathrm{F}}$ are given in [Chen 2002].

In the frame of the same concept, the manipulator stiffness model for the loaded mode was proposed in [Yi 1992], [Yi 1993], where numerous factors were taken into account (conventional external loading, gravity forces, antagonistic redundant actuation, etc.). The final results for the stiffness matrix is presented as

$$\mathbf{K}_C = \mathbf{J}_\theta^{-T}\, \mathbf{K}_u\, \mathbf{J}_\theta^{-1} \tag{1.13}$$

where $\mathbf{K}_u$ is a solution of a non-linear matrix equation, which includes the joint stiffness and the external/internal loadings as parameters. However, this approach is rather hard from computational point of view. Besides, in this work the Jacobians and all their derivatives have been computed not in a "true" equilibrium configuration (it was unreasonably replaced by unloaded one). For this reason, since the equilibrium obviously depends on the loading magnitude, some essential issues were omitted. As a result, any nonlinear effects have been detected in the stiffness behavior of the examined manipulators.

Another significant result, which should be mentioned here, is related to the stiffness modeling of the parallel manipulators with the cross-linkage. Firstly this problem was considered in [Yi 1992], [Yi 1993] where all coordinates where decomposed into two groups (dependent and independent ones). But no clear rule for such coordinate splitting has been proposed, besides the developed technique involved very non-trivial computations. Further, the cross-linkage was in the focus of [Quennouelle 2008a], [Quennouelle 2008c] where a rather compact expression for the stiffness matrix has been proposed

$$\mathbf{K}_C = \mathbf{J}_\theta^{-T} \left(\mathbf{K}_\theta - \mathbf{K}_F + \mathbf{K}_I \right) \mathbf{J}_\theta^{-1} \tag{1.14}$$

which, compared to (1.12), includes additional matrix $\mathbf{K}_I$ that is induced by the geometrical constraints (cross-linkage). However, there are still a number of open questions concerning the coordinate splitting rule (i.e. dividing them into dependent and independent ones) and computing of the equilibrium configuration corresponding to the applied loading.

It should be noted that this problem of (computing the loaded equilibrium) has been omitted in most of the related works. At the same time, it is clear that the changes in the manipulator configuration directly influence the Jacobians (and their derivatives) as well as on the end-effector location. For this reason, computing the Jacobians and Hessians in a traditional way (i.e. for the unloaded configuration) may lead to excessively rough simplification of the stiffness model. In particular, some non-linear phenomena in manipulator stiffness behavior can be hardly detected, while they should obviously exist from the point of view general theory of elastic structures.

Nonlinear-behavior of the manipulator under loading. In mechanics, it has been known since a long time that the elastic structures may suddenly change their configuration if the loading exceed some critical value. A classical example is the so-called Euler column that retains its straight shape until the loading (Figure 1.14) [www civildb], [www highline]. This effect (buckling) is well known in structural mechaniques, however in robotics this aspect has never been studied before.

Figure 1.14 Examples of buckling in column [www civildb], [www highline]

Non-linear behavior of force-deflection relation and possible buckling effects have been known since a long time. However in robotics, these questions did not attract much attention, mainly due to high rigidity of commercially available robots. But current trends in mechanical design of manipulators that are targeted at essential reduction of moving masses motivate relaxing this assumption. Hence, non-linear stiffness analysis is also important for the robotic manipulator. As it was mentioned before, existing stiffness analysis techniques for robots are strictly assumed that loading cannot change configurations of an examined manipulator or these changes are negligible. This simplification imposes crucial limitations for the stiffness analysis and, as a result, does not allow us to detect buckling and other non-linear phenomena known from general theory of elastic structures.

Similar to the classical mechanics three types of buckling can appear in a robotic system: buckling of the link, contact buckling and geometrical buckling. First type of buckling is defined by the mechanical properties of the link and easily can be detected by FEA analysis or critical loading for it can be computed via approximated equations. Normally these loadings are unreachable in robots, while minimization of the link cross-sections can make these limits reachable. Thus it is reasonable to check critical loads for the buckling of elements on the design step. The second type of buckling is caused by the contact of the links with environment. It can be avoided on the machining process designing stage. The nature of the geometrical buckling is closed to the buckling of the elements, while several elements should be analysed together. In this case the critical force is defined by the stiffness of the links and junctions between them. Since stiffness of the junction may be lower than stiffness of links, or even in parallel manipulators can be negligible (for the passive joints), the critical force can be reduced in times comparing with the critical loading of the separate elements. So, nonlinear effects and buckling can appear in robots and they require additional analysis, however these questions have been omitted before.

In practice, it is impossible to detect non-linear effect without finding the *loaded equilibrium,* while this question was omitted in previous works. Besides, the loading may potentially lead to multiple equilibriums, to bifurcations of the equilibriums and to static instability of the manipulator configurations. These effects are essentialy dangerous for parallel manipulators wich impose numerious passive joints. Some aspects of multiple-equilibrium problem for robotic manipulators have been examined in the works [Hines 1998], [Carricato 2002] who applied the Catastrophe theory for the stability analysis of the planar parallel manipulators with several flexural elements under external loading. However, they did not propose a general approach for stability analysis of the manipulator configurations. Therefore, it will be also in the focus of this research.

Summary of the VJM-based results. The above mentioned publications are briefly summarized in Table 1.6, where all notations are adopted to those used in this work. As it follows from their analysis, the stiffness modeling in loaded mode for both serial and parallel manipulators with passive joints needs further improvement. In particular, it is required to develop dedicated numerical techniques that are well adopted for robotic applications and provide a designer with capability of computing the loaded equilibriums (which may be non-unique), their stability analysis, local linearization of the force-deflection relation, and also evaluation of possible non-linear phenomena (such as buckling) that can be potentially dangerous in practical applications. This motivates the enhancement of previous results [Pashkevich 2010] and extending them for the case of the external and internal loadings.

Table 1.6 Summary of the related works and expressions for the Cartesian stiffness matrix

Publications	Model & assumptions	Stiffness matrix
Salisbury [Salisbury 1980]	Serial manipulator, elasticity in actuators	$\mathbf{K}_{\mathrm{C}} = \mathbf{J}_{\theta}^{-\mathrm{T}}\, \mathbf{K}_{\theta}\, \mathbf{J}_{\theta}^{-1}$
Gosselin [Gosselin 1990], Ciblak & Lipkin [Ciblak 1998], [Ciblak 1999], Pigoski et al., [Pigoski 1998]	Parallel manipulator, elasticity in actuators, non over-constrained	$\mathbf{K}_{\mathrm{C}} = \mathbf{J}_{\theta}^{-\mathrm{T}}\, \mathbf{K}_{\theta}\, \mathbf{J}_{\theta}^{-1}$
Zhang et al. [Zhang 2004], [Xi 2004]	Serial kinematic chain without passive joints, elasticity in virtual joints	$\mathbf{K}_{\mathrm{C}} = \left(\sum_i \mathbf{J}_{\theta i}\, \mathbf{K}_{\theta i}^{-1}\, \mathbf{J}_{\theta i}^{\mathrm{T}} \right)^{-1}$
Pashkevich et al. [Pashkevich 2010]	Serial kinematic chain with passive joints, elasticity in virtual joints	$\begin{bmatrix} \mathbf{K}_{\mathrm{C}} & * \\ * & * \end{bmatrix} = \begin{bmatrix} \mathbf{J}_{\theta} \mathbf{K}_{\theta}^{-1} \mathbf{J}_{\theta}^{\mathrm{T}} & \mathbf{J}_{\mathrm{q}} \\ \mathbf{J}_{\mathrm{q}}^{\mathrm{T}} & \mathbf{0} \end{bmatrix}^{-1}$
Zhang & Gosselin [Zhang 2002]	Parallel manipulator without cross-linking between kinematic chains	$\mathbf{K}_{\mathrm{C}} = \sum_i \mathbf{K}_{\mathrm{C}}^{(i)};\quad \mathbf{K}_{\mathrm{C}}^{(i)} = \left(\sum_j \mathbf{J}_{\theta j}\, \mathbf{K}_{\theta j}^{-1}\, \mathbf{J}_{\theta j}^{\mathrm{T}} \right)^{-1}$
Pashkevich et al., [Pashkevich 2010]	Parallel manipulator without cross-linking between kinematic chains	$\mathbf{K}_{C} = \sum_i \mathbf{K}_{\mathrm{C}}^{(i)};$ $\begin{bmatrix} \mathbf{K}_{\mathrm{C}}^{(i)} & * \\ * & * \end{bmatrix} = \begin{bmatrix} \mathbf{J}_{\theta i} \mathbf{K}_{\theta i}^{-1} \mathbf{J}_{\theta i}^{T} & \mathbf{J}_{\mathrm{q}i} \\ \mathbf{J}_{\mathrm{q}i}^{\mathrm{T}} & \mathbf{0} \end{bmatrix}^{-1}$
Alici & Shirinzadeh [Alici 2005] Chen & Kao [Chen 2000a] Marlet & Gosselin [Merlet 2008]	Serial or parallel manipulator with external loading (non over-constrained)	$\mathbf{K}_{\mathrm{C}} = \mathbf{J}_{\theta}^{-\mathrm{T}} \left(\mathbf{K}_{\theta} - \mathbf{K}_{\mathrm{F}} \right) \mathbf{J}_{\theta}^{-1}$
Quennouelle & Gosselin [Quennouelle 2008a], [Quennouelle 2008c]	Parallel manipulator with external loading and supplementary geometric constraints (cross-linkings)	$\mathbf{K}_{\mathrm{C}} = \mathbf{J}_{\theta}^{-\mathrm{T}} \left(\mathbf{K}_{\theta} - \mathbf{K}_{\mathrm{F}} + \mathbf{K}_{\mathrm{I}} \right) \mathbf{J}_{\theta}^{-1}$
Yi & Freeman [Yi 1992], [Yi 1993]	Parallel manipulator with external loading, inertia and gravity loads, joint stiffness, actuation redundancy	$\mathbf{K}_{\mathrm{C}} = \mathbf{J}_{\theta}^{-\mathrm{T}}\, \mathbf{K}_{\mathrm{u}}\, \mathbf{J}_{\theta}^{-1}$ $\mathbf{K}_{\mathrm{u}}$ - solution of non-linear matrix equation that includes joint stiffness and external/internal loadings as parameters

1.4 SUMMARY: THESIS GOAL AND RELATED PROBLEMS

As it follows from the presented review, the problem of stiffness analysis is very important for the robotic-based machining of high performance materials that are characterized by high loadings, which produce significant compliance errors. Besides, spesificity of serial and parallel robots is required to take into account influence of passive joints and different types of loading. Therefore, to evaluate errors and/or compensate them an accurate stiffness model of the manipulator with passive joints and different types of loading is required. However, existing stiffness modeling approaches substantially consider linear models.

Performed comparison analysis of existing stiffness modeling methods illustrated that for a considered problem the VJM-based approach is more attractive, however it still required essential enhancements. Existing approaches of the VJM methods are computationally attractive, provide some results for the stiffness modeling in the loaded mode, but they are still based on the linear models and, consequently, are not able to detect any non-linear effects in the stiffness behavior of manipulator under high loading (buckling for instance). Besides, current approaches still use crude approximations of manipulator links, which is not able to take into account real shape of links and contact surfaces of the adjacent ones. In addition, existing approaches are implicitly assumed that there are no internal forces in close kinematic chains, gravity forces are neglected both for serial and parallel manipulators and it is supposed that all components of the robot are perfect. Hence, in order to obtain a non-linear stiffness model of robots with passive joints, these limitations should be withdrawn.

For comparison, other methods have more essential limitations that do not allow us to consider all defined stiffness modeling aspects simultaniously.For instance, the FEA seems to be accurate but it is time consuming and is not suitable for non-linear stiffness analysis. Moreover, there is no general technique to define active and passive joints in the CAD model, which lead to some difficulties and indeterminacy of their definitions. The MSA method is less time consuming but still is not applicable for non-linear stiffness analysis and deals with crude approximations of the manipulator links. Besides, it has some difficulties of integration with CAD model. Howerever, in order to increase accuracy of the VJM model parameters, some ideas from the FEA modeling can be successfully used.

Hence, the goal of this thesis is ***enhancement of stiffness modeling techniques for serial and parallel manipulators in order to increase the accuracy and efficiency of robotic-based machining of high performance materials by means of compensation of the compliance errors***. To achieve this goal, several problems have to be solved:

Problem 1: Accuracy improvement of stiffness matrices used in the VJM model (taking into account complex shape of manipulator links, coupling between rotational/translational deflections and joint particularities);

Problem 2: Enhancement of VJM-based stiffness modeling technique for serial and parallel manipulators with arbitrary location of passive joints in the case of small deflections (unloaded mode);

Problem 3: Extension of the proposed VJM-based technique for the case of large deflections caused by internal and external loadings, taking into account related changes in Jacobians and equilibrium coordinates;

Problem 4: Application of the developed technique to the analysis of non-linear effects in manipulator stiffness behaviour under loadings and determining the potentially dangerous configurations and critical forces that may provoke undesired buckling phenomena, i.e. sudden change of current configuration of the loaded manipulator.

To address these problems, the remainder of the work is organized as it follows. Chapter 2 deals with stiffness matrix identification for the links with complex shape. Chapter 3 focuses on the manipulator stiffness modelling for the unloaded mode. Chapter 4 is devoted to the stiffness analysis of serial and parallel manipulators in the loaded mode. In Chapter 5, non-linear stiffness behaviour of serial and parallel manipulators under different types of loadings is considered.

CHAPTER 2

KINETOSTATIC MODELS OF MANIPULATOR ELEMENTS AND IDENTIFICATION OF THEIR PARAMETERS

This chapter is devoted to the accuracy improvement of the manipulator link elastostatic model. It proposes computationally efficient identification procedure, which is based on the FEA-modeling and allows us to obtain the stiffness matrix taking into account the complex shape of the link, couplings between rotational and translational deflections and joints particularities. Simulation study shows that it is able to evaluate stiffness matrix elements with an accuracy of about 0.1% and also to detect non-significant ones. The developed identification procedure is illustrated by several examples whose results will be used in the following chapters for the VJM-based modeling.

2.1 INTRODUCTION

The stiffness modeling approach developed in this work is based on the VJM-presentation of manipulator links/joints. Its core idea is that each mechanical element with distributed elasticity is replaced by a combination of a rigid body and a lumped virtual spring, whose properties are described by a 6×6 stiffness matrix. Therefore, the accuracy of the manipulator stiffness models considered here directly depends on the accuracy of the stiffness matrices incorporated in them. For this reason, this chapter focuses on accuracy improvement of the kinetostatic models of manipulator elements and identification of their parameters.

In robotic literature, there are several ways to obtain the stiffness matrix of a link. The simplest of them assumes that a real link (with rather complex shape) can be approximated by a simple beam, for which

the stiffness matrix can be easily expressed analytically. Another, more accurate, technique deals with multi-beam approximation where the link is presented as a serial chain of rigid bodies separated by virtual springs. For this presentation, the stiffness matrix of the whole link is computed using a common procedure known from stiffness analysis of serial manipulators. However, in spite of computational convenience and better accuracy, the second approach can be hardly applied to many industrial manipulators (where links may be nonhomogeneous, their shape is quite complex and cross-section is non-constant, etc). For instance, for the Orthoglide foot (Figure 2.1), even a four-beam approximation provides an accuracy of only 30-50% [Pashkevich 2010].

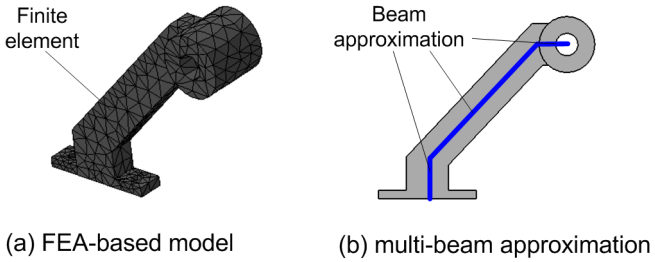

Figure 2.1 CAD model of the link with complex shape

To achieve desired accuracy, here it is proposed to apply the FEA-based identification methodology that was firstly introduced in [Pashkevich 2010] but needs some further development. The corresponding *algorithm* is schematically presented in Figure 2.2. At the *first step*, a CAD model of the link is created, which properly describes the link shape, cross-sections, distribution and physical properties of the material (density, Young's modulus, Poisson's ratio, etc.). Then, at the *second step*, one of the link ends is fixed in accordance with contact surfaces of an adjacent element (for example by cylindrical surface for the revolute joint). At the second end of the link, certain distributed (or localized) force/torque is applied in accordance with contact surfaces of an adjacent element. For these settings, the FEA-modeling is performed which yields the deflection field for a huge number of points generated by the meshing procedure. From this set, a subset (so called '*deflection field*') is extracted corresponding to the neighborhood of the reference point. This field contains desired information on the link compliance with respect to the applied force/torque. Such virtual experiments are repeated several times, for different directions of forces and torques (issue of their magnitude is discussed in the following sections). And finally, at the *third step,* the proposed identification procedure that gives the desired stiffness matrix of the link is applied.

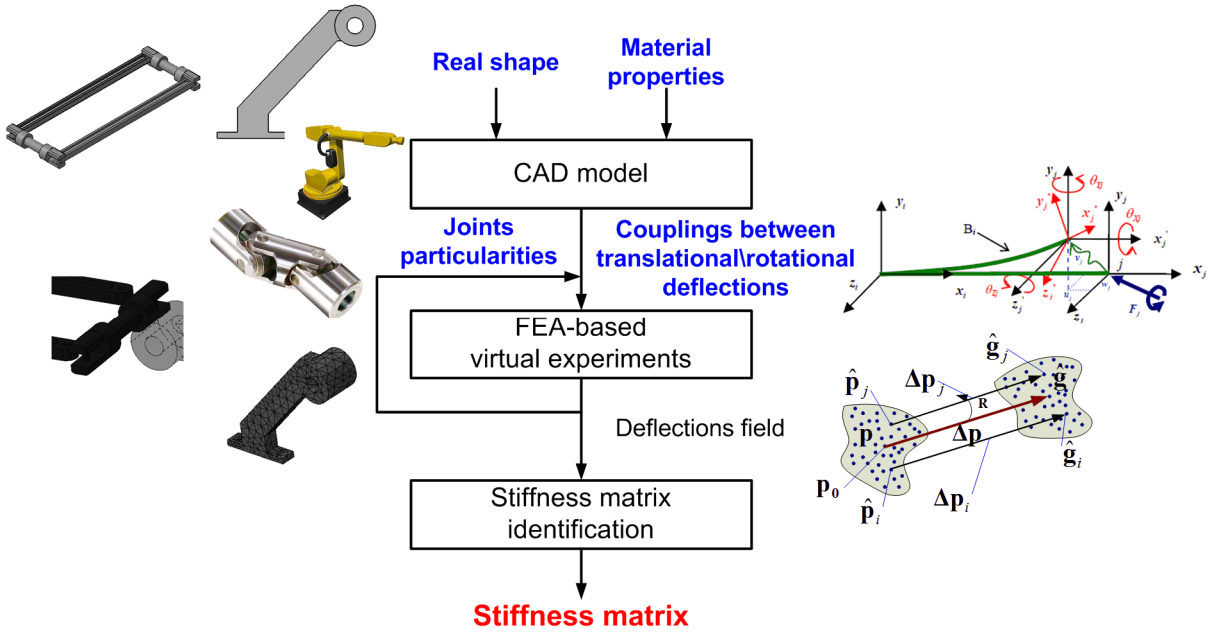

Figure 2.2 Algorithm for stiffness matrix identification procedure

It is worth mentioning that the above described algorithm has some essential advantages, which are not achievable while using any analytical technique. In particular, here it is possible to take into account (straightforwardly and explicitly) the joint elasticity that usually has a number of particularities, such as significant compliance of link/joint areas located closed to the contact points or surfaces. For instant, for a case study presented in Section 2.7 of this chapter, some of the stiffness matrix elements are reduced by the factor of 10-12 if the joint particularities are modeled properly. It is evident that existing analytical expressions do not take into account these issues.

Hence, the goal of this chapter is the accuracy improvement of the stiffness matrix identification for manipulator elements. As it follows from the related analysis, particular problems that should be considered here are the following:

(i) Further development of the FEA-based methodology for the link stiffness matrix identification, which allows us to take into account the link shape, coupling between rotational/translational deflections and joint particularities;

(ii) Development of numerical technique, which computes the stiffness matrix from the set of points (displacement field) extracted from the FEA-based virtual experiments;

(iii) Evaluation of this technique accuracy with respect to virtual experiment settings (meshing type\size, deflection range, fixing and force application method) and size\shape of virtual sensor;

(iv) Minimization of the identification errors by statistical processing of the experimental data (outlines elimination, determination of the confidence intervals and detecting "zero" elements of the stiffness matrix);

(v) Validation of the developed technique on application examples related to typical parallel manipulators and their comparison with conventional regular-shape approximation models.

To address these sub-problems, the remainder of this chapter is organized as follows. Section 2.2 introduces the FEA-based methodology for identification of the link stiffness matrix. Section 2.3 proposes a numerical technique for evaluating the stiffness matrix elements from the field of points. Section 2.4 focuses on the accuracy estimation. Section 2.5 deals with minimization of the identification errors. Section 2.6 is devoted to the extension of the developed technique for the case of double-side loading, which operates with 12×12 stiffness matrices instead of traditional 6×6 ones. In Section 2.7, the developed technique is applied to the links of Orthoglide manipulator. And finally, Section 2.8 summarizes main results and contributions of this chapter.

2.2 FEA-BASED APPROACH FOR IDENTIFICATION OF LINK STIFFNESS MATRIX

Let us start from a detailed description of the FEA-based methodology for the link stiffness matrix identification. It is based on a number of the virtual experiments that are conducted in the CAD-environment (CATIA with ANSYS, for instance). Each of these experiments gives some information on the resistance of an elastic body or mechanism to deformations caused by an external force or torque. The desired stiffness model is obtained by integrating data obtained from several different experiments, which differ in the direction of applied forces/torques.

For relatively small deformations, the stiffness properties are defined through the so-called *stiffness matrix* **K**, which defines the linear relation

$$\begin{bmatrix} \mathbf{F} \\ \mathbf{M} \end{bmatrix} = \mathbf{K} \cdot \begin{bmatrix} \mathbf{p} \\ \delta\boldsymbol{\varphi} \end{bmatrix} \tag{2.1}$$

between the three-dimensional translational/rotational displacements $\mathbf{p} = (p_x, p_y, p_z)^{\mathrm{T}}$; $\delta\boldsymbol{\varphi} = (\delta\varphi_x, \delta\varphi_y, \delta\varphi_z)^{\mathrm{T}}$ and the static forces/torques $\mathbf{F} = (F_x, F_y, F_z)^{\mathrm{T}}$, $\mathbf{M} = (M_x, M_y, M_z)^{\mathrm{T}}$ causing this transition. As known from mechanics, $\mathbf{K}$ is a 6×6 symmetrical semi-definite non-negative matrix, which may include non-diagonal elements to represent the coupling between the translations and rotations [Pashkevich 2010]. The inverse of $\mathbf{K}$ is usually called the *compliance matrix* and is denoted as $\mathbf{k}$.

It is worth mentioning, that there are a number of publications, which operate with non-symmetrical stiffness matrices that are derived via differentiation of the force-deflection relation under the assumption that the static loading is essential. However, as it was shown in [Zafran 2002], [Kövecses 2007], that non-symmetrical stiffness matrices are obtained for very specific definitions of the force and displacement only (for instance, when the displacement is defined with respect to moving frame and the scalar product of the force and displacement does not correspond to the work in common sense). On the other hand, for conservative mechanical systems the stiffness matrix can be defined as the second derivative of the potential energy, which is always symmetrical. Hence, since here we consider only conservative systems and classical definitions of the force and displacement, there are no reasons to obtain a non-symmetrical stiffness matrix from the identification procedure presented below.

For robotic manipulators, the matrix $\mathbf{K}$ can be computed semi-analytically provided that the stiffness matrices of all separate components (links, actuators, etc.) are known with desired precision [Pashkevich 2010]. However, explicit expressions for the link stiffness matrices can be obtained in simple cases only (truss, beam, etc.). For more sophisticated shapes that are commonly used in robotics, the stiffness matrix is usually estimated via the shape approximation, using relatively small set of primitives [Majou 2007]. However, as it follows from the studies [Pashkevich 2010], the accuracy of this approach is rather low. Hence, in a general case, it is prudent to apply to each link the FEA-based techniques, which hypothetically produce rather accurate result.

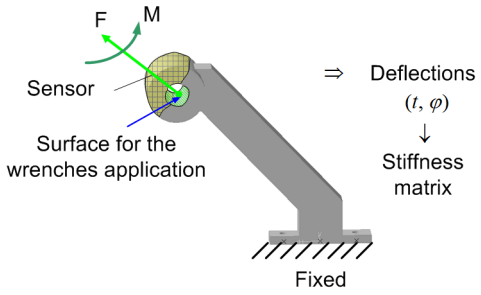

Figure 2.3 Identification experiment for the element with a complex shape

Using the FEA, the stiffness matrix $\mathbf{K}$ (or its inverse $\mathbf{k}$) is evaluated from several numerical experiments, each of which produces the vectors of linear and angular deflections ($\mathbf{p}$, $\delta\boldsymbol{\varphi}$) corresponding to the applied force and torque ($\mathbf{F}$, $\mathbf{M}$) (see Figure 2.3). Then, the desired matrix is computed from the linear system

$$\mathbf{k} = \begin{bmatrix} \mathbf{F}_1 & \dots & \mathbf{F}_m \\ \mathbf{M}_1 & \dots & \mathbf{M}_m \end{bmatrix}^{-1} \cdot \begin{bmatrix} \mathbf{p}_1 & \dots & \mathbf{p}_m \\ \delta\boldsymbol{\varphi}_1 & \dots & \delta\boldsymbol{\varphi}_m \end{bmatrix} \tag{2.2}$$

where m is the number of experiments ($m \ge 6$) and the matrix inverse is replaced by the pseudo-inverse in the case of $m > 6$. It is obvious that the case of $m = 6$ with special arrangement of the forces and torques is numerically attractive

$$\begin{aligned} &\mathbf{F}_1 = (F_x, 0, 0)^T \quad \mathbf{M}_1 = (0, 0, 0)^T; \qquad \mathbf{F}_4 = (0, 0, 0)^T \quad \mathbf{M}_4 = (M_z, 0, 0)^T \\ &\mathbf{F}_2 = (0, F_y, 0)^T \quad \mathbf{M}_2 = (0, 0, 0)^T; \qquad \mathbf{F}_5 = (0, 0, 0)^T \quad \mathbf{M}_5 = (0, M_y, 0)^T. \\ &\mathbf{F}_3 = (0, 0, F_y)^T \quad \mathbf{M}_3 = (0, 0, 0)^T; \qquad \mathbf{F}_6 = (0, 0, 0)^T \quad \mathbf{M}_6 = (0, 0, M_z)^T \end{aligned} \tag{2.3}$$

corresponding to the diagonal structure of the matrix to be inverted. In this case, each FEA-experiment produces exactly one column of the compliance matrix

$$\mathbf{k} = \begin{bmatrix} \mathbf{p}_1 / F_x & \mathbf{p}_2 / F_y & \mathbf{p}_3 / F_z & \mathbf{p}_4 / M_x & \mathbf{p}_5 / M_y & \mathbf{p}_6 / M_z \\ \delta\boldsymbol{\varphi}_1 / F_x & \delta\boldsymbol{\varphi}_2 / F_y & \delta\boldsymbol{\varphi}_3 / F_z & \delta\boldsymbol{\varphi}_4 / M_z & \delta\boldsymbol{\varphi}_5 / M_y & \delta\boldsymbol{\varphi}_6 / M_z \end{bmatrix} \tag{2.4}$$

and the values ($\mathbf{p}_i$, $\delta\boldsymbol{\varphi}_i$) may be clearly physically interpreted. On the other hand, by increasing the number of experiments ($m > 6$) it is possible to reduce the estimation error. Besides, it is worth mentioning that the

classical methodology of the optimal design of an experiment cannot be applied here directly, because it is not possible to include in equation (2.4) the measurement errors induced by virtual experiments as additive components. Some aspects of this problem are studied in sub-section 2.4.4.

Hence, to obtain the desired stiffness (compliance) matrix, it is required to estimate first the deflections ($\mathbf{p}$, $\delta\boldsymbol{\varphi}$) corresponding to each virtual experiment. This issue is in the focus of the following section.

2.3 NUMERICAL TECHNIQUE FOR EVALUATING THE STIFFNESS MATRIX ELEMENTS

Usually, in FEA-based experiments, the values ($\mathbf{p}$, $\delta\boldsymbol{\varphi}$) are computed from the spatial location of a single finite element enclosing the reference point. In contrast to this approach, here it is proposed to evaluate ($\mathbf{p}$, $\delta\boldsymbol{\varphi}$) from the set of points (*displacement field*) describing transitions of a rather large number of nodes located in the neighborhood of reference point. It is reasonable to assume that such modification will yield positive impact on the accuracy, since the FEA-modeling errors usually differ from node to node, exposing almost quasi-stochastic nature.

2.3.1 Related optimization problem

To formulate this problem strictly, let us denote the displacement field by a set of vector couples $\{\mathbf{p}_i, \Delta\mathbf{p}_i \,|\, i=\overline{1,n}\}$ (see Figure 2.4) where the first component $\mathbf{p}_i$ defines the node's initial location (before applying the force/torque), $\Delta\mathbf{p}_i$ refers to the node's displacement due to the applied force/torque, and n is the number of considered nodes. Then, assuming that all the nodes are close enough to the reference point, this set can be approximated by a "*rigid transformation*"

$$\mathbf{p}_i + \Delta\mathbf{p}_i = \mathbf{R}(\delta\boldsymbol{\varphi})\cdot\mathbf{p}_i + \mathbf{p}, \quad i=\overline{1,n}\,, \tag{2.5}$$

that includes as the parameters the linear displacement vector $\mathbf{p}$ and the orthogonal 3×3 matrix $\mathbf{R}$ that depends on the rotational displacement $\delta\boldsymbol{\varphi}$. Then, the problem of the deflection estimation can be presented as the best fit of the considered vector field by equation (2.5) with respect to the six scalar variables $(p_x, p_y, p_z, \delta\varphi_x, \delta\varphi_y, \delta\varphi_z)$ incorporated in the displacement vector $\mathbf{p}$ and the rotation matrix $\mathbf{R}$.

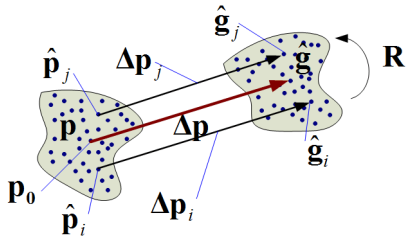

Figure 2.4 Field of points from FEA modeling

In practice, the FEA-modeling output provides the deflection vector fields for all nodes referring to all components of the mechanism. So, it is required to select a relevant subset corresponding to the neighborhood of the reference point $\mathbf{p}_0$. Besides, the node locations $\mathbf{p}_i$ must be expressed relative to this point, i.e. the origin of the coordinate system must be shifted to $\mathbf{p}_0$. The latter is specified by the physical meaning of the deflections in the stiffness analysis.

To estimate the desired deflections ($\mathbf{p}$, $\delta\boldsymbol{\varphi}$), let us apply the least square technique that leads to minimization of the sum of squared residuals

$$f = \sum_{i=1}^{n} \left\| \mathbf{p}_i + \Delta\mathbf{p}_i - \mathbf{R}(\delta\boldsymbol{\varphi})\mathbf{p}_i - \mathbf{p} \right\|^2 \to \min_{\mathbf{R},\mathbf{p}} \tag{2.6}$$

with respect to the vector $\mathbf{t}$ and the orthogonal matrix $\mathbf{R}$ representing the rotational deflections $\delta\boldsymbol{\varphi}$**.** The specificities of this problem (that does not allow direct application of the standard methods) are the orthogonal constraint $\mathbf{R}^{\mathrm{T}}\mathbf{R} = \mathbf{I}$ and non-trivial relation between elements of the matrix $\mathbf{R}$ and the vector $\delta\boldsymbol{\varphi}$**.** The following sub-sections present two methods for computing $\mathbf{p}$**,** $\delta\boldsymbol{\varphi}$, as well as their comparison study.

2.3.2 Problem solution using SVD-based method

For the comparison purposes, first let us briefly present the exact solution of the optimization problem (2.6). It relies on some results from the matrix algebra referred to as "Procrustes problem" [Gower 2004]. The corresponding estimation procedure is decomposed in two steps, which sequentially produce the rotation matrix **R** and the translation vector **p**. Then, the desired vector of rotation angles $\delta\boldsymbol{\varphi}$ is extracted from **R**.

Let us transform the original optimization problem (2.6) to the standard form. First, for the non-constrained variable **p**, straightforward differentiation and equating to zero gives an expression

$$\mathbf{p} = \frac{1}{n}\left(\sum_{i=1}^{n} \Delta\mathbf{p}_i - (\mathbf{R} - \mathbf{I}) \sum_{i=1}^{n} \mathbf{p}_i \right) \tag{2.7}$$

Then, after relevant substitution and denoting

$$\hat{\mathbf{p}}_i = \mathbf{p}_i - \frac{1}{n}\sum_{i=1}^{n} \mathbf{p}_i \; ; \qquad \hat{\mathbf{g}}_i = \mathbf{p}_i + \Delta\mathbf{p}_i - \frac{1}{n}\sum_{i=1}^{n} (\mathbf{p}_i + \Delta\mathbf{p}_i) \, , \tag{2.8}$$

the original optimization problem is reduced to the orthogonal Procrustes formulation

$$f = \sum_{i=1}^{n} \left\| \hat{\mathbf{g}}_i - \mathbf{R}\,\hat{\mathbf{p}}_i \right\|^2 \to \min_{\mathbf{R}} \, . \tag{2.9}$$

with the constraint $\mathbf{R}^T\mathbf{R} = \mathbf{I}$. The latter yields the solution [Gower 2004]

$$\mathbf{R} = \mathbf{V}\mathbf{U}^T \tag{2.10}$$

that is expressed via the singular value decomposition (SVD) of the matrix

$$\sum_{i=1}^{n} \hat{\mathbf{p}}_i \cdot \mathbf{g}_i^T = \mathbf{U}\,\boldsymbol{\Sigma}\,\mathbf{V}^T \, , \tag{2.11}$$

which requires some computational efforts. Hence, the above expressions (2.7), (2.10) allow to solve the optimization problem (2.6) in terms of variables **R** and **p**.

Further, to evaluate the vector of angular displacements $\delta\boldsymbol{\varphi}$, the orthogonal matrix **R** must be decomposed into a product of elementary rotations around the Cartesian axes x, y, z. It is obvious that, in a general case, this decomposition is not unique and depends on the rotation order. However, for a small $\delta\boldsymbol{\varphi}$ (that is implicitly assumed for FEA-experiments) this matrix may be uniquely presented in differential form

$$\mathbf{R} \cong \begin{bmatrix} 1 & -\delta\varphi_z & \delta\varphi_y \\ \delta\varphi_z & 1 & -\delta\varphi_x \\ -\delta\varphi_y & \delta\varphi_x & 1 \end{bmatrix} \tag{2.12}$$

Using this expression, the desired parameters $\delta\varphi_x, \delta\varphi_y, \delta\varphi_z$ may be extracted from $\mathbf{R} = [r_{ij}]$ in several ways (Table 2.1), which are formally equivalent but do not necessarily possess similar robustness with respect to round-off errors. A relevant comparison study will be presented in sub-section 2.4.2.

Table 2.1 Evaluation of the rotation angles from matrix **R**

Method	φ_x	φ_y	φ_z
SVD+	r_{32}	r_{13}	r_{21}
SVD-	$-r_{23}$	$-r_{31}$	$-r_{12}$
SVD±	$(r_{32} - r_{23})/2$	$(r_{13} - r_{31})/2$	$(r_{21} - r_{12})/2$
SVD+asin	$\operatorname{asin} r_{32}$	$\operatorname{asin} r_{13}$	$\operatorname{asin} r_{21}$
SVD-asin	$-\operatorname{asin} r_{23}$	$-\operatorname{asin} r_{31}$	$-\operatorname{asin} r_{12}$
SVD±asin	$\operatorname{asin}\left((r_{32} - r_{23})/2\right)$	$\operatorname{asin}\left((r_{13} - r_{31})/2\right)$	$\operatorname{asin}\left((r_{21} - r_{12})/2\right)$

2.3.3 Efficiency improvement of developed technique

To reduce the computational efforts and to avoid the SVD, let us introduce linearization of the rotational matrix **R** at the early stage, using explicit parameterization given by expression (2.12). This allows rewriteing the equation of the 'rigid transformation' (2.5) in the form

$$\Delta\mathbf{p}_i = \mathbf{p}_i \times \delta\boldsymbol{\varphi} + \mathbf{p}; \quad i = \overline{1,n} \tag{2.13}$$

that can be further transformed into a linear system of the following form

$$\begin{bmatrix}\mathbf{I} & \mathbf{P}_i\end{bmatrix}\begin{bmatrix}\mathbf{p} \\ \delta\boldsymbol{\varphi}\end{bmatrix} = \Delta\mathbf{p}_i; \quad i = \overline{1,n} \tag{2.14}$$

where $\mathbf{P}_i$ is a skew-symmetric matrix corresponding to the vector $\mathbf{p}_i$:

$$\mathbf{P}_i = \begin{bmatrix} 0 & p_{zi} & -p_{yi} \\ -p_{zi} & 0 & p_{xi} \\ p_{yi} & -p_{xi} & 0 \end{bmatrix} \tag{2.15}$$

Then, applying the standard least-square technique with the objective

$$f = \sum_{i=1}^{n} \left\| \Delta\mathbf{p}_i - \mathbf{P}_i\,\delta\boldsymbol{\varphi} - \mathbf{p} \right\|^2 \to \min_{\boldsymbol{\varphi},\mathbf{t}} \tag{2.16}$$

one can get the solution

$$\begin{bmatrix}\mathbf{p} \\ \delta\boldsymbol{\varphi}\end{bmatrix} = \begin{bmatrix} n\mathbf{I} & \sum_{i=1}^{n}\mathbf{P}_i \\ \sum_{i=1}^{n}\mathbf{P}_i^T & \sum_{i=1}^{n}\mathbf{P}_i^T\mathbf{P}_i \end{bmatrix}^{-1} \begin{bmatrix} \sum_{i=1}^{n}\Delta\mathbf{p}_i \\ \sum_{i=1}^{n}\mathbf{P}_i^T\Delta\mathbf{p}_i \end{bmatrix} \tag{2.17}$$

that employs the 6×6 matrix inversion. This solution can be simplified by shifting the origin of the coordinate system to the point $\mathbf{p}_c = n^{-1}\sum_{i=1}^{n}\mathbf{p}_i$ leading to expression

$$\begin{bmatrix}\mathbf{p} \\ \delta\boldsymbol{\varphi}\end{bmatrix} = \begin{bmatrix} n^{-1}\mathbf{I} & \mathbf{0} \\ \mathbf{0} & \left(\sum_{i=1}^{n}\hat{\mathbf{P}}_i^T\hat{\mathbf{P}}_i\right)^{-1} \end{bmatrix} \cdot \begin{bmatrix} \sum_{i=1}^{n}\Delta\mathbf{p}_i \\ \sum_{i=1}^{n}\hat{\mathbf{P}}_i^T\Delta\mathbf{p}_i \end{bmatrix} \tag{2.18}$$

that requires inversion of the matrix of size 3×3. Here, $\hat{\mathbf{P}}_i$ denotes a skew-symmetric matrix corresponding to the vector $\hat{\mathbf{p}}_i = \mathbf{p}_i - \mathbf{p}_c$.

It is evident that the obtained expression (2.18) is more computationally efficient compared to (2.8) and (2.10). Besides, for some typical cases corresponding to regular meshing patterns of the FEA, expression (2.18) can be further simplified as shown in the following subsection.

2.3.4 Analytical solutions for typical case studies

In practice, the points $\mathbf{p}_i$ are distributed in the space in a regular way, in accordance with the meshing options chosen for the FEA-modeling. This allows us to inverse the matrix $\sum_{i=1}^{n}\hat{\mathbf{P}}_i^T\hat{\mathbf{P}}_i$ analytically and to obtain very simple expressions for **p,** $\delta\boldsymbol{\varphi}$. Let us consider several patterns that are useful for practice and are presented in Figure 2.5.

Case 1: Symmetrical field (Figure 2.5a). If the field is symmetrical with respect to its centre $\mathbf{p}_c$, the solution (2.18) can be presented in a compact analytical form as

$$\mathbf{p} = n^{-1}\sum_{i=1}^{n}\Delta\mathbf{p}_i \;; \quad \delta\boldsymbol{\varphi} = \mathbf{D}^{-1}\sum_{i=1}^{n}\hat{\mathbf{P}}_i^T\Delta\mathbf{p}_i \tag{2.19}$$

where the matrix

$$\mathbf{D} = diag\left[\sum_{i=1}^{n}(\hat{p}_{yi}^2 + \hat{p}_{zi}^2) \quad \sum_{i=1}^{n}(\hat{p}_{xi}^2 + \hat{p}_{zi}^2) \quad \sum_{i=1}^{n}(\hat{p}_{xi}^2 + \hat{p}_{yi}^2)\right] \tag{2.20}$$

is diagonal and easily inverted.

Case 2: Cubic field (Figure 2.5b). If the field is symmetrical and, in addition, it is produced by uniform meshing of the cubic subspace $a \times a \times a$, the matrix D is expressed as $\mathbf{D} = d \cdot \mathbf{I}$ where $d = a^2\, n(\sqrt[3]{n} - 1)/6(\sqrt[3]{n} + 1)$.

Case 3: Planar square field (Figure 2.5c). For the field produced by uniform meshing of the square $a \times a$ located perpendicular to the *x*-axis, the expression for the matrix $\mathbf{D} = diag\left[d \quad d/2 \quad d/2\right]$

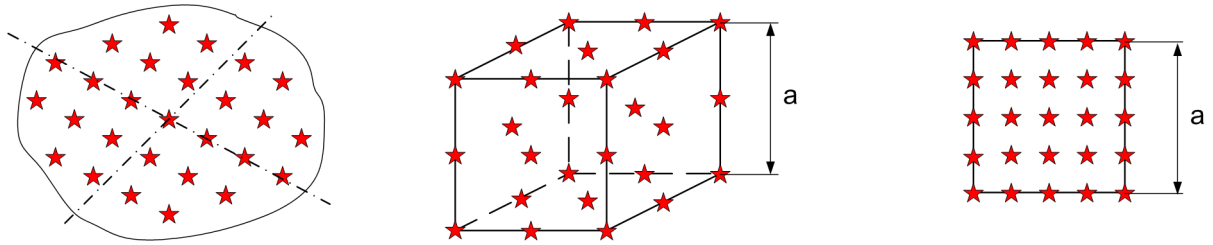

(a) Symmetrical field (b) Cubic field (c) Planar square field

Figure 2.5 Typical patterns of the deflection field

Summarizing Section 2.3, it should be noted that the proposed numerical technique is computationally attractive and allow simultaneous estimation both translational and rotational deflections **p,** $\delta\boldsymbol{\varphi}$ from the FEA-produced field. Below it is evaluated from the point of view of the precision and robustness.

2.4 ACCURACY OF THE DEVELOPED NUMERICAL TECHNIQUE

To be applied in practice, the accuracy of the developed numerical technique should be evaluated with respect to the virtual experiment settings (meshing type\size, deflection range, fixing and force application method) and size\shape of virtual sensor. Let us consider several case studies corresponding to typical industrial applications.

2.4.1 Error sources and their impact

It is obvious that the main source of estimation errors is related to the FEA-modeling that highly depends on the size and type of the finite elements, meshing options, incorporated numerical algorithms, computer word length and the round-off principle. Hypothetically, the accuracy can be essentially improved by reducing the mesh size and increasing the number of digits in presentation of all variables. But there are some evident technical constraints that do not allow ignoring the FEA limitations.

Another type of errors arises from numerical differentiation incorporated in the considered technique. Strictly speaking, the linear relation (2.1) is valid for rather small deflections that may be undetectable against the FEA-modeling defects. On the other side, large deflections may be out of the elasticity range. Hence, it is prudent to find a compromise for the applied forces/torques taking into account both factors.

2.4.2 Influence of linearization and round-offs

Since both of the considered algorithms (SVD-based and the proposed one, see Section 2.3) involve numerous matrix multiplications, they may accumulate the round-off errors. Besides, they employ the first-order approximation of the matrix **R** that may create another source of inaccuracy. Hence, it is prudent to obtain numerical assessments corresponding to a typical case study.

For these assessments, there were examined data sets corresponding to the cubic deflection field of size 10×10×10 mm^3 with the mesh step of 1 mm (1331 points). The deflections have been generated via the

'rigid transformation' (2.5) with the parameters $\mathbf{p} = (a, a, a)^T$ and $\delta\boldsymbol{\varphi} = (b, b, b)^T$ presented in Table 2.2, Table 2.3. All calculations have been performed using the double precision floating-point arithmetic.

Table 2.2 Identification errors for the rotation $\delta\boldsymbol{\varphi}$ [deg]

Method	Rotation amplitude b					
	0.01°	0.05°	0.1°	0.5°	1°	5°
SVD-based technique						
SVD+	$2\cdot10^{-6}$	$4\cdot10^{-5}$	$2\cdot10^{-4}$	$4\cdot10^{-3}$	$2\cdot10^{-2}$	0.48
SVD-	$2\cdot10^{-6}$	$4\cdot10^{-5}$	$2\cdot10^{-4}$	$4\cdot10^{-3}$	$2\cdot10^{-2}$	0.48
SVD±	$9\cdot10^{-7}$	$2\cdot10^{-5}$	$9\cdot10^{-5}$	$2\cdot10^{-3}$	$9\cdot10^{-3}$	0.24
SVD+asin	$2\cdot10^{-6}$	$4\cdot10^{-5}$	$2\cdot10^{-4}$	$4\cdot10^{-3}$	$2\cdot10^{-2}$	0.48
SVD-asin	$2\cdot10^{-6}$	$4\cdot10^{-5}$	$2\cdot10^{-4}$	$4\cdot10^{-3}$	$2\cdot10^{-2}$	0.48
SVD±ain	$9\cdot10^{-7}$	$2\cdot10^{-5}$	$9\cdot10^{-5}$	$2\cdot10^{-3}$	$9\cdot10^{-3}$	0.24
LIN-based technique						
LIN	$9\cdot10^{-7}$	$2\cdot10^{-5}$	$9\cdot10^{-5}$	$2\cdot10^{-3}$	$9\cdot10^{-3}$	0.24
LIN asin	$9\cdot10^{-7}$	$2\cdot10^{-5}$	$9\cdot10^{-5}$	$2\cdot10^{-3}$	$9\cdot10^{-3}$	0.24

Table 2.3 Identification errors for the translation [mm]

Method	Translation amplitude a			
	0.01 mm	0.1 mm	1.0 mm	10 mm
SVD	10^{-16}	10^{-16}	10^{-16}	$2\cdot10^{-14}$
LIN	10^{-16}	10^{-16}	10^{-16}	$3\cdot10^{-15}$

As it follows from the analysis, the influence of the linearization and round-offs is negligible for the translation (the induced errors are less than 10^{-14} mm). In contrast, for the rotation, practically acceptable results may be achieved for rather small angular deflections that are less than 1.0° (the errors are up to 0.01°). The latter imposes an essential constraint on the amplitude of the forces/torques in the FEA-modeling that must ensure reasonable deflections. Another conclusion concerns comparison of the SVD-based and LIN-based methods. It justifies advantages of the proposed LIN-based technique that provides the best robustness and lower computational complexity.

2.4.3 Influence of FEA-modeling errors

By its general principle, the FEA-modeling is an approximate method that produces some errors caused by the discretization. Beside, even for the perfect modeling, the deflections in the neighborhood of the reference point do not exactly obey the equation (2.5). Hence, it is reasonable to assume that the 'rigid transformation' (2.5) incorporates some additive random errors

$$\mathbf{p}_i + \Delta\mathbf{p}_i = \mathbf{R}(\delta\boldsymbol{\varphi})\cdot\mathbf{p}_i + \mathbf{p} + \boldsymbol{\varepsilon}_i; \quad i = \overline{1,n} \tag{2.21}$$

that are supposed to be independent and identically distributed Gaussian random variables with zero-mean and standard deviation σ.

In the frame of this assumption, the expression for the deflections (2.18) can be rewritten as

$$\mathbf{p} = \mathbf{p}^{\mathrm{o}} + n^{-1}\sum_{i=1}^{n}\boldsymbol{\varepsilon}_i; \quad \delta\boldsymbol{\varphi} = \delta\boldsymbol{\varphi}^{\mathrm{o}} + \left(\sum_{i=1}^{n}\hat{\mathbf{P}}_i^T\hat{\mathbf{P}}_i\right)^{-1}\sum_{i=1}^{n}\hat{\mathbf{P}}_i^T\boldsymbol{\varepsilon}_i \tag{2.22}$$

where the superscript 'o' corresponds to the 'true' parameter value. This justifies usual properties of the adopted point-type estimator (2.18), which is obviously unbiased and consistent. Furthermore, the variance-covariance matrices for **t**, δ**φ** may be expressed as

$$\mathrm{cov}[\mathbf{p}] = \frac{\sigma^2}{n}\mathbf{I}; \quad \mathrm{cov}[\delta\boldsymbol{\varphi}] = \sigma^2\left(\sum_{i=1}^{n}\hat{\mathbf{P}}_i^T\hat{\mathbf{P}}_i\right)^{-1} \tag{2.23}$$

allowing to evaluate the estimation accuracy using common confidence interval techniques.

As it follows from (2.21), for the translational deflection **p** the identification accuracy is defined by the standard deviation $\sigma/\sqrt{n}$ and depends on the number of the points only. In contrast, for the rotational deflection, the spatial location of the points is a very important issue. In particular, for the cubic field of the size $a \times a \times a$, the standard deviation of the rotation angles may be approximately expressed as $\sigma/a\sqrt{n/6}$.

To evaluate the standard deviation σ describing the random errors $\boldsymbol{\varepsilon}$, one may use the residual-based estimator obtained from the expression

$$\mathrm{E}\left(\sum_{i=1}^{n}\left\|\mathbf{p}_i + \Delta\mathbf{p}_i - \mathbf{R}(\delta\boldsymbol{\varphi})\cdot\mathbf{p}_i - \mathbf{p}\right\|^2\right) = (3n-6)\,\sigma^2. \tag{2.24}$$

The latter may be easily derived taking into account that, for each experiment, the deflection field consists of *n* three-dimensional vectors that are approximated by the model containing 6 scalar parameters. Moreover, to increase accuracy, it is prudent to aggregate the squared residuals for all FEA-experiments and to make relevant estimation using the coefficient $(3n-6)m\sigma^2$, where *m* is the experiments number.

In addition, to increase accuracy and robustness, it is reasonable to eliminate outliers in the experimental data. They may appear in the FEA-field due to some anomalous causes, such as insufficient meshing of some elements, violation of the boundary conditions in some areas of the mechanical joints, etc. The simplest and reliable method that is adopted in this research is based on the 'data filtering' with respect to the residuals (i.e. eliminating certain percentage of the points with the highest residual values). Another practical question is related to *detecting zero elements* in the compliance matrix or, in other words, evaluating the statistical significance of the computed values compared to zero. These issues will be studied in Section 2.5.

2.4.4 Optimal settings for identification experiments

Finally, to evaluate the combined influence of various error sources, let us focus on the deflection identification from the cubic field of size 10×10×10 mm^3 (1331 points, mesh step 1 mm). In particular, let us contaminate all deflections using the Gaussian noise with the s.t.d. 5×10^{-5} mm that is a typical value discovered from the examined FEA data sets (Table 2.4). Similar to the previous case, all calculations were performed using the double precision floating-point arithmetic (16 decimal digits).

Table 2.4 Parameters of the FEA-modeling noise for different mesh type

Meshing options			σ, mm
Type of the mesh	Notation	Size of the finite element	
Linear mesh	3L	3 mm	$4.10\cdot10^{-5}$
	2L	2 mm	$4.59\cdot10^{-5}$
	1L	1 mm	$3.87\cdot10^{-5}$
Parabolic mesh	5P	5 mm	$6.40\cdot10^{-5}$
	3P	3 mm	$5.26\cdot10^{-5}$
	2P	2 mm	$5.60\cdot10^{-5}$

The obtained results confirmed the main theoretical derivations of the previous subsections. The identification errors obey the normal distribution (Figure 2.6) but their s.t.d. should be evaluated taking into account some additional issues. Thus, the s.t.d. of the translational error is about $1.36 \cdot 10^{-6}$ mm and depends only on the FEA-induced component that is evaluated as $\sigma / \sqrt{n} \approx 1.37 \cdot 10^{-6}$ mm. The influence of the linearization and round-offs is negligible here (this component is less than 10^{-14} mm). Also, this type of the error does not depend on the translation amplitude.

In contrast, for the rotational deflections, there exists strong dependence on the amplitude (Figure 2.7). In particular, for the angular deflection 0.1°, the s.t.d. of the identification error is about $8.4 \cdot 10^{-5}$ deg, while the FEA-induced component is evaluated as $\sigma / a\sqrt{n/6} \approx 1.8 \cdot 10^{-5}$ deg and the linearization component is about $8.8 \cdot 10^{-5}$ deg (see Table 2.2). Moreover, the simulation results allow to define preferable values of the angular deflection that may be extracted from the FEA-data with the highest accuracy. They show that the deflection angles should be in the range 0.01 …0.2° to ensure the identification accuracy of about 0.2%

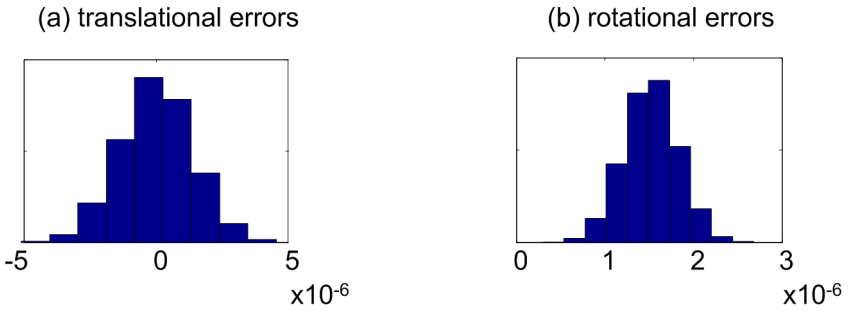

Figure 2.6 Histograms for the identification errors (a = 1.0 mm, b=0.1°, σ= 5×10^{-5} mm)

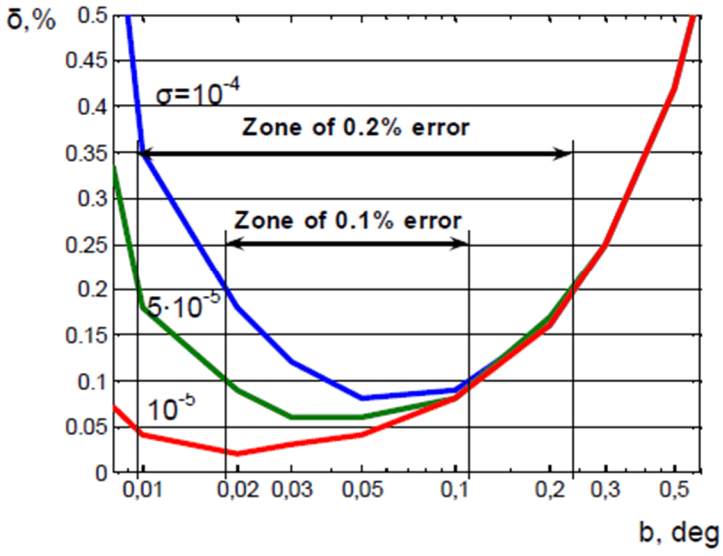

Figure 2.7 Identification errors for different amplitudes of the rotational deflections

Thus, the case studies considered in Section 2.4 confirm that the proposed LIN-based algorithm ensures the same accuracy as the SVD-based one, while possessing lower computational complexity. Besides, these results give some practical recommendations for setting the FEA-based experiments and evaluating the identification accuracy.

2.5 MINIMIZATION OF IDENTIFICATION ERRORS

To demonstrate efficiency of the developed technique and to evaluate its applicability to real-life situations, let us consider an example for which the desired compliance matrix can be obtained both numerically and analytically. A comparison of these two solutions provides convenient benchmarks for different FEA-modeling options and also gives some practical recommendations for achieving the required accuracy.

2.5.1 Benchmark example

As an example, let us consider a cantilever beam of size 1000×10×10 mm^3 (see Figure 2.8) with the Young's Modulus $E = 2{\cdot}10^5\, N/mm^2$ and the Poisson's Ratio $\nu = 0.266$. These data correspond to geometry and material properties of a typical robot link studied in this work.

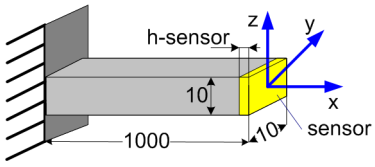

Figure 2.8 Examined cantilever beam

For this element, an analytical expression for the compliance matrix can be presented as

$$\mathbf{k} = \begin{bmatrix} k_{11} & 0 & 0 & 0 & 0 & 0 \\ 0 & k_{22} & 0 & 0 & 0 & k_{26} \\ 0 & 0 & k_{33} & 0 & k_{35} & 0 \\ 0 & 0 & 0 & k_{44} & 0 & 0 \\ 0 & 0 & k_{53} & 0 & k_{55} & 0 \\ 0 & k_{62} & 0 & 0 & 0 & k_{66} \end{bmatrix} \tag{2.25}$$

where non-zero elements are: $k_{35} = k_{53} = -L^2/2EI_y$, $k_{11} = L/EA$, $k_{22} = L^3/3EI_z$, $k_{33} = L^3/3EI_y$, $k_{44} = L/GJ$, $k_{55} = L/3EI_y$, $k_{66} = L/3EI_z$, $k_{26} = k_{62} = L^2/2EI_z$. Here L is the length of the beam, A is its cross-section area, I_y, I_z are the second moments, J is the cross-section property.

The FEA-modeling has been performed using the CATIA V5R16 CAD system. It is a complete tool for preparing parts geometry and generating finite element models with powerful meshing capabilities. The software was run on a computer with a 1.8 GHz processor and 1 GB memory, which impose essential constraints on the finite element dimensions even for this simple case (a single beam element) [Zamani 2005].

During modeling, the loads have been applied at one end of the beam with the other end fully clamped. The force/torque amplitudes were determined using expression (2.23) and the optimal accuracy settings for the deflections 0.1…1.0 mm and 0.01…0.20°, which yielded the following values: $F_x = 1000\,N$, $F_y = 1N$, $F_z = 1N$, $M_x = 1N{\cdot}m$, $M_y = 1N{\cdot}m$, $M_z = 1N{\cdot}m$. These loads were applied sequentially, providing 6 elementary FEA-experiments, each of which produced a single column of the compliance matrix **k**, in accordance with (2.4).

2.5.2 Optimal selections of FEA-modeling options

Since the identification errors, which are studied here, essentially depend on the discretization of the FEA-based model and definition of the deflection field, let us focus on the influence of the meshing parameters of the FEA-model and on dimensions of the virtual sensor that specifies this field.

Meshing options. The adopted software provides two basic options for the automatic mesh generation: linear and parabolic ones. It is known that, generally, the linear meshing is faster computationally but less accurate. On the other hand, the parabolic meshing requires more computational resources, but leads to more accurate results.

For the considered case study, both meshing options have been examined and compared with respect to the accuracy of the obtained compliance matrix. The mesh size was gradually reduced from 5 to 1 mm, until achieving the lower limit imposed by the computer memory size. The obtained results (Table 2.5 and Figure 2.9) clearly demonstrate advantages of the parabolic mesh, which allow achieving appropriate accuracy of 0.1% for the mesh step of 2 mm using standard computing capacities. In contrast, the best result for the linear mesh is 12% and corresponds to the step of 1 mm.

Table 2.5 Maximum errors in estimation of compliance matrix elements

Meshing options			Maximum errors in elements of identified matrix k_{ij}
Type of the mesh	Notation	Size of the finite element	
Linear mesh	3L	3 mm	27%
	2L	2 mm	20%
	1L	1 mm	12%
Parabolic mesh	5P	5 mm	3.3%
	3P	3 mm	0.19%
	2P	2 mm	0.10%

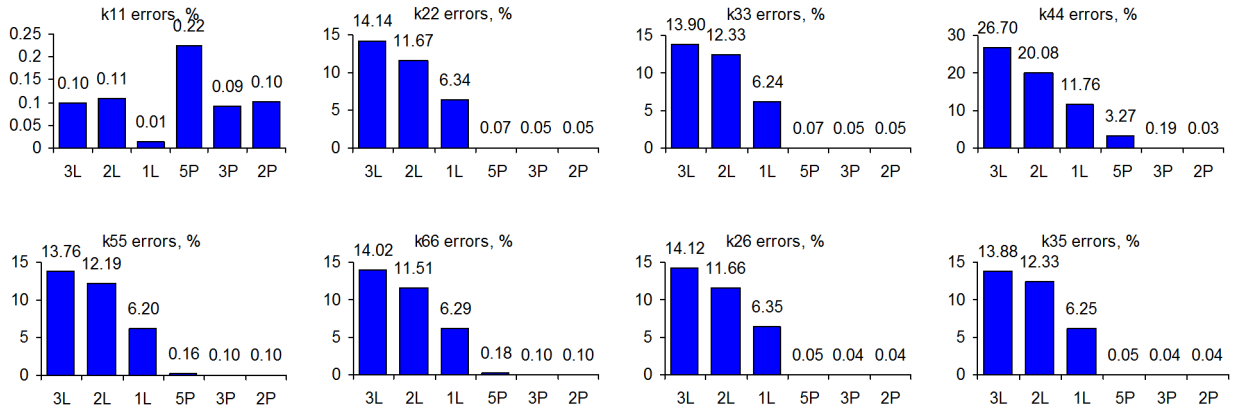

Figure 2.9 Errors (%) in estimations of non-zero elements of the compliance matrix (3L,2L,1L are linear mesh with steps 3,2,1 mm; 5P,3P,2P are parabolic mesh with steps 5,3,2 mm)

Accuracy of these results can also be evaluated by the difference between the deflections computed using analytical expression (2.25) and the identified compliance matrix (assuming that the link is under similar loadings as in virtual experiments). This allows us to simplify physical meaning of the identification errors and also to obtain a weighted performance measure that neglects some identification failures, whose impact on the reference point deflection is not essential. Relevant results are presented in Figure 2.10, where there are presented the worst values selected from six virtual experiments. They confirm that the mesh 2P (parabolic with step 2 mm) ensures accuracy of 0.1% and is preferable for practice. On the other hand, as it follows from separate study, further reduction of the mesh step does not lead to essential reduction of the identification errors. Obviously, this conclusion is valid for this case study only, but it can be applied to other cases using proper scaling of dimensions.

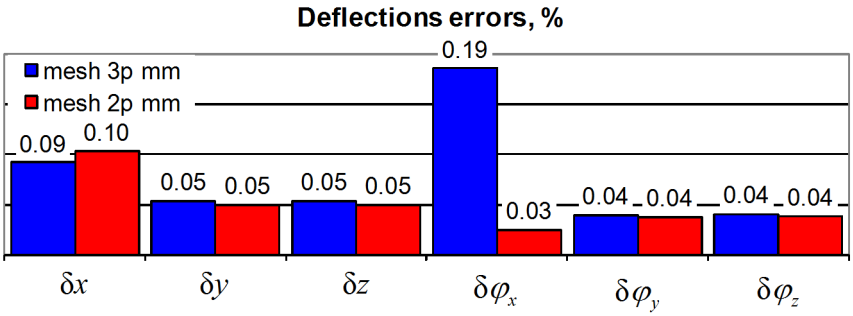

Figure 2.10 Influence of the stiffness matrix errors on the position accuracy

Defining the virtual sensor. The developed technique operates with the deflection field bounded by the virtual sensor (see Figure 2.3), which is located in the neighborhood of the reference point (RP). As stated above, this neighborhood should be large enough to neutralize the influence of the FEA-induced errors, but its unreasonable increase may lead to violation of some essential assumptions and, consequently, to a reduction in the accuracy.

To get a realistic inference concerning this issue, a number of experiments have been carried out, for different definitions of the RP-neighborhood (i.e., the virtual sensor size). The obtained results (Table 2.6) show that the highest accuracy 0.1% is achieved for the one-layer configuration of the deflection field, which is composed of the nodes located on the rare edge of the examined beam. This pattern is very close to the square-type field 10×10 mm^2 studied above (see sub-section 2.3.4). In contrast, increasing the sensor size up to the cubic-type of $10\times10\times10$ mm^3 leads to the identification error of about 0.08%. Hence, in practice, it is reasonable to estimate the deflection values from the field of points corresponding to the square-type virtual sensor.

Table 2.6 Evolution of the identification errors for different virtual sensors

h-sensor	k_{11}	k_{22}	k_{33}	k_{44}	k_{55}	k_{66}	k_{62}	k_{53}
1-layer	0.10%	0.05%	0.05%	0.03%	0.10%	0.10%	0.04%	0.04%
0.1%	0.11%	0.13%	0.13%	0.01%	0.08%	0.09%	0.09%	0.09%
0.2%	0.09%	0.2%	0.2%	0.05%	0.04%	0.04%	0.14%	0.14%
0.3%	0.04%	0.28%	0.28%	0.10%	0.02%	0.02%	0.19%	0.19%
0.5%	0.06%	0.42%	0.42%	0.20%	0.13%	0.13%	0.29%	0.29%
1%	0.33%	0.8%	0.80%	0.46%	0.41%	0.41%	0.54%	0.54%
2%	0.86%	1.55%	1.55%	0.98%	0.91%	0.92%	1.03%	1.03%

It is worth mentioning that, in practice, the reference point of the link may be located outside the the link material (see Figure 2.1). Consequently, the RP-neighborhood does not include any finite elements that may be used for creating the deflection field required by the identification procedure. In this case, the link CAD-model should be complemented with an additional solid body centered in the reference point and restrained by the surfaces of the corresponding joint (this body should be rigid enough to insure correctness of FEA-based simulations). After such modifications, the virtual sensor can be defined in the usual way. As it follows from our experience, proper definition of the virtual sensor (and additional solid body) as well as applied loading (distributed on the joint surfaces) play a crucial role in conducting of virtual experiments.

2.5.3 Statistical processing of FEA-based data

Though the finite element analysis is based on strictly deterministic assumptions, it includes tedious computations that may generate some errors, which may be treated statistically. This idea is applied below in order to improve the identification accuracy and to detect the stiffness matrix elements that may be set to zero (in practice, the stiffness matrices with strictly zero elements are rather common).

Eliminating outliers. As noticed above, the FEA-modeling data may include some anomalous samples that do not obey the assumed statistical properties. This phenomenon has been detected in 2 of 6 experiments, (see Figure 2.11) where the histograms demonstrated obvious presence of the outliers changing the regular distribution shape (local maximums around the tails). For this reason, a straightforward filtering technique was applied that eliminated 10% the nodes corresponding to the highest residual values (see Figure 2.12). This technique essentially improved the identification accuracy, the maximum error for the compliance matrix elements reduced from 0.1% to 0.05%.

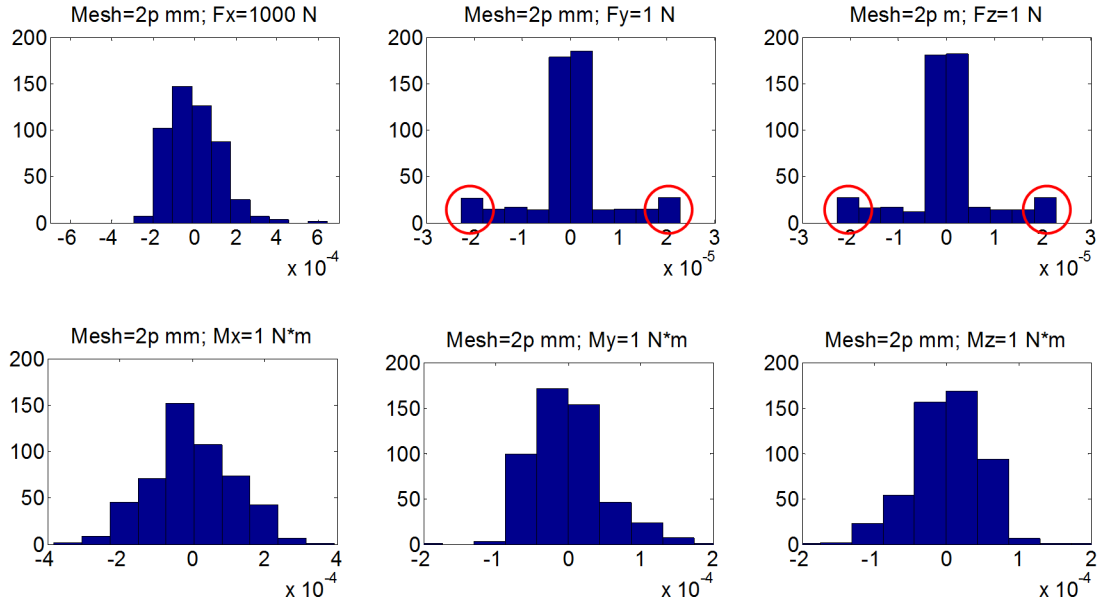

Figure 2.11 Residuals for stiffness model identification with parabolic mesh of 2 mm

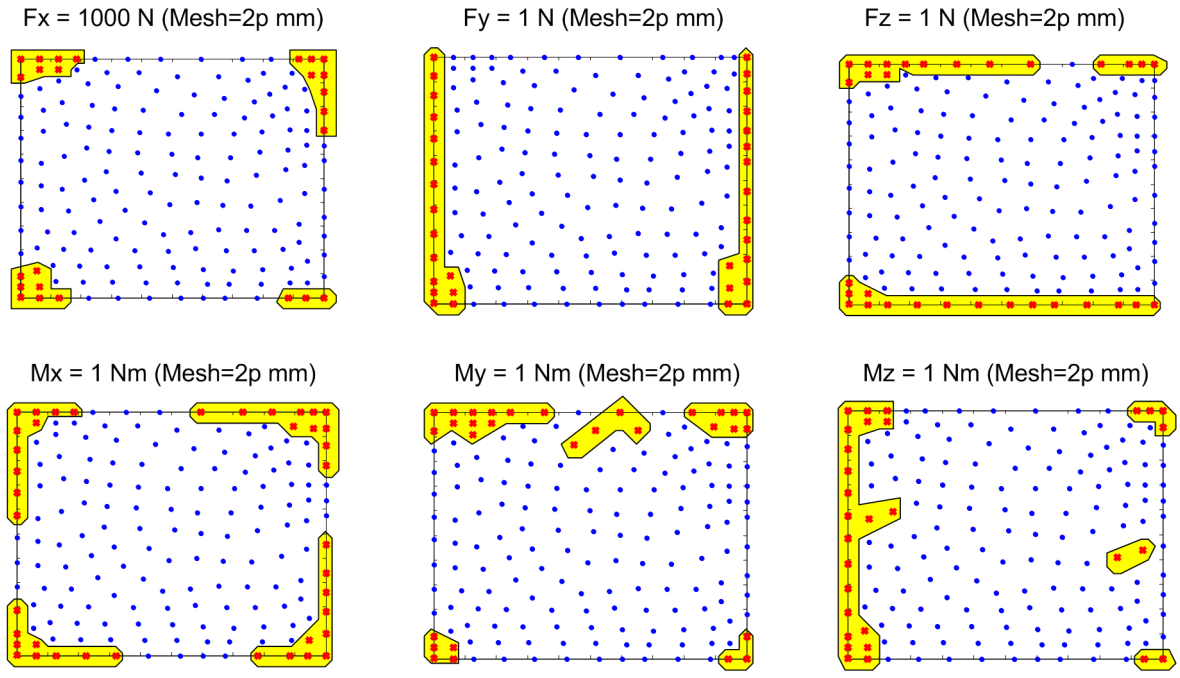

Figure 2.12 Filtering of the deflection field outliers

It is worth mentioning that here, because of the 3-dimensional nature of the problem, each node has been evaluated by three residuals and it was eliminated if any of these residuals was treated as an outlier. In addition, the detailed analysis showed that the outliers were concentrated at the beam edges, which confirms previous assumptions concerning the FEA-induced errors.

Eliminating non-significant elements. According to (2.23), the desired compliance matrix includes a number of zero elements (26 of 36), but the proposed identification procedure may produce some small non-zero values. To evaluate their statistical significance, for each element k_{ij} the confidence interval was computed. Relevant computations were performed using expressions for the variances of the deflections (2.21) and the s.t.d. value of the FEA-modeling noise, which was estimated as $\sigma = 5.6 \cdot 10^{-5}$ *mm* (by averaging for all 6 experiments). Then, the computed confidence intervals were scaled in accordance with (2.4), to be adopted to corresponding elements of the matrix **k** (this procedure involves simple division by the magnitude of the applied force or torque).

Using this approach, the compliance matrix was revised by assigning to zero all non-significant elements. The employed "decision support" algorithm treated an element as a non-significant one if its confidence interval included zero. As shown in Table 2.7, this technique allowed us to detect all 26 zero elements mentioned above. It should be also noted that all non-zero elements were evaluated as 'significant' ones, with essential 'safety factor' of 10^2 and higher.

Table 2.7 Eliminating non-significant elements

Parameter	Estimated value	CI	Exact value
k_{11}	$5.00 \cdot 10^{-5}$	$\pm 2.3 \cdot 10^{-8}$	$5.00 \cdot 10^{-5}$
k_{22}	$2.00 \cdot 10^{0}$	$\pm 2.4 \cdot 10^{-5}$	$2.00 \cdot 10^{0}$
k_{33}	$2.00 \cdot 10^{0}$	$\pm 2.4 \cdot 10^{-5}$	$2.00 \cdot 10^{0}$
k_{44}	$9.00 \cdot 10^{-6}$	$\pm 6.0 \cdot 10^{-9}$	$9.00 \cdot 10^{-6}$
k_{55}	$6.00 \cdot 10^{-6}$	$\pm 8.2 \cdot 10^{-9}$	$6.00 \cdot 10^{-6}$
k_{66}	$6.00 \cdot 10^{-6}$	$\pm 8.2 \cdot 10^{-9}$	$6.00 \cdot 10^{-6}$
k_{26}	$-3.00 \cdot 10^{-3}$	$\pm 2.4 \cdot 10^{-8}$	$-3.00 \cdot 10^{-3}$
k_{62}	$-3.00 \cdot 10^{-3}$	$\pm 8.5 \cdot 10^{-6}$	$-3.00 \cdot 10^{-3}$
k_{35}	$3.00 \cdot 10^{-3}$	$\pm 2.4 \cdot 10^{-8}$	$3.00 \cdot 10^{-3}$
k_{53}	$3.00 \cdot 10^{-3}$	$\pm 8.5 \cdot 10^{-6}$	$3.00 \cdot 10^{-3}$
k_{31}	$1.8 \cdot 10^{-8}$	$\pm 2.3 \cdot 10^{-8}$	0
k_{32}	$7.8 \cdot 10^{-6}$	$\pm 2.4 \cdot 10^{-5}$	0
k_{23}	$7.8 \cdot 10^{-6}$	$\pm 2.4 \cdot 10^{-5}$	0
k_{45}	$-6.2 \cdot 10^{-10}$	$\pm 8.4 \cdot 10^{-8}$	0
k_{54}	$-5.7 \cdot 10\text{-}^{10}$	$\pm 5.6 \cdot 10^{-8}$	0
k_{63}	$-6.7 \cdot 10^{-9}$	$\pm 2.4 \cdot 10^{-8}$	0

Remarks and comments. The presented illustrative example that deals with a classical element (cantilever beam) confirmed validity of the developed method but also demonstrated some limitations of the FEA-modeling with respect to the stiffness analysis. In particular, some (not very essential but non negligible) disagreement between numerical values of the applied forces/torques and their values extracted from the modeling protocol were detected. Besides, there are a number of non-trivial issues in defining modeling options that are normally set by default. All these factors contribute to the accuracy, but a practically acceptable level 0.1% can be achieved rather easily, using standard computing facilities. Some additional enhancement can be achieved symmetrizing the obtained matrix $\mathbf{k} := (\mathbf{k} + \mathbf{k}^T)/2$ that is motivated by the physical reasons.

2.6 STIFFNESS MATRIX FOR A DOUBLE-SIDE LOADED LINK

The above presented identification technique allows us to obtain stiffness matrices of size 6×6, which are common for the VJM-based modeling. These matrices describe the link stiffness behavior that is evaluated assuming that one of the link ends is fixed and the loading is applied to the second one. In mechanics, such arrangement is known as "cantilever beams" (Figure 2.13a). Though for kinematic chains studied in the following sections this assumption (fixing of one of the link ends) is not valid in strict sense. The stiffness model developed in the following chapters operate with 6×6 stiffness matrices only. This is achieved due to a special procedure of deriving the static equilibrium equations, where the links are considered sequentially, and one-by-one, assuming that each link is fixed in the previous joint and the loading is applied to the next one. This is an essential advantage of the VJM-modeling that operates with stiffness matrices of relatively small dimensions.

However, there is an alternative approach (the MSA-modeling) that operates with 12×12 stiffness matrices, which does not assume that any of the link ends is fixed. In contrast, it is assumed here that the links are subject to double-side loading and deflections are defined for both of this sides (Figure 2.13b). For such arrangement, the stiffness matrix should have size 12×12 because it defines the linear relations between two deflection vectors (of size 6 each) and two vectors of loading (of size 6 each). From a physical point of view, it is clear that both stiffness matrices (of size 6×6 and 12×12) describe the same properties of the link, while the smaller one contains exhaustive information on the stiffness. Hence, it is useful to obtain expressions that allow us to transform a 6×6 stiffness matrix into a 12×12 one, which is required for the MSA-modeling technique that usually deals with standard and simple link approximations (beams, truss, etc.).

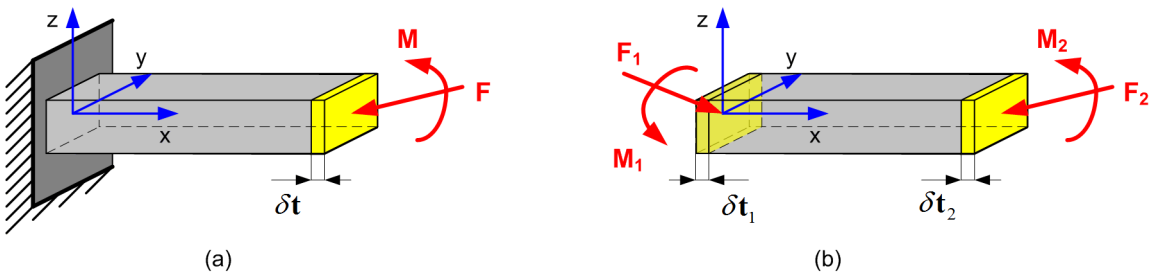

Figure 2.13 Physical models of cantilever beam (a) and double-side loaded beam (b)

To derive desired expressions, let us denote the above described stiffness matrices as $\mathbf{K}_{6\times6}$ and $\mathbf{K}_{12\times12}$. Let us also assume that the link geometry and its spatial location are defined by the vector $\mathbf{L}=(l_x, l_y, l_z)^{\mathrm{T}}$ connecting corresponding nodes. Besides taking into account that both of the matrices are symmetrical, it is convenient to present them in the block form as

$$\mathbf{K}_{6\times6}=\begin{bmatrix}\mathbf{K}_a & \mathbf{K}_b\\ \mathbf{K}_c & \mathbf{K}_d\end{bmatrix} \qquad \mathbf{K}_c=\mathbf{K}_b^{\mathrm{T}} \tag{2.26}$$

$$\mathbf{K}_{12\times12}=\begin{bmatrix}\mathbf{K}_{11} & \mathbf{K}_{12}\\ \mathbf{K}_{21} & \mathbf{K}_{22}\end{bmatrix}, \quad \mathbf{K}_{21}=\mathbf{K}_{12}^{\mathrm{T}},$$

$$\mathbf{K}_{ij}=\begin{bmatrix}\mathbf{K}_{ija} & \mathbf{K}_{ijb}\\ \mathbf{K}_{ijc} & \mathbf{K}_{ijd}\end{bmatrix} \quad \mathbf{K}_{ijc}=\mathbf{K}_{ijb}^{\mathrm{T}} \tag{2.27}$$

where $i=1,2$ and $j=1,2$.

Let us consider simultaneously two static equilibrium equations

$$\begin{bmatrix}\mathbf{F}\\ \mathbf{M}\end{bmatrix}=\begin{bmatrix}\mathbf{K}_a & \mathbf{K}_b\\ \mathbf{K}_c & \mathbf{K}_d\end{bmatrix}\cdot\begin{bmatrix}\delta\mathbf{p}\\ \delta\boldsymbol{\varphi}\end{bmatrix} \tag{2.28}$$

and

$$\begin{bmatrix}\mathbf{W}_1\\ \mathbf{W}_2\end{bmatrix}=\begin{bmatrix}\mathbf{K}_{11} & \mathbf{K}_{12}\\ \mathbf{K}_{21} & \mathbf{K}_{22}\end{bmatrix}\cdot\begin{bmatrix}\delta\mathbf{t}_1\\ \delta\mathbf{t}_2\end{bmatrix} \tag{2.29}$$

where the first one corresponds to the single-end loading (see Figure 2.13a) and the second equation corresponds to the double-side loading (see Figure 2.13b). Here, for the single-side loading case, $\mathbf{F}$ and $\mathbf{M}$ are the force and torque applied to the non-fixed link end, $\delta\mathbf{p}$ and $\delta\boldsymbol{\varphi}$ are translational and rotational deflections caused by external loading. Similarly, for the double-side loading case, $\mathbf{W}_1=(\mathbf{F}_1,\mathbf{M}_1)^{\mathrm{T}}$ and $\mathbf{W}_2=(\mathbf{F}_2,\mathbf{M}_2)^{\mathrm{T}}$ are the wrenches applied to the link ends, $\delta\mathbf{t}_1$ and $\delta\mathbf{t}_2$ are the deflections of corresponding link ends under the loadings $\mathbf{W}_1$ and $\mathbf{W}_2$. It is obvious that in both cases the model variables should satisfy the static equilibrium conditions, which eliminate some redundancy in notations for the second case.

To obtain desired matrices, let us assume first that for the double-side model $\delta\mathbf{t}_1=\mathbf{0}$. This allows us straightforwardly apply equation (2.28) and static equilibrium constrain that yield

$$\mathbf{W}_1=\begin{bmatrix}-\mathbf{F}\\ -\mathbf{M}+\mathbf{F}\times\mathbf{L}\end{bmatrix};\qquad \mathbf{W}_2=\begin{bmatrix}\mathbf{F}\\ \mathbf{M}\end{bmatrix};\qquad \delta\mathbf{t}_2=\begin{bmatrix}\delta\mathbf{t}\\ \delta\boldsymbol{\varphi}\end{bmatrix} \tag{2.30}$$

That leads to the following presentation of equation (2.29)

$$\begin{bmatrix}-\mathbf{F}\\ -\mathbf{M}+\mathbf{F}\times\mathbf{L}\\ \mathbf{F}\\ \mathbf{M}\end{bmatrix}=\begin{bmatrix}\mathbf{K}_{11} & \mathbf{K}_{12}\\ \mathbf{K}_{21} & \mathbf{K}_{22}\end{bmatrix}\cdot\begin{bmatrix}\mathbf{0}\\ \mathbf{0}\\ \delta\mathbf{p}\\ \delta\boldsymbol{\varphi}\end{bmatrix} \tag{2.31}$$

which leads to

$$\mathbf{K}_{22}=\mathbf{K}_{6\times 6} \tag{2.32}$$

Further, taking into account that $\mathbf{F}\times\mathbf{L}=-(\mathbf{L}\times)\cdot\mathbf{F}$ and using symmetrical properties of stiffness matrix,

$$\begin{gathered}\mathbf{K}_{12}=\begin{bmatrix}-\mathbf{K}_a & -\mathbf{K}_b\\ -\mathbf{K}_c-(\mathbf{L}\times)\cdot\mathbf{K}_a & -\mathbf{K}_d-(\mathbf{L}\times)\cdot\mathbf{K}_b\end{bmatrix};\\ \mathbf{K}_{21}=\mathbf{K}_{12}^{\mathrm{T}}=\begin{bmatrix}-\mathbf{K}_a & -\mathbf{K}_b+\mathbf{K}_a\cdot(\mathbf{L}\times)\\ -\mathbf{K}_c & -\mathbf{K}_d+\mathbf{K}_c\cdot(\mathbf{L}\times)\end{bmatrix}\end{gathered} \tag{2.33}$$

where

$$(\mathbf{L}\times)=\begin{bmatrix}0 & -l_z & l_y\\ l_z & 0 & -l_x\\ -l_y & l_x & 0\end{bmatrix} \tag{2.34}$$

Similarly, assuming that $\delta\mathbf{t}_2=\mathbf{0}$, the model (2.29) can be re-written using expressions

$$\mathbf{W}_1=\begin{bmatrix}\mathbf{F}\\ \mathbf{M}\end{bmatrix};\qquad \mathbf{W}_2=\begin{bmatrix}-\mathbf{F}\\ -\mathbf{M}+\mathbf{F}\times\mathbf{L}\end{bmatrix};\qquad \delta\mathbf{t}_1=\begin{bmatrix}\delta\mathbf{t}\\ \delta\boldsymbol{\varphi}\end{bmatrix} \tag{2.35}$$

and presented in the form

$$\begin{bmatrix}\mathbf{F}\\ \mathbf{M}\\ -\mathbf{F}\\ -\mathbf{M}+\mathbf{F}\times\mathbf{L}\end{bmatrix}=\begin{bmatrix}\mathbf{K}_{11} & \mathbf{K}_{12}\\ \mathbf{K}_{21} & \mathbf{K}_{22}\end{bmatrix}\cdot\begin{bmatrix}\delta\mathbf{p}_1\\ \delta\boldsymbol{\varphi}_1\\ \mathbf{0}\\ \mathbf{0}\end{bmatrix} \tag{2.36}$$

that after substitution of $\mathbf{K}_{12}$, $\mathbf{K}_{21}$, $\mathbf{K}_{22}$ and relevant transformations gives the following expression

$$\mathbf{K}_{11}=\begin{bmatrix}\mathbf{K}_a & \mathbf{K}_b-\mathbf{K}_a\cdot(\mathbf{L}\times)\\ \mathbf{K}_c+(\mathbf{L}\times)\cdot\mathbf{K}_a & \mathbf{K}_d-\mathbf{K}_c\cdot(\mathbf{L}\times)+(\mathbf{L}\times)\cdot\mathbf{K}_b-(\mathbf{L}\times)\cdot\mathbf{K}_a\cdot(\mathbf{L}\times)\end{bmatrix} \tag{2.37}$$

Finally, integrating all sub-matrices, the desired matrix of size 12×12 can be presented in the form

$$\mathbf{K}_{12\times12}=\left[\begin{array}{cc:cc}\mathbf{K}_a & \mathbf{K}_b-\mathbf{K}_a\cdot(\mathbf{L}\times) & -\mathbf{K}_a & -\mathbf{K}_b\\ \mathbf{K}_c+(\mathbf{L}\times)\cdot\mathbf{K}_a & \mathbf{K}_d-\mathbf{K}_c\cdot(\mathbf{L}\times)+(\mathbf{L}\times)\cdot\mathbf{K}_b-(\mathbf{L}\times)\cdot\mathbf{K}_a\cdot(\mathbf{L}\times) & -\mathbf{K}_c-(\mathbf{L}\times)\cdot\mathbf{K}_a & -\mathbf{K}_d-(\mathbf{L}\times)\cdot\mathbf{K}_b\\ -\mathbf{K}_a & -\mathbf{K}_b+\mathbf{K}_a\cdot(\mathbf{L}\times) & \mathbf{K}_a & \mathbf{K}_b\\ -\mathbf{K}_c & -\mathbf{K}_d+\mathbf{K}_c\cdot(\mathbf{L}\times) & \mathbf{K}_c & \mathbf{K}_d\end{array}\right] \tag{2.38}$$

which includes elements of $\mathbf{K}_{6\times6}$ and the link's geometrical parameters $(\mathbf{L}\times)$ only.

Therefore, the stiffness matrix identification technique developed in sections 2.1-2.5, can also produce 12×12 matrices required for the manipulator stiffness modeling based on the MSA-approach. This also enhances previous results of [Deblaise 2006b] where the manipulator topology was quite general (parallel and with cross-linkage), but the links stiffness properties were described rather roughly.

2.7 Application example: stiffness matrices for Orthoglide links

Let us apply the proposed methodology to the identification of the link stiffness matrices for a parallel manipulator of Orthoglide family [Chablat 2003]. The principal components of the manipulator are presented in Figure 2.14, where the elements (b, e, f) are treated as flexible ones and the element (c) is assumed to be rigid. In previous works, relevant stiffness matrices have been obtained either via single-beam approximation [Majou 2007] or by using FEA-based identification procedure with linear meshing option [Pashkevich 2010]. Besides, joints particularities have not been taken into account and their influence on the elements of the stiffness matrix was not studied. Hence, it is quite possible that some stiffness matrix elements have been identified with essential errors.

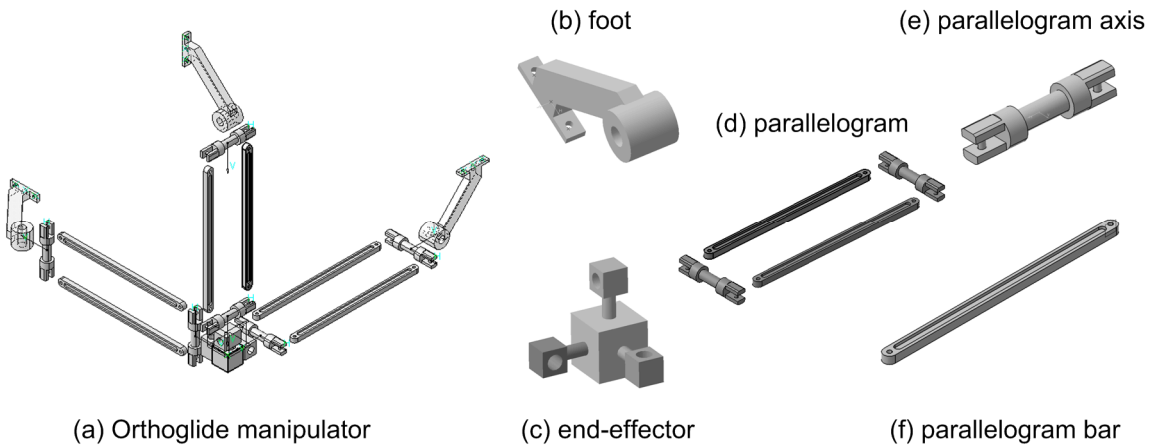

Figure 2.14 CAD model of Orthoglide and its principal components:
Orthoglide (a), foot (b), end-effector (c), parallelogram (d), parallelogram axis (e) and bar (f)

In accordance with sub-section 2.5.1, the FEA-based virtual experiments were performed using the parabolic mesh of size 2 mm (2P in Figure 2.9) and the test forces/torques of 1 N and 1 N·m respectively,

which, for considered link size and material properties, correspond to the area of linear force-deflection relation (see 0). As it follows from Table 2.5, such settings ensure accuracy of about 0.1%. Identification results are presented in Table 2.8, where the obtained matrices include a number of zero elements that were detected using the technique presented in sub-section 2.5.2. It is also worth mentioning that these matrices are symmetrical, which confirms validity of the developed method.

For comparison purposes, similar matrices have been computed using other methods (single- and multi-beam approximations, the FEA-modeling with linear meshing). They are presented in Table 2.9 and show essential dissimilarity in the evaluation of some matrix elements by different methods. For instance, for the parallelogram bar (i.e., link (f) in 0), the torsional compliance defined by the element k_{44} differs by a factor of 13. The main reason for this is that the developed technique takes into account the joint particularities that define the force distribution rule for the applied loadings (previous results assumed that the loading was localized in the reference point). However, the final conclusion concerning accuracy of the obtained stiffness matrices can be obtained after integration of these matrices in the stiffness model of the entire manipulator and comparing it with a straightforward FEA-modeling of the manipulator assembly.

Hence, presented examples confirm advantages of the developed stiffness matrix identification technique and demonstrate its ability to take into account complex link shapes as well as joint particularities related to the force/torque distribution. In addition, it produces symmetrical matrices with some zero elements in accordance with physical properties of the considered manipulator components. In the following chapters, these matrices will be used for the VJM-based stiffness modeling of parallel manipulators.

Table 2.8 Compliance matrices of Orhoglide links

Link	Compliance matrix
foot	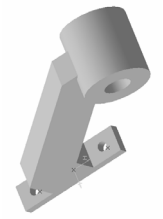 $k_{Foot} = \begin{bmatrix} 2.77\cdot10^{-4} & -3.28\cdot10^{-4} & 0 & 0 & 0 & -4.03\cdot10^{-6} \\ -3.28\cdot10^{-4} & 4.14\cdot10^{-4} & 0 & 0 & 0 & 5.41\cdot10^{-6} \\ 0 & 0 & 1.94\cdot10^{-3} & 1.12\cdot10^{-5} & -1.49\cdot10^{-5} & 0 \\ 0 & 0 & 1.12\cdot10^{-5} & 2.29\cdot10^{-7} & 0 & 0 \\ 0 & 0 & -1.49\cdot10^{-5} & 0 & 2.30\cdot10^{-7} & 0 \\ -4.03\cdot10^{-6} & 5.41\cdot10^{-6} & 0 & 0 & 0 & 8.42\cdot10^{-8} \end{bmatrix}$
axis	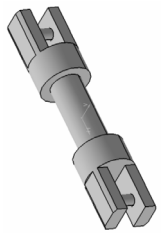 $k_{Axis} = \begin{bmatrix} 6.23\cdot10^{-6} & 0 & 0 & 0 & 0 & 0 \\ 0 & 2.83\cdot10^{-5} & 0 & 0 & 0 & 1.40\cdot10^{-7} \\ 0 & 0 & 2.59\cdot10^{-5} & 0 & -9.65\cdot10^{-7} & 0 \\ 0 & 0 & 0 & 2.77\cdot10^{-7} & 0 & 0 \\ 0 & 0 & -9.65\cdot10^{-7} & 0 & 4.84\cdot10^{-7} & 0 \\ 0 & 1.40\cdot10^{-7} & 0 & 0 & 0 & 1.20\cdot10^{-7} \end{bmatrix}$
bar	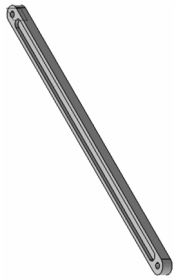 $k_{Bar} = \begin{bmatrix} 4.55\cdot10^{-5} & 0 & 0 & 0 & 0 & 0 \\ 0 & 2.33\cdot10^{-1} & 0 & 0 & 0 & 1.13\cdot10^{-4} \\ 0 & 0 & 5.08\cdot10^{-2} & 0 & -2.39\cdot10^{-4} & 0 \\ 0 & 0 & 0 & 2.88\cdot10^{-5} & 0 & 0 \\ 0 & 0 & -2.39\cdot10^{-4} & 0 & 1.50\cdot10^{-6} & 0 \\ 0 & 1.13\cdot10^{-3} & 0 & 0 & 0 & 7.19\cdot10^{-6} \end{bmatrix}$

Table 2.9 Comparison of the compliance matrix elements obtained from different methods

Method	Compliance matrix elements					
	k_{11} [mm/N]	k_{22} [mm/N]	k_{33} [mm/N]	k_{44} [rad/N·mm]	k_{55} [rad/N·mm]	k_{66} [rad/N·mm]
Link (b): foot						
Single-beam approximation	$3.45 \cdot 10^{-4}$	$3.45 \cdot 10^{-4}$	$18.1 \cdot 10^{-4}$	$2.10 \cdot 10^{-7}$	$2.10 \cdot 10^{-7}$	$0.91 \cdot 10^{-7}$
Four-beam approximation	$2.77 \cdot 10^{-4}$	$4.34 \cdot 10^{-4}$	$17.9 \cdot 10^{-4}$	$2.11 \cdot 10^{-7}$	$1.95 \cdot 10^{-7}$	$0.91 \cdot 10^{-7}$
FEA-based evaluation (linear mesh)	$2.45 \cdot 10^{-4}$	$3.24 \cdot 10^{-4}$	$15.9 \cdot 10^{-4}$	$2.07 \cdot 10^{-7}$	$2.06 \cdot 10^{-7}$	$1.71 \cdot 10^{-7}$
FEA-based evaluation (parabolic mesh)	$2.77 \cdot 10^{-4}$	$4.15 \cdot 10^{-4}$	$19.4 \cdot 10^{-4}$	$2.29 \cdot 10^{-7}$	$2.30 \cdot 10^{-7}$	$0.84 \cdot 10^{-7}$
Link (e): parallelogram axis						
Single beam approximation	$1.34 \cdot 10^{-6}$	$2.65 \cdot 10^{-5}$	$2.65 \cdot 10^{-5}$	$4.29 \cdot 10^{-8}$	$3.18 \cdot 10^{-8}$	$3.18 \cdot 10^{-8}$
FEA-based evaluation (linear mesh)	$1.99 \cdot 10^{-6}$	$1.29 \cdot 10^{-5}$	$1.50 \cdot 10^{-5}$	$6.81 \cdot 10^{-6}$	$8.23 \cdot 10^{-6}$	$2.67 \cdot 10^{-6}$
FEA-based evaluation (parabolic mesh)	$6.23 \cdot 10^{-6}$	$2.83 \cdot 10^{-5}$	$2.59 \cdot 10^{-5}$	$2.77 \cdot 10^{-7}$	$4.84 \cdot 10^{-7}$	$1.20 \cdot 10^{-7}$
Link (f): parallelogram bar						
Single-beam approximation	$3.75 \cdot 10^{-5}$	$4.38 \cdot 10^{-2}$	$1.09 \cdot 10^{-1}$	$3.96 \cdot 10^{-6}$	$3.40 \cdot 10^{-6}$	$1.37 \cdot 10^{-6}$
FEA-based evaluation (linear mesh)	$4.50 \cdot 10^{-5}$	$3.64 \cdot 10^{-2}$	$8.01 \cdot 10^{-2}$	$3.76 \cdot 10^{-6}$	$2.65 \cdot 10^{-6}$	$1.09 \cdot 10^{-6}$
FEA-based evaluation (parabolic mesh)	$4.55 \cdot 10^{-5}$	$5.08 \cdot 10^{-2}$	$2.33 \cdot 10^{-1}$	$2.88 \cdot 10^{-5}$	$7.19 \cdot 10^{-6}$	$1.50 \cdot 10^{-6}$

2.8 SUMMARY

The chapter is devoted to the development of the FEA-based methodology for stiffness matrix identification of the manipulator links with the complex shape. The main contributions are in the areas of virtual experiments planning and algorithmic data processing that produce the desired stiffness matrix with required accuracy. In contrast to other works, the developed technique operates with the deflection field in the neighborhood of the reference point, which provides higher identification accuracy (about 0.1% for stiffness matrix element). In addition, it allows us to estimate confidence intervals for the matrix elements and to set to zero non-significant ones.

In more details, new results and contributions of Chapter 2 can be formulated as

(i) FEA-based methodology for stiffness matrix identification, which allows to evaluate the stiffness matrix from the deflection field produced by virtual experiments in a CAD environment, taking into account the link shape, coupling between rotational/translational deflections and joint particularities

(ii) Numerical technique for computing the stiffness matrix from the deflection field extracted from FEA-based virtual experiments; comparative study of several versions (SVD-based, LIN-based etc.) with respect to computational efficiency and speed.

(iii) Analytical expressions for accuracy evaluation of the developed identification technique, which allow to determine the optimal settings for the FEA-based experiments and to improve the identification accuracy

(iv) Technique for statistical processing of the experimental data, which allows us to minimise the identification errors by eliminating outliers, to determine the confidence intervals and to detect "zero" elements of the stiffness matrix.

(v) Application of the developed technique to case studies (Orthoglide links) and comparison with previous methods (based on approximated models), which confirmed advantages of the developed method: reduction of errors in significant elements of the stiffness matrix from 20-50% to 0.1%

In spite of the fact that the developed technique produces 6×6 stiffness matrices (which are used in the VJM method), it is also useful to the MSA-based modeling that operates with matrices of the size 12×12. Required transformation is performed using the derived analytical expressions that are applicable in general cases. Thus, the developed identification technique allows us to increase the accuracy of both methods, the VJM- and the MSA-based ones.

Besides, this technique can be efficiently applied not only to separate links but also to the entire manipulators, whose stiffness is evaluated through the FEA-modeling. In the case of constrained and over-constrained manipulator, this application is straightforward. While for under-constrained manipulators, the CAD model should be slightly modified by introducing an additional constraint.

Concerning limitations of the developed technique, they are related to the use of the lumped presentation for the stiffness of the manipulator link, whose properties are distributed by its nature. It is obvious that such idealization can be justified for some range of force/torque only. Moreover, the obtained stiffness matrices correspond to the linear model, whose applicability is also limited. However, as it will be shown in the following sections, the VJM-model of the entire manipulator may demonstrate essentially non-linear behavior (though the stiffness of each link is described by a linear model).

Main results of Chapter 2 are published in the following works: [Klimchik 2009b], [Klimchik 2011b].

CHAPTER 3

STIFFNESS MODELING OF MANIPULATORS WITH PASSIVE JOINTS IN UNLOADED MODE

This chapter is devoted to the enhancement of the VJM-based stiffness modeling technique for serial and parallel manipulators with arbitrary location of passive joints in the case of small deflections (unloaded mode). It proposes computationally efficient procedure, which is able to produce singular and non-singular Cartesian stiffness matrix for the kinematic chain both in numerical and in an analytical form. This allows to extend the classical stiffness mapping equation for the case of manipulators with passive joints and to evaluate stiffness matrix properties analytically. It also proposes a new aggregation technique, which is able to take into account the geometry of the mobile platform and to compute internal deflections and forces/torques as well as the displacement of the end-platform caused by geometrical errors in the kinematic chains. The developed stiffness analysis technique is illustrated by several examples, which deal with parallel manipulators.

3.1 INTRODUCTION

Stiffness of an industrial manipulator is one of the most important performance indicators in any applications [Park 2008] [Angeles 2008] [Luca 2008]. For industrial robots the primary target is an accurate location of a technological tool during workpiece processing, while manipulator compliance introduces positioning errors arising due to the external loading during machining. Similarly, in the fast pick-and-place manipulations the stiffness defines admissible velocity and acceleration in order to avoid undesirable displacements due to inertia forces [Nof 1999]. In the case of large robotic manipulators, elastic deformations of mechanical components under the task load (and under own link-weight) also introduce

significant position errors [Meggiolaro 2005]. It is obvious that in all of these cases, the desired stiffness should be high enough to meet the requirements of the relevant application.

Similar to the general structural mechanics [Timoshenko 1970] [Hjelmstad 1997], the robot stiffness analysis evaluates the manipulator resistance to the deformations caused by an external force/torque applied to the end-effector [Duffy 1996]. As it follows from Chapter 1, in robotics the stiffness modeling is usually based on the *Virtual Joint Method* (VJM), which describes flexible elements as rigid, while a localized virtual spring located in the manipulator joints take into account it compliance. Manipulator stiffness, as well as other manipulator properties (kinematical, for instance), depend on the manipulator configuration [Alici 2005]. Moreover, in general, the force-deflection relation is nonlinear, while for small deformations or so called unloaded mode (which is normally in the engineering practice it is considered as an operational condition), they can be approximated by the linear function. Numerically this property is defined by the stiffness matrix **K** (or the compliance matrix **k**), which gives the linear relation between end-effector displacement and external loading which cause this transition (assuming that all of them are small enough) [Koseki 2000]. As it follows from related works, for the conservative systems, that are considered in this work, stiffness matrix **K** is 6×6 semi-definite non-negative symmetrical matrix but to represent the coupling between the translation and rotation its structure may be non-diagonal.

In robotics 6×6 stiffness matrix **K** is usually referred to as the Cartesian Stiffness Matrix $\mathbf{K}_C$ and it should be distinguished from the "Joint-Space Stiffness Matrix" $\mathbf{K}_\theta$ that describes forces-deflections relation in the joint coordinates [Ciblak 1999]. These stiffness matrices can be mapped to each other using the Conservative Congruency Transformation [Chen 2000a]. Mathematical background for this computation originates from the work of Salisbury [Salisbury 1980] who derived a closed-form expression for the Cartesian stiffness matrix of a serial manipulator assuming that the mechanical elasticity is concentrated in the actuated joints. Retaining this assumption, Gosselin [Gosselin 1990] extended this result for the case of parallel manipulators (where the links were assumed to be rigid, and the passive joints to be perfect). Further development of this approach allowed to take into account links stiffness by supplementating the rigid beam with linear and torsional springs [Gosselin 2002]. Recent modification of VJM-modelling proposed by Pashkevich et. al. [Pashkevich 2010] and further developed in this thesis (see Chapter 2 for details) deals with 6×6 stiffness matrices which are computed from FEA experiments and are able to take into account couplings between translational and rotational deflections, the real shape of complex link and joints particularities. The latter essentially increased accuracy of the VJM-modeling while preserving its high computational efficiency. At present, there are different variations of VJM, which differ in modeling assumptions and numerical techniques [Majou 2007], [Corradini 2002]. They were developed for different kinematic architectures [Company 2002], [Arumugan 2004], but there are still a number of open questions that are considered in this Chapter.

Currently, most of the related works are devoted to stiffness modeling of *serial chains*. They include both stiffness analysis of classical serial manipulators (without passive joints) [Salisbury 1980], [Ciblak 1999], [Pigoski 1998] and also some results for serial chains with passive joints. In particular, in [Pashkevich 2010] an algorithmic solution has been proposed. This solution is capable of producing rank-deficient stiffness matrices. In spite of its computational simplicity, the method is not able to produce an analytical expression for the desired matrix. This limitation motivates us to revise this technique. Also it is useful to evaluate impact of passive joints on the separate elements of the stiffness matrix.

For *parallel manipulators*, stiffness modelling is usually performed for all kinematic chains simultaneously [Gosselin 1990] [Wei 2010], using the aggregated elastostatic equilibrium equations [Yi 1993], [Quennouelle 2008b]. In contrast to these works, our approach is based on a two-step procedure, which includes stiffness modelling of all kinematic chains *separately* and then *aggregates* them in a unique model. This approach has been used by several authors [Zhang 2004], [Xi 2004], [Pashkevich 2010], but related aggregation technique was reduced to simple summations of Cartesian stiffness matrices for the kinematic chains and the external loadings applied to their end-points. This corresponds to "pure" parallel architectures where the end-point location of all kinematic chains are aligned and matched at the end-platform reference point. Besides, in this work it has been implicitly assumed that the kinematic chains are perfect, i.e. their geometrical parameters are strictly nominal and the parallel manipulator can be assembled without additional internal stresses. However, in practice, the parallel manipulator architecture is usually

quite complex. In particular, the kinematic chains may be attached to different points of the end-platform. Besides the kinematic chain geometry usually differs from the nominal one, which causes some internal forces/torques while assembling. These motivate further development of the stiffness model aggregation technique for parallel manipulators.

Hence, as it follows from the above analysis, the manipulator stiffness modeling for unloaded mode needs further improvement. So, the goal of this chapter is the enhancement of VJM-based stiffness modeling technique for serial and parallel manipulators with arbitrary location of passive joints in the case of small deflections (unloaded mode). To achieve this goal, several sub-problems have to be solved:

(i) Enhancement of the VJM-based stiffness modeling technique for small deformations on the case of serial chains with the arbitrary location of passive joints

(ii) Investigation of a passive joints influence on the stiffness matrix elements and development of analytical technique for the relevant stiffness matrix modification (for serial kinematic chain);

(iii) Development of the stiffness model-assembling technique that allows to aggregate the elastostatic models of separate kinematic chains in the stiffness model of the parallel manipulator and to evaluate the deflections and the internal forces/torques caused by the geometrical errors in the chains

To address these sub-problems, the remainder of this chapter is organised as follows. Section 3.2 deals with numerical computing of the stiffness matrix and evaluating of internal deflections for serial chains with passive joints. Section 3.3 proposes an analytical solution of the problem. Further, Sections 3.4 and 3.5 focus on stiffness modelling of parallel manipulators, where the stiffness model aggregation technique is proposed for both perfect and non-perfect serial chains. And finally, Section 3.6 summarises main results and contributions of this Chapter.

3.2 STIFFNESS MODELING OF SERIAL CHAIN OF PARALLEL MANIPULATOR

Typical examples of the examined kinematic chains can be found in the 3-PUU translational parallel kinematic machine [Li 2008], in the Delta parallel robot [Clavel 1988] or in the parallel manipulators of the Orthoglide family [Chablat 2003] and other manipulators [Merlet 2006] (see Figure 3.1). It is worth mentioning that here a specific spatial arrangement of under-constrained chains yields the over-constrained mechanism that posses a high structural rigidity with respect to the external force. In particular, for Orthoglide, each kinematic chain prevents the platform from rotating around two orthogonal axes and any combination of two kinematic chains suppresses all possible rotations of the platform. Hence, the whole set of three kinematic chains produces a non-singular stiffness matrix while for each separate chain the stiffness matrix is singular. This motivated the development of dedicated stiffness analysis techniques that are presented below.

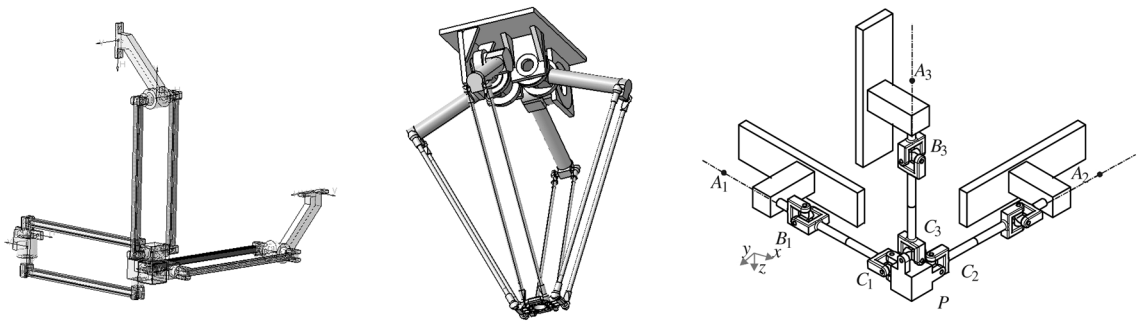

(a) Orthoglide manipulator (b) Fatronik manipulator (c) 3-PUU-manipulator

Figure 3.1 Architecture of typical parallel manipulators and their kinematics chains

3.2.2 Serial chain with passive joints and its VJM-model

Let us consider a general serial kinematic chain, which consists of a fixed "Base", a number of flexible actuated joints "Ac", a serial chain of flexible "Links", a number of passive joints "Ps" and a moving "Platform" at the end of the chain (Figure 3.2). It is assumed that all links are separated by joints (actuated or passive, rotational or translational) and the joint type order is arbitrary. Besides, it is admitted that some links may be separated by actuated and passive joints simultaneously. Such architecture can be found in most of the parallel manipulators (Figure 3.1) where several similar kinematic chains are connected to the same base and the platform in a different way (with the rotation of 90° or 120°, for instance), in order to eliminate the redundancy caused by the passive joints. It is obvious that such kinematic chains are statically *under-constrained* and their stiffness analysis cannot be performed by the direct application of the standard methods.

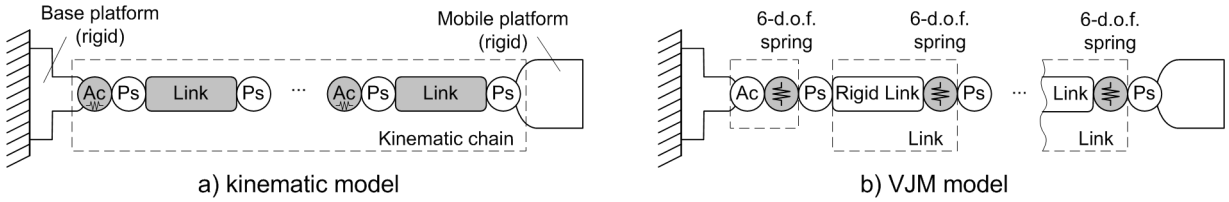

Figure 3.2 General serial kinematic chain and its VJM model (Ac – actuated joint, Ps – passive joint).

In order to evaluate the stiffness of the considered serial chain, let us apply a modification of the virtual joint method (VJM), which is based on the lump modelling approach [Gosselin 1990]. According to this approach, the original rigid model should be extended by adding virtual joints (localized springs), which describe elastic deformations of the links. Besides, virtual springs are included in the actuating joints, to take into account the stiffness of the control loop. Under such assumptions, the kinematic chain can be described by the following serial structure:

(a) a rigid link between the manipulator base and the first actuating joint described by the constant homogenous transformation matrix $\mathbf{T}_{\text{Base}}$;

(b) the 6-d.o.f. actuating joints defining three translational and three rotational actuator coordinates, which are described by the homogenous matrix function $\mathbf{T}_{3\text{D}}(\boldsymbol{\theta}_{\text{a}}^{i})$ where $\boldsymbol{\theta}_{\text{a}}^{i} = (\theta_{\text{x}}^{ai}, \theta_{\text{y}}^{ai}, \theta_{\text{z}}^{ai}, \theta_{\varphi\text{x}}^{ai}, \theta_{\varphi\text{y}}^{ai}, \theta_{\varphi\text{z}}^{ai})$ are the virtual spring coordinates;

(c) the 6-d.o.f. passive joints defining three translational and three rotational passive joints coordinates, which are described by the homogenous matrix function $\mathbf{T}_{3\text{D}}(\mathbf{q}_{\text{p}}^{i})$ where $\mathbf{q}_{\text{p}}^{i} = (q_{\text{x}}^{i}, q_{\text{y}}^{i}, q_{\text{z}}^{i}, q_{\varphi\text{x}}^{i}, q_{\varphi\text{y}}^{i}, q_{\varphi\text{z}}^{i})$ are the passive joint coordinates;

(d) the rigid links, which are described by the constant homogenous transformation matrix $\mathbf{T}_{\text{Link}}^{i}$;

(e) a 6-d.o.f. virtual joint defining three translational and three rotational link-springs, which are described by the homogenous matrix function $\mathbf{T}_{3\text{D}}(\boldsymbol{\theta}_{\text{Link}}^{i})$, where $\boldsymbol{\theta}_{\text{Link}}^{i} = (\theta_{\text{x}}^{i}, \theta_{\text{y}}^{i}, \theta_{\text{z}}^{i}, \theta_{\varphi\text{x}}^{i}, \theta_{\varphi\text{y}}^{i}, \theta_{\varphi\text{z}}^{i})$, $(\theta_{\text{x}}^{i}, \theta_{\text{y}}^{i}, \theta_{\text{z}}^{i})$ and $(\theta_{\varphi\text{x}}^{i}, \theta_{\varphi\text{y}}^{i}, \theta_{\varphi\text{z}}^{i})$ correspond to the elementary translations and rotations respectively;

(f) a rigid link from the last link to the end-effector, described by the homogenous matrix transformation $\mathbf{T}_{\text{Tool}}$.

In the frame of these notations, the final expression defining the end-effector location subject to variations of all joint coordinates of a single kinematic chain may be written as the product of the following homogenous matrices

$$\mathbf{T} = \mathbf{T}_{\text{Base}} \cdot \prod_{i} \left(\mathbf{T}_{3\text{D}}\left(\boldsymbol{\theta}_{\text{a}}^{i}\right) \cdot \mathbf{T}_{3\text{D}}\left(\mathbf{q}_{\text{p}}^{2i-1}\right) \cdot \mathbf{T}_{\text{Link}}^{i} \cdot \mathbf{T}_{3\text{D}}\left(\boldsymbol{\theta}_{\text{Link}}^{i}\right) \cdot \mathbf{T}_{3\text{D}}\left(\mathbf{q}_{\text{p}}^{2i}\right) \right) \cdot \mathbf{T}_{\text{Tool}} \tag{3.1}$$

where the components $\mathbf{T}_{\text{Base}}$, $\mathbf{T}_{\text{3D}}(...)$, $\mathbf{T}^{i}_{\text{Link}}$, $\mathbf{T}_{\text{Tool}}$ may be factorized with respect to the terms including the joint variables, in order to simplify computing of the derivatives (Jacobian and Hessian).

This expression includes both traditional geometric variables (passive and active joint coordinates) and stiffness variables (virtual joint coordinates). The explicit position and orientation of the end-effector can by extracted from the matrix $\mathbf{T}$ in a standard way [Angeles 2007], so finally the kinematic model can be rewritten as the vector function

$$\mathbf{t} = \mathbf{g}(\mathbf{q}, \boldsymbol{\theta}) \tag{3.2}$$

where the vector $\mathbf{t} = (\mathbf{p}, \boldsymbol{\varphi})^{\mathrm{T}}$ includes the position $\mathbf{p} = (x, y, z)^{\mathrm{T}}$ and orientation $\boldsymbol{\varphi} = (\varphi_{\mathrm{x}}, \varphi_{\mathrm{y}}, \varphi_{\mathrm{z}})^{\mathrm{T}}$ of the end-platform, the vector $\mathbf{q} = (q_1, q_2, ..., q_{\mathrm{nq}})^{T}$ contains all passive joint coordinates, the vector $\boldsymbol{\theta} = (\theta_1, \theta_2, ..., \theta_{\mathrm{n}\theta})^{\mathrm{T}}$ collects all virtual joint coordinates, n_{q} is the number of the passive joins, n_{θ} is the number of the virtual joints.

3.2.3 Cartesian stiffness matrix of a serial chain

For the serial chain the unloaded configuration can be defined as $\mathbf{t}_0 = f(\mathbf{q}_0, \boldsymbol{\theta}_0)$, where $\mathbf{q}_0$ is computed via the inverse kinematic and $\boldsymbol{\theta}_0$ is equal to zero (since there are no preloads in the springs). Let us assume that the external force $\mathbf{F}$ relocates the manipulator to the position $\mathbf{t} = f(\mathbf{q}_0 + \Delta\mathbf{q}, \boldsymbol{\theta}_0 + \Delta\boldsymbol{\theta})$, which for small displacements may be expressed as

$$\mathbf{t} = \mathbf{t}_0 + \mathbf{J}_{\theta} \cdot \Delta\boldsymbol{\theta} + \mathbf{J}_{\mathrm{q}} \cdot \Delta\mathbf{q} \tag{3.3}$$

where $\mathbf{J}_{\theta} = \partial f(\mathbf{q}, \boldsymbol{\theta}) / \partial \boldsymbol{\theta}$ and $\mathbf{J}_{\mathrm{q}} = \partial f(\mathbf{q}, \boldsymbol{\theta}) / \partial \mathbf{q}$ are the kinematic Jacobians with respect to the coordinates $\boldsymbol{\theta}$, $\mathbf{q}$, which may be computed from (3.1) analytically or semi-analytically, using the factorization technique proposed in [Pashkevich 2010].

For the kinetostatic model, which describes the force-and-motion relation, it is necessary to introduce additional equations that define the virtual joint reactions to the corresponding spring deformations. For analytical convenience, all relevant expressions may be collected in a single matrix equation

$$\boldsymbol{\tau}_{\theta} = \mathbf{K}_{\theta} \cdot \boldsymbol{\theta} \tag{3.4}$$

where $\boldsymbol{\tau}_{\theta} = (\tau_{\theta,1}, \tau_{\theta,2}, ..., \tau_{\theta,\mathrm{n}\theta})^{\mathrm{T}}$ is the aggregated vector of the virtual joint reactions, $\mathbf{K}_{\theta} = diag(\mathbf{K}_{\theta,1}, \mathbf{K}_{\theta,2}, ..., \mathbf{K}_{\theta,\mathrm{n}\theta})$ is the aggregated spring stiffness matrix of the size $n_{\theta} \times n_{\theta}$, and $\mathbf{K}_{\theta,i}$ is the spring stiffness matrix of the corresponding link. Similarly, one can define the aggregated vector of the passive joint reactions $\boldsymbol{\tau}_{\mathrm{q}} = (\tau_{\mathrm{q},1}, \tau_{\mathrm{q},2}, ..., \tau_{\mathrm{q},\mathrm{nq}})^{\mathrm{T}}$ but, at the equilibrium, all its components must be equal to zero ($\boldsymbol{\tau}_{\mathrm{q}} = \mathbf{0}$).

Further, let us apply the principle of virtual work assuming that the joints are given small, arbitrary virtual displacements $\Delta\boldsymbol{\theta}$ in the equilibrium neighborhood. Then, the virtual work of the external force $\mathbf{F}$ applied to the end-effector along the corresponding displacement $\Delta\mathbf{t} = \mathbf{J}_{\theta} \cdot \Delta\boldsymbol{\theta} + \mathbf{J}_{\mathrm{q}} \cdot \Delta\mathbf{q}$ is equal to the sum $(\mathbf{F}^{\mathrm{T}} \cdot \mathbf{J}_{\theta}) \cdot \Delta\boldsymbol{\theta} + (\mathbf{F}^{\mathrm{T}} \cdot \mathbf{J}_{\mathrm{q}}) \cdot \Delta\mathbf{q}$. For the internal forces, the virtual work includes only one component $-\boldsymbol{\tau}_{\theta}{}^{\mathrm{T}} \cdot \Delta\boldsymbol{\theta}$, since the passive joints do not produce the force/torque reactions (the minus sign takes into account the adopted directions for the virtual spring forces/torques). Therefore, since in the static equilibrium the total virtual work is equal to zero for any virtual displacement, the equilibrium conditions may be written as

$$\mathbf{J}_{\theta}{}^{\mathrm{T}} \cdot \mathbf{F} = \boldsymbol{\tau}_{\theta}; \quad \mathbf{J}_{\mathrm{q}}{}^{\mathrm{T}} \cdot \mathbf{F} = \boldsymbol{\tau}_{\mathrm{q}} \tag{3.5}$$

This gives additional expressions describing the force/torque propagation from the joints to the end-effector.

Hence, the complete kinetostatic model consists of four matrix equations (3.3)-(3.5) where either $\mathbf{F}$ or $\Delta\mathbf{t}$ are treated as known, and the remaining variables are considered as unknown. Thus, relevant equations of statics may be written as

$$\mathbf{J}_{\theta} \cdot \boldsymbol{\theta} + \mathbf{J}_{\mathrm{q}} \cdot \Delta\mathbf{q} = \Delta\mathbf{t}; \qquad \mathbf{F} \cdot \mathbf{J}_{\theta}{}^{\mathrm{T}} - \mathbf{K}_{\theta} \cdot \boldsymbol{\theta} = 0; \qquad \mathbf{F} \cdot \mathbf{J}_{\mathrm{q}}{}^{\mathrm{T}} = 0 \tag{3.6}$$

here $\Delta\mathbf{t} = \mathbf{t} - \mathbf{t}_0$, and the general relation between the increments $\mathbf{F}$, $\Delta\mathbf{t}$, $\boldsymbol{\theta}$, $\mathbf{q}$ can be presented as

$$\begin{bmatrix} \mathbf{0} & \mathbf{J}_\theta & \mathbf{J}_q \\ \mathbf{J}_\theta^{\mathrm{T}} & -\mathbf{K}_\theta & \mathbf{0} \\ \mathbf{J}_q^{\mathrm{T}} & \mathbf{0} & \mathbf{0} \end{bmatrix} \cdot \begin{bmatrix} \mathbf{F} \\ \boldsymbol{\theta} \\ \Delta\mathbf{q} \end{bmatrix} = \begin{bmatrix} \Delta\mathbf{t} \\ \mathbf{0} \\ \mathbf{0} \end{bmatrix} \tag{3.7}$$

The latter gives a straightforward numerical technique for computing the desired stiffness matrix: direct inversion of the matrix in the left-hand side of (3.7) and extracting from it the upper-left sub-matrix of size 6×6

$$\begin{bmatrix} \mathbf{0} & \mathbf{J}_\theta & \mathbf{J}_q \\ \mathbf{J}_\theta^{\mathrm{T}} & -\mathbf{K}_\theta & \mathbf{0} \\ \mathbf{J}_q^{\mathrm{T}} & \mathbf{0} & \mathbf{0} \end{bmatrix}^{-1} = \left[\begin{array}{c|c|c} \mathbf{K}_C & * & * \\ \hline * & * & * \\ \hline * & * & * \end{array}\right] \tag{3.8}$$

Since the matrix $\mathbf{K}_\theta$ is non-singular (it describes the stiffness of the virtual springs), the variables $\boldsymbol{\theta}$ can be expressed via $\mathbf{F}$ using the equations (3.6) $\boldsymbol{\theta} = \mathbf{K}_\theta^{-1} \cdot \mathbf{J}_\theta^{\mathrm{T}} \cdot \mathbf{F}$. This leads to a reduced system of matrix equations with unknown $\mathbf{F}$ and $\Delta\mathbf{q}$

$$\begin{bmatrix} \mathbf{J}_\theta \cdot \mathbf{K}_\theta^{-1} \cdot \mathbf{J}_\theta^{\mathrm{T}} & \mathbf{J}_q \\ \mathbf{J}_q^{\mathrm{T}} & \mathbf{0} \end{bmatrix} \cdot \begin{bmatrix} \mathbf{F} \\ \Delta\mathbf{q} \end{bmatrix} = \begin{bmatrix} \Delta\mathbf{t} \\ \mathbf{0} \end{bmatrix}. \tag{3.9}$$

that may be treated in the similar way, i.e. the desired stiffness matrix is also obtained by the direct inversion of the matrix in the left-hand side of (3.9) and extracting from it the upper-left sub-matrix of size 6×6:

$$\begin{bmatrix} \mathbf{J}_\theta \cdot \mathbf{K}_\theta^{-1} \cdot \mathbf{J}_\theta^{\mathrm{T}} & \mathbf{J}_q \\ \mathbf{J}_q^{\mathrm{T}} & \mathbf{0} \end{bmatrix}^{-1} = \left[\begin{array}{c|c} \mathbf{K}_C & * \\ \hline * & * \end{array}\right] \tag{3.10}$$

where the sub-matrix $\mathbf{J}_\theta \cdot \mathbf{K}_\theta^{-1} \cdot \mathbf{J}_\theta^{\mathrm{T}}$ describes the spring compliance relative to the end-effector, and the sub-matrix $\mathbf{J}_q$ takes into account the passive joint influence on the end-effector motions. Therefore, for a separate kinematic chain, the desired stiffness matrix $\mathbf{K}_C$ can be computed by the direct inversion of the $(6+n_q)\times(6+n_q)$ matrix in the left-hand side of (3.10) and extracting from it the 6×6 sub-matrix.

3.2.4 Deflections in serial chains with passive joints

Cartesian stiffness matrix $\mathbf{K}_C$ computed in the previous sub-section, allows us to obtain the linear relation between the end-effector displacement $\Delta\mathbf{t}$ and the external loading $\mathbf{F}$

$$\mathbf{F} = \mathbf{K}_C \cdot \Delta\mathbf{t}, \tag{3.11}$$

that defines the kinematic chain elastostatic properties in a traditional way. However, due to specificity of the robotic mechanism, it is useful to propose the additional performance measures that evaluate variations in passive $\Delta\mathbf{q}$ and virtual joint coordinates $\boldsymbol{\theta}$ because of the end-point displacement. These values provide the designer a supplementary information on the manipulator properties, such as the weakest and strongest links with respect to the compliance errors, the most significant displacements in the passive joints caused by the shifting of the end-point location etc. It is worth mentioning that these values cannot be directly computed from kinematic equations due to redundant number of the joint variables (in fact, it is necessary to take into account additional relations derived from static equilibrium equations).

The desired performance measures can be introduced in a similar manner, via the stiffness matrices $\mathbf{K}_{C\theta}$ and $\mathbf{K}_{Cq}$ defining linear mappings of the end-point displacement to the internal coordinates deflections $\boldsymbol{\theta}$ and $\Delta\mathbf{q}$:

$$\boldsymbol{\theta} = \mathbf{K}_{C\theta} \cdot \Delta\mathbf{t}; \qquad \Delta\mathbf{q} = \mathbf{K}_{Cq} \cdot \Delta\mathbf{t} \tag{3.12}$$

These matrices $\mathbf{K}_{C\theta}$ and $\mathbf{K}_{Cq}$ can be computed from the full scale force deflection relation (3.7) by the direct inversion of $(6+n_q+n_\theta)\times(6+n_q+n_\theta)$ matrix in the left-hand side of (3.8) and extracting from it $n_\theta \times 6$ and $n_q \times 6$ sub-matrices, which correspond to $\mathbf{K}_{C\theta}$ and $\mathbf{K}_{Cq}$ respectively (see (3.8) for details).

Moreover, since the virtual joint coordinates $\boldsymbol{\theta}$ and external loading $\mathbf{F}$ are defined, the internal loadings $\boldsymbol{\tau}_\theta$ in virtual joints can be computed using the expressions (3.4) and (3.5).

To avoid high-dimensional matrix inversion, some transformations can be performed analytically assuming that the matrix $\mathbf{K}_C$ is known. In particular, using expressions $\boldsymbol{\theta} = \mathbf{K}_\theta^{-1} \cdot \mathbf{J}_\theta^{\,T} \cdot \mathbf{F}$ and $\mathbf{F} = \mathbf{K}_C \cdot \Delta\mathbf{t}$ that follow from (3.4) and (3.5), the desired matrix $\mathbf{K}_{C\theta}$ can be expressed as

$$\mathbf{K}_{C\theta} = \mathbf{K}_\theta^{-1} \cdot \mathbf{J}_\theta^{\,T} \cdot \mathbf{K}_C \tag{3.13}$$

and relevant torques in the virtual joints can be computed as

$$\boldsymbol{\tau}_\theta = \mathbf{J}_\theta^{\,T} \cdot \mathbf{K}_C \cdot \Delta\mathbf{t} \tag{3.14}$$

Further, to compute the matrix $\mathbf{K}_{Cq}$, let us consider the first equation of the system (3.6) and substitute $\boldsymbol{\theta} = \mathbf{K}_{C\theta} \cdot \Delta\mathbf{t}$. This yields the redundant system of linear equations

$$\mathbf{J}_\theta \cdot \mathbf{K}_{C\theta} \cdot \Delta\mathbf{t} + \mathbf{J}_q \cdot \Delta\mathbf{q} = \Delta\mathbf{t}\ , \tag{3.15}$$

which can be solved using the common pseudo-inversion technique that gives the following expression for the second matrix

$$\mathbf{K}_{Cq} = \left(\mathbf{J}_q^{\,T} \cdot \mathbf{J}_q\right)^{-1} \cdot \mathbf{J}_q^{\,T} \cdot \left(\mathbf{I} - \mathbf{J}_\theta \cdot \mathbf{K}_{C\theta}\right) \tag{3.16}$$

that includes inversion of dimension $n_q \times n_q$. Hence, using expressions (3.13) and (3.16), the designer can obtain additional information allowing to evaluate resistance of the internal joint variables with respect to the deflection of the end-platform and to make the relevant modifications of the manipulator parameters.

Summarising Section 3.2 it should be stressed that the developed technique can be applied to a serial kinematic chain with the arbitrary location of passive joints and allows us obtain even rank-deficient stiffness matrices caused by the presence of the passive joints or singular configuration of the chain. Also, it evaluates internal deflections (and corresponding forces/torques) that are useful for mechanical design. In contrast to previous works, the proposed technique is more computationally efficient and includes low-order matrix inversion. However, to evaluate properties of the considered matrices, it is worth to obtain an analytical solution.

3.3 ANALYTICAL COMPUTING OF CARTESIAN STIFFNESS MATRIX

The expressions proposed in Section 3.2 allow us to compute the Cartesian stiffness matrix $\mathbf{K}_C$ for serial kinematic chains with the passive joints in the numerical form, by the inversion of $(6+n_q+n_\theta)\times(6+n_q+n_\theta)$ matrix (3.8) and extracting the 6×6 sub-matrix from it. Another more efficient solution, requires matrix inversion of dimension $(6+n_q)\times(6+n_q)$ in accordance with (3.10). This Section gives the analytical solution of the problem, which requires several matrix inversions of dimension 6×6 only. Besides, it allows us to explicitly separate the influence of virtual elastic joints and passive joints. For illustration purposes, it also includes several case studies that show how the stiffness matrix is modified due to the presence of the passive joints.

3.3.1 Extended stiffness mapping equation

For the manipulators without the passive joints, the desired equation is well-known [Gosselin 1990], [Chen 1999] and is expressed as $\mathbf{K}_C = \mathbf{J}_\theta^{-1} \cdot \mathbf{K}_\theta \cdot \mathbf{J}_\theta^{-T}$ or $\mathbf{K}_\theta = \mathbf{J}_\theta \cdot \mathbf{K}_C \cdot \mathbf{J}_\theta^{\,T}$. In literature, it is also often called the "stiffness mapping" expression, which defines relation between the stiffness properties in the joint and Cartesian spaces. It is worth mentioning that in the previous works, it has been implicitly assumed that the Jacobian $\mathbf{J}_\theta$ is a 6×6 invertible non-singular matrix, while in a general case the considered kinematic chains may produce non-square Jacobians of size $6\times n_\theta$, but $rank(\mathbf{J}_\theta) = 6$ due to the special arrangement of virtual springs. Let us generalize the stiffness mapping equation for the case of the manipulators with passive joints and a redundant number of virtual joints $n_\theta > 6$.

In order to derive the desired equation, it is reasonable to consider matrix expression (3.10) and apply the blockwise inversion technique of Frobenius [Gantmacher 1959]

$$\begin{bmatrix} \mathbf{A} & \mathbf{B} \\ \mathbf{C} & \mathbf{D} \end{bmatrix}^{-1} = \left[\begin{array}{c|c} \mathbf{A^{-1}} + \mathbf{A^{-1}BH^{-1}CA^{-1}} & -\mathbf{A^{-1}BH^{-1}} \\ \hline -\mathbf{H^{-1}CA^{-1}} & \mathbf{H^{-1}} \end{array}\right]; \qquad \mathbf{H} = \mathbf{D} - \mathbf{CA^{-1}B} \tag{3.17}$$

where the sub-matrices $\mathbf{A},...,\mathbf{H}$ are expressed as

$$\mathbf{A} = \mathbf{J}_\theta \cdot \mathbf{K}_\theta^{-1} \cdot \mathbf{J}_\theta^{\mathrm{T}}; \quad \mathbf{B} = \mathbf{J}_\mathrm{q}; \quad \mathbf{C} = \mathbf{J}_\mathrm{q}^{\mathrm{T}}; \quad \mathbf{D} = \mathbf{0}; \quad \mathbf{H} = -\mathbf{J}_\mathrm{q}^{\mathrm{T}} \cdot (\mathbf{J}_\theta \cdot \mathbf{K}_\theta^{-1} \cdot \mathbf{J}_\theta^{\mathrm{T}})^{-1} \cdot \mathbf{J}_\mathrm{q} \tag{3.18}$$

This yields the following presentation of the left-hand side of (3.10)

$$\begin{bmatrix} \mathbf{J}_\theta \cdot \mathbf{K}_\theta^{-1} \cdot \mathbf{J}_\theta^{T} & \mathbf{J}_\mathrm{q} \\ \mathbf{J}_\mathrm{q}^{\mathrm{T}} & \mathbf{0} \end{bmatrix}^{-1} = \begin{bmatrix} \mathbf{A}' & \mathbf{B}' \\ \mathbf{C}' & \mathbf{D}' \end{bmatrix} \tag{3.19}$$

where

$$\begin{aligned} \mathbf{A}' &= \left(\mathbf{J}_\theta \cdot \mathbf{K}_\theta^{-1} \cdot \mathbf{J}_\theta^{\mathrm{T}}\right)^{-1} - \left(\mathbf{J}_\theta \cdot \mathbf{K}_\theta^{-1} \cdot \mathbf{J}_\theta^{\mathrm{T}}\right)^{-1} \cdot \mathbf{J}_\mathrm{q} \cdot \left(\mathbf{J}_\mathrm{q}^{\mathrm{T}} \cdot \left(\mathbf{J}_\theta \cdot \mathbf{K}_\theta^{-1} \cdot \mathbf{J}_\theta^{\mathrm{T}}\right)^{-1} \cdot \mathbf{J}_\mathrm{q}\right)^{-1} \cdot \mathbf{J}_\mathrm{q}^{\mathrm{T}} \cdot \left(\mathbf{J}_\theta \cdot \mathbf{K}_\theta^{-1} \cdot \mathbf{J}_\theta^{\mathrm{T}}\right)^{-1} \\ \mathbf{B}' &= \left(\mathbf{J}_\theta \cdot \mathbf{K}_\theta^{-1} \cdot \mathbf{J}_\theta^{\mathrm{T}}\right)^{-1} \cdot \mathbf{J}_\mathrm{q} \cdot \left(\mathbf{J}_\mathrm{q}^{\mathrm{T}} \cdot \left(\mathbf{J}_\theta \cdot \mathbf{K}_\theta^{-1} \cdot \mathbf{J}_\theta^{T}\right)^{-1} \cdot \mathbf{J}_\mathrm{q}\right)^{-1}; \\ \mathbf{C}' &= \left(\mathbf{J}_\mathrm{q}^{\mathrm{T}} \cdot \left(\mathbf{J}_\theta \cdot \mathbf{K}_\theta^{-1} \cdot \mathbf{J}_\theta^{\mathrm{T}}\right)^{-1} \cdot \mathbf{J}_\mathrm{q}\right)^{-1} \cdot \mathbf{J}_\mathrm{q}^{\mathrm{T}} \cdot \left(\mathbf{J}_\theta \cdot \mathbf{K}_\theta^{-1} \cdot \mathbf{J}_\theta^{\mathrm{T}}\right)^{-1} \\ \mathbf{D}' &= -\left(\mathbf{J}_\mathrm{q}^{\mathrm{T}} \cdot (\mathbf{J}_\theta \cdot \mathbf{K}_\theta^{-1} \cdot \mathbf{J}_\theta^{\mathrm{T}})^{-1} \cdot \mathbf{J}_\mathrm{q}\right)^{-1} \end{aligned} \tag{3.20}$$

Hence, the desired Cartesian stiffness matrix $\mathbf{K}_\mathrm{C}$ can be presented analytically as

$$\mathbf{K}_\mathrm{C} = \left(\mathbf{J}_\theta \cdot \mathbf{K}_\theta^{-1} \cdot \mathbf{J}_\theta^{T}\right)^{-1} - \left(\mathbf{J}_\theta \cdot \mathbf{K}_\theta^{-1} \cdot \mathbf{J}_\theta^{T}\right)^{-1} \cdot \mathbf{J}_\mathrm{q} \cdot \left(\mathbf{J}_\mathrm{q}^{\mathrm{T}} \cdot \left(\mathbf{J}_\theta \cdot \mathbf{K}_\theta^{-1} \cdot \mathbf{J}_\theta^{\mathrm{T}}\right)^{-1} \cdot \mathbf{J}_\mathrm{q}\right)^{-1} \cdot \mathbf{J}_\mathrm{q}^{\mathrm{T}} \cdot \left(\mathbf{J}_\theta \cdot \mathbf{K}_\theta^{-1} \cdot \mathbf{J}_\theta^{\mathrm{T}}\right)^{-1}. \tag{3.21}$$

Similarly, the matrix $\mathbf{K}_{\mathrm{Cq}}$ defining mapping from the Cartesian space to the passive joint space can also be expressed analytically as

$$\mathbf{K}_{\mathrm{Cq}} = \left(\mathbf{J}_\mathrm{q}^{\mathrm{T}} \cdot \left(\mathbf{J}_\theta \cdot \mathbf{K}_\theta^{-1} \cdot \mathbf{J}_\theta^{\mathrm{T}}\right)^{-1} \cdot \mathbf{J}_\mathrm{q}\right)^{-1} \cdot \mathbf{J}_\mathrm{q}^{\mathrm{T}} \cdot \left(\mathbf{J}_\theta \cdot \mathbf{K}_\theta^{-1} \cdot \mathbf{J}_\theta^{\mathrm{T}}\right)^{-1}. \tag{3.22}$$

To compare these results with the classical stiffness mapping equation $\mathbf{K}_\mathrm{C} = \mathbf{J}_\theta^{-1} \cdot \mathbf{K}_\theta \cdot \mathbf{J}_\theta^{-\mathrm{T}}$, the expression (3.21) can be rewritten as the difference of two 6×6 matrices

$$\mathbf{K}_\mathrm{C} = \mathbf{K}_\mathrm{C}^0 - \mathbf{K}_\mathrm{C}^0 \cdot \mathbf{J}_\mathrm{q} \cdot \mathbf{K}_{\mathrm{Cq}} \tag{3.23}$$

where the first term $\mathbf{K}_\mathrm{C}^0$ is the stiffness matrix of the corresponding serial chain without passive joints

$$\mathbf{K}_\mathrm{C}^0 = \left(\mathbf{J}_\theta \cdot \mathbf{K}_\theta^{-1} \cdot \mathbf{J}_\theta^{\mathrm{T}}\right)^{-1} \tag{3.24}$$

and the second term $\mathbf{K}_\mathrm{C}^0 \cdot \mathbf{J}_\mathrm{q} \cdot \mathbf{K}_{\mathrm{Cq}}$ defines influence of the passive joints on the Cartesian stiffness matrix $\mathbf{K}_\mathrm{C}$. Hence, the obtained expression (3.23) extends the classical stiffness mapping technique for the case of manipulators with passive joints by adding an additional component to it. The latter allows us to estimate the impact of passive joints on the kinematic chain stiffness in an explicit form and to obtain some useful analytical results presented in the following sub-section.

It is worth mentioning that in contrast to previous works, the proposed extended stiffness mapping equation (3.23) can be also applied to the kinematic chains with non-square Jacobians $\mathbf{J}_\theta$ of full rank, since the matrix inversion is applied to the 6×6 matrix $\mathbf{J}_\theta \cdot \mathbf{K}_\theta^{-1} \cdot \mathbf{J}_\theta^{\mathrm{T}}$, which is always invertible (even for singular postures of kinematic chain). Besides, it is in a good agreement with other relevant works [Quennouelle 2008a], [Quennouelle 2008c], [Chen 2008] where $\mathbf{K}_\mathrm{C}$ was presented as the difference between the two matrices but the second one was computed in a different way (to take into account impact of geometrical constrains).

3.3.2 Stiffness matrix properties

Let us analyze in details expression (3.21) that allows computing the stiffness matrix of a serial chain with passive joints $\mathbf{K}_C$ from the corresponding matrix of the chain without passive joints $\mathbf{K}_C^0$. Assuming that $rank(\mathbf{K}_C^0)=6$, this matrix can be factorised into the product of two non-singular square matrices $\mathbf{K}_C^0=\mathbf{S}^T\mathbf{S}$. This yields a compact presentation of the desired matrix in the form

$$\mathbf{K}_C=\mathbf{S}^{\mathrm{T}}\cdot\mathbf{M}\cdot\mathbf{S} \tag{3.25}$$

where

$$\mathbf{M}=\mathbf{I}-(\mathbf{S}\cdot\mathbf{J}_q)\cdot\left(\mathbf{J}_q^{\mathrm{T}}\cdot\mathbf{S}^{\mathrm{T}}\cdot\mathbf{S}\cdot\mathbf{J}_q\right)^{-1}\cdot(\mathbf{J}_q^{\mathrm{T}}\cdot\mathbf{S}^{\mathrm{T}}) \tag{3.26}$$

and the inverse $(\mathbf{J}_q^{\mathrm{T}}\cdot\mathbf{S}^{\mathrm{T}}\cdot\mathbf{S}\cdot\mathbf{J}_q)^{-1}$ exists due to the assumption $rank(\mathbf{J}_q)=n_q$. Further, the product $\mathbf{S}\cdot\mathbf{J}_q$ can be also factorised using the SVD-technique [Strang 1998] as

$$\mathbf{S}\cdot\mathbf{J}_q=\mathbf{U}\,\boldsymbol{\Sigma}\,\mathbf{V}^{\mathrm{T}}=\left[u_{ij}\right]_{6\times6}\cdot\begin{bmatrix}\boldsymbol{\Sigma}_q\\ \mathbf{0}\end{bmatrix}_{6\times n_q}\cdot\left[v_{ij}\right]_{n_q\times n_q} \tag{3.27}$$

where $\mathbf{U}$, $\mathbf{V}$ are the orthogonal matrices and the matrix $\boldsymbol{\Sigma}_q=diag(\sigma_1,\sigma_2,...)$ is composed of n_q non-zero singular values σ_i (provided that $rank(\mathbf{J}_q)=n_q$). The latter gives the following presentation of $\mathbf{M}$

$$\mathbf{M}=\mathbf{U}\cdot\left(\mathbf{I}-\boldsymbol{\Sigma}\cdot\left(\boldsymbol{\Sigma}^{\mathrm{T}}\cdot\boldsymbol{\Sigma}\right)^{-1}\cdot\boldsymbol{\Sigma}^{\mathrm{T}}\right)\cdot\mathbf{U}^{\mathrm{T}}. \tag{3.28}$$

where the product $\boldsymbol{\Sigma}\cdot(\boldsymbol{\Sigma}^T\cdot\boldsymbol{\Sigma})^{-1}\cdot\boldsymbol{\Sigma}^{\mathrm{T}}$ may be computed in a straightforward way:

$$\boldsymbol{\Sigma}\cdot\left(\boldsymbol{\Sigma}^{\mathrm{T}}\cdot\boldsymbol{\Sigma}\right)^{-1}\cdot\boldsymbol{\Sigma}^{\mathrm{T}}=\begin{bmatrix}\boldsymbol{\Sigma}_q\\ \mathbf{0}\end{bmatrix}\cdot\left(\begin{bmatrix}\boldsymbol{\Sigma}_q & \mathbf{0}\end{bmatrix}\cdot\begin{bmatrix}\boldsymbol{\Sigma}_q\\ \mathbf{0}\end{bmatrix}\right)^{-1}\cdot\begin{bmatrix}\boldsymbol{\Sigma}_q & \mathbf{0}\end{bmatrix}=\begin{bmatrix}\mathbf{I}_{n_q} & \mathbf{0}\\ \mathbf{0} & \mathbf{0}\end{bmatrix}_{6\times6}. \tag{3.29}$$

So, the inner part of $\mathbf{M}$ may be presented as

$$\mathbf{M}'=\mathbf{I}-\boldsymbol{\Sigma}\cdot\left(\boldsymbol{\Sigma}^T\cdot\boldsymbol{\Sigma}\right)^{-1}\cdot\boldsymbol{\Sigma}^{\mathrm{T}}=\left[\begin{array}{c|c}\mathbf{0}_{n_q} & \mathbf{0}\\ \hline \mathbf{0} & \mathbf{I}_{6-n_q}\end{array}\right]_{6\times6} \tag{3.30}$$

This leads to the final expression

$$\mathbf{K}_C=\mathbf{S}^T\cdot\mathbf{U}\cdot\mathbf{M}'\cdot\mathbf{U}^T\cdot\mathbf{S} \tag{3.31}$$

that allows to evaluate the rank of the stiffness matrix $\mathbf{K}_C$

$$rank(\mathbf{K}_C)=rank(\mathbf{M}')=6-n_q \tag{3.32}$$

For computational convenience, the orthogonal matrix $\mathbf{U}$ may be split into six vector columns $\left[\mathbf{u}_1,...,\mathbf{u}_6\right]$ and the matrix product $\mathbf{U}\cdot\mathbf{M}'\cdot\mathbf{U}^{\mathrm{T}}$ is expressed as a subsum of $\mathbf{u}_i\mathbf{u}_i^{\mathrm{T}}$ corresponding to the non-zero elements of $\mathbf{M}'$. This gives another presentation of the desired Cartesian stiffness matrix

$$\mathbf{K}_C=\mathbf{S}^{\mathrm{T}}\cdot\left(\sum_{i=nq+1}^{6}\mathbf{u}_i\mathbf{u}_i^{\mathrm{T}}\right)\cdot\mathbf{S} \tag{3.33}$$

where the middle term includes only those unit vectors $\mathbf{u}_i$ that are not "compensated" by the passive joints (for this notation, the directions $\mathbf{u}_1,...\mathbf{u}_{nq}$ correspond to the end-effector motions, which do not produce elastostatic reactions because of the passive joints). It should be noted that in the case of $n_q=0$, i.e. without passive joints, the total sum of $\mathbf{u}_i\mathbf{u}_i^{\mathrm{T}}$ produces a unit matrix $\mathbf{I}_6$ and the latter expression is reduced to $\mathbf{K}_C^0=\mathbf{S}^{\mathrm{T}}\cdot\mathbf{S}$.

All this leads to the following conclusion concerning computational singularities:

Remark 1. The first term of the expression (3.21) is non-singular if and only if $rank\left(\mathbf{J}_\theta\right)=6$, i.e. if the VJM model of the chain includes at least 6 independent virtual springs.

Remark 2. The second term of the expression (3.21) is non-singular if and only if $rank\left(\mathbf{J}_{\mathrm{q}}\right)=n_{\mathrm{q}}$, i.e. if the VJM model of the chain does not include redundant passive joints.

Remark 3. If both terms of (3.21) are non-singular, their difference produces a symmetrical stiffness matrix, which is always singular and $rank\left(\mathbf{K}_{\mathrm{C}}\right)=6-n_{\mathrm{q}}$.

Remark 4. If the matrix $\mathbf{K}_{\mathrm{C}}^{0}$ of the chain without passive joints is symmetrical and positive-definite, the stiffness matrix of the chain with passive joints $\mathbf{K}_{\mathrm{C}}$ is also symmetrical but positive-semidefinite.

Hence, in practice, expression (3.21) does not cause any computational difficulties and always produce a singular stiffness matrix of rank $6-n_{\mathrm{q}}$. In analytical computations, it can be also useful in modifying the original stiffness matrix $\mathbf{K}_{\mathrm{C}}^{0}$ sequentially, which will be the focus in the next sub-section

3.3.3 Recursive computation of the stiffness matrix

To simplify the Cartesian stiffness matrix computation technique and to specify the impact of each passive joint on resulting matrix $\mathbf{K}_{\mathrm{C}}$, it is useful to obtain recursive procedure which allows us sequentially modify the original stiffness matrix $\mathbf{K}_{\mathrm{C}}^{0}$. To obtain relevant recursive procedure, let us assume that it is possible to take into account passive joints sequentially, in two steps. Let us group these joints into two vectors $\mathbf{q}_1$ and $\mathbf{q}_2$ and decompose the Jacobian $\mathbf{J}_{\mathrm{q}}$ of size $6\times n_{\mathrm{q}}$ into two sub-matrices $[\mathbf{J}_{\mathrm{q1}},\mathbf{J}_{\mathrm{q2}}]$ of sizes $6\times n_{\mathrm{q1}}$ and $6\times n_{\mathrm{q2}}$ correspondingly. Then, recursive expressions corresponding to (3.21) can be written as

$$\mathbf{K}_{\mathrm{C}}^{1}=\mathbf{K}_{\mathrm{C}}^{0}-\mathbf{K}_{\mathrm{C}}^{0}\mathbf{J}_{\mathrm{q1}}\left(\mathbf{J}_{\mathrm{q1}}^{\mathrm{T}}\mathbf{K}_{\mathrm{C}}^{0}\mathbf{J}_{\mathrm{q1}}\right)^{-1}\mathbf{J}_{\mathrm{q1}}^{T}\mathbf{K}_{\mathrm{C}}^{0};\qquad \mathbf{K}_{\mathrm{C}}^{2}=\mathbf{K}_{\mathrm{C}}^{1}-\mathbf{K}_{\mathrm{C}}^{1}\mathbf{J}_{\mathrm{q2}}\left(\mathbf{J}_{\mathrm{q2}}^{\mathrm{T}}\mathbf{K}_{\mathrm{C}}^{1}\mathbf{J}_{\mathrm{q2}}\right)^{-1}\mathbf{J}_{\mathrm{q2}}^{\mathrm{T}}\mathbf{K}_{\mathrm{C}}^{1} \tag{3.34}$$

In order to evaluate the obtained matrix $\mathbf{K}_{\mathrm{C}}^{2}$, let us substitute the first expression in the second one and perform some equivalent transformations using notations

$$\begin{aligned}&\mathbf{A}=\mathbf{J}_{\mathrm{q1}}^{\mathrm{T}}\mathbf{K}_{\mathrm{C}}^{0}\mathbf{J}_{\mathrm{q1}};\quad \mathbf{B}=\mathbf{J}_{\mathrm{q1}}^{\mathrm{T}}\mathbf{K}_{\mathrm{C}}^{0}\mathbf{J}_{\mathrm{q2}};\quad \mathbf{C}=\mathbf{J}_{\mathrm{q2}}^{\mathrm{T}}\mathbf{K}_{\mathrm{C}}^{0}\mathbf{J}_{\mathrm{q1}};\quad \mathbf{D}=\mathbf{J}_{\mathrm{q2}}^{\mathrm{T}}\mathbf{K}_{\mathrm{C}}^{0}\mathbf{J}_{\mathrm{q2}}\\&\mathbf{H}=\mathbf{D}-\mathbf{C}\mathbf{A}^{-1}\mathbf{B}=\mathbf{J}_{\mathrm{q2}}^{\mathrm{T}}\mathbf{K}_{\mathrm{C}}^{0}\mathbf{J}_{\mathrm{q2}}-\mathbf{J}_{\mathrm{q2}}^{\mathrm{T}}\mathbf{K}_{\mathrm{C}}^{0}\mathbf{J}_{\mathrm{q1}}\cdot\left(\mathbf{J}_{\mathrm{q1}}^{\mathrm{T}}\mathbf{K}_{\mathrm{C}}^{0}\mathbf{J}_{\mathrm{q1}}\right)^{-1}\cdot\mathbf{J}_{\mathrm{q1}}^{\mathrm{T}}\mathbf{K}_{\mathrm{C}}^{0}\mathbf{J}_{\mathrm{q2}}\end{aligned} \tag{3.35}$$

This allows converting the original bulky expression

$$\begin{aligned}\mathbf{K}_{\mathrm{C}}^{2}=&\left\{\mathbf{K}_{\mathrm{C}}^{0}-\mathbf{K}_{\mathrm{C}}^{0}\cdot\mathbf{J}_{\mathrm{q1}}\cdot\left(\mathbf{J}_{\mathrm{q1}}^{\mathrm{T}}\cdot\mathbf{K}_{\mathrm{C}}^{0}\cdot\mathbf{J}_{\mathrm{q1}}\right)^{-1}\cdot\mathbf{J}_{\mathrm{q1}}^{\mathrm{T}}\cdot\mathbf{K}_{\mathrm{C}}^{0}\right\}-\left\{\mathbf{K}_{\mathrm{C}}^{0}-\mathbf{K}_{\mathrm{C}}^{0}\cdot\mathbf{J}_{\mathrm{q1}}\cdot\left(\mathbf{J}_{\mathrm{q1}}^{\mathrm{T}}\cdot\mathbf{K}_{\mathrm{C}}^{0}\cdot\mathbf{J}_{\mathrm{q1}}\right)^{-1}\cdot\mathbf{J}_{\mathrm{q1}}^{T}\cdot\mathbf{K}_{\mathrm{C}}^{0}\right\}\times\\&\times\mathbf{J}_{\mathrm{q2}}\cdot\left(\mathbf{J}_{\mathrm{q2}}^{\mathrm{T}}\cdot\left\{\mathbf{K}_{\mathrm{C}}^{0}-\mathbf{K}_{\mathrm{C}}^{0}\cdot\mathbf{J}_{\mathrm{q1}}\cdot\left(\mathbf{J}_{\mathrm{q1}}^{\mathrm{T}}\cdot\mathbf{K}_{\mathrm{C}}^{0}\cdot\mathbf{J}_{\mathrm{q1}}\right)^{-1}\cdot\mathbf{J}_{\mathrm{q1}}^{\mathrm{T}}\cdot\mathbf{K}_{\mathrm{C}}^{0}\right\}\cdot\mathbf{J}_{\mathrm{q2}}\right)^{-1}\cdot\mathbf{J}_{\mathrm{q2}}^{\mathrm{T}}\cdot\left\{\mathbf{K}_{\mathrm{C}}^{0}-\mathbf{K}_{\mathrm{C}}^{0}\cdot\mathbf{J}_{\mathrm{q1}}\cdot\left(\mathbf{J}_{\mathrm{q1}}^{\mathrm{T}}\cdot\mathbf{K}_{\mathrm{C}}^{0}\cdot\mathbf{J}_{\mathrm{q1}}\right)^{-1}\cdot\mathbf{J}_{\mathrm{q1}}^{\mathrm{T}}\cdot\mathbf{K}_{\mathrm{C}}^{0}\right\}\end{aligned} \tag{3.36}$$

into a more compact form

$$\mathbf{K}_{\mathrm{C}}^{2}=\mathbf{K}_{\mathrm{C}}^{0}-\mathbf{K}_{\mathrm{C}}^{0}\cdot(\mathbf{J}_{\mathrm{q1}}\mathbf{A}^{-1}\mathbf{J}_{\mathrm{q1}}^{\mathrm{T}}+\mathbf{J}_{\mathrm{q2}}\mathbf{H}^{-1}\mathbf{J}_{\mathrm{q2}}^{\mathrm{T}}+\mathbf{J}_{\mathrm{q2}}\mathbf{H}^{-1}\mathbf{C}\mathbf{A}^{-1}\mathbf{J}_{\mathrm{q1}}^{\mathrm{T}}-\mathbf{J}_{\mathrm{q1}}\mathbf{A}^{-1}\mathbf{B}\,\mathbf{H}^{-1}\mathbf{J}_{\mathrm{q2}}^{\mathrm{T}}+\mathbf{J}_{\mathrm{q1}}\mathbf{A}^{-1}\mathbf{B}\,\mathbf{H}^{-1}\mathbf{C}\mathbf{A}^{-1}\mathbf{J}_{\mathrm{q1}}^{\mathrm{T}})\cdot\mathbf{K}_{\mathrm{C}}^{0} \tag{3.37}$$

or, using block-matrix presentation, it can be written as

$$\mathbf{K}_{\mathrm{C}}^{2}=\mathbf{K}_{\mathrm{C}}^{0}-\mathbf{K}_{\mathrm{C}}^{0}\cdot\begin{bmatrix}\mathbf{J}_{\mathrm{q1}} & \mathbf{J}_{\mathrm{q2}}\end{bmatrix}\cdot\left[\begin{array}{c|c}\mathbf{A}^{-1}+\mathbf{A}^{-1}\mathbf{B}\,\mathbf{H}^{-1}\mathbf{C}\mathbf{A}^{-1} & -\mathbf{A}^{-1}\mathbf{B}\,\mathbf{H}^{-1}\\\hline -\mathbf{H}^{-1}\mathbf{C}\mathbf{A}^{-1} & \mathbf{H}^{-1}\end{array}\right]\cdot\begin{bmatrix}\mathbf{J}_{\mathrm{q1}}^{\mathrm{T}}\\ \mathbf{J}_{\mathrm{q2}}^{\mathrm{T}}\end{bmatrix}\cdot\mathbf{K}_{\mathrm{C}}^{0} \tag{3.38}$$

Furthermore, using Frobenius formula for the blockwise matrix inverse (3.17), the derived expression can be presented in the form

$$\mathbf{K}_{\mathrm{C}}^{2}=\mathbf{K}_{\mathrm{C}}^{0}-\mathbf{K}_{\mathrm{C}}^{0}\cdot\begin{bmatrix}\mathbf{J}_{\mathrm{q1}} & \mathbf{J}_{\mathrm{q2}}\end{bmatrix}\cdot\left[\begin{array}{c|c}\mathbf{J}_{\mathrm{q1}}^{\mathrm{T}}\cdot\mathbf{K}_{\mathrm{C}}^{0}\cdot\mathbf{J}_{\mathrm{q1}} & \mathbf{J}_{\mathrm{q1}}^{\mathrm{T}}\cdot\mathbf{K}_{\mathrm{C}}^{0}\cdot\mathbf{J}_{\mathrm{q2}}\\\hline \mathbf{J}_{\mathrm{q2}}^{\mathrm{T}}\cdot\mathbf{K}_{\mathrm{C}}^{0}\cdot\mathbf{J}_{\mathrm{q1}} & \mathbf{J}_{\mathrm{q2}}^{\mathrm{T}}\cdot\mathbf{K}_{\mathrm{C}}^{0}\cdot\mathbf{J}_{\mathrm{q2}}\end{array}\right]^{-1}\cdot\begin{bmatrix}\mathbf{J}_{\mathrm{q1}}^{\mathrm{T}}\\ \mathbf{J}_{\mathrm{q2}}^{\mathrm{T}}\end{bmatrix}\cdot\mathbf{K}_{\mathrm{C}}^{0}, \tag{3.39}$$

or

$$\mathbf{K}_{\mathrm{C}}^{2}=\mathbf{K}_{\mathrm{C}}^{0}-\mathbf{K}_{\mathrm{C}}^{0}\cdot\begin{bmatrix}\mathbf{J}_{\mathrm{q1}} & \mathbf{J}_{\mathrm{q2}}\end{bmatrix}\cdot\left(\begin{bmatrix}\mathbf{J}_{\mathrm{q1}}^{\mathrm{T}}\\ \mathbf{J}_{\mathrm{q2}}^{\mathrm{T}}\end{bmatrix}\cdot\mathbf{K}_{\mathrm{C}}^{0}\cdot\begin{bmatrix}\mathbf{J}_{\mathrm{q1}} & \mathbf{J}_{\mathrm{q2}}\end{bmatrix}\right)^{-1}\cdot\begin{bmatrix}\mathbf{J}_{\mathrm{q1}}^{\mathrm{T}}\\ \mathbf{J}_{\mathrm{q2}}^{\mathrm{T}}\end{bmatrix}\cdot\mathbf{K}_{\mathrm{C}}^{0} \tag{3.40}$$

that exactly coincide with the expression for the stiffness matrix $\mathbf{K}_{\mathrm{C}}$ corresponding to the aggregated Jacobian $\mathbf{J}_{\mathrm{q}}=[\mathbf{J}_{\mathrm{q1}},\mathbf{J}_{\mathrm{q2}}]$. Hence, it proves that the desired stiffness matrix of the kinematic chain with passive joints can be computed recursively, using arbitrary partitioning of the Jacobian $\mathbf{J}_{\mathrm{q}}$. Obviously, it is more convenient to apply column-wise splitting that allows sequential modification of the matrix $\mathbf{K}_{\mathrm{C}}^{0}$ taking into account the geometry of each passive joint separately (and reducing sequentially by one the rank of Cartesian stiffness matrix).

Proposition. If the chain does not include redundant passive joints, expression (3.21) allows recursive presentation

$$\mathbf{K}_{\mathrm{C}}^{i+1}=\mathbf{K}_{\mathrm{C}}^{i}-\mathbf{K}_{\mathrm{C}}^{i}\cdot\mathbf{J}_{\mathrm{q}}^{i}\cdot\left(\mathbf{J}_{\mathrm{q}}^{i\,\mathrm{T}}\cdot\mathbf{K}_{\mathrm{C}}^{i}\cdot\mathbf{J}_{\mathrm{q}}^{i}\right)^{-1}\cdot\mathbf{J}_{\mathrm{q}}^{i\,\mathrm{T}}\cdot\mathbf{K}_{\mathrm{C}}^{i} \tag{3.41}$$

in which the sub-Jacobians $\mathbf{J}_{\mathrm{q}}^{i}\subset\mathbf{J}_{\mathrm{q}}$ are extracted from $\mathbf{J}_{\mathrm{q}}=[\mathbf{J}_{\mathrm{q}}^{1},\mathbf{J}_{\mathrm{q}}^{2},...]$ in arbitrary order (column-by-column, or by groups of columns).

Corollary. The desired stiffness matrix $\mathbf{K}_{\mathrm{C}}$ can be computed in n_{q} steps, by sequential application of expression (3.41) for each column of the Jacobian $\mathbf{J}_{\mathrm{q}}$ (i.e. for each passive joint separately).

The latter motivates an additional analysis that is presented below and gives very simple and practically convenient expressions for the modifications of original stiffness matrix $\mathbf{K}_{\mathrm{C}}^{0}$.

3.3.4 Single-joint decomposition in stiffness matrix computing

Recursive equation (3.41) allows us to essentially simplify the computational procedure using the sequential modification of the original stiffness matrix $\mathbf{K}_{\mathrm{C}}^{0}$ for each passive joint independently, using separate columns of $\mathbf{J}_{\mathrm{q}}=[\mathbf{J}_{\mathrm{q1},}\,\mathbf{J}_{\mathrm{q2}},...]$. Moreover, for some typical cases, relevant computations may be easily performed analytically. Here, some useful techniques related to this approach are presented.

Let us assume that a current recursion deals with a single passive joint corresponding to the *i*-th column of the Jacobian $\mathbf{J}_{\mathrm{q}}$, which is denoted as $\mathbf{J}_{\mathrm{q}}^{i}$ and has size 6×1. In this case, the matrix expression $(\mathbf{J}_{\mathrm{q}}^{i\,\mathrm{T}}\mathbf{K}_{\mathrm{C}}^{i}\mathbf{J}_{\mathrm{q}}^{i})^{-1}$ is reduced to the size of 1×1 and the matrix inversion is replaced by a simple scalar division. Besides, the term $\mathbf{K}_{\mathrm{C}}^{i}\mathbf{J}_{\mathrm{q}}^{i}$ has size 6×1, so the recursion (3.41) is simplified to

$$\mathbf{K}_{\mathrm{C}}^{i+1}=\mathbf{K}_{\mathrm{C}}^{i}-\frac{1}{\mu}\mathbf{u}_{i}\cdot\mathbf{u}_{i}^{\mathrm{T}}\ \ or\ \left[K_{jk}^{(i+1)}\right]=\left[K_{jk}^{(i)}\right]-\frac{1}{\mu}\left[u_{j}^{(i)}u_{k}^{(i)}\right] \tag{3.42}$$

where $\mathbf{u}_{i}=\mathbf{K}_{C}^{i}\mathbf{J}_{q}^{i}$ is a 6×1 vector and $\mu=\mathbf{J}_{\mathrm{q}}^{i\,\mathrm{T}}\mathbf{K}_{\mathrm{C}}^{i}\mathbf{J}_{\mathrm{q}}^{i}$ is a scalar. Using the methodology presented in Section 3.3.1, it can be also proved that each recursions reduces the rank of the stiffness matrix by 1

$$rank\left(\mathbf{K}_{\mathrm{C}}^{i+1}\right)=rank\left(\mathbf{K}_{\mathrm{C}}^{i}\right)-1 \tag{3.43}$$

provided that the current Jacobian $\mathbf{J}_{\mathrm{q}}^{i}$ is independent of the previous ones $\mathbf{J}_{\mathrm{q}}^{1},\mathbf{J}_{\mathrm{q}}^{2}...$ (i.e. the *i*-th passive joint is not redundant relatively to the joints $1,...,i-1$).

Since in practice any combination of passive joints can be decomposed into elementary translational and rotational ones, it is enough to consider only two types of the Jacobian columns $\mathbf{J}_{qi}$:

$$\mathbf{J}_{\mathrm{tran}}=\begin{bmatrix}e_1 & e_2 & e_3 & 0 & 0 & 0\end{bmatrix}^{\mathrm{T}};\qquad \mathbf{J}_{\mathrm{rot}}=\begin{bmatrix}d_1 & d_2 & d_3 & e_1 & e_2 & e_3\end{bmatrix}^{\mathrm{T}} \tag{3.44}$$

where the unit vector $\mathbf{e}=\begin{bmatrix} e_1 & e_2 & e_3 \end{bmatrix}$, $\mathbf{e}^T\mathbf{e}=1$ defines the orientation of the passive joint axis (both for translational and rotational ones) and the vector $\mathbf{d}=\begin{bmatrix} d_1 & d_2 & d_3 \end{bmatrix}$ defines the influence of the rotational passive joints on the linear velocity at the reference point, i.e. $\mathbf{d}=\mathbf{e}\times\mathbf{r}$ where $\mathbf{r}$ is a vector from the joint centre point to the reference point. After relevant substitutions, one can obtain the following expression for the translational joint

$$\mu=\sum_{j=1}^{3}\sum_{k=1}^{3}K_{jk}^{(i)}e_j e_k; \qquad u_j=\sum_{k=1}^{3}K_{jk}^{(i)}e_k \tag{3.45}$$

And for the rotational joint

$$\mu=\sum_{j=1}^{3}\sum_{k=1}^{3}K_{jk}^{(i)}d_j d_k+2\sum_{j=1}^{3}\sum_{k=4}^{6}K_{jk}^{(i)}d_j e_{k-3}+\sum_{j=4}^{6}\sum_{k=4}^{6}K_{jk}^{(i)}e_{j-3}e_{k-3}; \qquad u_j=\sum_{k=1}^{3}K_{jk}^{(i)}d_k+\sum_{k=4}^{6}K_{jk}^{(i)}e_{k-3} \tag{3.46}$$

Hence, the single-joint decomposition allows to replace the matrix computations (3.41) by simple scalar calculations (3.42) that deal with the modification of the stiffness matrix elements, in accordance with the passive joint location defined by the vectors $\mathbf{d}$ and $\mathbf{e}$. It is worth mentioning that in general case, the transformation (3.42) affects all elements of the matrix $\mathbf{K}_{\mathrm{C}}^{i}$, which differs from simple setting to zero the corresponding row and/or column that has been proposed in some publications [Taghvaeipour 2010]. Let us consider now several specific (but rather typical) cases where the transformation rules are more simple and elegant.

3.3.5 Analytical computations: chains with trivial passive joints

For practical purposes, let us consider a special type of kinematic chains where the passive joint axes are collinear to the axes x, *y* or *z* of the Cartesian coordinate system. Such passive joints will be further referred to as "trivial" or "quasi-trivial" ones. For such cases, the vector-columns of the Jacobian $\mathbf{J}_{\mathrm{q}}$ include a number of zero elements, so the expressions (3.42) can be essentially simplified.

Let us start from a set of *trivial* cases where the Jacobians $\mathbf{J}_{\mathrm{q}}^{i}$ are created from the columns of the identity matrix $\mathbf{I}_{6\times 6}$:

$$\mathbf{J}_{\mathrm{q}}^{(1)}=\begin{bmatrix}1\\0\\0\\0\\0\\0\end{bmatrix}, \qquad \mathbf{J}_{\mathrm{q}}^{(2)}=\begin{bmatrix}0\\1\\0\\0\\0\\0\end{bmatrix}, \qquad ..., \qquad \mathbf{J}_{\mathrm{q}}^{(6)}=\begin{bmatrix}0\\0\\0\\0\\0\\1\end{bmatrix} \tag{3.47}$$

It can be easily proved that they cover the following types of the joint geometry:

- *translational passive joints* with arbitrary spatial position (but with the joint axis directed along *x*, *y* or *z*);
- *rotational passive joints* positioned at the reference point (and with the joint axis directed along *x*, *y* or *z*) or rotational passive joint $\mathrm{R_x}$ located at any point at the *x*-axis.

For these cases, assuming that $\mathbf{J}_{\mathrm{q}}^{(p)}$ denotes the vector-column with a single non-zero element in the *p*-th position, a straightforward substitution into (3.42) yields $u_j=K_{jp}^{(i)}$; $\mu=K_{pp}^{(i)}$. So, the recursive expression for the Cartesian stiffness matrix is simplified to

$$\left[K_{jk}^{(i+1)}\right]=\left[K_{jk}^{(i)}\right]-\left[\frac{K_{jk}^{(i)}K_{kj}^{(i)}}{K_{pp}^{(i)}}\right] \tag{3.48}$$

and the *p*–th row and column of the matrix $\mathbf{K}_{\mathrm{C}}^{i+1}$ become equal to zero

$$K_{pk}^{(i+1)}=0; \quad K_{kp}^{(i+1)}=0; \quad \forall p=1,...6\,. \tag{3.49}$$

So, the recursive computations are easily performed analytically.

For the trivial passive joints, the results are summarized in Table 3.1 where the original stiffness matrix $[K_{ij}]$ is assumed to be sparse in accordance with the structure corresponding to a symmetric beam-type link (see Section 2.5). As it follows from them, here in all cases the stiffness matrix modifications includes setting to zero of an appropriate row and column, but in some cases some elements of other rows and columns are also modified (by simple division by 4).

Table 3.1 Stiffness matrix transformations caused by trivial passive joints

Type of joint	Jacobian	Modified Stiffness matrix
Translational T_x 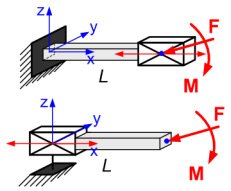	$\mathbf{J}_q^{(1)} = \begin{bmatrix} 1 \\ 0 \\ 0 \\ 0 \\ 0 \\ 0 \end{bmatrix}$	$\begin{bmatrix} 0 & 0 & 0 & 0 & 0 & 0 \\ 0 & K_{22} & 0 & 0 & 0 & K_{26} \\ 0 & 0 & K_{33} & 0 & K_{35} & 0 \\ 0 & 0 & 0 & K_{44} & 0 & 0 \\ 0 & 0 & K_{53} & 0 & K_{55} & 0 \\ 0 & K_{62} & 0 & 0 & 0 & K_{66} \end{bmatrix}$
Translational T_y 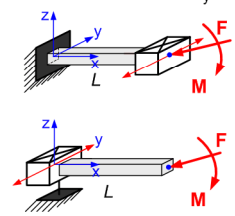	$\mathbf{J}_q^{(2)} = \begin{bmatrix} 0 \\ 1 \\ 0 \\ 0 \\ 0 \\ 0 \end{bmatrix}$	$\begin{bmatrix} K_{11} & 0 & 0 & 0 & 0 & 0 \\ 0 & 0 & 0 & 0 & 0 & 0 \\ 0 & 0 & K_{33} & 0 & K_{35} & 0 \\ 0 & 0 & 0 & K_{44} & 0 & 0 \\ 0 & 0 & K_{53} & 0 & K_{55} & 0 \\ 0 & 0 & 0 & 0 & 0 & \frac{K_{66}}{4} \end{bmatrix}$
Translational T_z 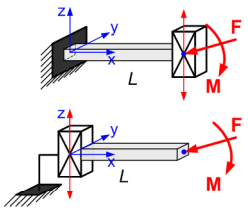	$\mathbf{J}_q^{(3)} = \begin{bmatrix} 0 \\ 0 \\ 1 \\ 0 \\ 0 \\ 0 \end{bmatrix}$	$\begin{bmatrix} K_{11} & 0 & 0 & 0 & 0 & 0 \\ 0 & K_{22} & 0 & 0 & 0 & K_{26} \\ 0 & 0 & 0 & 0 & 0 & 0 \\ 0 & 0 & 0 & K_{44} & 0 & 0 \\ 0 & 0 & 0 & 0 & \frac{K_{55}}{4} & 0 \\ 0 & K_{62} & 0 & 0 & 0 & K_{66} \end{bmatrix}$
Rotational R_x 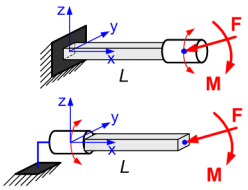	$\mathbf{J}_q^{(4+)} = \begin{bmatrix} 0 \\ 0 \\ 0 \\ 1 \\ 0 \\ 0 \end{bmatrix}$	$\begin{bmatrix} K_{11} & 0 & 0 & 0 & 0 & 0 \\ 0 & K_{22} & 0 & 0 & 0 & K_{26} \\ 0 & 0 & K_{33} & 0 & K_{35} & 0 \\ 0 & 0 & 0 & 0 & 0 & 0 \\ 0 & 0 & K_{53} & 0 & K_{55} & 0 \\ 0 & K_{62} & 0 & 0 & 0 & K_{66} \end{bmatrix}$
Rotational R_y 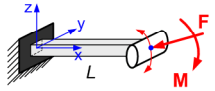	$\mathbf{J}_q^{(5+)} = \begin{bmatrix} 0 \\ 0 \\ 0 \\ 0 \\ 1 \\ 0 \end{bmatrix}$	$\begin{bmatrix} K_{11} & 0 & 0 & 0 & 0 & 0 \\ 0 & K_{22} & 0 & 0 & 0 & K_{26} \\ 0 & 0 & \frac{K_{33}}{4} & 0 & 0 & 0 \\ 0 & 0 & 0 & K_{44} & 0 & 0 \\ 0 & 0 & 0 & 0 & 0 & 0 \\ 0 & K_{62} & 0 & 0 & 0 & K_{66} \end{bmatrix}$
Rotational R_z 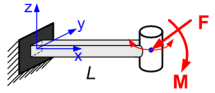	$\mathbf{J}_q^{(6+)} = \begin{bmatrix} 0 \\ 0 \\ 0 \\ 0 \\ 0 \\ 1 \end{bmatrix}$	$\begin{bmatrix} K_{11} & 0 & 0 & 0 & 0 & 0 \\ 0 & \frac{K_{22}}{4} & 0 & 0 & 0 & 0 \\ 0 & 0 & K_{33} & 0 & K_{35} & 0 \\ 0 & 0 & 0 & K_{44} & 0 & 0 \\ 0 & 0 & K_{53} & 0 & K_{55} & 0 \\ 0 & 0 & 0 & 0 & 0 & 0 \end{bmatrix}$

Further, let us consider a set of *quasi-trivial* cases where the Jacobians $\mathbf{J}_{\mathrm{q}}^{i}$ are of a more complicated structure compared to $\mathbf{J}_{\mathrm{q}}^{(4)}, \mathbf{J}_{\mathrm{q}}^{(5)}, \mathbf{J}_{\mathrm{q}}^{(6)}$

$$\mathbf{J}_{\mathrm{q}}^{(4+)} = \begin{bmatrix} 0 \\ d_{\mathrm{y}} \\ d_{\mathrm{z}} \\ 1 \\ 0 \\ 0 \end{bmatrix}, \qquad \mathbf{J}_{\mathrm{q}}^{(5+)} = \begin{bmatrix} d_{\mathrm{x}} \\ 0 \\ d_{\mathrm{z}} \\ 0 \\ 1 \\ 0 \end{bmatrix}, \qquad \mathbf{J}_{\mathrm{q}}^{(6+)} = \begin{bmatrix} d_{\mathrm{x}} \\ d_{\mathrm{y}} \\ 0 \\ 0 \\ 0 \\ 1 \end{bmatrix} \tag{3.50}$$

where d_x, d_y, d_z denote the elements of the vector $\mathbf{d}$ defining the passive joint location. It can be proved that such types of Jacobians describe

- *rotational passive joints* shifted by a distance L with respect to the reference point in the direction either x, y or z (and with the joint axis directed along x, y or z),

and the values of d_x, d_y, d_z are equal to either $\pm L$ or 0.

For these case studies, relevant results are presented in Table 3.2 where the original stiffness matrix $[K_{ij}]$ is assumed to be the same as above. As it follows from them, here the resulting stiffness matrix is singular but does not include purely zero rows and columns. Hence, the existing technique [Taghvaeipour 2010] based on simple zeroing of the rows and columns cannot be applied for such types of passive joints.

Using results obtained for the trivial and quasi-trivial passive joints, in many practically significant cases we can easily modify analytically the original stiffness matrix by sequentially taking into account each passive joint in accordance with the developed recursive technique. Relevant examples will be presented in sub-section 3.4.2

Table 3.2 Examples of stiffness matrix transformations for quasi-trivial passive joints

Type of joint	Jacobian	Modified Stiffness matrix
Rotational R_y 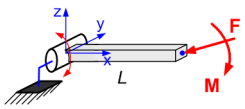	$\mathbf{J}_{q}^{(5+)} = \begin{bmatrix} 0 \\ 0 \\ -L \\ 0 \\ 1 \\ 0 \end{bmatrix}$	$\begin{bmatrix} K_{11} & 0 & 0 & 0 & 0 & 0 \\ 0 & K_{22} & 0 & 0 & 0 & K_{26} \\ 0 & 0 & \frac{K_{33}}{4} & 0 & \frac{K_{35}}{2} & 0 \\ 0 & 0 & 0 & K_{44} & 0 & 0 \\ 0 & 0 & \frac{K_{53}}{2} & 0 & \frac{3 \cdot K_{55}}{4} & 0 \\ 0 & K_{62} & 0 & 0 & 0 & K_{66} \end{bmatrix}$
Rotational R_z 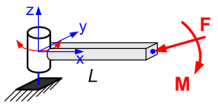	$\mathbf{J}_{q}^{(6+)} = \begin{bmatrix} 0 \\ L \\ 0 \\ 0 \\ 0 \\ 1 \end{bmatrix}$	$\begin{bmatrix} K_{11} & 0 & 0 & 0 & 0 & 0 \\ 0 & \frac{K_{22}}{4} & 0 & 0 & 0 & \frac{K_{26}}{2} \\ 0 & 0 & K_{33} & 0 & K_{35} & 0 \\ 0 & 0 & 0 & K_{44} & 0 & 0 \\ 0 & 0 & K_{53} & 0 & K_{55} & 0 \\ 0 & \frac{K_{62}}{2} & 0 & 0 & 0 & \frac{3 \cdot K_{66}}{4} \end{bmatrix}$

Summarising Section 3.3, its main contribution can be defined as the development of the analytical technique for computing of Cartesian stiffness matrices for serial kinematic chains with passive joints. It is based on the extended stiffness mapping equation, which separates the impact of passive joints and compliant elements presented by actuated and virtual elastic joints. This technique can be applied in one-step manner or recursively, by sequentially modifying the stiffness matrix taking into account the effect of each passive joint separately. The latter significantly simplifies related analytical computation reducing them to elementary algebraic transformations. Advantages of the proposed technique are illustrated by several case studies that give simple and practically convenient rules for stiffness matrix modification for kinematic chains with trivial and quasi-trivial passive joints.

3.4 AGGREGATION OF STIFFNESS MODELS OF PERFECT SERIAL CHAINS

The stiffness modelling technique proposed in Sections 3.2 and 3.3 allows us to compute the stiffness matrix for a serial chain with an arbitrary location of passive joints and to evaluate its properties. It also provides an analytical solution of the problem. But this technique is limited by the stiffness modelling of serial kinematic chains or serial manipulators. Hence, it is reasonable to extend this technique for parallel architectures and to propose the method of aggregation of the elastostatic models of separate kinematic chains to the stiffness model of the parallel manipulator. Let us consider this problem in details.

3.4.1 Stiffness model aggregation technique

Let us assume that a parallel manipulator may be presented as a strictly parallel system of the actuated serial legs connecting the base and the end-platform (Figure 3.1) [Merlet 2006]. Using the methodology described in the previous sections and applying it to each leg, a set of m Cartesian stiffness matrices $\mathbf{K}_{\mathrm{C}}^{(i)}$ expressed with respect to the same coordinate system but corresponding to different platform points can be computed. If initially the chain stiffness matrices have been computed in local coordinate systems, their transformation is performed in a standard way [Angeles 2007], as

$$\mathbf{K}_{\mathrm{C}}^{\mathrm{glob}} = \begin{bmatrix} \mathbf{R} & \mathbf{0} \\ \mathbf{0} & \mathbf{R} \end{bmatrix} \cdot \mathbf{K}_{\mathrm{C}}^{\mathrm{loc}} \cdot \begin{bmatrix} \mathbf{R}^{\mathrm{T}} & \mathbf{0} \\ \mathbf{0} & \mathbf{R}^{\mathrm{T}} \end{bmatrix} \tag{3.51}$$

where $\mathbf{R}$ is a 3×3 rotation matrix describing orientation of the local coordinate system with respect to the global one.

To aggregate these matrices $\mathbf{K}_{\mathrm{C}}^{(i)}$, they must be also re-computed with respect to the same reference point of the platform. Assuming that the platform is rigid enough (as compared to the compliance of the legs), this conversion can be performed by extending the legs by a virtual rigid link connecting the end-point of the leg and the reference point of the platform (see Figure 3.3 where these extensions are defined by the vectors $\mathbf{v}_i$).

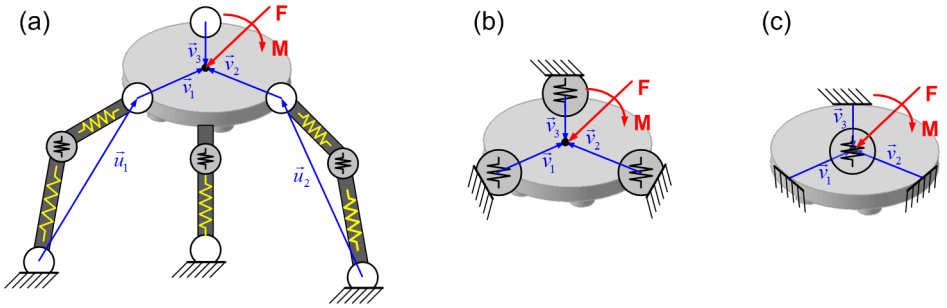

Figure 3.3 Typical parallel manipulator (a) and transformation of its VJM models (b, c)

After such extension, an equivalent stiffness matrix of the leg may be expressed using relevant expression for a usual serial chain, i.e. as $\mathbf{J}_{\mathrm{v}}^{(i)-\mathrm{T}} \cdot \mathbf{K}_{\mathrm{C}}^{(i)} \cdot \mathbf{J}_{\mathrm{v}}^{(i)-1}$, where the Jacobian $\mathbf{J}_{\mathrm{v}}^{(i)}$ defines differential relation between the coordinates of the i-th virtual spring and the reference frame of the end-platform. Hence, the final expression for the stiffness matrix of the considered parallel manipulator can be written as

$$\mathbf{K}_{\mathrm{C}}^{(m)} = \sum_{i=1}^{m} \left(\mathbf{J}_{\mathrm{v}}^{(i)^{-\mathrm{T}}} \cdot \mathbf{K}_{\mathrm{C}}^{(i)} \cdot \mathbf{J}_{\mathrm{v}}^{(i)^{-1}} \right) \tag{3.52}$$

where m is the number of serial kinematic chains in the manipulator architecture.

As a result, expression (3.52) allows us to compute Cartesian stiffness matrix for the parallel manipulator based on stiffness matrices for serial chains and transformation Jacobians $\mathbf{J}_{\mathrm{v}}^{(i)}$, which define geometrical mapping between end-points of serial chains and reference point frame (end-effector). Moreover, it is implicitly assumed here that all stiffness matrices (both for the serial chains and for the whole manipulator) are expressed in the same global coordinate system, otherwise they should be recomputed to

requisite coordinates. Hence, the axes of all virtual springs are parallel to the axes x, y, z of this system. This allows to evaluate Jacobians $\mathbf{J}_{\mathrm{v}}^{(i)}$ and their inverses from the geometry of the end-platform analytically

$$\mathbf{J}_{\mathrm{v}}^{(i)} = \begin{bmatrix} \mathbf{I}_3 & (\mathbf{v}_i\times) \\ \mathbf{0} & \mathbf{I}_3 \end{bmatrix}_{6\times 6}, \qquad \mathbf{J}_{\mathrm{v}}^{(i)-1} = \begin{bmatrix} \mathbf{I}_3 & -(\mathbf{v}_i\times) \\ \mathbf{0} & \mathbf{I}_3 \end{bmatrix}_{6\times 6} \tag{3.53}$$

where $\mathbf{I}_3$ is 3×3 identity matrix, and $(\mathbf{v}\times)$ is a skew-symmetric matrix corresponding to the vector $\mathbf{v}$:

$$(\mathbf{v}\times) = \begin{bmatrix} 0 & -v_{\mathrm{z}} & v_{\mathrm{y}} \\ v_{\mathrm{z}} & 0 & -v_{\mathrm{x}} \\ -v_{\mathrm{y}} & v_{\mathrm{x}} & 0 \end{bmatrix} \tag{3.54}$$

Therefore, expression (3.52) represents explicit aggregation of the leg stiffness matrices with respect to any given reference point of the platform. It is worth mentioning that in practice, the matrices $\mathbf{K}_{\mathrm{C}}^{(i)}$ are always singular while the aggregation usually produces non-singular matrix. Relevant examples are presented in the following sub-section.

3.4.2 Application example: Gough platform

Let us apply now the developed technique to computing of the stiffness matrix for two versions of a general Stewart-Gough platform presented in Figure 3.4 [Chen 2008], [Li 2002b], [El-Khasawneh 1999], [Arumugam 2004]. It is assumed that in both cases the manipulator base and the moving plate (platform) are connected by six similar extensible legs (Figure 3.5) but their spatial arrangements are different:

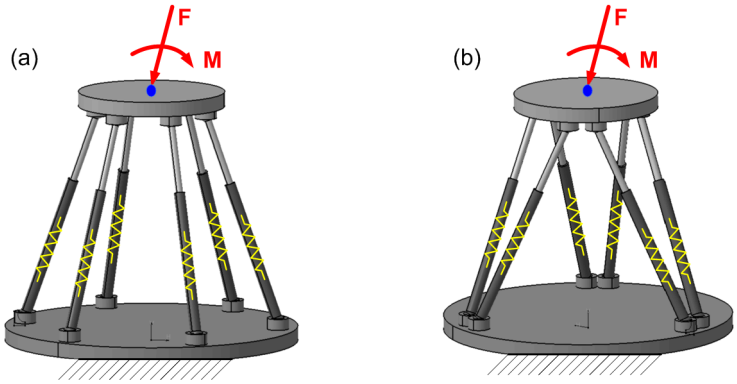

Figure 3.4 Geometry of the Stewart-Gough platforms under study

Figure 3.5 Geometry of the manipulator leg and its VJM model

Case A: the legs are regularly connected to the base and platform, with the same angular distance 60° (it is obviously a degenerated design, where the stiffness matrix should be singular)

Case B: the legs are connected to the base and platform in three pairs, with the angular distance of 120° between the mounting points (it is a classical design of Stewart-Gough where the stiffness matrix should be non-singular).

For both designs, the original leg stiffness (i.e. without the passive joints) can be described by the sparse matrix corresponding to the symmetric beam (see Chapter 2). Further, to take into account the

influence of the passive joints, it should be applied recursively to the procedure (3.41) with the elementary Jacobians

$$\mathbf{J}_{\mathrm{Rx}}^{(1)}=\begin{bmatrix}0\\0\\0\\1\\0\\0\end{bmatrix};\quad \mathbf{J}_{\mathrm{Ry}}^{(2)}=\begin{bmatrix}0\\0\\0\\0\\1\\0\end{bmatrix};\quad \mathbf{J}_{\mathrm{Rz}}^{(3)}=\begin{bmatrix}0\\0\\0\\0\\0\\1\end{bmatrix};\quad \mathbf{J}_{\mathrm{Ry+}}^{(4)}=\begin{bmatrix}0\\0\\-L\\0\\1\\0\end{bmatrix};\quad \mathbf{J}_{\mathrm{Rz+}}^{(5)}=\begin{bmatrix}0\\L\\0\\0\\0\\1\end{bmatrix} \tag{3.55}$$

where L is the leg length. It is obvious that, due to the trivial structure of $\mathbf{J}_{\mathrm{q}}^{\,i}$, the recursive computations can be easily performed analytically (see Section 3.3.3). They sequentially produce the following results:

$$\mathbf{K}_C^0=\left[\begin{array}{ccc:ccc}K_{11}&0&0&0&0&0\\0&K_{22}&0&0&0&K_{26}\\0&0&K_{33}&0&K_{35}&0\\\hdashline 0&0&0&K_{44}&0&0\\0&0&K_{53}&0&K_{55}&0\\0&K_{62}&0&0&0&K_{66}\end{array}\right]\qquad \mathbf{K}_C^1=\left[\begin{array}{ccc:ccc}K_{11}&0&0&0&0&0\\0&K_{22}&0&0&0&K_{26}\\0&0&K_{33}&0&K_{35}&0\\\hdashline 0&0&0&0&0&0\\0&0&K_{53}&0&K_{55}&0\\0&K_{62}&0&0&0&K_{66}\end{array}\right]$$

$$\mathbf{K}_C^2=\left[\begin{array}{ccc:ccc}K_{11}&0&0&0&0&0\\0&K_{22}&0&0&0&K_{26}\\0&0&K_{33}/4&0&0&0\\\hdashline 0&0&0&0&0&0\\0&0&0&0&0&0\\0&K_{62}&0&0&0&K_{66}\end{array}\right]\qquad \mathbf{K}_C^3=\left[\begin{array}{ccc:ccc}K_{11}&0&0&0&0&0\\0&K_{22}/4&0&0&0&0\\0&0&K_{33}/4&0&0&0\\\hdashline 0&0&0&0&0&0\\0&0&0&0&0&0\\0&0&0&0&0&0\end{array}\right]$$

$$\mathbf{K}_C^4=\left[\begin{array}{ccc:ccc}K_{11}&0&0&0&0&0\\0&K_{22}/4&0&0&0&0\\0&0&0&0&0&0\\\hdashline 0&0&0&0&0&0\\0&0&0&0&0&0\\0&0&0&0&0&0\end{array}\right]\qquad \mathbf{K}_C^5=\left[\begin{array}{ccc:ccc}K_{11}&0&0&0&0&0\\0&0&0&0&0&0\\0&0&0&0&0&0\\\hdashline 0&0&0&0&0&0\\0&0&0&0&0&0\\0&0&0&0&0&0\end{array}\right]$$

Hence, in the final form, the derived matrix includes only the traction/compression terms (and not bending, torsion, etc.) that agrees perfectly with other results on Stewart-Gough platforms.

Further, in order to be applied to each leg, the obtained matrix must be transformed from the local to the global coordinate system. In this specific case, due to the special structure of $\mathbf{K}_{\mathrm{C}}^5$, relevant transformation [Deblaise 2006a], [Angeles 2007]

$$\mathbf{K}_{\mathrm{C}_i}=\begin{bmatrix}\mathbf{R}_i&\mathbf{0}\\\mathbf{0}&\mathbf{R}_i\end{bmatrix}\cdot K_{11}\cdot\left[\begin{array}{cc:c}1&&\\&0&\mathbf{0}_{3\times3}\\&0&\\\hdashline &\mathbf{0}_{3\times3}&\mathbf{0}_{3\times3}\end{array}\right]\cdot\begin{bmatrix}\mathbf{R}_i^{\mathrm{T}}&\mathbf{0}\\\mathbf{0}&\mathbf{R}_i^{\mathrm{T}}\end{bmatrix} \tag{3.56}$$

expressed via the orthogonal rotation matrix $\mathbf{R}_i$ describing orientation of the i-th local coordinate system with respect to the global one, is easily reduced to

$$\mathbf{K}_{\mathrm{C}_i}=K_{11}\cdot\left[\begin{array}{c:c}\mathbf{u}_i^0\cdot\mathbf{u}_i^{0T}&\mathbf{0}_{3\times3}\\\hdashline \mathbf{0}_{3\times3}&\mathbf{0}_{3\times3}\end{array}\right]. \tag{3.57}$$

where $\mathbf{u}_i^0$ is the unit vector directed along the leg axis $\mathbf{u}_i$ (see Figure 3.3). Besides, before aggregating, the stiffness matrices of the separate legs $\mathbf{K}_{\mathrm{C}_i}$ must be re-computed with respect to the same reference point in accordance with expressions (3.51) (3.52) which yields

$$\mathbf{K}_{\mathrm{C}} = K_{11} \cdot \sum_{i=1}^{6} \left[\begin{array}{c|c} \mathbf{I}_3 & \mathbf{0} \\ \hline (\mathbf{v}_i\times) & \mathbf{I}_3 \end{array} \right] \cdot \left[\begin{array}{c|c} \mathbf{u}_i^0 \cdot \mathbf{u}_i^{0\mathrm{T}} & \mathbf{0}_{3\times3} \\ \hline \mathbf{0}_{3\times3} & \mathbf{0}_{3\times3} \end{array} \right] \cdot \left[\begin{array}{c|c} \mathbf{I}_3 & (\mathbf{v}_i\times)^{\mathrm{T}} \\ \hline \mathbf{0} & \mathbf{I}_3 \end{array} \right] \tag{3.58}$$

where $\mathbf{v}_i$ is the vector from the leg end-point to the platform reference point (see Figure 3.3). So, after relevant transformations, one can get the final expression of the manipulator stiffness matrix

$$\mathbf{K}_{\mathrm{C}} = K_{11} \cdot \sum_{i=1}^{6} \left[\begin{array}{c|c} (\mathbf{u}_i^0\mathbf{u}_i^{0\mathrm{T}}) & (\mathbf{u}_i^0\mathbf{u}_i^{0\mathrm{T}}) \cdot (\mathbf{v}_i\times)^{\mathrm{T}} \\ \hline (\mathbf{v}_i\times) \cdot (\mathbf{u}_i^0\mathbf{u}_i^{0\mathrm{T}}) & (\mathbf{v}_i\times) \cdot (\mathbf{u}_i^0\mathbf{u}_i^{0\mathrm{T}}) \cdot (\mathbf{v}_i\times)^{\mathrm{T}} \end{array} \right] \tag{3.59}$$

or

$$\mathbf{K}_{\mathrm{C}} = K_{11} \cdot \sum_{i=1}^{6} \left[\begin{array}{c} \mathbf{u}_i^0 \\ \hline (\mathbf{v}_i\times \mathbf{u}_i^0) \end{array} \right] \cdot \left[\begin{array}{c|c} \mathbf{u}_i^{0\mathrm{T}} & (\mathbf{v}_i\times \mathbf{u}_i^0)^{\mathrm{T}} \end{array} \right] \tag{3.60}$$

where the vector $\mathbf{u}_i$, $\mathbf{v}_i$ describing spatial locations of the legs and computed via the direct kinematics, and $\mathbf{v}_i\times\mathbf{u}_i^0$ denotes the vector product (in contrast to the above notation $(\mathbf{v}_i\times)$ which is referred to the corresponding skew-symmetric matrix).

The derived equation has been applied to both case studies, assuming that the manipulators are in their "*home*" configurations when the platform is parallel to the base and it is symmetrical with respect to the vertical axis. Corresponding expressions for the leg vectors are

$$\mathbf{u}_i = \begin{bmatrix} r\cos(\psi_i) - R\cos(\phi_i) \\ r\sin(\psi_i) - R\sin(\phi_i) \\ h \end{bmatrix}, \qquad \mathbf{v}_i = \begin{bmatrix} -r\cos(\psi_i) \\ -r\sin(\psi_i) \\ 0 \end{bmatrix} \tag{3.61}$$

where $\phi_i = \psi_i \in \{0, 60°, 120°, 180°, 240°, 300°\}$ for the case A, and $\phi_i \in \{0, 120°, 120°, 240°, 240°, 360°\}$; $\psi_i \in \{60, 60, 180°, 180°, 300°, 300°\}$ for the case B. Substitution of these vectors into the expression (3.59) leads to the following stiffness matrices

$$\mathbf{K}_{\mathrm{C}}^{(A)} = \frac{3K_{11}}{L^2} \left[\begin{array}{ccc|ccc} d_{\mathrm{a}}^2 & 0 & 0 & 0 & rhd_{\mathrm{a}} & 0 \\ 0 & d_{\mathrm{a}}^2 & 0 & -rhd_{\mathrm{a}} & 0 & 0 \\ 0 & 0 & 2h^2 & 0 & 0 & 0 \\ \hline 0 & -rhd_{\mathrm{a}} & 0 & r^2h^2 & 0 & 0 \\ rhd_{\mathrm{a}} & 0 & 0 & 0 & r^2h^2 & 0 \\ 0 & 0 & 0 & 0 & 0 & 0 \end{array} \right] \tag{3.62}$$

and

$$\mathbf{K}_{\mathrm{C}}^{(B)} = \frac{3K_{11}}{L^2} \left[\begin{array}{ccc|ccc} d_{\mathrm{a}}^2 + Rr & 0 & 0 & 0 & rhd_{\mathrm{b}} & 0 \\ 0 & d_{\mathrm{a}}^2 + Rr & 0 & -rhd_{\mathrm{b}} & 0 & 0 \\ 0 & 0 & 2h^2 & 0 & 0 & 0 \\ \hline 0 & -rhd_{\mathrm{b}} & 0 & r^2h^2 & 0 & 0 \\ rhd_{\mathrm{b}} & 0 & 0 & 0 & r^2h^2 & 0 \\ 0 & 0 & 0 & 0 & 0 & 1.5\,r^2R^2 \end{array} \right] \tag{3.63}$$

where R and r denote the circle radius which comprise the leg connection point at the base and moving platform respectively, $d_{\mathrm{a}} = R - r$; $d_{\mathrm{b}} = R/2 - r$; L is the leg length, h is the vertical distance between the base and the platform, and the superscripts 'A' and 'B' define the relevant case study. As it follows from these expressions, in 'zero' location the matrix $\mathbf{K}_{\mathrm{C}}^{(A)}$ is singular and allows "free" rotation of the end-platform around the vertical axis. In contrast, for the same location the matrix $\mathbf{K}_{\mathrm{C}}^{(B)}$ is non-singular and the manipulator resists to all external forces/torques applied to the platform. These results are in good agreement with previous research on the Stewart-Gough platforms and confirm efficiency of the developed computational technique for manipulator stiffness modeling [Svinin 2001], [Li 2002b].

Hence, proposed stiffness model assembling technique allows us to aggregate elastostatic models of separate kinematic chains in the stiffness model of the parallel manipulator. It is also able to take into account the geometry of the end-platform and its connection with kinematic chains in an explicit form.

3.5 AGGREGATION OF STIFFNESS MODELS OF NON-PERFECT SERIAL CHAINS

In the previous Section, it was implicitly assumed that kinematic chains of the parallel manipulator are "*perfect*", i.e. their geometrical parameters are strictly nominal and their end-frames can be aligned and matched without additional efforts and/or internal stresses, while assembling. However, in practice, the kinematic chain geometry may differ from the nominal one (i.e. be "*non-perfect*"), and the assembling causes internal stresses and shifting of the end-points location. Thus, let us extend the above aggregation procedure to the case of non-perfect serial chains and develop a technique, which is able to evaluate deflections and internal forces/torques caused by geometrical errors in the chains.

3.5.1 Stiffness model aggregation technique

Let us consider a parallel manipulator, which may be presented as a strictly parallel system of the actuated serial legs connecting the fixed base and mobile end-platform [Merlet 2006]. Using the methodology described in the previous sections, each *i*-th leg (serial chain) may be characterized by the geometrical function $\mathbf{t}_i = \mathbf{g}_i(\mathbf{q}_i, \boldsymbol{\theta}_i)$, where $\mathbf{t}_i$ defines the end-frame location and $\mathbf{q}_i, \boldsymbol{\theta}_i$ are passive and virtual joint coordinates respectively, which define kinematic chain configuration. For perfect kinematic chains, the joint coordinates $\mathbf{q}_i, \boldsymbol{\theta}_i$ are computed using nominal geometrical model of the leg $\mathbf{g}_i^0(\mathbf{q}_i, \boldsymbol{\theta}_i)$, for the given end-platform location $\mathbf{t}^0$. These notations are illustrated by Figure 3.6a where A_i correspond to the end-points of the perfect chains and O is the platform reference point. Similar to Section 3.4, the vectors $\overrightarrow{A_i O}$ are denoted as $\mathbf{v}_i$. Using the above presented technique, it is possible to compute the Cartesian stiffness matrices of the chains and express them with respect to the same reference point O. Let us denote this matrix as $\mathbf{K}_C^{(i)}$ (see sub-section 3.4.1 for the details).

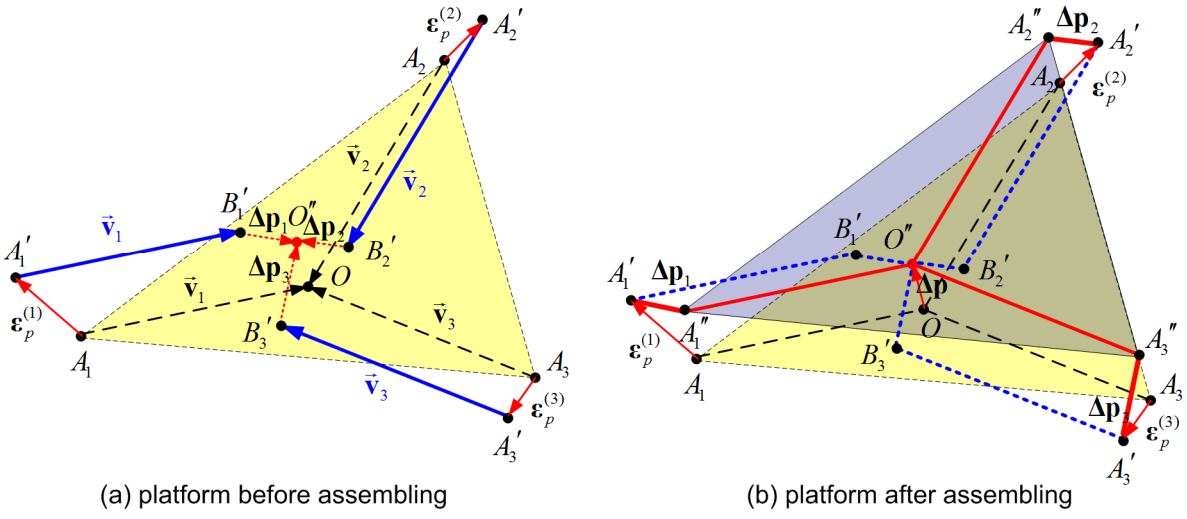

Figure 3.6 Transformation of characteristic points of serial chains in assembling of non-perfect parallel manipulator; (A_i , A_i' - end-point locations of serial chain before assembling for perfect and non-perfect manipulators respectively, A_i'' - end-point location of serial chain after assembling for non-perfect manipulator)

For the non-perfect chain before assembling, similar configurations $\mathbf{q}_i, \boldsymbol{\theta}_i$ produce slightly different end-point locations of the chains $\mathbf{t}_i = \mathbf{g}_i^0(\mathbf{q}_i, \boldsymbol{\theta}_i) + \boldsymbol{\varepsilon}_i$, which are denoted as A_i' in Figure 3.6a. Correspondently, assuming that the platform is rigid enough, the points A_i' can be mapped to B_i' that differ from O by $\boldsymbol{\varepsilon}_i$. Hence, geometrical errors do not allow assembling parallel manipulator at the original reference point.

To assemble all chains in the same reference point, it is required to apply additional efforts. Geometrically, it leads to relocation of the frames corresponding to the points B_i' to a new position B_i'', and relocations of the point A_i' to A_i'' that is defined by the vector $\Delta\mathbf{t}_i$. In Figure 3.6b, relevant reference point of the platform is denoted as O''. Hence, the stiffness model aggregation problem is reduced to computing of a new end-platform location $\mathbf{t}^0 + \Delta\mathbf{t}$ for which end-frames of all kinematic chains are aligned and matched.

Consequently, a manipulator will occupy the most advantageous configuration with respect to the potential energy of the elastic elements.

To compute the end-platform deflection $\Delta\mathbf{t}$, let us assume that the geometrical errors are small enough and corresponding shifting of the chain end-points and end-effector do not change Cartesian stiffness matrices $\mathbf{K}_{\mathrm{C}}^{(i)}$ or their influences are negligible. So, the stiffness matrices of the serial chains $\mathbf{K}_{\mathrm{C}}^{(i)}$ are the same at the points O, B_i' and O'' and computed for the nominal configurations $\mathbf{q}_i, \boldsymbol{\theta}_i$. Let us also assume that the point O'' is shifted from O by $\Delta\mathbf{p}$ and the mobile platform orientations for the parallel manipulator with perfect and non-perfect serial chains differ by $\Delta\boldsymbol{\varphi}$. This allows us to express the potential energy of the parallel manipulator with geometrical errors in kinematic chains as

$$E = \frac{1}{2}\sum_{i=1}^{m}\left(\left(\boldsymbol{\varepsilon}_i - \Delta\mathbf{t}\right)^{\mathrm{T}} \cdot \mathbf{K}_{\mathrm{C}}^{(i)} \cdot \left(\boldsymbol{\varepsilon}_i - \Delta\mathbf{t}\right)\right) \tag{3.64}$$

where $\Delta\mathbf{t} = (\Delta\mathbf{p}, \Delta\boldsymbol{\varphi})$ is displacement (position and orientation) of the reference point.

It is obvious that after assembling, the considered mechanical system will occupy the most advantageous configuration with respect to the potential energy, i.e. $E \to \min\limits_{\Delta\mathbf{t}}$. It means that the desired vector $\Delta\mathbf{t}$ can be found from the expression

$$\frac{\partial E}{\partial \Delta\mathbf{t}} = \sum_{i=1}^{m}\left(\mathbf{K}_{\mathrm{C}}^{(i)} \cdot \left(\Delta\mathbf{t} - \boldsymbol{\varepsilon}_i\right)\right) = 0 \tag{3.65}$$

that yields the following linear equation

$$\sum_{i=1}^{m}\mathbf{K}_{\mathrm{C}}^{(i)} \cdot \Delta\mathbf{t} = \sum_{i=1}^{m}\left(\mathbf{K}_{\mathrm{C}}^{(i)} \cdot \boldsymbol{\varepsilon}_i\right) \tag{3.66}$$

which allows us to evaluate the end-platform deflection

$$\Delta\mathbf{t} = \left(\sum_{i=1}^{m}\mathbf{K}_{\mathrm{C}}^{(i)}\right)^{-1} \cdot \sum_{i=1}^{m}\left(\mathbf{K}_{\mathrm{C}}^{(i)} \cdot \boldsymbol{\varepsilon}_i\right) \tag{3.67}$$

and the end-platform location after assembling

$$\mathbf{t}' = \mathbf{t}^0 + \Delta\mathbf{t} \tag{3.68}$$

For each separate kinematic chain, the end-frame deflections due to assembling can be expressed as

$$\Delta\mathbf{t}_i = \Delta\mathbf{t} - \boldsymbol{\varepsilon}_i = \left(\sum_{i=1}^{m}\mathbf{K}_{\mathrm{C}}^{(i)}\right)^{-1} \cdot \sum_{i=1}^{m}\left(\mathbf{K}_{\mathrm{C}}^{(i)} \cdot \boldsymbol{\varepsilon}_i\right) - \boldsymbol{\varepsilon}_i \tag{3.69}$$

This allows us to compute the loading for each kinematic chain applied to the end-point (due to interaction with other non-perfect chains)

$$\mathbf{F}_i = \mathbf{K}_{\mathrm{C}}^{(i)} \cdot \Delta\mathbf{t}_i \tag{3.70}$$

and corresponding loadings in the virtual joints $\boldsymbol{\tau}_{\theta}^{(i)}$

$$\boldsymbol{\tau}_{\theta}^{(i)} = \mathbf{J}_{\theta}^{(i)\mathrm{T}} \cdot \mathbf{F}_i = \mathbf{J}_{\theta}^{(i)\mathrm{T}} \cdot \mathbf{K}_{\mathrm{C}}^{(i)} \cdot \Delta\mathbf{t}_i \tag{3.71}$$

It is worth mentioning that here $\sum_{i=1}^{m}\mathbf{F}_i = \mathbf{0}$, since there is no external loading applied to the platform reference point after the assembling. Besides, it is possible to compute relevant deflections of the virtual and passive joint coordinates of the chains

$$\boldsymbol{\theta}_i = \mathbf{K}_{\mathrm{C}\theta}^{(i)} \cdot \Delta\mathbf{t}_i; \qquad \Delta\mathbf{q}_i = \mathbf{K}_{\mathrm{Cq}}^{(i)} \cdot \Delta\mathbf{t}_i \tag{3.72}$$

caused by the assembling.

Thus, the above expressions allow us to evaluate the end-platform deflection and internal forces/torques caused by assembling of kinematic chains with geometrical errors. However, the total manipulator Cartesian stiffness matrix $\mathbf{K}_{\mathrm{C}}$ is assumed to be the same as in Section 3.4, since the geometrical errors are assumed to be small enough.

3.5.2 Application examples: parallel translational manipulators

Let us illustrate the developed stiffness model aggregation technique by examples that deal with assembling of Orthoglide and 3-PUU parallel translational manipulators with geometrical errors in kinematic chains (Figure 3.7). Both manipulators consist of three kinematic chains with one translational actuator along the axes x, y or z, two passive U-joints (or two separate rotational joints) and the bar or the kinematic parallelogram between them. These manipulators have the working area of size 200×200×200 mm with the transmission factor from 0.5 to 2; the detailed geometrical parameters are presented in [Chablat 2003], the link stiffness matrices were computed using an approach developed in Chapter 2. Their numerical values are presented in sub-section 2.7. Let us assume that the manipulators have geometrical errors in the kinematic chains, which have effects on the end-point location and provoke internal loadings in the joints.

Taking into account the shape of the dexterous workspace, let us focus on the stiffness analysis of these manipulators in five characteristic points: isotropic point Q_0, two limit points Q_1 and Q_2. with symmetrical configuration and two limit points Q_3 and Q_4. with non-symmetrical configuration [Pashkevich 2005] (see Figure 3.7). Let us estimate the end-effector location and internal deflections/loadings caused by the geometrical errors in the chains. The stiffness matrices of the chains for both manipulators in the points Q_0...Q_4 have been computed using the technique proposed in Section 3.2.3.

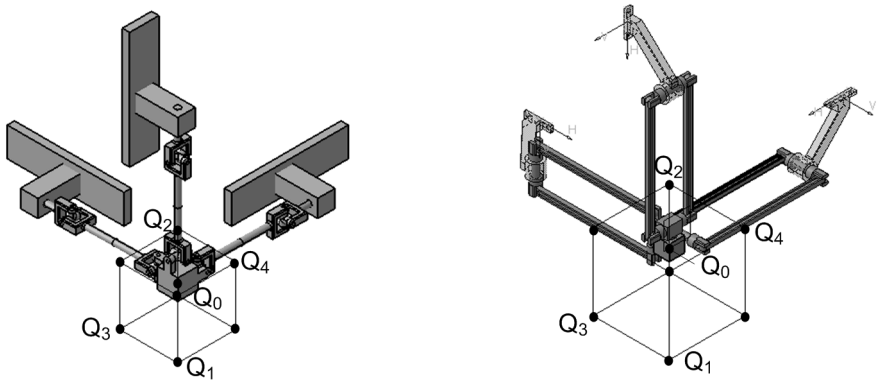

(a) 3-PUU manipultor (b) Orthoglide manipultor

Figure 3.7 CAD models of 3-PUU and Orthoglide manipulators

For illustration purposes, let us investigate two types of geometrical errors

Case A: Each actuator of the manipulator has a *position error* 1 mm in actuator location $\boldsymbol{\varepsilon}_1^0 = (1, 0, 0, 0, 0, 0)^T$; $\boldsymbol{\varepsilon}_2^0 = (0, 1, 0, 0, 0, 0)^T$; $\boldsymbol{\varepsilon}_3^0 = (0, 0, 1, 0, 0, 0)^T$;

Case B: Each actuator of the manipulator has an *angular error* 1° in actuator location $\boldsymbol{\varepsilon}_1^0 = (0, 0, 0, 1^\circ, 0, 0)^T$; $\boldsymbol{\varepsilon}_2^0 = (0, 0, 0, 0, 1^\circ, 0)^T$; $\boldsymbol{\varepsilon}_3^0 = (0, 0, 0, 0, 0, 1^\circ)^T$.

In case A, as it follows from the chains geometry, the deflections of the chain end-points before assembling $\boldsymbol{\varepsilon}_i$ may be expressed as

points $\mathbf{Q}_0$...$\mathbf{Q}_4$

$$\boldsymbol{\varepsilon}_1 = \boldsymbol{\varepsilon}_1^0; \quad \boldsymbol{\varepsilon}_2 = \boldsymbol{\varepsilon}_2^0; \quad \boldsymbol{\varepsilon}_3 = \boldsymbol{\varepsilon}_3^0.$$

In case B, the values $\boldsymbol{\varepsilon}_i$ should be computed using the geometrical model $\mathbf{g}_i(\mathbf{q}_i, \boldsymbol{\theta}_i)$:

point $\mathbf{Q}_0$:

$$\boldsymbol{\varepsilon}_1 = \left(0 \quad -1.68{\cdot}10^{-2} \quad 1.92 \;\vdots\; 1^\circ \quad 0 \quad 0\right)^T;$$

$$\boldsymbol{\varepsilon}_2 = \left(1.92 \quad 0 \quad -1.68{\cdot}10^{-2} \;\vdots\; 0 \quad 1^\circ \quad 0\right)^T;$$

$$\boldsymbol{\varepsilon}_3 = \left(-1.68{\cdot}10^{-2} \quad 1.92 \quad 0 \;\vdots\; 0 \quad 0 \quad 1^\circ\right)^T;$$

point Q_1:

$$\boldsymbol{\varepsilon}_1 = \left(0 \quad -2.24 \quad 4.11 \;\vdots\; 1^\circ \quad 0 \quad 0\right)^T;$$
$$\boldsymbol{\varepsilon}_2 = \left(4.11 \quad 0 \quad -2.24 \;\vdots\; 0 \quad 1^\circ \quad 0\right)^T;$$
$$\boldsymbol{\varepsilon}_3 = \left(-2.24 \quad 4.11 \quad 0 \;\vdots\; 0 \quad 0 \quad 1^\circ\right)^T;$$

point Q_2:

$$\boldsymbol{\varepsilon}_1 = \left(0 \quad 1.28 \quad 6.46\cdot10^{-1} \;\vdots\; 1^\circ \quad 0 \quad 0\right)^T;$$
$$\boldsymbol{\varepsilon}_2 = \left(6.46\cdot10^{-1} \quad 0 \quad 1.28 \;\vdots\; 0 \quad 1^\circ \quad 0\right)^T;$$
$$\boldsymbol{\varepsilon}_3 = \left(1.28 \quad 6.46\cdot10^{-1} \quad 0 \;\vdots\; 0 \quad 0 \quad 1^\circ\right)^T;$$

point Q_3:

$$\boldsymbol{\varepsilon}_1 = \left(\ 0 \quad 1.25 \quad 4.14 \;\vdots\; 1^\circ \quad 0 \quad 0\right)^T;$$
$$\boldsymbol{\varepsilon}_2 = \left(0.62 \quad 0 \quad -2.21 \;\vdots\; 0 \quad 1^\circ \quad 0\right)^T;$$
$$\boldsymbol{\varepsilon}_3 = \left(-2.24 \quad 4.11 \quad 0 \;\vdots\; 0 \quad 0 \quad 1^\circ\right)^T;$$

point Q_4:

$$\boldsymbol{\varepsilon}_1 = \left(0 \quad -2.21 \quad 0.62 \;\vdots\; 1^\circ \quad 0 \quad 0\right)^T;$$
$$\boldsymbol{\varepsilon}_2 = \left(4.14 \quad 0 \quad 1.25 \;\vdots\; 0 \quad 1^\circ \quad 0\right)^T;$$
$$\boldsymbol{\varepsilon}_3 = \left(1.28 \quad 0.65 \quad 0 \;\vdots\; 0 \quad 0 \quad 1^\circ\right)^T;$$

Further, substituting these deflections $\boldsymbol{\varepsilon}_i$ and corresponding chain stiffness matrices $\mathbf{K}_{\mathrm{C}}^{(i)}$ into formulas (3.67) - (3.72), we can compute the desired assembling-induced values of the end-platform displacement, the internal forces/torques and the relevant displacements in virtual and passive joints. Main results of this study for Orthoglide and 3-PUU manipulators are summarised in Tables 3-3 – 3-6, where $\Delta q^{\max}$ is the maximum rotational displacement of passive joints, $\theta_{\mathrm{p}}^{\max}, \theta_{\varphi}^{\max}$ are maximum displacement of translational and rotational virtual springs respectively, $\tau_{\mathrm{p}}^{\max}$, $\tau_{\varphi}^{\max}$ are maximum torques in translational and rotational virtual joints respectively, $M^{\max}$ is the maximum moment in the chains, caused by assembling of a parallel manipulator with the non-perfect kinematic chains.

These results show that in the Case A (Tables 3-3 and 3-5), the geometrical errors in the kinematic chains do not cause any internal loading for both manipulators. However, they provoke the shift of the end-platform location up to 2.02 mm (point Q_2). Corresponding changes in passive joint coordinates are about 0.42° (point Q_2).

In contrast, in the Case B, the geometrical errors in the kinematic chains of Orthoglide (Table 3.4) cause essential internal loadings. For instance, in point Q_1 the torque applied to the end-point of the chain can reach up to $8.91\,\mathrm{N\cdot m}$. This loading induces displacements up to $0.41\,\mathrm{mm}$ and 0.62° for translational and rotational virtual springs respectively. It should be noted that here the loadings for rotational virtual springs are up to $11.96\,\mathrm{N\cdot m}$, but for translational virtual springs they are equal to zero (in spite of non-zero deflections in them). Nevertheless, this result is reasonable due to the non-diagonal structure of the matrices $\mathbf{K}_{\mathrm{C}}^{(i)}$ representing couplings between rotational and translational deflections. Variations in the passive joint coordinates can reach up to 0.67° (Point Q_3). For the end-platform, this case study gives the positional deflection up to 1.31 mm (Point Q_3) and the rotational deflection up to 0.62° (Point Q_1). It is obvious that the total sum of all internal loadings is equal to zero.

However, in the Case B for the 3-PUU manipulator (Table 3.6), there is no internal loading caused by assembling of non-perfect kinematic chains, while the end-platform deflections can reach up to 0.98 mm and

1.33° which is slightly lower than for Orthoglide. This essential difference in properties of these two manipulators is explained by their geometrical structures (Orthoglide is over-constrained manipulator, while 3-PUU is non over-constrained one).

Table 3.3 Assembling of Orthoglide manipulator with non-perfect chains: loadings and displacements for the case A ($\Delta\mathbf{t} = \left[\delta_1, \delta_2, \delta_3, 0, 0, 0\right]^T$, $\mathbf{F}_1 = \mathbf{0}$, $\mathbf{F}_2 = \mathbf{0}$, $\mathbf{F}_3 = \mathbf{0}$)

Point	Displacement of end-point $\Delta\mathbf{t}$	Deflections and loadings in joints and links
Q_0	$\delta_1 = \delta_2 = \delta_3 = 1\,\text{mm};$	$\Delta q^{\max} = 0.18^\circ;$ $\theta_{\text{p}}^{\max} = 0;$ $\theta_{\varphi}^{\max} = 0$ $\tau_{\text{p}}^{\max} = 0;$ $\tau_{\varphi}^{\max} = 0$
Q_1	$\delta_1 = \delta_2 = \delta_3 = 0.50\,\text{mm}$	$\Delta q^{\max} = 0.14^\circ;$ $\theta_{\text{p}}^{\max} = 0;$ $\theta_{\varphi}^{\max} = 0$ $\tau_{\text{p}}^{\max} = 0;$ $\tau_{\varphi}^{\max} = 0$
Q_2	$\delta_1 = \delta_2 = \delta_3 = 2.02\,\text{mm};$	$\Delta q^{\max} = 0.42^\circ;$ $\theta_{\text{p}}^{\max} = 0;$ $\theta_{\varphi}^{\max} = 0$ $\tau_{\text{p}}^{\max} = 0;$ $\tau_{\varphi}^{\max} = 0$
Q_3	$\delta_1 = \delta_2 = 0.73\,\text{mm};$ $\delta_3 = 0.27\,\text{mm}$	$\Delta q^{\max} = 0.20^\circ;$ $\theta_{\text{p}}^{\max} = 0;$ $\theta_{\varphi}^{\max} = 0$ $\tau_{\text{p}}^{\max} = 0;$ $\tau_{\varphi}^{\max} = 0$
Q_4	$\delta_1 = \delta_2 = 0.56\,\text{mm};$ $\delta_3 = 1.28\,\text{mm}$	$\Delta q^{\max} = 0.26^\circ;$ $\theta_{\text{p}}^{\max} = 0;$ $\theta_{\varphi}^{\max} = 0$ $\tau_{\text{p}}^{\max} = 0;$ $\tau_{\varphi}^{\max} = 0$

Table 3.4 Assembling of Orthoglide manipulator with non-perfect chains: loadings and displacements for the case B ($\Delta\mathbf{t} = \left[\delta_1, \delta_2, \delta_3, \varphi_1, \varphi_2, \varphi_3\right]^T$, $\mathbf{F}_1 \neq \mathbf{0}$, $\mathbf{F}_2 \neq \mathbf{0}$, $\mathbf{F}_3 \neq \mathbf{0}$)

Point	Displacement of end-point $\Delta\mathbf{t}$	Deflections and loadings in joints and links
Q_0	$\delta_1 = \delta_2 = \delta_3 = 0\,\text{mm};$ $\varphi_1 = \varphi_2 = \varphi_3 = 0.03^\circ;$	$M^{\max} = 2.09\,\text{N}\cdot\text{m}$ $\Delta q^{\max} = 0.31^\circ;$ $\theta_{\text{p}}^{\max} = 0.05\,\text{mm};$ $\theta_{\varphi}^{\max} = 0.94^\circ;$ $\tau_{\text{p}}^{\max} = 0;$ $\tau_{\varphi}^{\max} = 2.09\,\text{N}\cdot\text{m};$
Q_1	$\delta_1 = \delta_2 = \delta_3 = 0.41\,\text{mm};$ $\varphi_1 = \varphi_2 = \varphi_3 = -0.62^\circ;$	$M^{\max} = 8.91\,\text{N}\cdot\text{m}$ $\Delta q^{\max} = 0.63^\circ;$ $\theta_{\text{p}}^{\max} = 0.54\,\text{mm};$ $\theta_{\varphi}^{\max} = 1.74^\circ;$ $\tau_{\text{p}}^{\max} = 0;$ $\tau_{\varphi}^{\max} = 11.96\,\text{N}\cdot\text{m};$
Q_2	$\delta_1 = \delta_2 = \delta_3 = -0.96\,\text{mm};$ $\varphi_1 = \varphi_2 = \varphi_3 = 0.21^\circ;$	$M^{\max} = 1.48\,\text{N}\cdot\text{m}$ $\Delta q^{\max} = 0.52^\circ;$ $\theta_{\text{p}}^{\max} = 0.14\,\text{mm};$ $\theta_{\varphi}^{\max} = 0.80^\circ;$ $\tau_{\text{p}}^{\max} = 0;$ $\tau_{\varphi}^{\max} = 1.75\,\text{N}\cdot\text{m};$
Q_3	$\delta_1 = -0.91\,\text{mm};$ $\delta_2 = 1.31\,\text{mm};$ $\delta_3 = 0.58\,\text{mm};$ $\varphi_1 = -0.19^\circ;$ $\varphi_2 = -0.49^\circ;$ $\varphi_3 = 0.44^\circ;$	$M^{\max} = 4.33\,\text{N}\cdot\text{m};$ $\Delta q^{\max} = 0.67^\circ;$ $\theta_{\text{p}}^{\max} = 0.99\,\text{mm};$ $\theta_{\varphi}^{\max} = 1.49^\circ;$ $\tau_{\text{p}}^{\max} = 0;$ $\tau_{\varphi}^{\max} = 4.84\,\text{N}\cdot\text{m};$
Q_4	$\delta_1 = 0.93\,\text{mm};$ $\delta_2 = -0.10\,\text{mm};$ $\delta_3 = -0.25\,\text{mm};$ $\varphi_1 = 0.33^\circ;$ $\varphi_2 = 0.22^\circ;$ $\varphi_3 = -0.31^\circ;$	$M^{\max} = 2.98\,\text{N}\cdot\text{m};$ $\Delta q^{\max} = 0.59^\circ;$ $\theta_{\text{p}}^{\max} = 0.62\,\text{mm};$ $\theta_{\varphi}^{\max} = 1.30^\circ;$ $\tau_{\text{p}}^{\max} = 0;$ $\tau_{\varphi}^{\max} = 4.0\,\text{N}\cdot\text{m};$

Table 3.5 Assembling of 3-PUU manipulator with non-perfect chains: loadings and displacements for the case A ($\Delta\mathbf{t}=\left[\delta_1, \delta_2, \delta_3, 0, 0, 0\right]^T$, $\mathbf{F}_1=\mathbf{0}$, $\mathbf{F}_2=\mathbf{0}$, $\mathbf{F}_3=\mathbf{0}$)

Point	Displacement of end-point $\Delta\mathbf{t}$	Deflections and loadings in joints and links
Q_0	$\delta_1=\delta_2=\delta_3=1\,\text{mm};$	$\Delta q^{\max}=0.18^\circ;$ $\theta_{\text{p}}^{\max}=0;\ \theta_{\varphi}^{\max}=0$ $\tau_{\text{p}}^{\max}=0;\ \tau_{\varphi}^{\max}=0$
Q_1	$\delta_1=\delta_2=\delta_3=0.50\,\text{mm};$	$\Delta q^{\max}=0.14^\circ;$ $\theta_{\text{p}}^{\max}=0;\ \theta_{\varphi}^{\max}=0$ $\tau_{\text{p}}^{\max}=0;\ \tau_{\varphi}^{\max}=0$
Q_2	$\delta_1=\delta_2=\delta_3=2.02\,\text{mm};$	$\Delta q^{\max}=0.42^\circ;$ $\theta_{\text{p}}^{\max}=0;\ \theta_{\varphi}^{\max}=0$ $\tau_{\text{p}}^{\max}=0;\ \tau_{\varphi}^{\max}=0$
Q_3	$\delta_1=\delta_2=0.73\,\text{mm};$ $\delta_3=0.27\,\text{mm};$	$\Delta q^{\max}=0.20^\circ;$ $\theta_{\text{p}}^{\max}=0;\ \theta_{\varphi}^{\max}=0$ $\tau_{\text{p}}^{\max}=0;\ \tau_{\varphi}^{\max}=0$
Q_4	$\delta_1=\delta_2=0.56\,\text{mm};$ $\delta=1.28\,\text{mm};$	$\Delta q^{\max}=0.26^\circ;$ $\theta_{\text{p}}^{\max}=0;\ \theta_{\varphi}^{\max}=0$ $\tau_{\text{p}}^{\max}=0;\ \tau_{\varphi}^{\max}=0$

Table 3.6 Assembling of 3-PUU manipulator with non-perfect chains: loadings and displacements for the case B ($\Delta\mathbf{t}=\left[\delta_1, \delta_2, \delta_3, \varphi_1, \varphi_2, \varphi_3\right]^T$, $\mathbf{F}_1=\mathbf{0}$, $\mathbf{F}_2=\mathbf{0}$, $\mathbf{F}_3=\mathbf{0}$)

Point	Displacement of end-point $\Delta\mathbf{t}$	Deflections and loadings in joints and links
Q_0	$\delta_1=\delta_2=\delta_3=0\,\text{mm};$ $\varphi_1=\varphi_2=\varphi_3=1^\circ;$	$\Delta q^{\max}=0.13^\circ;$ $\theta_{\text{p}}^{\max}=0;\ \theta_{\varphi}^{\max}=0$ $\tau_{\text{p}}^{\max}=0;\ \tau_{\varphi}^{\max}=0$
Q_1	$\delta_1=\delta_2=\delta_3=0.47\,\text{mm};$ $\varphi_1=\varphi_2=\varphi_3=0.66^\circ;$	$\Delta q^{\max}=0.64^\circ;$ $\theta_{\text{p}}^{\max}=0;\ \theta_{\varphi}^{\max}=0$ $\tau_{\text{p}}^{\max}=0;\ \tau_{\varphi}^{\max}=0$
Q_2	$\delta_1=\delta_2=\delta_3=-0.98\,\text{mm};$ $\varphi_1=\varphi_2=\varphi_3=1.33^\circ;$	$\Delta q^{\max}=1.97^\circ;$ $\theta_{\text{p}}^{\max}=0;\ \theta_{\varphi}^{\max}=0$ $\tau_{\text{p}}^{\max}=0;\ \tau_{\varphi}^{\max}=0$
Q_3	$\delta_1=-0.23\,\text{mm};\ \delta_2=-0.89\,\text{mm};\ \delta_3=-0.87\,\text{mm};$ $\varphi_1=0.44^\circ;\ \varphi_2=1.21^\circ;\ \varphi_3=0.78^\circ;$	$\Delta q^{\max}=1.08^\circ;$ $\theta_{\text{p}}^{\max}=0;\ \theta_{\varphi}^{\max}=0$ $\tau_{\text{p}}^{\max}=0;\ \tau_{\varphi}^{\max}=0$
Q_4	$\delta_1=0.64\,\text{mm};\ \delta_2=0.29\,\text{mm};\ \delta_3=-0.13\,\text{mm};$ $\varphi_1=1.11^\circ;\ \varphi_2=0.41^\circ;\ \varphi_3=1.28^\circ;$	$\Delta q^{\max}=1.50^\circ;$ $\theta_{\text{p}}^{\max}=0;\ \theta_{\varphi}^{\max}=0$ $\tau_{\text{p}}^{\max}=0;\ \tau_{\varphi}^{\max}=0$

Hence, here the stiffness model assembling technique from Section 3.4 has been extended for the case of parallel manipulators with geometrical errors in serial chains. In addition to computing of aggregated Cartesian stiffness matrix, it allows us to evaluate internal deflections and forces/torques in joints, as well as deflections of the reference point caused by geometrical errors in kinematic chains. In spite of this issue has essential practical significance for evaluating the desired tolerances in links/joints geometry and corresponding internal stresses in over-constrained mechanisms, it has never been studied before.

3.6 SUMMARY

The chapter is devoted to the stiffness modeling of serial and parallel manipulators in the unloaded mode (i.e. under the assumption of small deformations). The main contributions are in the area of the VJM modelling approach that has been enhanced for serial and parallel manipulators with arbitrary location of passive joints. In contrast to other works, the developed technique starts from stiffness modelling of all kinematic chains *separately* and then *aggregates* them in a unique model. Besides, for each kinematic chain, this technique is able to obtain *both non-singular and singular stiffness matrices* that take into account passive joints or kinematic singularities. Relevant assembling procedure allows to compute the *aggregated Cartesian stiffness matrix* of the parallel manipulator and also to evaluate the *internal forces/torques* and *end-platform deflections* caused by geometrical errors in the kinematic chains of over-constrained mechanism. The developed method combines advantages of the FEA and the VJM modeling approaches (accuracy and computational efficiency respectively) and allows to obtain stiffness matrices either in a numerical or in an analytical form.

In more details, new results and contributions of Chapter 3 can be formulated as

(i) Enhanced VJM-based stiffness modeling technique for serial kinematic chains with arbitrary location of passive joints, which allows to take into account passive joints in an explicit form and to compute the stiffness matrix for any configuration (even for singular ones). Also, it evaluates internal deflections (and corresponding forces/torques) for the chains with arbitrary number of passive and actuated joints. In contrast to previous results, the developed technique is more computationally efficient, includes low-order matrix inversion, and is able to obtain even rank-deficient stiffness matrices caused by the presences of passive joints or singular configuration of the chain.

(ii) Analytical expression for stiffness matrix modification induced by passive joints, which extends the classical stiffness mapping notion for serial manipulators, and related recursive procedure for stiffness matrix elements computing, which allows to treat passive joints sequentially (one-by-one). For typical industrial architectures, which include trivial passive joints (where axes are collinear with Cartesian ones), simple and practically convenient rules for stiffness matrix modification have been proposed. These results significantly simplify computation of the desired stiffness matrix and reduce them to elementary algebraic transformations.

(iii) Stiffness model assembling technique that allows to aggregate elastostatic models of separate kinematic chains in the stiffness model of the parallel manipulator. It also allows to evaluate internal deflections and forces/torques in joints, as well as deflections of the reference point, caused by geometrical errors in kinematic chains. This issue has never been studied before and has essential practical significance for evaluating desired tolerances in links/joints geometry and corresponding internal stresses in over-constrained mechanisms.

However, these results are limited to the case of small deformations (corresponding to unloaded mode). Besides, it is assumed here that a parallel manipulator has strictly parallel architecture, i.e. there are no cross-linkages and internal loops in kinematic chains of the legs. The first of these problems will be considered in Chapter 4, which focuses on stiffness modeling of serial and parallel manipulators in the loaded mode (case of large deformations case).

Main results of Chapter 3 are published in the following works: [Klimchik 2009a], [Klimchik 2011c], [Klimchik 2011d].

CHAPTER 4

STIFFNESS MODELING OF MANIPULATORS WITH PASSIVE JOINTS IN LOADED MODE

This chapter is devoted to the extension of the VJM-based stiffness modeling technique developed in the previous Section for the case of large deflections (loaded mode). It proposes a computationally efficient procedure, which is able to take into account the internal and external loadings and to obtain a non-linear force-deflection relation. It also produces Cartesian stiffness matrix both in numerical and analytical form. This allows us to extend the classical stiffness mapping equation for the case of manipulators with passive joints in the loaded mode. The stiffness model aggregation technique is also extended for the case of the loaded parallel manipulator. It is able to produce non-linear force-deflection and deflection-force relations as well as to compute internal deflections and forces/torques caused by different types of loadings and geometrical errors in kinematic chains. In addition, it proposes a non-linear compliance errors compensation technique that is based on the developed stiffness model. These results are illustrated by several examples.

4.1 INTRODUCTION

In the previous Chapter, it was explicitly assumed that the loading causes rather *small changes* in all manipulator variables (and also in equilibrium configuration). It allowed us to obtain *linear relation* between all considered variables and to limit our study by computing *of stiffness matrices*. This case was also referred to as the *'unloaded mode*'. However in practice, the loading may cause essential deflections in manipulator elastic elements, so the stiffness model should be definitely non-linear. For this reason, in this Chapter the 'small deflections' assumption is released and the study focuses on obtaining *non-linear force-deflection relations* and their linearization in the neighborhood of the elastostatic equilibriums, which produces relevant stiffness matrices. Below, the 'large deflections' case will be referred to as the *'loaded mode'*.

In literature, the manipulator stiffness modeling for the loaded mode has not been studied in details yet. The majority of the related works focus on computing of Cartesian stiffness matrix taking into account the loading value but implicitly assuming that the *equilibrium* is exactly the same as for the unloaded mode. To our knowledge, at present there are no robotic papers where non-linear force-deflection relation has been obtained strictly and for wide range of the external loading. In particular, in the works [Alici 2005], [Chen 2002] and [Li 2002a] one could obtain an *extended expression* for the stiffness matrix of a robotic manipulator, where in addition to the classical term $\mathbf{J}_\theta^{-T}\cdot\mathbf{K}_\theta\cdot\mathbf{J}_\theta^{-1}$, the second term $\mathbf{J}_\theta^{-T}\cdot\mathbf{K}_F\cdot\mathbf{J}_\theta^{-1}$ that takes into account the configuration changes due to the loading has been introduced (here, $\mathbf{J}_\theta$ is the Jacobian, $\mathbf{K}_\theta$ is the joint stiffness matrix and $\mathbf{K}_F$ is computed in a special way). From a mathematical point of view, this result can be treated as the second order approximation of the force-deflection relation in the neighborhood of the unloaded equilibrium. It means that, strictly speaking, this expression cannot be applied for a wide range of the external loading. Another limitation is related to the influence of the passive joints that have not been considered within the frame in the above mentioned papers. Other related works include [Alici 2005], [Chen 2000a], [Li 2002a], [Merlet 2008], [Quennouelle 2008a], [Quennouelle 2008a], [Quennouelle 2008c], where detailed analysis has been presented in Chapter 1. In our opinion, the most advanced results were obtained in [Yi 1992] and [Yi 1993], but the issue of computing of loaded equilibrium has been omitted.

In industrial robotics it is usually assumed that the loading is caused by an interaction between the robot end-effector and a workpiece. However, there may exist other types of external or internal forces/torques that affect the manipulator stiffness properties. For instance, for heavy manipulators [Meggiolaro 1998], [Meggiolaro 2004], the gravity forces produce essential end-effector deflections. So, they are usually compensated by supplementary mechanisms that generate additional loadings applied to the manipulator elements. It is obvious that such type of *external loading* (both gravity itself and gravity compensation) must be taken into account in the stiffness model. Further, these types of forces/torques are referred to as the *'auxiliary loading'*.

Furthermore, kinematic chains of robotic manipulators may include some additional elastic elements in the actuated or/and passive joints that are intended to increase the robot positioning accuracy or to improve the stiffness properties in certain workspace areas. For example, to eliminate the backlash, the gear trains may include spring-loaded scissor elements that generate the internal forces, which must be also integrated in the stiffness model [Wei 2010]. Similar forces may also arise in the parallel manipulators with antagonistic actuating [Chakarov 1999], [Chakarov 2004]. Other examples include parallel manipulators with springs interposed in the passive joints in order to improve stiffness in the singularity neighborhood. For this type of force/torque a term *'internal preloading'* will be used below.

As it follows from our analysis, non-linear stiffness modeling of robotic manipulators must include explicit computation of the coordinates corresponding to the *loaded equilibrium*. These coordinates should be used while calculating Jacobians (and Hessians) of the manipulator geometrical model that are obviously included in the desired stiffness model. One of the potential problems here is that, in general, the static equilibrium equation of the loaded manipulator cannot be solved unambiguously, i.e. for the same loading multiple equilibriums may exist, either stable or unstable. Hypothetically, this may create very specific manipulator behavior while the loading is increasing or decreasing (sudden jump from one equilibrium configuration to another). Some aspects of this problem have been studied in [Hines 1998], [Carricato 2002].

In the frame of the non-linear stiffness modeling technique being developed in this Chapter, it is also worth to revise the *stiffness models aggregation* technique presented in Chapter 3. Here, in addition to the

aggregated Cartesian stiffness matrix, it is required to obtain the aggregated force-deflection relation assuming that the kinematic chain may include geometrical errors. Moreover, in practice, it is often necessary to solve the inverse problem that is equivalent to obtaining the non-linear deflection-force relation. These problems have not been studied in literature yet. Though, they are very important for the *compliance errors compensation* (via proper adjusting of the actuated coordinates). At present, the compliance errors compensation problems have been solved for linear stiffness model only [Salisbury 1980], [Surdilovic 1996], [Seo 1998] [Gong 2000], [Wang 2009].

Hence, as it follows from the above analysis, the manipulator stiffness modeling for the loaded mode needs further improvement. Thus, the goal of this chapter is to extend the results of Chapter 3 for the case of large deflections (loaded mode). To achieve this goal, several sub-problems have to be solved:

(i-a) Development of non-linear stiffness modeling technique for kinematic chains with the passive joints in the case of the external loading at the end-point and preloading in the joints;

(i-b) Extension of this technique for manipulators with external and internal loading applied to the node-points (auxiliary loading);

(ii) Stability analysis of kinematic chain configuration under loading in the case of single and multiple equilibriums

(iii) Enhancement of the stiffness model aggregation technique for parallel manipulators with internal and external loadings (composed of perfect and/or non-perfect kinematic chains)

(iv) Development of the compliance errors compensation technique for over-constrained parallel manipulators under external and internal loadings.

To address these sub-problems, the remainder of this chapter is organized as follows. Section 4.2 deals with the serial chains with the loading at the end-point and preloadings in the joints. It proposes numerical technique for computing the loaded static equilibrium and obtaining the non-linear force-deflection relation as well as expressions for computing the stiffness matrices. In Section 4.3, this technique is extended for the case of serial chains with the auxiliary loading. Section 4.4 is devoted to the stability analysis of serial chain configuration. Section 4.5 focuses on non-linear stiffness models aggregation technique for parallel manipulators with perfect or/and non-perfect serial chains. Section 4.6 proposes the non-linear compliance errors compensation technique. And finally, Section 4.7 summarizes main results and contributions of this Chapter.

4.2 SERIAL KINEMATIC CHAIN OF PARALLEL MANIPULATOR WITH LOADING AT THE END-POINT AND PRELOADING IN JOINTS

Let us start the development of non-linear stiffness modeling technique assuming that the most essential loading is applied to the end-point of the kinematic chain. Besides, let us assume that some joints may include special springs, which eliminate backlash and/or modify the manipulator stiffness properties. Under these assumptions, the results of Section 3.2 cannot be applied in a straightforward way due to significant changes in the manipulator configuration under the loading. In particular, for loaded equilibrium, the values of virtual and passive joint coordinates $\boldsymbol{\theta}$, $\mathbf{q}$ cannot be computed pure geometrically (in contrast to Chapter 3). Moreover, here the stiffness properties should depend on the loading magnitude [Yi 1993], [Chen 2002], [Quennouelle 2009a] and some non-linear effects in the stiffness behavior can be discovered [Timoshenko 1970]. Let us focus on these issues.

4.2.1 Problem statement

Similar to Section 3.2, the serial chain under study includes flexible actuated joints and flexible links that may be separated by passive joints. Its geometry is described by the vector function

$$\mathbf{t} = \mathbf{g}(\mathbf{q}, \boldsymbol{\theta}) \tag{4.1}$$

where the vector $\mathbf{t} = (\mathbf{p}, \boldsymbol{\varphi})^{\mathrm{T}}$ includes the position $\mathbf{p} = (x, y, z)^{\mathrm{T}}$ and orientation $\boldsymbol{\varphi} = (\varphi_x, \varphi_y, \varphi_z)^{\mathrm{T}}$ of the end-effector in the Cartesian space; the vector $\mathbf{q} = (q_1, q_2, ..., q_{\mathrm{nq}})^{\mathrm{T}}$ contains "perfect passive joint" coordinates (i.e., without internal preloading); the vector $\boldsymbol{\theta} = (\theta_1, \theta_2, ..., \theta_{\mathrm{n}\theta})^{\mathrm{T}}$ collects coordinates of all virtual joints and "preloaded passive joints" (with auxiliary internal springs); n_{q}, n_{θ} are the sizes of $\mathbf{q}$ and $\boldsymbol{\theta}$ respectively.

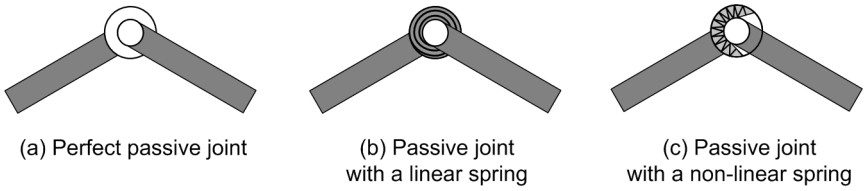

Figure 4.1 Examples of auxiliary springs in preloaded passive joints.

Several types of passive joints with and without internal preloading are presented in Figure 4.1. Such joints include internal springs, as such their statics is described by the following expression

$$\tau_{\theta i} = K_{\theta i} \cdot \left(\theta_i - \theta_{0i}\right) \tag{4.2}$$

where $\tau_{\theta i}$ is the torque/force caused by the deviation of the joint coordinate θ_i from its unloaded ("zero") value θ_{0i}, and coefficient $K_{\theta i}$ defines the spring stiffness. For the purpose of generality, let us introduce similar "zero" values θ_{0i} for the virtual springs that described flexibility of the links (obviously they are equal to zero for this subset of $\boldsymbol{\theta}$). This allows us to define vector $\boldsymbol{\theta}_0$ of the same size as $\boldsymbol{\theta}$ and to present the static equations corresponding to all variables (corresponding to perfect and preloaded passive joints, virtual springs of links and actuators) in general form

$$\boldsymbol{\tau}_{\theta} = \mathbf{K}_{\theta} \cdot (\boldsymbol{\theta} - \boldsymbol{\theta}_0), \qquad \boldsymbol{\tau}_{\mathrm{q}} = \mathbf{0} \tag{4.3}$$

Here $\boldsymbol{\tau}_{\theta}, \boldsymbol{\tau}_{\mathrm{q}}$ are the generalized torque/force in joints corresponding to the variables $\boldsymbol{\theta}$ and $\mathbf{q}$; the matrix $\mathbf{K}_{\theta}$ collects stiffness coefficients of all springs of the kinematic chain.

It is worth mentioning that in the case without internal preloading, the vector $\boldsymbol{\theta}$ describes only flexibility of manipulator links/actuators that are presented by virtual springs, while vector $\mathbf{q}$ collects entire set of passive joint coordinates. In contrast, here, the passive joint coordinates are divided into two subsets: (i) "perfect passive joints" included in $\mathbf{q}$, and (ii) "preloaded passive joints" included in $\boldsymbol{\theta}$ together with traditional virtual springs. Besides, if a passive joint includes a nonlinear spring (see Figure 4.1), the corresponding joint variable may be included either in $\boldsymbol{\theta}$ or $\mathbf{q}$, depending on the current configuration of the manipulator. However, for each configuration, this assignment is strictly unique.

In contrast to Section 3.2, here the desired stiffness model is defined by a non-linear relation

$$\mathbf{F} = f(\Delta\mathbf{t}), \tag{4.4}$$

where $f(...)$ is a so-called "force-deflections" function that associates a deflection $\Delta\mathbf{t}$ with an external force $\mathbf{F}$ that causes deformations. It is worth mentioning that the function $f(...)$ can be determined even for the singular configurations (or redundant kinematics) while the inverse statement is not generally true. Hence, enhanced stiffness analysis must include the computation of this function and the detailed analysis of its singularities that may provoke various nonlinear phenomena (such as buckling). In the unloaded case, this function is usually defined through the "stiffness matrix" $\mathbf{K}$, which describes the linear relation $\mathbf{F} = \mathbf{K}(\mathbf{q}_0, \boldsymbol{\theta}_0) \cdot \Delta\mathbf{t}$ between small six-dimensional translational/rotational displacements $\Delta\mathbf{t}$, and the external forces/torques $\mathbf{F}$ causing this transition. Here, it is assumed that $\Delta\mathbf{t}$ includes three positional components $(\Delta x, \Delta y, \Delta z)$ describing the displacement in Cartesian space and three angular components

$(\Delta\varphi_x, \Delta\varphi_y, \Delta\varphi_z)$ that describe the end-platform rotation around the Cartesian axes, while the vectors $\mathbf{q}_0, \boldsymbol{\theta}_0$ correspond to the manipulator equilibrium configuration for which the loadings (both internal and external) are equal to zero. However, for the loaded mode, similar linear relation is defined in the neighborhood of another static equilibrium, which corresponds to a different manipulator configuration $(\mathbf{q},\boldsymbol{\theta})$, that is modified by external forces/torques $\mathbf{F}$. Respectively, in this case, the stiffness model describes the relation between the increments of the force $\boldsymbol{\delta}\mathbf{F}$ and the position $\boldsymbol{\delta}\mathbf{t}$

$$\boldsymbol{\delta}\mathbf{F} = \mathbf{K}^F(\mathbf{q},\boldsymbol{\theta})\cdot\boldsymbol{\delta}\mathbf{t} \tag{4.5}$$

where $\mathbf{q} = \mathbf{q_0} + \boldsymbol{\Delta}\mathbf{q}$ and $\boldsymbol{\theta} = \boldsymbol{\theta_0} + \boldsymbol{\Delta\theta}$ denote the new configuration of the manipulator, and $\boldsymbol{\Delta}\mathbf{q}$, $\boldsymbol{\Delta\theta}$ are the deviations in the coordinates $\mathbf{q}$, $\boldsymbol{\theta}$ respectively.

Hence, the considered problem of enhanced stiffness modeling may be separated in two sequential sub-problems: (a) computing *full-scale "force-deflections relation*" for the loaded manipulator; (b) the *linearization* of the relevant force-deflection relations in the neighborhood of the equilibrium and computing corresponding stiffness matrix (that in a general case can be singular due to the presence of passive joints). Let us focus on these sub-problems.

4.2.2 Static equilibrium configuration for serial chain in the loaded mode

To solve the first sub-problem, it is desired to obtain a relation between the external loading $\mathbf{F}$ and internal coordinates of the kinematic chain $(\mathbf{q},\boldsymbol{\theta})$ corresponding to the static equilibrium. Based on this data, the desired value of the end-point displacement can be computed straightforwardly, using geometric equation (4.1). In previous works, this issue was usually ignored and the linearization was performed in the neighborhood of the unloaded configuration assuming that the external load is small enough. It is obvious that the latter essentially limits relevant results and does not allow detecting non-linear effects such as buckling. From a mathematical point of view, the problem is reduced to solving of a system of the non-linear static equilibrium equations that may produce unique or non-unique, stable or unstable solutions.

For computational reasons, let us consider the *dual problem* that deals with determining the external force $\mathbf{F}$ and the manipulator equilibrium configuration $(\mathbf{q}, \boldsymbol{\theta})$ that corresponds to the end-effector location $\mathbf{t}$ taking into account internal preloading in the joints. Let us assume that the joints are given small, arbitrary virtual displacements $\delta\mathbf{q}, \delta\boldsymbol{\theta}$ in the neighborhood of $(\mathbf{q}, \boldsymbol{\theta})$. According to the principle of virtual displacements, the virtual work of the external force $\mathbf{F}$ applied to the end-effector along the corresponding displacement $\delta\mathbf{t} = \mathbf{J}_\theta\cdot\delta\boldsymbol{\theta} + \mathbf{J}_\mathrm{q}\cdot\delta\mathbf{q}$ is equal to the sum $(\mathbf{F}^\mathrm{T}\cdot\mathbf{J}_\theta)\cdot\delta\boldsymbol{\theta} + (\mathbf{F}^\mathrm{T}\cdot\mathbf{J}_\mathrm{q})\cdot\delta\mathbf{q}$ (here $\mathbf{J}_\theta$ and $\mathbf{J}_\mathrm{q}$ are the kinematic Jacobians with respect to the coordinates $\boldsymbol{\theta}$, $\mathbf{q}$). Since the passive joints do not produce any force/torque reactions, the virtual work corresponding to the generalized forces/torques $\boldsymbol{\tau}_\theta, \boldsymbol{\tau}_\mathrm{q}$ includes only one component $-\boldsymbol{\tau}_\theta^\mathrm{T}\cdot\delta\boldsymbol{\theta}$. The minus sign takes into account the force-displacement directions for the virtual springs. In the static equilibrium, the total virtual work of all forces is equal to zero for any virtual displacement, therefore, the equilibrium conditions may be written as $\mathbf{J}_\theta^\mathrm{T}\cdot\mathbf{F} = \boldsymbol{\tau}_\theta$; $\mathbf{J}_\mathrm{q}^\mathrm{T}\cdot\mathbf{F} = \mathbf{0}$, and taking into account assumptions and notations from the previous section, the static equilibrium conditions can be presented as

$$\mathbf{J}_\theta^\mathrm{T}\cdot\mathbf{F} = \mathbf{K}_\theta\cdot(\boldsymbol{\theta}-\boldsymbol{\theta}_0); \qquad \mathbf{J}_\mathrm{q}^\mathrm{T}\cdot\mathbf{F} = \mathbf{0}; \qquad \mathbf{t} = \mathbf{g}(\mathbf{q},\boldsymbol{\theta}) \tag{4.6}$$

where the vector $\boldsymbol{\theta}_0$ defines internal preloading in the joints, the matrix $\mathbf{K}_\theta$ describes stiffness of all springs in the adopted VJM model, while the external loading $\mathbf{F}$ and the configuration $(\mathbf{q}, \boldsymbol{\theta})$ are treated as the unknown for the given end-effector location $\mathbf{t} = \mathbf{g}(\mathbf{q}, \boldsymbol{\theta})$. Hence, the designed equilibrium configuration must satisfy the system of nonlinear equations (4.6).

Since there is no general method to determine an analytical solution of this system, a numerical technique is required. Let us linearize the kinematic equation in the neighborhood of the current position $(\mathbf{q}_i, \boldsymbol{\theta}_i)$

$$\mathbf{t} = \mathbf{g}(\mathbf{q}_i,\boldsymbol{\theta}_i) + \mathbf{J}_\mathrm{q}(\mathbf{q}_i,\boldsymbol{\theta}_i)\cdot(\mathbf{q}_{i+1}-\mathbf{q}_i) + \mathbf{J}_\theta(\mathbf{q}_i,\boldsymbol{\theta}_i)\cdot(\boldsymbol{\theta}_{i+1}-\boldsymbol{\theta}_i) \tag{4.7}$$

and rewrite the static equilibrium equations as

$$\mathbf{J}_\theta^{\mathrm{T}}(\mathbf{q}_i,\boldsymbol{\theta}_i)\cdot\mathbf{F}_{i+1}=\mathbf{K}_\theta\left(\boldsymbol{\theta}_{i+1}-\boldsymbol{\theta}_0\right);\qquad \mathbf{J}_{\mathrm{q}}^{\mathrm{T}}(\mathbf{q}_i,\boldsymbol{\theta}_i)\cdot\mathbf{F}_{i+1}=\mathbf{0}\,, \tag{4.8}$$

which leads to a system of linear algebraic equations with respect to $(\mathbf{q}_{i+1},\boldsymbol{\theta}_{i+1},\mathbf{F}_{i+1})$ that includes the Jacobians $\mathbf{J}_\theta(\mathbf{q}_i,\boldsymbol{\theta}_i)$, $\mathbf{J}_{\mathrm{q}}(\mathbf{q}_i,\boldsymbol{\theta}_i)$ and the geometrical location function $\mathbf{g}(\mathbf{q}_i,\boldsymbol{\theta}_i)$ computed in the previous point $(\mathbf{q}_i,\boldsymbol{\theta}_i)$:

$$\begin{aligned}
&\mathbf{J}_{\mathrm{q}}(\mathbf{q}_i,\boldsymbol{\theta}_i)\cdot\mathbf{q}_{i+1}+\mathbf{J}_\theta(\mathbf{q}_i,\boldsymbol{\theta}_i)\cdot\boldsymbol{\theta}_{i+1}=\mathbf{t}-\mathbf{g}(\mathbf{q}_i,\boldsymbol{\theta}_i)+\mathbf{J}_{\mathrm{q}}(\mathbf{q}_i,\boldsymbol{\theta}_i)\cdot\mathbf{q}_i+\mathbf{J}_\theta(\mathbf{q}_i,\boldsymbol{\theta}_i)\cdot\boldsymbol{\theta}_i;\\
&\mathbf{J}_{\mathrm{q}}^{\mathrm{T}}(\mathbf{q}_i,\boldsymbol{\theta}_i)\cdot\mathbf{F}_{i+1}=\mathbf{0}\\
&\mathbf{J}_\theta^{\mathrm{T}}(\mathbf{q}_i,\boldsymbol{\theta}_i)\cdot\mathbf{F}_{i+1}-\mathbf{K}_\theta\cdot\boldsymbol{\theta}_{i+1}=-\mathbf{K}_\theta\cdot\boldsymbol{\theta}_0
\end{aligned} \tag{4.9}$$

This gives the following iterative scheme

$$\begin{bmatrix}\mathbf{F}_{i+1}\\ \mathbf{q}_{i+1}\\ \boldsymbol{\theta}_{i+1}\end{bmatrix}=\begin{bmatrix}\mathbf{0} & \mathbf{J}_{\mathrm{q}}(\mathbf{q}_i,\boldsymbol{\theta}_i) & \mathbf{J}_\theta(\mathbf{q}_i,\boldsymbol{\theta}_i)\\ \mathbf{J}_{\mathrm{q}}^{\mathrm{T}}(\mathbf{q}_i,\boldsymbol{\theta}_i) & \mathbf{0} & \mathbf{0}\\ \mathbf{J}_\theta^{\mathrm{T}}(\mathbf{q}_i,\boldsymbol{\theta}_i) & \mathbf{0} & -\mathbf{K}_\theta\end{bmatrix}^{-1}\cdot\begin{bmatrix}\mathbf{t}-\mathbf{g}\left(\mathbf{q}_i,\boldsymbol{\theta}_i\right)+\mathbf{J}_{\mathrm{q}}(\mathbf{q}_i,\boldsymbol{\theta}_i)\cdot\mathbf{q}_i+\mathbf{J}_\theta(\mathbf{q}_i,\boldsymbol{\theta}_i)\cdot\boldsymbol{\theta}_i\\ \mathbf{0}\\ -\mathbf{K}_\theta\cdot\boldsymbol{\theta}_0\end{bmatrix} \tag{4.10}$$

that may be reduced down to

$$\begin{aligned}
&\begin{bmatrix}\mathbf{F}_{i+1}\\ \mathbf{q}_{i+1}\end{bmatrix}=\begin{bmatrix}\mathbf{J}_\theta(\mathbf{q}_i,\boldsymbol{\theta}_i)\cdot\mathbf{K}_\theta^{-1}\cdot\mathbf{J}_\theta^{\mathrm{T}}(\mathbf{q}_i,\boldsymbol{\theta}_i) & \mathbf{J}_{\mathrm{q}}(\mathbf{q}_i,\boldsymbol{\theta}_i)\\ \mathbf{J}_{\mathrm{q}}^{\mathrm{T}}(\mathbf{q}_i,\boldsymbol{\theta}_i) & 0\end{bmatrix}^{-1}\cdot\begin{bmatrix}\mathbf{t}-\mathbf{g}(\mathbf{q}_i,\boldsymbol{\theta}_i)+\mathbf{J}_{\mathrm{q}}(\mathbf{q}_i,\boldsymbol{\theta}_i)\cdot\mathbf{q}_i+\mathbf{J}_\theta(\mathbf{q}_i,\boldsymbol{\theta}_i)\cdot\boldsymbol{\theta}_i\\ 0\end{bmatrix}\\
&\boldsymbol{\theta}_{i+1}=\mathbf{K}_\theta^{-1}\cdot\mathbf{J}_\theta^{\mathrm{T}}(\mathbf{q}_i,\boldsymbol{\theta}_i)\cdot\mathbf{F}_{i+1}+\boldsymbol{\theta}_0
\end{aligned} \tag{4.11}$$

The latter is more convenient computationally, since it requires the inversion of a lower dimension matrix $(n+6)\times(n+6)$ instead of $(n+m+6)\times(n+m+6)$, where n, m are the sizes of the vectors $\mathbf{q}$ and $\boldsymbol{\theta}$ respectively. For instance, for the kinematic chains of the Orthoglide manipulator (see example in Chapter 5), the expression (4.10) requires the inversion of 34×34 matrix, while iterative scheme (4.11) needs the inversion of 10×10 matrix only. It should be mentioned that $\mathbf{K}_\theta^{-1}$ is computed only once, outside of the iterative loop.

Similar to the other iterative schemes, convergence of this algorithm highly depends on the starting point. However, due to the physical nature of the considered problem, it is possible to start iterations from the non-loaded configuration $(\mathbf{q}_0,\boldsymbol{\theta}_0)$. Besides, it is useful to modify the target point for each iteration in accordance with the expression $\mathbf{t}_i=\alpha_i\cdot\mathbf{t}+(1-\alpha_i)\cdot\mathbf{t}_0$ using scalar variable α_i that is monotonically increasing from 0 up to 1. Another approach can be used for computing the force-deflection curve. Here, the starting point can be taken from previously computed loaded configuration corresponding to another value of deflection that is very close to the target one. For typical values of deformations, the proposed iterative procedure convergences in 3-5 iterations if the configuration is stable. In the simulation studies, the convergence has been evaluated as the weighted sum of residual norms corresponding to equations (4.6) and the algorithm stops when this criterion achieved the prescribed value.

However, some computational difficulties may arise in the case of buckling or in the area of multiple equilibriums, where the convergence problem becomes rather critical and highly depends on an initial point. Here, the number of iterations increases significantly and the computational time becomes non-negligible. To overcome these difficulties, it is proposed to modify the developed iterative scheme and to repeat the computations several times, with slightly modified initial points that are obtained by adding small random noise to $\mathbf{q}_0,\boldsymbol{\theta}_0$. Another option is to add small disturbances to $(\boldsymbol{\theta}_i,\mathbf{q}_i)$ at each iteration. These techniques were used in case studies presented in Chapter 5.

The proposed iterative scheme can also be slightly modified to solve the *original problem*, i.e. computing the equilibrium configuration corresponding to given external loading $\mathbf{F}$ (instead of given $\mathbf{t}$). In this case, expressions (4.10), (4.11) are used in the internal loop, while the designed algorithm is supplemented by an external loop, which provides iterative searching for $\mathbf{t}$ corresponding to the given $\mathbf{F}$

$$\mathbf{t}_{i+1}=\mathbf{t}_i+\mathbf{K}_i^{-1}\cdot\left(\mathbf{F}-\mathbf{F}_i\right) \tag{4.12}$$

where $\mathbf{t}_i$, $\mathbf{F}_i$ and $\mathbf{K}_i$ are the location, the loading and stiffness matrix at the i-th iteration respectively. It is worth mentioning that the dual problem is meaningful only if the stiffness matrix $\mathbf{K}_i$ is non-singular. It is obvious that for a separate serial chain with passive joints the matrix $\mathbf{K}_i$ is always singular, while for a serial manipulator it is usually non-singular (the same as for a parallel manipulator due to specific assembling of kinematic chains). On the other hand, the dual problem considered in this Section (i.e. computing $\mathbf{F}$ corresponding to $\mathbf{t}$) is always physically meaningful and has at least one solution.

4.2.3 Stiffness matrix of serial chain in the loaded mode

The previous sub-section presents a technique that generally allows us to obtain the relation between the elastic deformations and corresponding external force/torque. It is based on sequential computations of loaded equilibriums (and relevant force/torque) for various displacements of the manipulator end-point with respect to its unloaded location. However, though this relation is highly non-linear, common engineering practice operates with the stiffness matrix derived via its linearization.

To compute the desired stiffness matrix, let us consider the neighborhood of the loaded configuration and assume that the external force and the end-effector location are incremented by some small values $\delta\mathbf{F}$, $\delta\mathbf{t}$. Besides, let us assume that a new configuration also satisfies the equilibrium conditions. Hence, it is necessary to consider simultaneously two equilibriums corresponding to the manipulator state variables $(\mathbf{F}, \mathbf{q}, \boldsymbol{\theta}, \mathbf{t})$ and $(\mathbf{F}+\delta\mathbf{F}, \mathbf{q}+\delta\mathbf{q}, \boldsymbol{\theta}+\delta\boldsymbol{\theta}, \mathbf{t}+\delta\mathbf{t})$. Relevant equations of statics may be written as

$$\mathbf{J}_\theta^{\mathrm{T}} \cdot \mathbf{F} = \mathbf{K}_\theta \cdot (\boldsymbol{\theta} - \boldsymbol{\theta}_0); \qquad \mathbf{J}_q^{\mathrm{T}} \cdot \mathbf{F} = 0 \tag{4.13}$$

and

$$\begin{aligned} &(\mathbf{J}_\theta + \delta\mathbf{J}_\theta)^{\mathrm{T}} \cdot (\mathbf{F} + \delta\mathbf{F}) = \mathbf{K}_\theta \cdot (\boldsymbol{\theta} - \boldsymbol{\theta}_0 + \delta\boldsymbol{\theta}); \\ &(\mathbf{J}_q + \delta\mathbf{J}_q)^{\mathrm{T}} \cdot (\mathbf{F} + \delta\mathbf{F}) = 0 \end{aligned} \tag{4.14}$$

where $\delta\mathbf{J}_q(\mathbf{q}, \boldsymbol{\theta})$ and $\delta\mathbf{J}_\theta(\mathbf{q}, \boldsymbol{\theta})$ are the differentials of the Jacobians due to changes in $(\mathbf{q}, \boldsymbol{\theta})$. Besides, in the neighborhood of $(\mathbf{q}, \boldsymbol{\theta})$, the kinematic equation may also be presented in the linearized form:

$$\delta\mathbf{t} = \mathbf{J}_\theta(\mathbf{q}, \boldsymbol{\theta}) \cdot \delta\boldsymbol{\theta} + \mathbf{J}_q(\mathbf{q}, \boldsymbol{\theta}) \cdot \delta\mathbf{q} \tag{4.15}$$

Hence, after neglecting the high-order small terms and expanding the differentials via the Hessians of the function $\Psi = \mathbf{g}(\mathbf{q}, \boldsymbol{\theta})^{\mathrm{T}} \cdot \mathbf{F}$, equations (4.13), (4.14) may be rewritten as

$$\begin{aligned} &\mathbf{J}_\theta^{\mathrm{T}}(\mathbf{q}, \boldsymbol{\theta}) \cdot \delta\mathbf{F} + \mathbf{H}_{\theta q}^{\mathrm{F}}(\mathbf{q}, \boldsymbol{\theta}) \cdot \delta\mathbf{q} + \mathbf{H}_{\theta\theta}^{\mathrm{F}}(\mathbf{q}, \boldsymbol{\theta}) \cdot \delta\boldsymbol{\theta} = \mathbf{K}_\theta \cdot \delta\boldsymbol{\theta} \\ &\mathbf{J}_q^{\mathrm{T}}(\mathbf{q}, \boldsymbol{\theta}) \cdot \delta\mathbf{F} + \mathbf{H}_{qq}^{\mathrm{F}}(\mathbf{q}, \boldsymbol{\theta}) \cdot \delta\mathbf{q} + \mathbf{H}_{q\theta}^{\mathrm{F}}(\mathbf{q}, \boldsymbol{\theta}) \cdot \delta\boldsymbol{\theta} = \mathbf{0} \end{aligned} \tag{4.16}$$

where

$$\mathbf{H}_{qq}^{\mathrm{F}} = \partial^2\Psi / \partial\mathbf{q}^2; \qquad \mathbf{H}_{\theta\theta}^{\mathrm{F}} = \partial^2\Psi / \partial\boldsymbol{\theta}^2; \qquad \mathbf{H}_{q\theta}^{\mathrm{F}} = \mathbf{H}_{\theta q}^{\mathrm{F}} = \partial^2\Psi / \partial\mathbf{q}\,\partial\boldsymbol{\theta} \tag{4.17}$$

and the general relation between the increments of the state variables can be presented as

$$\begin{bmatrix} \mathbf{0} & \mathbf{J}_q & \mathbf{J}_\theta \\ \mathbf{J}_q^{\mathrm{T}} & \mathbf{H}_{qq}^{\mathrm{F}} & \mathbf{H}_{q\theta}^{\mathrm{F}} \\ \mathbf{J}_\theta^{\mathrm{T}} & \mathbf{H}_{\theta q}^{\mathrm{F}} & \mathbf{H}_{\theta\theta}^{\mathrm{F}} - \mathbf{K}_\theta \end{bmatrix} \cdot \begin{bmatrix} \delta\mathbf{F} \\ \delta\mathbf{q} \\ \delta\boldsymbol{\theta} \end{bmatrix} = \begin{bmatrix} \delta\mathbf{t} \\ \mathbf{0} \\ \mathbf{0} \end{bmatrix} \tag{4.18}$$

The latter gives a straightforward numerical technique for computing the desired stiffness matrix: direct inversion of the matrix in the left-hand side of (4.18) and extracting from it the upper-left sub-matrix of size 6×6. Similarly, the matrices defining linear relations between the end-effector increment $\delta\mathbf{t}$ and the increments of the joint variables $\delta\boldsymbol{\theta}$, $\delta\mathbf{q}$ can be computed, i.e.:

$$\delta\mathbf{F} = \mathbf{K}_C \cdot \delta\mathbf{t}; \qquad \delta\boldsymbol{\theta} = \mathbf{K}_{C\theta} \cdot \delta\mathbf{t}; \qquad \delta\mathbf{q} = \mathbf{K}_{Cq} \cdot \delta\mathbf{t} \tag{4.19}$$

where

$$\left[\begin{array}{c|c|c} \mathbf{K}_{\mathrm{C}} & * & * \\ \hline \mathbf{K}_{\mathrm{C}\mathrm{q}} & * & * \\ \hline \mathbf{K}_{\mathrm{C}\theta} & * & * \end{array}\right] = \left[\begin{array}{ccc} \mathbf{0} & \mathbf{J}_{\mathrm{q}} & \mathbf{J}_{\theta} \\ \mathbf{J}_{\mathrm{q}}^{\mathrm{T}} & \mathbf{H}_{\mathrm{qq}}^{\mathrm{F}} & \mathbf{H}_{\mathrm{q}\theta}^{\mathrm{F}} \\ \mathbf{J}_{\theta}^{\mathrm{T}} & \mathbf{H}_{\theta\mathrm{q}}^{\mathrm{F}} & \mathbf{H}_{\theta\theta}^{\mathrm{F}} - \mathbf{K}_{\theta} \end{array}\right]^{-1} \tag{4.20}$$

It is worth mentioning that the internal preloading (expressed by the variable $\boldsymbol{\theta}_0$) is not included in the latter expression in the explicit way, but it directly influences on the variables $(\mathbf{q}, \boldsymbol{\theta})$ describing the equilibrium configuration and corresponding Jacobians and Hessians, which are elements of (4.20). Besides, in contrast to previous works, here it is possible to obtain supplementary matrices $\mathbf{K}_{\mathrm{C}\theta}, \mathbf{K}_{\mathrm{C}\mathrm{q}}$ that give additional measures of the manipulator stiffness which evaluate sensitivity of the joint coordinates $(\mathbf{q}, \boldsymbol{\theta})$ with respect to the external loading.

In the case when the matrix inverse (4.20) is computationally hard, the variable $\delta\boldsymbol{\theta}$ can be eliminated analytically, using corresponding static equation: $\delta\boldsymbol{\theta} = \mathbf{k}_{\theta}^{\mathrm{F}} \cdot \mathbf{J}_{\theta}^{\mathrm{T}} \cdot \delta\mathbf{F} + \mathbf{k}_{\theta}^{\mathrm{F}} \cdot \mathbf{H}_{\theta\mathrm{q}}^{\mathrm{F}} \cdot \delta\mathbf{q}$, where $\mathbf{k}_{\theta}^{\mathrm{F}} = (\mathbf{K}_{\theta} - \mathbf{H}_{\theta\theta}^{\mathrm{F}})^{-1}$. This leads to a reduced system of matrix equations with unknowns $\delta\mathbf{F}$ and $\delta\mathbf{q}$

$$\left[\begin{array}{cc} \mathbf{J}_{\theta} \cdot \mathbf{k}_{\theta}^{\mathrm{F}} \cdot \mathbf{J}_{\theta}^{\mathrm{T}} & \mathbf{J}_{\mathrm{q}} + \mathbf{J}_{\theta} \cdot \mathbf{k}_{\theta}^{\mathrm{F}} \cdot \mathbf{H}_{\theta\mathrm{q}}^{\mathrm{F}} \\ \mathbf{J}_{\mathrm{q}}^{\mathrm{T}} + \mathbf{H}_{\mathrm{q}\theta}^{\mathrm{F}} \cdot \mathbf{k}_{\theta}^{\mathrm{F}} \cdot \mathbf{J}_{\theta}^{\mathrm{T}} & \mathbf{H}_{\mathrm{qq}}^{\mathrm{F}} + \mathbf{H}_{\mathrm{q}\theta}^{\mathrm{F}} \cdot \mathbf{k}_{\theta}^{\mathrm{F}} \cdot \mathbf{H}_{\theta\mathrm{q}}^{\mathrm{F}} \end{array}\right] \cdot \left[\begin{array}{c} \delta\mathbf{F} \\ \delta\mathbf{q} \end{array}\right] = \left[\begin{array}{c} \delta\mathbf{t} \\ \mathbf{0} \end{array}\right] \tag{4.21}$$

that may be treated in the similar way, i.e. the desired stiffness matrix is also obtained by direct inversion of the matrix in the left-hand side of (4.21) and extracting from it the upper-left sub-matrix of size 6×6:

$$\left[\begin{array}{c|c} \mathbf{K}_{\mathrm{C}} & * \\ \hline \mathbf{K}_{\mathrm{C}\mathrm{q}} & * \end{array}\right] = \left[\begin{array}{cc} \mathbf{J}_{\theta} \cdot \mathbf{k}_{\theta}^{\mathrm{F}} \cdot \mathbf{J}_{\theta}^{\mathrm{T}} & \mathbf{J}_{\mathrm{q}} + \mathbf{J}_{\theta} \cdot \mathbf{k}_{\theta}^{\mathrm{F}} \cdot \mathbf{H}_{\theta\mathrm{q}}^{\mathrm{F}} \\ \mathbf{J}_{\mathrm{q}}^{\mathrm{T}} + \mathbf{H}_{\mathrm{q}\theta}^{\mathrm{F}} \cdot \mathbf{k}_{\theta}^{\mathrm{F}} \cdot \mathbf{J}_{\theta}^{\mathrm{T}} & \mathbf{H}_{\mathrm{qq}}^{\mathrm{F}} + \mathbf{H}_{\mathrm{q}\theta}^{\mathrm{F}} \cdot \mathbf{k}_{\theta}^{\mathrm{F}} \cdot \mathbf{H}_{\theta\mathrm{q}}^{\mathrm{F}} \end{array}\right]^{-1} \tag{4.22}$$

Similar to subsection 4.1, this approach allows us to reduce the dimension of the inverted matrix from $(n+m+6)\times(n+m+6)$ to $(n+6)\times(n+6)$, that in the case of Orthoglide (see Chapter 5) corresponds to 34×34 and 10×10 respectively.

It is worth mentioning that the structure of the latter matrix is similar to the one obtained for the unloaded manipulator and differs only by Hessians that take into account the influence of the external load. It should also be noted that, because of the presence of the passive joints, the stiffness matrix of a separate serial kinematic chain is always singular, but aggregation of all the chains for a parallel manipulator produces a non-singular stiffness matrix.

Further simplification of (4.22) can be obtained by applying the block matrix inversion technique of Frobenius [Gantmacher 1959] that yields the following expressions

$$\mathbf{K}_{\mathrm{C}} = \mathbf{K}_{C}^{0(F)} - \mathbf{K}_{C}^{0(F)} \cdot \left(\mathbf{J}_{\mathrm{q}} + \mathbf{J}_{\theta} \cdot \mathbf{k}_{\theta}^{\mathrm{F}} \cdot \mathbf{H}_{\theta\mathrm{q}}^{\mathrm{F}}\right) \cdot \mathbf{K}_{\mathrm{C}\mathrm{q}} \tag{4.23}$$

where the first term $\mathbf{K}_{C}^{0(F)} = (\mathbf{J}_{\theta} \cdot \mathbf{k}_{\theta}^{\mathrm{F}} \cdot \mathbf{J}_{\theta}^{\mathrm{T}})^{-1}$ exactly corresponds to the classical formula defining stiffness of the kinematic chain without passive joints in the loaded mode [Chen 2000a], [Alici 2005] and

$$\mathbf{K}_{\mathrm{C}\mathrm{q}} = -\left(\mathbf{H}_{\mathrm{qq}}^{\mathrm{F}} + \mathbf{H}_{\mathrm{q}\theta}^{\mathrm{F}} \cdot \mathbf{k}_{\theta}^{\mathrm{F}} \cdot \mathbf{H}_{\theta\mathrm{q}}^{\mathrm{F}} - \left(\mathbf{J}_{\mathrm{q}}^{\mathrm{T}} + \mathbf{H}_{\mathrm{q}\theta}^{\mathrm{F}} \cdot \mathbf{k}_{\theta}^{\mathrm{F}} \cdot \mathbf{J}_{\theta}^{\mathrm{T}}\right) \cdot \mathbf{K}_{C}^{0(F)} \cdot \left(\mathbf{J}_{\mathrm{q}} + \mathbf{J}_{\theta} \cdot \mathbf{k}_{\theta}^{\mathrm{F}} \cdot \mathbf{H}_{\theta\mathrm{q}}^{\mathrm{F}}\right)\right)^{-1} \cdot \left(\mathbf{J}_{\mathrm{q}}^{\mathrm{T}} + \mathbf{H}_{\mathrm{q}\theta}^{\mathrm{F}} \cdot \mathbf{k}_{\theta}^{\mathrm{F}} \cdot \mathbf{J}_{\theta}^{\mathrm{T}}\right) \cdot \mathbf{K}_{C}^{0(F)} \tag{4.24}$$

Similarly, the matrix $\mathbf{K}_{\mathrm{C}\theta}$ can be expressed analytically as

$$\mathbf{K}_{\mathrm{C}\theta} = \mathbf{k}_{\theta}^{\mathrm{F}} \cdot \mathbf{J}_{\theta}^{\mathrm{T}} \cdot \mathbf{K}_{\mathrm{C}} + \mathbf{k}_{\theta}^{\mathrm{F}} \cdot \mathbf{H}_{\theta\mathrm{q}}^{\mathrm{F}} \cdot \mathbf{K}_{\mathrm{C}\mathrm{q}} \tag{4.25}$$

Hence, the technique presented in Section 4.2 allows us to compute the static equilibrium configuration and Cartesian stiffness matrix for serial chains with external loading applied to the end-point and with preloading in the joints. In Chapter 5, it will be applied to several case studies that deal with kinematic chains employed in typical parallel manipulators and demonstrate particularities of stiffness analysis of loaded manipulator with passive joints. However, this technique does not cover heavy manipulators, where the own weight of the robot is significant and the external loading is applied to both the end-point and internal points of the kinematic chain. Furthermore, this type of loading will be called an auxiliary one.

4.3 SERIAL KINEMATIC CHAIN OF PARALLE MANIPULATOR WITH AUXILIARY LOADINGS IN INTERMEDIATE NODES

4.3.1 Problem statement

For stiffness modeling of serial kinematic chain with auxiliary loading let us use the same VJM model as in Sections 3.2 and 4.2, but let us assume that the serial chain has the additional external loadings applied to the internal node points (Figure 4.2). These loadings can be caused by gravity forces (generally they are distributed, but in practice they can be approximated by localized ones) and/or gravity compensators. These forces will be denoted as $\mathbf{G}_j$, where $j = 1,...,n$ is the node number in the serial chain starting from the fix base (here, $j = n$ corresponds to the end-point). It should be noted that for computational convenience, it is assumed that the end point loading consists of two components $\mathbf{G}_n$ and $\mathbf{F}$ of different nature.

It is evident that in general the auxiliary forces $\mathbf{G}_i$ depend on the manipulator configuration. So, let us assume that they are described by the functions

$$\mathbf{G}_j = \mathbf{G}_j(\mathbf{q},\boldsymbol{\theta}), \tag{4.26}$$

where $\mathbf{q}$ and $\boldsymbol{\theta}$ collect all passive joints and virtual joints coordinates respectively. In contrast, for the external force $\mathbf{F}$, it is assumed that there is no direct relation with the manipulator configuration.

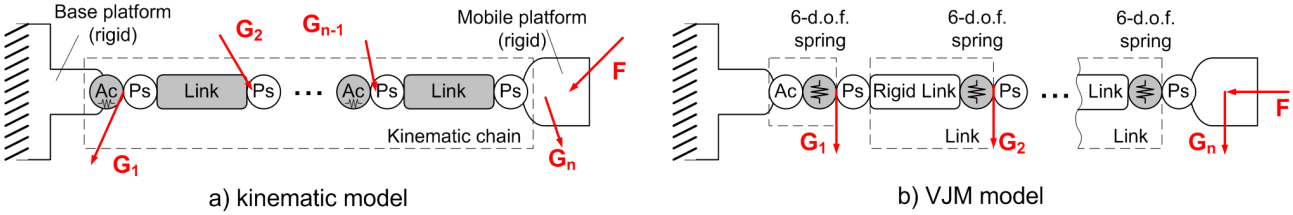

Figure 4.2 General structure of kinematic chain with auxiliary loading and its VJM model

For the serial chains with the auxiliary loadings it is also required to extend the geometrical model. In particular, in addition to the equation (4.1) defining the end-point location, it is necessary to introduce the additional functions

$$\mathbf{t}_j = \mathbf{g}_j(\mathbf{q},\boldsymbol{\theta}), \quad j = 1,...,n \tag{4.27}$$

defining locations of the nodes. It is worth mentioning that for the serial chain, the position $\mathbf{t}_j$ depends on a sub-set of the joint coordinates (corresponding to the passive and virtual joints located between the base and the *j*-th node), but for the purpose of analytical simplicity let us use the whole set of the joint coordinates $(\mathbf{q}, \boldsymbol{\theta})$ as the arguments of the functions $\mathbf{g}_i(...)$.

Using these assumptions and the methodology of Section 4.2, the problem of stiffness modeling of serial chains with auxiliary loadings can be split in the following sub-problems: (a) deriving the static equilibrium equations for the chain with auxiliary loadings; (b) computing *full-scale "force-deflections relation"* for the end-point and intermediate nodes; (c) *linearization* of the relevant force-deflection relations in the neighborhood of the equilibrium and computing corresponding stiffness matrix. Let us focus on these sub-problems.

4.3.2 Static equilibrium equations for serial chain with auxiliary loadings

To obtain a desired stiffness model, let us derive first the static equilibrium equations that differ from the equations (4.6) used in the previous Section due to the influence of auxiliary loadings $\mathbf{G}_j$. Let us apply the principle of the virtual work and assume that the kinematic chain under external loadings $\mathbf{F}$ and $\mathbf{G} = [\mathbf{G}_1 ... \mathbf{G}_n]$ has the configuration $(\mathbf{q}, \boldsymbol{\theta})$ and the locations of the end-point and the nodes are $\mathbf{t} = \mathbf{g}(\mathbf{q},\boldsymbol{\theta})$ and $\mathbf{t}_j = \mathbf{g}_j(\mathbf{q},\boldsymbol{\theta})$, $j = \overline{1,n}$ respectively.

According to the principle of virtual work, the work of external forces $\mathbf{G}, \mathbf{F}$ is equal to the work of internal forces $\boldsymbol{\tau}_\theta$ caused by displacement of the virtual springs $\delta\boldsymbol{\theta}$

$$\sum_{j=1}^{n}\left(\mathbf{G}_j{}^{\mathrm{T}}\cdot\delta\mathbf{t}_j\right)+\mathbf{F}^{\mathrm{T}}\cdot\delta\mathbf{t}=\boldsymbol{\tau}_\theta{}^{\mathrm{T}}\cdot\delta\boldsymbol{\theta} \tag{4.28}$$

where the virtual displacements $\delta\mathbf{t}_j$ can be computed from the linearized geometrical model derived from (4.27)

$$\delta\mathbf{t}_j=\mathbf{J}_\theta^{(j)}\cdot\delta\boldsymbol{\theta}+\mathbf{J}_\mathrm{q}^{(j)}\cdot\delta\mathbf{q},\quad j=1..n, \tag{4.29}$$

which includes the Jacobian matrices

$$\mathbf{J}_\theta^{(j)}=\frac{\partial}{\partial\boldsymbol{\theta}}\mathbf{g}_j\left(\mathbf{q},\boldsymbol{\theta}\right);\qquad \mathbf{J}_\mathrm{q}^{(j)}=\frac{\partial}{\partial\mathbf{q}}\mathbf{g}_j\left(\mathbf{q},\boldsymbol{\theta}\right) \tag{4.30}$$

with respect to the virtual and passive joint coordinates respectively.

Substituting (4.29) to (4.28) we can obtain the equation

$$\sum_{j=1}^{n}\left(\mathbf{G}_j{}^{\mathrm{T}}\cdot\mathbf{J}_\theta^{(j)}\cdot\delta\boldsymbol{\theta}+\mathbf{G}_j{}^{\mathrm{T}}\cdot\mathbf{J}_\mathrm{q}^{(j)}\cdot\delta\mathbf{q}\right)+\left(\mathbf{F}^{\mathrm{T}}\cdot\mathbf{J}_\theta^{(n)}\cdot\delta\boldsymbol{\theta}+\mathbf{F}^{\mathrm{T}}\cdot\mathbf{J}_\mathrm{q}^{(n)}\cdot\delta\mathbf{q}\right)=\boldsymbol{\tau}_\theta{}^{\mathrm{T}}\cdot\delta\boldsymbol{\theta} \tag{4.31}$$

which has to be satisfied for any variation of $\delta\boldsymbol{\theta}$, $\delta\mathbf{q}$. It means that the terms regrouping the variables $\delta\boldsymbol{\theta}$, $\delta\mathbf{q}$ have the coefficients equal to zero, hence the force-balance equations can be written as

$$\boldsymbol{\tau}_\theta=\sum_{j=1}^{n}\mathbf{J}_\theta^{(j)\mathrm{T}}\cdot\mathbf{G}_j+\mathbf{J}_\theta^{(n)\mathrm{T}}\cdot\mathbf{F};\qquad \mathbf{0}=\sum_{j=1}^{n}\mathbf{J}_\mathrm{q}^{(j)\mathrm{T}}\cdot\mathbf{G}_j+\mathbf{J}_\mathrm{q}^{(n)\mathrm{T}}\cdot\mathbf{F},\qquad j=1..n. \tag{4.32}$$

Also, these equations can be re-written in block-matrix form as

$$\boldsymbol{\tau}_\theta=\mathbf{J}_\theta^{(\mathrm{G})\mathrm{T}}\cdot\mathbf{G}+\mathbf{J}_\theta^{(\mathrm{F})\mathrm{T}}\cdot\mathbf{F};\qquad \mathbf{0}=\mathbf{J}_\mathrm{q}^{(\mathrm{G})\mathrm{T}}\cdot\mathbf{G}+\mathbf{J}_\mathrm{q}^{(\mathrm{F})\mathrm{T}}\cdot\mathbf{F} \tag{4.33}$$

where

$$\begin{gathered}\mathbf{J}_\theta^{(\mathrm{F})}=\mathbf{J}_\theta^{(n)};\qquad \mathbf{J}_\mathrm{q}^{(F)}=\mathbf{J}_\mathrm{q}^{(n)};\\ \mathbf{J}_\theta^{(\mathrm{G})}=\left[\mathbf{J}_\theta^{(1)\mathrm{T}}...\mathbf{J}_\theta^{(n)\mathrm{T}}\right]^{\mathrm{T}};\qquad \mathbf{J}_\mathrm{q}^{(\mathrm{G})}=\left[\mathbf{J}_\mathrm{q}^{(1)\mathrm{T}}...\mathbf{J}_\mathrm{q}^{(n)\mathrm{T}}\right]^{\mathrm{T}};\qquad \mathbf{G}=\left[\mathbf{G}_1{}^{\mathrm{T}}...\mathbf{G}_n{}^{\mathrm{T}}\right]^{\mathrm{T}}\end{gathered} \tag{4.34}$$

Finally, taking into account the virtual spring reaction $\boldsymbol{\tau}_\theta=\mathbf{K}_\theta\cdot\left(\boldsymbol{\theta}-\boldsymbol{\theta}^0\right)$, where $\mathbf{K}_\theta=diag\left(\mathbf{K}_{\theta_1},...,\mathbf{K}_{\theta_n}\right)$, the desired static equilibrium equations can be presented as

$$\begin{aligned}\mathbf{J}_\theta^{(\mathrm{G})\mathrm{T}}\cdot\mathbf{G}+\mathbf{J}_\theta^{(\mathrm{F})\mathrm{T}}\cdot\mathbf{F}&=\mathbf{K}_\theta\cdot\left(\boldsymbol{\theta}-\boldsymbol{\theta}^0\right)\\ \mathbf{J}_\mathrm{q}^{(\mathrm{G})\mathrm{T}}\cdot\mathbf{G}+\mathbf{J}_\mathrm{q}^{(\mathrm{F})\mathrm{T}}\cdot\mathbf{F}&=\mathbf{0}\end{aligned} \tag{4.35}$$

It should be noted that compared to previously used equilibrium equations (4.6), here there are two additional terms $\mathbf{J}_\theta^{(\mathrm{G})\mathrm{T}}\mathbf{G}$ and $\mathbf{J}_\mathrm{q}^{(\mathrm{G})\mathrm{T}}\mathbf{G}$ that take into account the influence of the auxiliary loading $\mathbf{G}$. Further, these equations will be used for computing the static equilibrium configuration and corresponding Cartesian stiffness matrix.

4.3.3 Static equilibrium configuration for serial chain with auxiliary loadings

To obtain a relation between the external loading $\mathbf{F}$ and internal coordinates of the kinematic chain $(\mathbf{q},\boldsymbol{\theta})$ corresponding to the static equilibrium, equations (4.35) should be solved either for the different given values of $\mathbf{F}$ or for the different given values of $\mathbf{t}$. In sub-section 4.2.2 these problems were referred to as the original and the dual ones respectively, but the dual problem has been discovered to be the most convenient from a computational point of view. Hence, let us solve static equilibrium equations with respect to the manipulator configuration $\left(\mathbf{q},\boldsymbol{\theta}\right)$ and external loading $\mathbf{F}$ for given end-effector position $\mathbf{t}=\mathbf{g}\left(\mathbf{q},\boldsymbol{\theta}\right)$ and function of auxiliary-loadings $\mathbf{G}\left(\mathbf{q},\boldsymbol{\theta}\right)$

$$\begin{aligned} &\mathbf{K}_\theta \cdot \left(\boldsymbol{\theta} - \boldsymbol{\theta}^0\right) = \mathbf{J}_\theta^{(\mathrm{G})\mathrm{T}} \cdot \mathbf{G} + \mathbf{J}_\theta^{(\mathrm{F})\mathrm{T}} \cdot \mathbf{F}; \qquad \mathbf{J}_\mathrm{q}^{(\mathrm{G})\mathrm{T}} \cdot \mathbf{G} + \mathbf{J}_\mathrm{q}^{(\mathrm{F})\mathrm{T}} \cdot \mathbf{F} = \mathbf{0} \\ &\mathbf{t} = \mathbf{g}\left(\mathbf{q}, \boldsymbol{\theta}\right); \qquad \mathbf{G} = \mathbf{G}\left(\mathbf{q}, \boldsymbol{\theta}\right) \end{aligned} \tag{4.36}$$

Compared to sub-section 4.2.2, here the unknown variables are the same $\left(\mathbf{q}, \boldsymbol{\theta}, \mathbf{F}\right)$, but the equation structure is more complicated.

Since this system of equations usually has no analytical solution, an iterative numerical technique can be applied. Similar to the previous Section, the kinematic equations may be linearized in the neighborhood of the current configuration $(\mathbf{q}_i, \boldsymbol{\theta}_i)$

$$\mathbf{t}_{i+1} = \mathbf{g}\left(\mathbf{q}_i, \boldsymbol{\theta}_i\right) + \mathbf{J}_\theta^{(\mathrm{F})}\left(\mathbf{q}_i, \boldsymbol{\theta}_i\right) \cdot \left(\boldsymbol{\theta}_{i+1} - \boldsymbol{\theta}_i\right) + \mathbf{J}_\mathrm{q}^{(\mathrm{F})}\left(\mathbf{q}_i, \boldsymbol{\theta}_i\right) \cdot \left(\mathbf{q}_{i+1} - \mathbf{q}_i\right); \tag{4.37}$$

where the subscript '*i*' indicates the iteration number and the changes in Jacobians $\mathbf{J}_\theta^{(\mathrm{G})}$, $\mathbf{J}_\theta^{(\mathrm{F})}$, $\mathbf{J}_\mathrm{q}^{(\mathrm{G})}$, $\mathbf{J}_\mathrm{q}^{(\mathrm{F})}$ and the auxiliary loadings $\mathbf{G}\left(\mathbf{q}, \boldsymbol{\theta}\right)$ are assumed to be negligible from iteration to iteration. Correspondingly, the static equilibrium equations in the neighborhood of $(\mathbf{q}_i, \boldsymbol{\theta}_i)$ may be rewritten as

$$\begin{aligned} &\mathbf{J}_\theta^{(\mathrm{G})\mathrm{T}}\left(\mathbf{q}_i, \boldsymbol{\theta}_i\right) \cdot \mathbf{G}\left(\mathbf{q}_i, \boldsymbol{\theta}_i\right) + \mathbf{J}_\theta^{(\mathrm{F})\mathrm{T}}\left(\mathbf{q}_i, \boldsymbol{\theta}_i\right) \cdot \mathbf{F}_{i+1} = \mathbf{K}_\theta \cdot \left(\boldsymbol{\theta}_{i+1} - \boldsymbol{\theta}^0\right) \\ &\mathbf{J}_\mathrm{q}^{(\mathrm{G})\mathrm{T}}\left(\mathbf{q}_i, \boldsymbol{\theta}_i\right) \cdot \mathbf{G}\left(\mathbf{q}_i, \boldsymbol{\theta}_i\right) + \mathbf{J}_\mathrm{q}^{(\mathrm{F})\mathrm{T}}\left(\mathbf{q}_i, \boldsymbol{\theta}_i\right) \cdot \mathbf{F}_{i+1} = \mathbf{0} \end{aligned}. \tag{4.38}$$

Thus, combining (4.37) and (4.38), the iterative algorithm for computing of the static equilibrium configuration for the given end-effector location can be presented as

$$\begin{bmatrix} \mathbf{F}_{i+1} \\ \mathbf{q}_{i+1} \\ \boldsymbol{\theta}_{i+1} \end{bmatrix} = \begin{bmatrix} \mathbf{0} & \mathbf{J}_\mathrm{q}^{(\mathrm{F})}\left(\mathbf{q}_i, \boldsymbol{\theta}_i\right) & \mathbf{J}_\theta^{(\mathrm{F})}\left(\mathbf{q}_i, \boldsymbol{\theta}_i\right) \\ \mathbf{J}_\mathrm{q}^{(\mathrm{F})\mathrm{T}}\left(\mathbf{q}_i, \boldsymbol{\theta}_i\right) & \mathbf{0} & \mathbf{0} \\ \mathbf{J}_\theta^{(\mathrm{F})\mathrm{T}}\left(\mathbf{q}_i, \boldsymbol{\theta}_i\right) & \mathbf{0} & -\mathbf{K}_\theta \end{bmatrix}^{-1} \begin{bmatrix} \mathbf{t}_{i+1} - \mathbf{g}\left(\mathbf{q}_i, \boldsymbol{\theta}_i\right) + \mathbf{J}_\theta^{(\mathrm{F})}\left(\mathbf{q}_i, \boldsymbol{\theta}_i\right) \cdot \boldsymbol{\theta}_i + \mathbf{J}_\mathrm{q}^{(\mathrm{F})}\left(\mathbf{q}_i, \boldsymbol{\theta}_i\right) \cdot \mathbf{q}_i \\ -\mathbf{J}_\mathrm{q}^{(\mathrm{G})\mathrm{T}}\left(\mathbf{q}_i, \boldsymbol{\theta}_i\right) \cdot \mathbf{G}_i \\ -\mathbf{J}_\theta^{(\mathrm{G})\mathrm{T}}\left(\mathbf{q}_i, \boldsymbol{\theta}_i\right) \cdot \mathbf{G}_i - \mathbf{K}_\theta \cdot \boldsymbol{\theta}^0 \end{bmatrix} \tag{4.39}$$

where $\mathbf{G}_{i+1} = \mathbf{G}(\mathbf{q}_{i+1}, \boldsymbol{\theta}_{i+1})$.

To reduce the size of a matrix to be inverted, the above system can be slightly simplified. In particular, applying the same approach as in section 4.2.2 (based on analytical expression for $\boldsymbol{\theta} = \mathbf{K}_\theta^{-1}(\mathbf{J}_\theta^{(\mathrm{G})\mathrm{T}} \cdot \mathbf{G} + \mathbf{J}_\theta^{(\mathrm{F})\mathrm{T}} \cdot \mathbf{F}) + \boldsymbol{\theta}^0$), the unknown variables can be separated in two groups $(\mathbf{F}, \mathbf{q})$ and $\boldsymbol{\theta}$. This yields the iterative scheme

$$\begin{aligned} \begin{bmatrix} \mathbf{F}_{i+1} \\ \mathbf{q}_{i+1} \end{bmatrix} = &\begin{bmatrix} \mathbf{J}_\theta^{(\mathrm{F})}\left(\mathbf{q}_i, \boldsymbol{\theta}_i\right) \cdot \mathbf{K}_\theta^{-1} \cdot \mathbf{J}_\theta^{(\mathrm{F})\mathrm{T}}\left(\mathbf{q}_i, \boldsymbol{\theta}_i\right) & \mathbf{J}_\mathrm{q}^{(\mathrm{F})}\left(\mathbf{q}_i, \boldsymbol{\theta}_i\right) \\ \mathbf{J}_\mathrm{q}^{(\mathrm{F})\mathrm{T}}\left(\mathbf{q}_i, \boldsymbol{\theta}_i\right) & \mathbf{0} \end{bmatrix}^{-1} \times \\ &\times \begin{bmatrix} \mathbf{t}_{i+1} - \mathbf{g}\left(\mathbf{q}_i, \boldsymbol{\theta}_i\right) + \mathbf{J}_\theta^{(\mathrm{F})}\left(\mathbf{q}_i, \boldsymbol{\theta}_i\right) \cdot \boldsymbol{\theta}_i + \mathbf{J}_\mathrm{q}^{(\mathrm{F})}\left(\mathbf{q}_i, \boldsymbol{\theta}_i\right) \cdot \mathbf{q}_i - \mathbf{J}_\theta^{(\mathrm{F})}\left(\mathbf{q}_i, \boldsymbol{\theta}_i\right) \cdot \mathbf{K}_\theta^{-1} \cdot \mathbf{J}_\theta^{(\mathrm{G})\mathrm{T}}\left(\mathbf{q}_i, \boldsymbol{\theta}_i\right) \cdot \mathbf{G}_i \\ -\mathbf{J}_\mathrm{q}^{(\mathrm{G})\mathrm{T}}\left(\mathbf{q}_i, \boldsymbol{\theta}_i\right) \cdot \mathbf{G}_i \end{bmatrix} \\ \boldsymbol{\theta}_{i+1} = &\mathbf{K}_\theta^{-1}\left(\mathbf{J}_\theta^{(\mathrm{G})\mathrm{T}}\left(\mathbf{q}_i, \boldsymbol{\theta}_i\right) \cdot \mathbf{G}_i + \mathbf{J}_\theta^{(\mathrm{F})\mathrm{T}}\left(\mathbf{q}_i, \boldsymbol{\theta}_i\right) \cdot \mathbf{F}_{i+1}\right) + \boldsymbol{\theta}^0 \end{aligned} \tag{4.40}$$

that requires matrix inversion of the essentially lower order (for example, for the 3-link manipulator with two passive joints and two actuated joints, the size of matrix inversion reduces from 34 to 14).

The proposed algorithm allows us to compute static equilibrium configuration for the serial chains with passive joints and all types of loadings (internal preloading, external loadings applied to any point of the manipulator and loading from the technological process). The convergence properties of this algorithm are similar to one presented in sub-section 4.2.2. It can also be modified in a similar way to solve the problem of computing the equilibrium configuration corresponding to the given external loading $\mathbf{F}$ (instead of the given $\mathbf{t}$). Some examples illustrating its application will be presented in Chapter 5.

4.3.4 Stiffness matrix for serial chain with auxiliary loadings

The previous sub-section allows us to obtain the non-linear relation between elastic deflections $\Delta\mathbf{t}$ and external loading $\mathbf{F}$. Since common engineering practice operates with the stiffness matrix, let us linearize this relation in the neighborhood of the equilibrium. Following the virtual work technique, let us assume that the external force and the end-effector location are incremented by some small values $\delta\mathbf{F}$, $\delta\mathbf{t}$ in

the neighborhood of current equilibrium configuration. Let us also assume that a new configuration also satisfies the equilibrium conditions. Hence, it is necessary to consider the two equilibriums corresponding to the manipulator state variables $(\mathbf{F}, \mathbf{q}, \boldsymbol{\theta}, \mathbf{t})$ and $(\mathbf{F}+\delta\mathbf{F}, \mathbf{q}+\delta\mathbf{q}, \boldsymbol{\theta}+\delta\boldsymbol{\theta}, \mathbf{t}+\delta\mathbf{t})$ simultaneously. The relevant static equilibrium equations may be written as

$$\begin{aligned}
&\mathbf{t} = \mathbf{g}\left(\mathbf{q}, \boldsymbol{\theta}\right) \\
&\mathbf{K}_{\theta} \cdot \left(\boldsymbol{\theta} - \boldsymbol{\theta}^{0}\right) = \mathbf{J}_{\theta}^{(\mathrm{G})\mathrm{T}} \cdot \mathbf{G} + \mathbf{J}_{\theta}^{(\mathrm{F})\mathrm{T}} \cdot \mathbf{F} \\
&\mathbf{J}_{\mathrm{q}}^{(\mathrm{G})\mathrm{T}} \cdot \mathbf{G} + \mathbf{J}_{\mathrm{q}}^{(\mathrm{F})\mathrm{T}} \cdot \mathbf{F} = \mathbf{0}
\end{aligned} \tag{4.41}$$

and

$$\begin{aligned}
&\mathbf{t} + \delta\mathbf{t} = \mathbf{g}\left(\mathbf{q} + \delta\mathbf{q}, \boldsymbol{\theta} + \delta\boldsymbol{\theta}\right) \\
&\mathbf{K}_{\theta} \cdot \left(\boldsymbol{\theta} + \delta\boldsymbol{\theta} - \boldsymbol{\theta}^{0}\right) = \left(\mathbf{J}_{\theta}^{(\mathrm{G})} + \delta\mathbf{J}_{\theta}^{(\mathrm{G})}\right)^{\mathrm{T}} \cdot \left(\mathbf{G} + \delta\mathbf{G}\right) + \left(\mathbf{J}_{\theta}^{(\mathrm{F})} + \delta\mathbf{J}_{\theta}^{(\mathrm{F})}\right)^{\mathrm{T}} \cdot \left(\mathbf{F} + \delta\mathbf{F}\right) \\
&\left(\mathbf{J}_{\mathrm{q}}^{(\mathrm{G})} + \delta\mathbf{J}_{\mathrm{q}}^{(\mathrm{G})}\right)^{\mathrm{T}} \cdot \left(\mathbf{G} + \delta\mathbf{G}\right) + \left(\mathbf{J}_{\mathrm{q}}^{(\mathrm{F})} + \delta\mathbf{J}_{\mathrm{q}}^{(\mathrm{F})}\right)^{\mathrm{T}} \cdot \left(\mathbf{F} + \delta\mathbf{F}\right) = \mathbf{0}
\end{aligned} \tag{4.42}$$

where the variables $\mathbf{t}$, $\mathbf{F}$, $\mathbf{G}$, $\mathbf{K}_{\theta}$, $\mathbf{q}$, $\boldsymbol{\theta}$, $\boldsymbol{\theta}^{0}$ are assumed to be known.

After linearization of the function $\mathbf{g}(\mathbf{q}, \boldsymbol{\theta})$ in the neighborhood of loaded equilibrium, the system (4.41), (4.42) is reduced to three equations

$$\begin{aligned}
&\delta\mathbf{t} = \mathbf{J}_{\theta}^{(\mathrm{F})} \cdot \delta\boldsymbol{\theta} + \mathbf{J}_{\mathrm{q}}^{(\mathrm{F})} \cdot \delta\mathbf{q} \\
&\mathbf{K}_{\theta} \cdot \delta\boldsymbol{\theta} = \delta\mathbf{J}_{\theta}^{(\mathrm{G})} \cdot \mathbf{G} + \mathbf{J}_{\theta}^{(\mathrm{G})} \cdot \delta\mathbf{G} + \delta\mathbf{J}_{\theta}^{(\mathrm{F})} \cdot \mathbf{F} + \mathbf{J}_{\theta}^{(\mathrm{F})} \cdot \delta\mathbf{F} \\
&\delta\mathbf{J}_{\mathrm{q}}^{(\mathrm{G})} \cdot \mathbf{G} + \mathbf{J}_{\mathrm{q}}^{(\mathrm{G})} \cdot \delta\mathbf{G} + \delta\mathbf{J}_{\mathrm{q}}^{(\mathrm{F})} \cdot \mathbf{F} + \mathbf{J}_{\mathrm{q}}^{(\mathrm{F})} \cdot \delta\mathbf{F} = \mathbf{0}
\end{aligned} \tag{4.43}$$

which define the desired linear relations between $\delta\mathbf{t}$ and $\delta\mathbf{F}$, $\delta\mathbf{q}$, $\delta\boldsymbol{\theta}$ that are expressed by the stiffness matrices $\mathbf{K}_{\mathrm{C}}$, $\mathbf{K}_{\mathrm{Cq}}$, $\mathbf{K}_{\mathrm{C}\theta}$ (see equations (4.19)). In this system, small variations of Jacobians may be expressed via the second order derivatives

$$\begin{aligned}
&\delta\mathbf{J}_{\mathrm{q}}^{(\mathrm{F})} = \mathbf{H}_{\mathrm{q}\theta}^{(\mathrm{F})} \cdot \delta\boldsymbol{\theta} + \mathbf{H}_{\mathrm{qq}}^{(\mathrm{F})} \cdot \delta\mathbf{q}; \qquad &&\delta\mathbf{J}_{\theta}^{(\mathrm{F})} = \mathbf{H}_{\theta\theta}^{(\mathrm{F})} \cdot \delta\boldsymbol{\theta} + \mathbf{H}_{\theta\mathrm{q}}^{(\mathrm{F})} \cdot \delta\mathbf{q}; \\
&\delta\mathbf{J}_{\mathrm{q}}^{(\mathrm{G})} = \mathbf{H}_{\mathrm{q}\theta}^{(\mathrm{G})} \cdot \delta\boldsymbol{\theta} + \mathbf{H}_{\mathrm{qq}}^{(\mathrm{G})} \cdot \delta\mathbf{q}; \qquad &&\delta\mathbf{J}_{\theta}^{(\mathrm{G})} = \mathbf{H}_{\theta\theta}^{(\mathrm{G})} \cdot \delta\boldsymbol{\theta} + \mathbf{H}_{\theta\mathrm{q}}^{(\mathrm{G})} \cdot \delta\mathbf{q};
\end{aligned} \tag{4.44}$$

where

$$\begin{aligned}
&\mathbf{H}_{\theta\theta}^{(\mathrm{G})} = \sum_{j=1}^{n} \frac{\partial^2}{\partial\boldsymbol{\theta}^2}\left(\mathbf{g}_j{}^{T}(\mathbf{q}, \boldsymbol{\theta}) \cdot \mathbf{G}_j\right); \qquad &&\mathbf{H}_{\mathrm{qq}}^{(\mathrm{G})} = \sum_{j=1}^{n} \frac{\partial^2}{\partial\mathbf{q}^2}\left(\mathbf{g}_j{}^{T}(\mathbf{q}, \boldsymbol{\theta}) \cdot \mathbf{G}_j\right); \\
&\mathbf{H}_{\theta\mathrm{q}}^{(\mathrm{G})} = \sum_{j=1}^{n} \frac{\partial^2}{\partial\boldsymbol{\theta}\,\partial\mathbf{q}}\left(\mathbf{g}_j{}^{T}(\mathbf{q}, \boldsymbol{\theta}) \cdot \mathbf{G}_j\right); \qquad &&\mathbf{H}_{\mathrm{q}\theta}^{(\mathrm{G})} = \sum_{j=1}^{n} \frac{\partial^2}{\partial\mathbf{q}\,\partial\boldsymbol{\theta}}\left(\mathbf{g}_j{}^{T}(\mathbf{q}, \boldsymbol{\theta}) \cdot \mathbf{G}_j\right); \\
&\mathbf{H}_{\theta\theta}^{(\mathrm{F})} = \frac{\partial^2}{\partial\boldsymbol{\theta}^2}\left(\mathbf{g}^{T}(\mathbf{q}, \boldsymbol{\theta}) \cdot \mathbf{F}\right); \qquad &&\mathbf{H}_{\mathrm{qq}}^{(\mathrm{F})} = \frac{\partial^2}{\partial\mathbf{q}^2}\left(\mathbf{g}^{T}(\mathbf{q}, \boldsymbol{\theta}) \cdot \mathbf{F}\right); \\
&\mathbf{H}_{\theta\mathrm{q}}^{(\mathrm{F})} = \frac{\partial^2}{\partial\boldsymbol{\theta}\,\partial\mathbf{q}}\left(\mathbf{g}^{T}(\mathbf{q}, \boldsymbol{\theta}) \cdot \mathbf{F}\right); \qquad &&\mathbf{H}_{\mathrm{q}\theta}^{(\mathrm{F})} = \frac{\partial^2}{\partial\mathbf{q}\,\partial\boldsymbol{\theta}}\left(\mathbf{g}^{T}(\mathbf{q}, \boldsymbol{\theta}) \cdot \mathbf{F}\right);
\end{aligned} \tag{4.45}$$

Also, the auxiliary loading $\mathbf{G}$ may be computed via the first order derivatives as

$$\delta\mathbf{G} = \frac{\partial\mathbf{G}}{\partial\boldsymbol{\theta}} \cdot \delta\boldsymbol{\theta} + \frac{\partial\mathbf{G}}{\partial\mathbf{q}} \cdot \delta\mathbf{q} \tag{4.46}$$

Furthermore, to insure similarity between the results of this subsection and sub-section 4.2.3, let us introduce the additional notation

$$\begin{aligned}
&\mathbf{H}_{\theta\theta} = \mathbf{H}_{\theta\theta}^{(\mathrm{F})} + \mathbf{H}_{\theta\theta}^{(\mathrm{G})} + \mathbf{J}_{\theta}^{(\mathrm{G})\mathrm{T}} \cdot \frac{\partial}{\partial\boldsymbol{\theta}}\mathbf{G}; \qquad &&\mathbf{H}_{\theta\mathrm{q}} = \mathbf{H}_{\theta\mathrm{q}}^{(\mathrm{G})} + \mathbf{H}_{\theta\mathrm{q}}^{(\mathrm{F})} + \mathbf{J}_{\theta}^{(\mathrm{G})\mathrm{T}} \cdot \frac{\partial}{\partial\mathbf{q}}\mathbf{G}; \\
&\mathbf{H}_{\mathrm{q}\theta} = \mathbf{H}_{\mathrm{q}\theta}^{(\mathrm{G})} + \mathbf{H}_{\mathrm{q}\theta}^{(\mathrm{F})} + \mathbf{J}_{\mathrm{q}}^{(\mathrm{G})\mathrm{T}} \cdot \frac{\partial}{\partial\boldsymbol{\theta}}\mathbf{G}; \qquad &&\mathbf{H}_{\mathrm{qq}} = \mathbf{H}_{\mathrm{qq}}^{(\mathrm{G})} + \mathbf{H}_{\mathrm{qq}}^{(\mathrm{F})} + \mathbf{J}_{\mathrm{q}}^{(\mathrm{G})\mathrm{T}} \cdot \frac{\partial}{\partial\mathbf{q}}\mathbf{G}
\end{aligned}, \tag{4.47}$$

which allows us to present the system (4.43) in the form

$$\begin{bmatrix} \delta\mathbf{t} \\ \mathbf{0} \\ \mathbf{0} \end{bmatrix} = \begin{bmatrix} \mathbf{0} & \mathbf{J}_{q}^{(F)} & \mathbf{J}_{\theta}^{(F)} \\ \mathbf{J}_{q}^{(F)T} & \mathbf{H}_{qq} & \mathbf{H}_{q\theta} \\ \mathbf{J}_{\theta}^{(F)T} & \mathbf{H}_{\theta q} & -\mathbf{K}_{\theta} + \mathbf{H}_{\theta\theta} \end{bmatrix} \cdot \begin{bmatrix} \delta\mathbf{F} \\ \delta\mathbf{q} \\ \delta\boldsymbol{\theta} \end{bmatrix} \tag{4.48}$$

that has the same structure as (4.18). Hence, similar to sub-section 4.2.3, the desired stiffness matrices can be computed via either a high order matrix inversion

$$\left[\begin{array}{c|c|c} \mathbf{K}_{C} & * & * \\ \hline \mathbf{K}_{Cq} & * & * \\ \hline \mathbf{K}_{C\theta} & * & * \end{array}\right] = \begin{bmatrix} \mathbf{0} & \mathbf{J}_{q}^{(F)} & \mathbf{J}_{\theta}^{(F)} \\ \mathbf{J}_{q}^{(F)T} & \mathbf{H}_{qq} & \mathbf{H}_{q\theta} \\ \mathbf{J}_{\theta}^{(F)T} & \mathbf{H}_{\theta q} & -\mathbf{K}_{\theta} + \mathbf{H}_{\theta\theta} \end{bmatrix}^{-1} \tag{4.49}$$

or lower order inversion

$$\left[\begin{array}{c|c} \mathbf{K}_{C} & * \\ \hline \mathbf{K}_{Cq} & * \end{array}\right] = \begin{bmatrix} \mathbf{J}_{\theta}^{(F)} \cdot \mathbf{k}_{\theta}^{F} \cdot \mathbf{J}_{\theta}^{(F)T} & \mathbf{J}_{q}^{(F)} + \mathbf{J}_{\theta}^{(F)} \cdot \mathbf{k}_{\theta}^{F} \cdot \mathbf{H}_{\theta q} \\ \mathbf{J}_{q}^{(F)T} + \mathbf{H}_{q\theta} \cdot \mathbf{k}_{\theta}^{F} \cdot \mathbf{J}_{\theta}^{(F)T} & \mathbf{H}_{qq} + \mathbf{H}_{q\theta} \cdot \mathbf{k}_{\theta}^{F} \cdot \mathbf{H}_{\theta q} \end{bmatrix}^{-1} \tag{4.50}$$

where $\mathbf{k}_{\theta}^{F}$ denotes the modified joint compliance matrix $\mathbf{k}_{\theta}^{F} = (\mathbf{K}_{\theta} - \mathbf{H}_{\theta\theta})^{-1}$. It is obvious that, using these notations, the matrices $\mathbf{K}_{C}$, $\mathbf{K}_{Cq}$, $\mathbf{K}_{C\theta}$ can be also computed analytically in accordance with expressions (4.23), (4.24) and (4.25) respectively.

Thus, in this Section, the non-linear stiffness modeling technique for serial chains was extended for the manipulators with external and internal loading applied to the node-points (auxiliary loading). It allows us to compute values of the internal variables corresponding to the equilibrium, to obtain the non-linear force-deflection relation and to compute the related stiffness matrices. However, the question related to the stability of the equilibrium configuration of the kinematic chain still remain open.

4.4 STABILITY OF KINEMATIC CHAIN CONFIGURATION UNDER LOADINGS

External and internal loadings applied to the serial chains may have influence on their configurations (i.e. on their shape). Moreover, for the same end-point location, due to the kinematic redundancy the kinematic chain can have multiple equilibrium configurations, either stable or unstable. For this reason let us concentrate on the stability analysis of the kinematic chains configuration under the loading. It is worth mentioning that in parallel manipulators, the considered configurations of the chains are equivalent with respect to the location of end-platform. But in practice only stable configurations may be observed.

4.4.1 Definition of configuration stability for a serial chain under loading

To investigate possible non-linear effects that may be caused by an external and internal loading, it is necessary to extend the notion of stability associated with the stiffness analysis. Traditionally, the stability of compliant mechanical systems (including manipulators) is defined as *resistance of the end-point location* $\mathbf{t}$ with respect to the "disturbing" effects of an external force $\mathbf{F}$ applied at this point. In such formulation, the stability is completely defined by the stiffness matrix $\mathbf{K}_{C}$ that describes the linear relations (4.5) between the force and deflection deviations $\delta\mathbf{F}$, $\delta\mathbf{t}$ with respect to the values $\mathbf{F}$, $\mathbf{t}$. It is obvious that the matrix $\mathbf{K}_{C}$ is a positive definite for the stable location $\mathbf{t}$.

However, in the compliant manipulators with the passive joints, the equilibrium configuration $(\mathbf{q},\boldsymbol{\theta})$ corresponding to the same end-point location $\mathbf{t}$ cannot be unique. Moreover, these configurations may be both "stable" and "unstable" and may correspond to different values of potential energy stored in the virtual springs. From this point of view, it is worth to distinguish stability of the end-point location $\mathbf{t}$ from stability of the corresponding equilibrium configuration of the kinematic chain $(\mathbf{q},\boldsymbol{\theta})$, which may be defined as a *resistance of the chain shape* with respect to disturbances in redundant kinematic variables. This issue becomes extremely important for the loaded mode, due to the kinematic redundancy caused by the passive joints and excessive number of virtual springs. As such, small disturbances in $(\mathbf{q},\boldsymbol{\theta})$ may provoke an

essential change of current equilibrium configuration leading to the reduction of the potential energy and transition to another equilibrium state, while keeping the same end-point location. Hence, it is necessary to evaluate internal properties of the kinematic chain in the state of the loaded equilibrium that may correspond either to minimum or maximum of the potential energy for a fixed value of **t** .

Let us illustrate this notion on the example of three-link chain (Figure 4.3a), which includes passive joints at both ends and two virtual torsional springs between the links, which insure the "straight" configuration for the unloaded mode. It is assumed that both ends of the chain are fixed by the external geometrical constrains while the internal configuration may change without shifting of the end-points, in accordance with redundant parameter value. It is evident that this chain is loaded, but the corresponding value of the force **F** depends on a particular configuration. Besides, among variety of possible configurations (corresponding to given end-point locations), only the equilibrium ones are in the focus of interest.

For this case study, it is convenient to give an energy-based interpretation. The considered kinematic chain has one redundant parameter (rotation angle of any passive joint) and under geometrical constrains may occupy configurations with the different shape. Relevant relation between the energy stored in the virtual springs and the redundant parameter value is presented in Figure 4.3b. Due to the physical nature of this chain, for each given end-point displacement Δ, the examined plot presents a continuous closed criss-cross curve that has exactly two minimum and maximum points, that correspond to the stable and unstable equilibriums respectively. Hence, numerical solution of static equilibrium equations presented in sections 4.2.2 and 3.3.3 may yield both stable and unstable configurations, while in practice only stable ones should be considered. Thus, in addition, to the above mentioned algorithms, the criterion that allows to distinguish stable and unstable configurations of the kinematic chain is required.

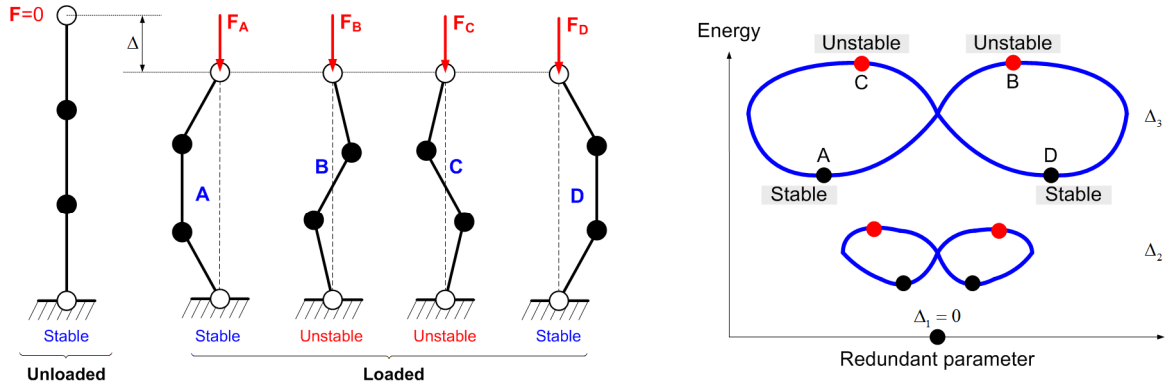

(a) equilibrium configurations (b) energy diagram

Figure 4.3 Stable and non-stable configurations of 3-link serial chain and their energy-based interpretation (○ - passive join, ● - virtual torsional spring)

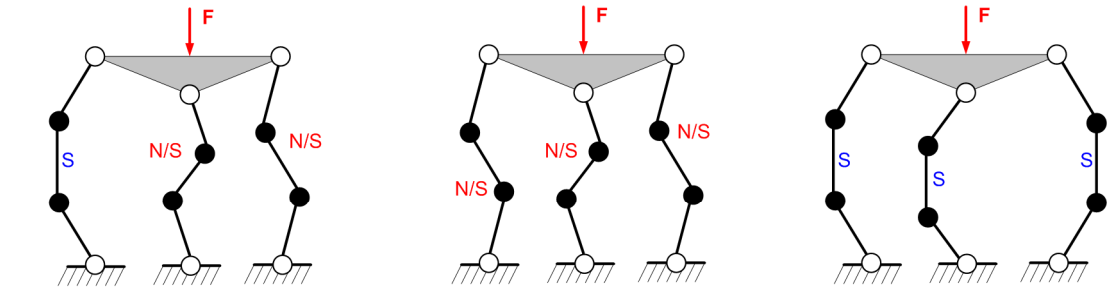

(a) parallel manipulator with stable and unstable configurations of serial chains

(b) parallel manipulator with unstable configurations of serial chains

(c) parallel manipulator with stable configurations of serial chains

Figure 4.4 2D parallel manipulators with serial chains in stable and unstable configurations (○ - passive join, ● - virtual torsional spring)

Physical meaning of this stability notion (related to the kinematic chain shape) is illustrated in Figure 4.4, which contains several postures of the same parallel manipulator with exactly the same end-platform location. These postures differ in the shapes of serial kinematic chains that may be treated as internal configuration of the parallel manipulator, which is not "visible" from the end-platform side whose static stability is completely defined by the Cartesian stiffness matrix. In particular, Figure 4.4a,b present parallel manipulators that include at least one kinematic chain in unstable configuration that cannot be observed in practice but satisfy the general static equilibrium equation. In contrast, Figure 4.4c shows physically realizable posture of the same manipulator (with exactly the same location of the chain end-points) where for all kinematic chains the shapes are stable.

Hence, a full-scale investigation into the stiffness properties of the loaded parallel manipulator must include the stability analysis of the internal kinematic chain configurations as presented in the following sub-section.

4.4.2 Stability criterion for kinematic chain configuration

To evaluate stability of the static equilibrium configuration $(\mathbf{q}, \boldsymbol{\theta})$ of a separate kinematic chain, let us assume that the end-point is fixed at the point $\mathbf{t} = (\mathbf{p}, \boldsymbol{\varphi})^{\mathrm{T}}$ corresponding to the external load $\mathbf{F}$, but the joint coordinates are given small virtual displacements $\delta\mathbf{q}$, $\delta\boldsymbol{\theta}$ satisfying the geometrical constraint (4.1), i.e.

$$\mathbf{t} = \mathbf{g}(\mathbf{q}, \boldsymbol{\theta}); \qquad \mathbf{t} = \mathbf{g}(\mathbf{q} + \delta\mathbf{q}, \boldsymbol{\theta} + \delta\boldsymbol{\theta}) \tag{4.51}$$

For these assumptions, let us compute the total virtual work in the joints that must be positive for a stable equilibrium and negative for an unstable one. To achieve the virtual configuration $(\mathbf{q} + \delta\mathbf{q}, \boldsymbol{\theta} + \delta\boldsymbol{\theta})$ and restore the equilibrium conditions, each of the joints must include virtual motors that generate the generalized forces/torques $\delta\boldsymbol{\tau}_{\mathrm{q}}$, $\delta\boldsymbol{\tau}_{\theta}$ which satisfy the equations:

$$\begin{aligned} &\mathbf{J}_{\theta}^{\mathrm{T}} \cdot \mathbf{F} = \mathbf{K}_{\theta} \cdot (\boldsymbol{\theta} - \boldsymbol{\theta}_0); && (\mathbf{J}_{\theta} + \delta\mathbf{J}_{\theta})^{\mathrm{T}} \cdot \mathbf{F} = \mathbf{K}_{\theta} \cdot (\boldsymbol{\theta} - \boldsymbol{\theta}_0 + \delta\boldsymbol{\theta}) + \delta\boldsymbol{\tau}_{\theta} \\ &\mathbf{J}_{\mathrm{q}}^{\mathrm{T}} \cdot \mathbf{F} = 0; && (\mathbf{J}_{\mathrm{q}} + \delta\mathbf{J}_{\mathrm{q}})^{\mathrm{T}} \cdot \mathbf{F} = \delta\boldsymbol{\tau}_{q} \end{aligned} \tag{4.52}$$

After relevant transformations, the virtual torques may be expressed as

$$\delta\boldsymbol{\tau}_{\theta} = \delta(\mathbf{J}_{\theta}^{\mathrm{T}} \cdot \mathbf{F}) - \mathbf{K}_{\theta} \cdot \delta\boldsymbol{\theta}; \qquad \delta\boldsymbol{\tau}_{\mathrm{q}} = \delta(\mathbf{J}_{\mathrm{q}}^{\mathrm{T}} \cdot \mathbf{F}) \tag{4.53}$$

where $\delta(...)$ denotes the differential with respect to $\delta\mathbf{q}$, $\delta\boldsymbol{\theta}$ that may be expanded via Hessians of the scalar function $\Psi = \mathbf{g}(\mathbf{q}, \boldsymbol{\theta})^{\mathrm{T}} \cdot \mathbf{F}$:

$$\delta(\mathbf{J}_{\theta}^{\mathrm{T}} \cdot \mathbf{F}) = \mathbf{H}_{\theta\mathrm{q}}^{\mathrm{F}} \cdot \delta\mathbf{q} + \mathbf{H}_{\theta\theta}^{\mathrm{F}} \cdot \delta\boldsymbol{\theta}; \qquad \delta(\mathbf{J}_{\mathrm{q}}^{\mathrm{T}} \cdot \mathbf{F}) = \mathbf{H}_{\mathrm{qq}}^{\mathrm{F}} \cdot \delta\mathbf{q} + \mathbf{H}_{\mathrm{q}\theta}^{\mathrm{F}} \cdot \delta\boldsymbol{\theta} \tag{4.54}$$

provided that

$$\mathbf{H}_{\mathrm{qq}}^{\mathrm{F}} = \partial^2\Psi / \partial\mathbf{q}^2; \qquad \mathbf{H}_{\theta\theta}^{\mathrm{F}} = \partial^2\Psi / \partial\boldsymbol{\theta}^2; \qquad \mathbf{H}_{\mathrm{q}\theta}^{\mathrm{F}} = \mathbf{H}_{\theta\mathrm{q}}^{\mathrm{F}\ \mathrm{T}} = \partial^2\Psi / \partial\mathbf{q}\,\partial\boldsymbol{\theta} \tag{4.55}$$

Furthermore, taking into account that the virtual displacement from $(\mathbf{q}, \boldsymbol{\theta})$ to $(\mathbf{q} + \delta\mathbf{q}, \boldsymbol{\theta} + \delta\boldsymbol{\theta})$ leads to a gradual change of the virtual motor torques from $(\mathbf{0}, \mathbf{0})$ to $(\delta\boldsymbol{\tau}_{\mathrm{q}}, \delta\boldsymbol{\tau}_{\theta})$, the virtual work may be computed as a half of the corresponding scalar products

$$\delta W = -\frac{1}{2}\left(\delta\boldsymbol{\tau}_{\theta}^{\mathrm{T}} \cdot \delta\boldsymbol{\theta} + \delta\boldsymbol{\tau}_{\mathrm{q}}^{\mathrm{T}} \cdot \delta\mathbf{q}\right) \tag{4.56}$$

where the minus sign takes into account the adopted conventions for the positive directions of the forces and displacements. Hence, after appropriate substitutions and transformations to the matrix form, the desired stability condition may be written as

$$\delta W = -\frac{1}{2}\begin{bmatrix}\delta\boldsymbol{\theta}^{\mathrm{T}} & \delta\mathbf{q}^{\mathrm{T}}\end{bmatrix} \cdot \begin{bmatrix}\mathbf{H}_{\theta\theta}^{\mathrm{F}} - \mathbf{K}_{\theta} & \mathbf{H}_{\mathrm{q}\theta}^{\mathrm{F}} \\ \mathbf{H}_{\theta\mathrm{q}}^{\mathrm{F}} & \mathbf{H}_{\mathrm{qq}}^{\mathrm{F}}\end{bmatrix} \cdot \begin{bmatrix}\delta\boldsymbol{\theta} \\ \delta\mathbf{q}\end{bmatrix} > 0 \tag{4.57}$$

where $\delta\mathbf{q}$ and $\delta\boldsymbol{\theta}$ must satisfy the geometrical constraints (4.51).

In order to take into account the relation between $\delta\mathbf{q}$ and $\delta\boldsymbol{\theta}$ that is imposed by (4.51), let us apply the first-order expansion of the function $\mathbf{g}(\boldsymbol{\theta}, \mathbf{q})$ that yields the following linear relation

$$\begin{bmatrix}\mathbf{J}_\theta & \mathbf{J}_q\end{bmatrix}\cdot\begin{bmatrix}\delta\boldsymbol{\theta}\\ \delta\mathbf{q}\end{bmatrix}=\mathbf{0} \tag{4.58}$$

Then, applying the SVD- factorization [Strang 1998] of the integrated Jacobian

$$\begin{bmatrix}\mathbf{J}_\theta & \mathbf{J}_q\end{bmatrix}=\begin{bmatrix}\mathbf{U}_\theta & \mathbf{U}_q\end{bmatrix}\cdot\begin{bmatrix}\mathbf{S}_r & \\ & \mathbf{0}\end{bmatrix}\cdot\begin{bmatrix}\mathbf{V}_\theta^{\mathrm{T}}\\ \mathbf{V}_q^{\mathrm{T}}\end{bmatrix} \tag{4.59}$$

and extracting from $\mathbf{V}_\theta$, $\mathbf{V}_q$ the sub-matrices $\mathbf{V}_\theta^{\mathrm{o}}$, $\mathbf{V}_q^{\mathrm{o}}$ corresponding to zero singular values, a relevant null-space of the system (4.58) may be presented as

$$\delta\boldsymbol{\theta}=\mathbf{V}_\theta^{\mathrm{o}}\cdot\delta\boldsymbol{\mu};\qquad \delta\mathbf{q}=\mathbf{V}_q^{\mathrm{o}}\cdot\delta\boldsymbol{\mu} \tag{4.60}$$

where $\delta\boldsymbol{\mu}$ is the arbitrary vector of the appropriate dimension (equal to the rank-deficiency of the integrated Jacobian). Hence, the stability condition (4.57) may be rewritten as an inequality

$$\delta W=-\frac{1}{2}\delta\boldsymbol{\mu}^{\mathrm{T}}\cdot\begin{bmatrix}\mathbf{V}_\theta^{\mathrm{o}}\\ \mathbf{V}_q^{\mathrm{o}}\end{bmatrix}^{\mathrm{T}}\cdot\begin{bmatrix}\mathbf{H}_{\theta\theta}^{\mathrm{F}}-\mathbf{K}_\theta & \mathbf{H}_{q\theta}^{\mathrm{F}}\\ \mathbf{H}_{\theta q}^{\mathrm{F}} & \mathbf{H}_{qq}^{\mathrm{F}}\end{bmatrix}\cdot\begin{bmatrix}\mathbf{V}_\theta^{\mathrm{o}}\\ \mathbf{V}_q^{\mathrm{o}}\end{bmatrix}\cdot\delta\boldsymbol{\mu}>0 \tag{4.61}$$

that must be satisfied for all arbitrary non-zero $\delta\boldsymbol{\mu}$. In other words, the considered static equilibrium configuration $(\mathbf{q}, \boldsymbol{\theta})$ is stable if (and only if) the matrix

$$\begin{bmatrix}\mathbf{V}_\theta^{\mathrm{o}}\\ \mathbf{V}_q^{\mathrm{o}}\end{bmatrix}^{\mathrm{T}}\cdot\begin{bmatrix}\mathbf{H}_{\theta\theta}^{\mathrm{F}}-\mathbf{K}_\theta & \mathbf{H}_{q\theta}^{\mathrm{F}}\\ \mathbf{H}_{\theta q}^{\mathrm{F}} & \mathbf{H}_{qq}^{\mathrm{F}}\end{bmatrix}\cdot\begin{bmatrix}\mathbf{V}_\theta^{\mathrm{o}}\\ \mathbf{V}_q^{\mathrm{o}}\end{bmatrix}<0 \tag{4.62}$$

is negative-definite. It is worth mentioning that the obtained result is in a good agreement with the previous studies [Chen 2002], where (for manipulators without passive joints) the stiffness properties were defined by the matrix $\mathbf{K}_\theta-\mathbf{H}_{\theta\theta}^{\mathrm{F}}$ that evidently must be positive-definite for the stable configurations. In Chapter 5 these results are applied for detecting bifurcations and buckling phenomena in typical serial kinematic chains and relevant parallel manipulators.

Thus, proposed stability analysis techniques for serial chain with the passive joints and related matrix stability criterion for the kinematic chain configuration allow estimating the stability of the serial chain configuration under external loading in the case of single and multiple equilibriums.

4.5 STIFFNESS MODEL OF PARALLEL MANIPULATORS IN LOADED MODE

The non-linear stiffness modeling technique proposed in Sections 4.2-4.4 deals with separate kinematic chains. In order to be applied to the parallel manipulators, it should be extended by appropriate stiffness model aggregation routines, as in Sections 3.4 and 3.5. Similar to the unloaded mode, these routines have to be applicable for both perfect and non-perfect kinematic chains. Besides, it is required to develop numerical algorithms for computing both direct and inverse force-deflection relations that are referred below to as non-linear stiffness and compliance models respectively.

4.5.1 Aggregation of chains stiffness models

Let us focus on the aggregation of stiffness models of separate serial chains into the stiffness model of the whole parallel manipulator in the loaded mode. To solve this problem, it is necessary to obtain the non-linear force-deflection relation, which takes into account elastostatic properties of all kinematic chains, and to compute corresponding Cartesian stiffness matrix.

Let us assume that the end-points of all kinematic chains are aligned and matched in the same target point $\mathbf{t}_0$, which corresponds to the desired end-platform location. This point is assumed to be known and allows us to compute, from the inverse kinematic model, the actuator and passive joint coordinates defining nominal configurations of the chains $(\mathbf{q}_{0i}, \boldsymbol{\theta}_{0i})$. It is also assumed that the stiffness models of all kinematic

chains have been already obtained using techniques proposed in Sections 4.2 or 4.3 and are presented in the form of partial non-linear force-deflection relations $\mathbf{F}_i = f_i(\mathbf{t} \mid \mathbf{t}_0)$ corresponding to the target point $\mathbf{t}_0$.

It is evident that the external loading $\mathbf{F}$ changes the end-platform location $\mathbf{t}_0$, hence it is reasonable to consider the set of locations $\mathbf{t}$ in the neighborhood of target one. Under the above assumptions, for any given point $\mathbf{t}$ from neighborhood of $\mathbf{t}_0$ it is possible to compute both the partial forces $\mathbf{F}_i$ and corresponding equilibrium configurations $(\mathbf{q}_i, \boldsymbol{\theta}_i)$ as well as to evaluate their stability (applying a criterion from Section 4.4). Then, in accordance with the superposition principle, the desired non-linear force-deflection relation for the whole parallel manipulator can be found by straightforward summation of all partial forces $\mathbf{F}_i$, i.e.

$$\mathbf{F} = \sum_{i=1}^{m} f_i\left(\mathbf{t} \mid \mathbf{t}_0\right) \tag{4.63}$$

where $\mathbf{F}$ denotes the total external loading applied to the end-platform. As a result, corresponding curves can be obtained by multiple repetition of the above described procedures for different values of the end-platform location $\mathbf{t}$.

Furthermore, for each given $\mathbf{t}$, the stiffness matrices $\mathbf{K}_{\mathrm{C}}^{(i)}$ of all kinematic chains can be computed using expression (4.23) or its modified version that includes the auxiliary loadings $\mathbf{G}_i$ (see sub-section 4.3.4 for details). This allows us to compute the Cartesian stiffness matrix $\mathbf{K}_{\mathrm{C}}$ of the whole parallel manipulator as a sum

$$\mathbf{K}_{\mathrm{C}} = \sum_{i=1}^{m} \mathbf{K}_{\mathrm{C}}^{(i)} \tag{4.64}$$

However, the matrices $\mathbf{K}_{\mathrm{Cq}}^{(i)}$ and $\mathbf{K}_{\mathrm{C}\theta}^{(i)}$ defining the "sensitivity" of the chain joint coordinates $(\mathbf{q}_i, \boldsymbol{\theta}_i)$ to the end-platform displacement cannot be aggregated in this way, they should be used separately to evaluate stresses in joints/links and resistance of the chain configurations with respect to external loading $\mathbf{F}$

$$\boldsymbol{\tau}_{\theta}^{(i)} = \mathbf{J}_{\theta}^{(i)\mathrm{T}} \cdot \mathbf{K}_{\mathrm{C}}^{(i)} \cdot \left(\mathbf{t} - \mathbf{t}_0\right); \qquad \delta\mathbf{q}_i = \mathbf{K}_{\mathrm{Cq}}^{(i)} \cdot \left(\mathbf{t} - \mathbf{t}_0\right); \qquad \delta\boldsymbol{\theta}_i = \mathbf{K}_{\mathrm{C}\theta}^{(i)} \cdot \left(\mathbf{t} - \mathbf{t}_0\right) \tag{4.65}$$

where $\mathbf{J}_{\theta}^{(i)}$ is Jacobian matrix of *i*-th kinematic chain with respect to virtual joint coordinates.

It is worth mentioning that above it was implicitly assumed that the manipulator assembling is equivalent to the aligning and matching of the chain end-frames. To deal with more general case, when the chains are connected to the different points of the platform, it is necessary to slightly modify the chain geometrical models and to re-compute the forces/torques and the stiffness matrices by adding a virtual rigid link connecting the end-point of the chain and the reference point of the platform (see Figure 3-3 where these extensions are defined by the vectors $\mathbf{v}_i$). After the relevant transformations that are described in details in sub-section 3.4.1, the above presented technique can be applied straightforwardly.

Besides, in contrast to Chapter 3, here there are no evident differences in stiffness models aggregation of perfect and non-perfect kinematic chains. However, here the chain geometrical errors are implicitly included in the functions $\mathbf{g}_i^{\varepsilon}(\mathbf{q}_i, \boldsymbol{\theta}_i)$. In particular for non-perfect chains, it is assumed that the nominal values of the joint coordinates $(\mathbf{q}_{0i}, \boldsymbol{\theta}_{0i})$ produce the end-point location vector which differs from $\mathbf{t}_0$:

$$\mathbf{g}_i^{\varepsilon}(\mathbf{q}_{0i}, \boldsymbol{\theta}_{0i}) = \mathbf{t}_0 + \boldsymbol{\varepsilon}_i \tag{4.66}$$

where $\boldsymbol{\varepsilon}_i$ accumulates influences of all geometrical errors on the end-point location of *i*-th chain. As a result, the end-platform cannot be located in the target point $\mathbf{t}_0$ without external loading, i.e.

$$\sum_{i=1}^{m} f_i\left(\mathbf{t} \mid \mathbf{t}_0\right)\Big|_{\mathbf{t}=\mathbf{t}_0} \neq \mathbf{0} \tag{4.67}$$

Moreover, without external loading, the end-platform location $\mathbf{t}_{\varepsilon}$ is different from the target one $\mathbf{t}_0$. The vector $\mathbf{t}_{\varepsilon}$ can be computed from the equation

$$\sum_{i=1}^{m} f_i\left(\mathbf{t}_{\varepsilon} \mid \mathbf{t}_0\right) = \mathbf{0} \tag{4.68}$$

which will be considered in the next sub-section. Corresponding internal forces $\mathbf{F}_i^{\varepsilon}$ defining the chain loadings due to the geometrical errors in the chains can be computed by simple substitution $\mathbf{t}_{\varepsilon}$ to the partial force deflection relations

$$\mathbf{F}_i^{\varepsilon} = f_i(\mathbf{t} \mid \mathbf{t}_0)\big|_{\mathbf{t}=\mathbf{t}_{\varepsilon}} \tag{4.69}$$

It is obvious that the sum of the $\mathbf{F}_i^{\varepsilon}$ is equal to zero but they produce stresses in the links and joints if the parallel manipulator is over-constrained.

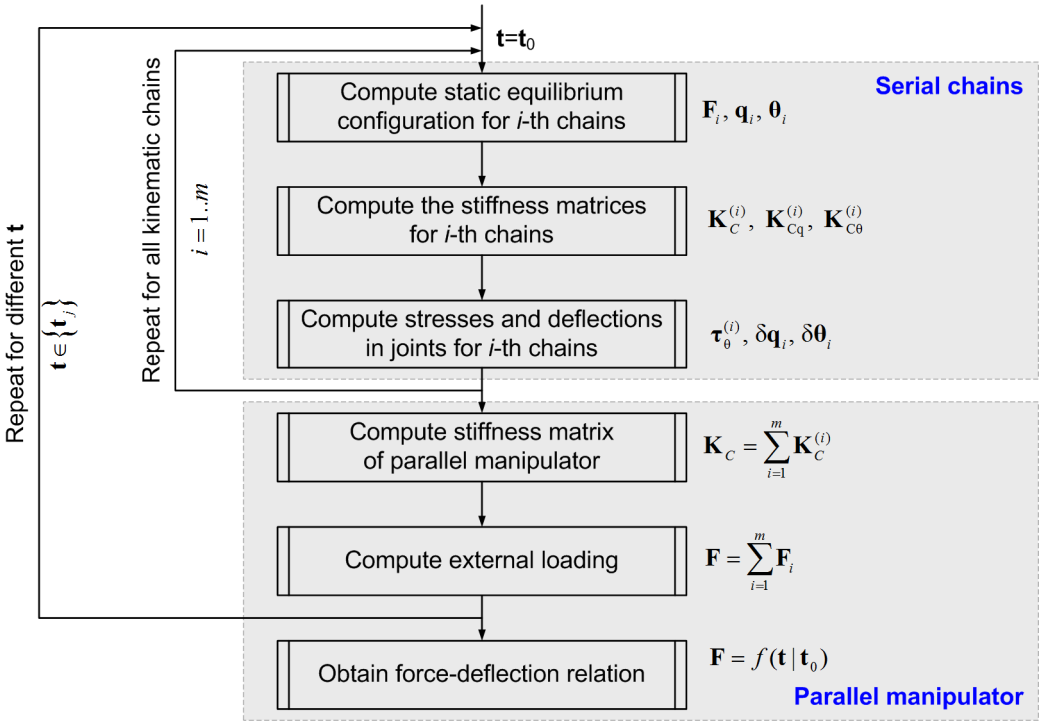

Figure 4.5 Aggregation of serial chains stiffness models technique

Hence, the developed aggregation technique allows us to obtain the non-linear force-deflection relation for a parallel manipulator in the loaded mode as well as to compute Cartesian stiffness matrices for any given target point $\mathbf{t}_0$ and given set of the end-point locations $\{\mathbf{t}\}$. This technique is summarized in Figure 4.5.

4.5.2 Compliance model of parallel manipulator

The non-linear force-deflection relation (4.63) allows us to evaluate the external force/torque $\mathbf{F}$ required to locate the manipulator in the target point $\mathbf{t}$ (assuming that the actuated coordinates are computed for the end-platform location $\mathbf{t}_0$ corresponding to the unloaded configuration). However in practice, it is often necessary to determine the end platform resistance to the external loading, i.e. to compute the deflection caused by the force $\mathbf{F}$ applied to the end-platform. The desired value can be found from the non-linear compliance model that in general case is expressed as

$$\mathbf{t} = f^{-1}(\mathbf{F} \mid \mathbf{t}_0) \tag{4.70}$$

and is defined by the inverse $f^{-1}(...)$ which for parallel manipulators usually exists (due to over-constrained structure). In contrast, for serial chains with passive joints, the function $f^{-1}(...)$ cannot be computed since the corresponding Cartesian stiffness matrix $\mathbf{K}_C^{(i)}$ is singular.

It is obvious that in a general case, the function $f^{-1}(...)$ cannot be expressed analytically. Hence, it is required that a dedicated iterative procedure, which is able to solve the non-linear equation (4.70) for $\mathbf{t}$ (assuming that $\mathbf{F}$ is given). It is proposed here to apply a modification of Newton-Raphson technique which iteratively updates the desired value $\mathbf{t}$ in accordance with the expression

$$\mathbf{t}' = \mathbf{t} + \mathbf{K}_{\mathrm{C}}^{-1}\left(\mathbf{t}\,|\,\mathbf{t}_0\right)\cdot\left(\mathbf{F} - f\left(\mathbf{t}\,|\,\mathbf{t}_0\right)\right) \tag{4.71}$$

where $\mathbf{t}'$ corresponds to the next iteration, $\mathbf{K}_{\mathrm{C}}\left(\mathbf{t}\,|\,\mathbf{t}_0\right)$ is the Cartesian stiffness matrix computed in the point $\mathbf{t}$, and $\mathbf{t}_0$ denotes the unloaded location of the end-platform. For this iterative scheme, $\mathbf{t}_0$ can be also used as the initial value of $\mathbf{t}$. Similar to sub-section 4.5.1, within each iterative loop, corresponding configurations $(\mathbf{q}_i, \boldsymbol{\theta}_i)$, the loadings $\mathbf{F}_i$ and stiffness matrices $\mathbf{K}_{\mathrm{C}}^{(i)}$ for each kinematic chain are computed using equations (4.10), (4.20) or (4.39), (4.49), depending on the external loading type.

As it follows from the relevant study, convergence of this iterative procedure is good enough if the function $f(...)$ is smooth and non-singular in the neighborhood of $\mathbf{t}_0$. If it is required to improve convergence, it is possible to apply the same technique as in sub-section 4.2.2, when the force $\mathbf{F}$ is modified from iteration to iteration in accordance with the expression $\mathbf{F}' = \alpha\cdot\mathbf{F}$, where a scalar variable α is monotonically increasing from 0 up to 1. The stopping criterion can be expressed in a straightforward way as

$$\left\|\mathbf{F} - f\left(\mathbf{t}\,|\,\mathbf{t}_0\right)\right\| < \varepsilon_{\mathrm{F}} \tag{4.72}$$

where ε_{F} is the desired accuracy. More details presentation of the developed iterative routines is given in Figure 4.6

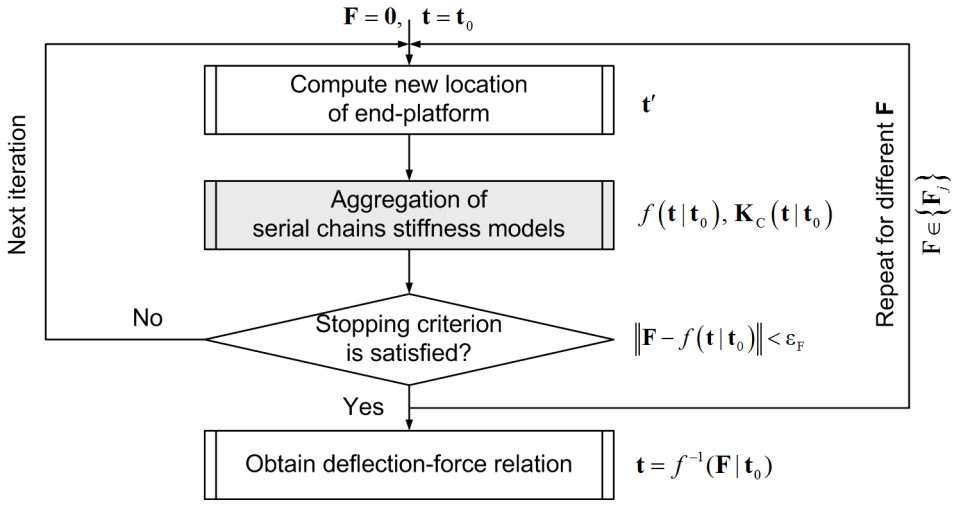

Figure 4.6 Procedure for obtaining deflection-force relation for loaded parallel manipulator

Summarising this sub-section, it is worth mentioning that the developed technique allows to obtain the desired non-linear deflection-force relation describing the end-platform resistance with respect to the external force for a given $\mathbf{t}_0$, which corresponds to the unloaded (nominal) manipulator configuration. However in practice, it is often required to compensate the compliance errors by proper adjusting of actuated coordinates (see Section 4.6). This procedure is equivalent to the modification of $\mathbf{t}_0$. Before considering this problem in details, let us illustrate the developed aggregation technique by an example.

4.5.3 Illustrative example: 2D translational manipulator with preloading in joints

Let us apply the proposed techniques to the stiffness analysis of the planar parallel manipulator of the Orthoglide family (Figure 4.7a). For illustration purposes, let us assume that the only source of the manipulator elasticity is concentrated in actuated drives, while the passive joints may be preloaded by (i) standard linear springs, or (ii) non-linear springs with mechanical stop-limit (see Figure 4.7 for details).

For this manipulator, the kinematic model includes a single parameter L (the leg length) and the dexterous workspace was defined as the maximum square area that provides the velocity (and force) transmission factors in the range [0.5, 2.0]. Using the critical point technique developed for this type of manipulators [Chablat 2003], it was proved that the desired square vertices are located in the points $Q_1(-p,-p)$ and $Q_2(p, p)$, where p=0.45 L. Besides, the square centre $Q_0(0, 0)$ is isotropic with respect to the velocity and force transmission. The parameters of the actuating drives are also assumed identical and their linear stiffness is denoted as K_θ. The auxiliary springs (incorporated in the passive joints) are described by two

parameters: the angular stiffness coefficient K_ϑ and the activation angle ϑ_0 that defines the preloading activation point. During simulation, the manipulator end-point has been displaced by value Δ in the direction Q_0Q_1 or Q_0Q_2, and the corresponding magnitude of the external force F has been computed.

The stiffness analysis results are summarized in Figure 4.8, Figure 4.9 and in Table 4.1. As it follows from them, the original manipulator (without preloading in passive joints) demonstrates rather low stiffness in the neighborhood of the point Q_2, which is roughly 4 times lower than in the isotropic point Q_0. In contrast, the linear stiffness in the point Q_1 is twice higher than in the point Q_0. Besides, in the point Q_2, the external loading may provoke the buckling phenomenon that is caused by a local minimum of the force-deflection relation. In this case, the distance-to-singularity is essentially lower than it is estimated from the kinematical model and the manipulator may easily lose its structural stability.

To improve the manipulator stiffness and to avoid the buckling in the neighborhood of Q_2, the passive joints were first preloaded by linear springs with activation angle $\vartheta_0 = 0$. As it follows from Figure 4.8, the preloading with parameter $K_\vartheta = 0.1 \cdot K_\theta \cdot L^2$ allows to eliminate buckling completely and to improve the stiffness by the factor of 2.3. On the other hand, the stiffness in the points Q_0 and Q_1 changes non-essentially, by 10% and 5% respectively. Hence, with respect to the stiffness, such preloading has a positive impact.

The only negative consequence of such preloading is related to the changes of the actuator control strategy. In fact, instead of standard kinematic control, it is necessary to apply the kinetostatic control algorithm (see next Section for details). It allows compensating the position errors caused by elastic deformations due to the internal preloading and to achieve the target end-point location with modified values of the actuated joint coordinates. As it follows from Table 4.1, corresponding adjustments of the joint coordinates may reach $0.1 \cdot L$ and are not negligible for most of the applications.

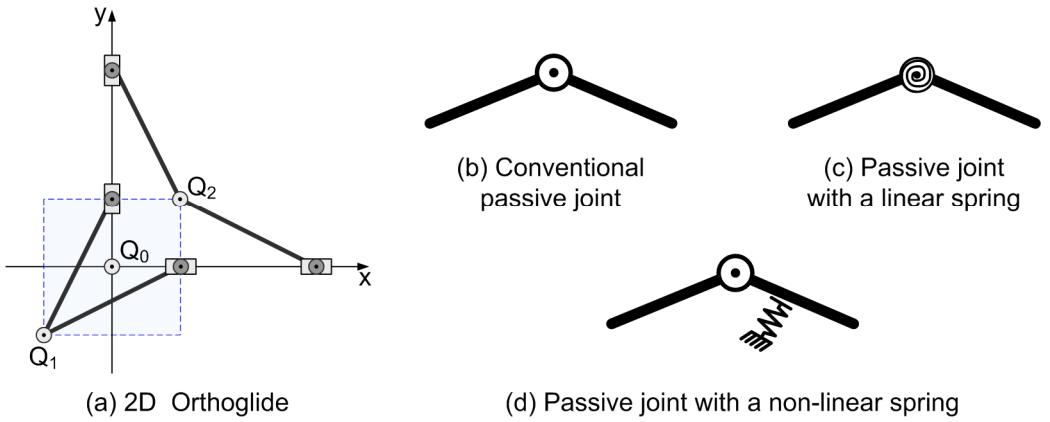

Figure 4.7 Architecture planar version of the Orthoglide manipulator (a), and passive joints and alternatives for them (b)-(d)

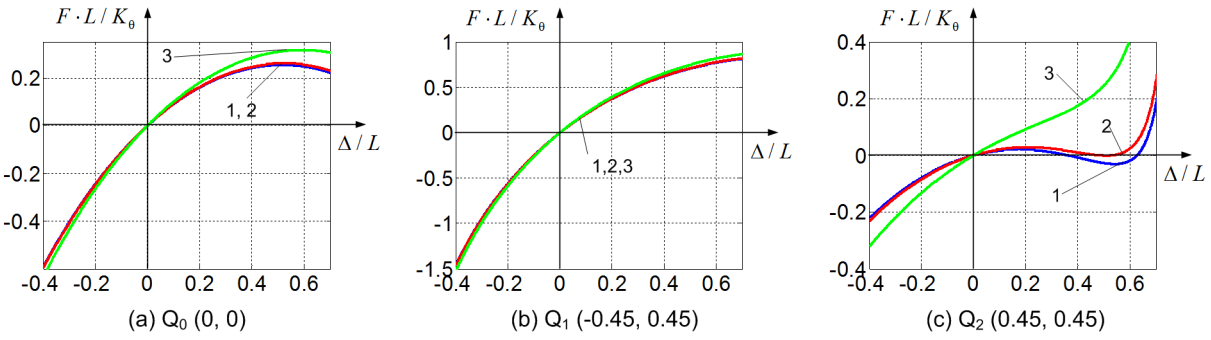

Figure 4.8 Force-deflection relations $F = f(\Delta / L)$ in critical points: (1) $K_\vartheta = 0$, (2) $K_\vartheta = 0.05\, K_\theta\, L^2$, (3) $K_\vartheta = 0.1\, K_\theta\, L^2$

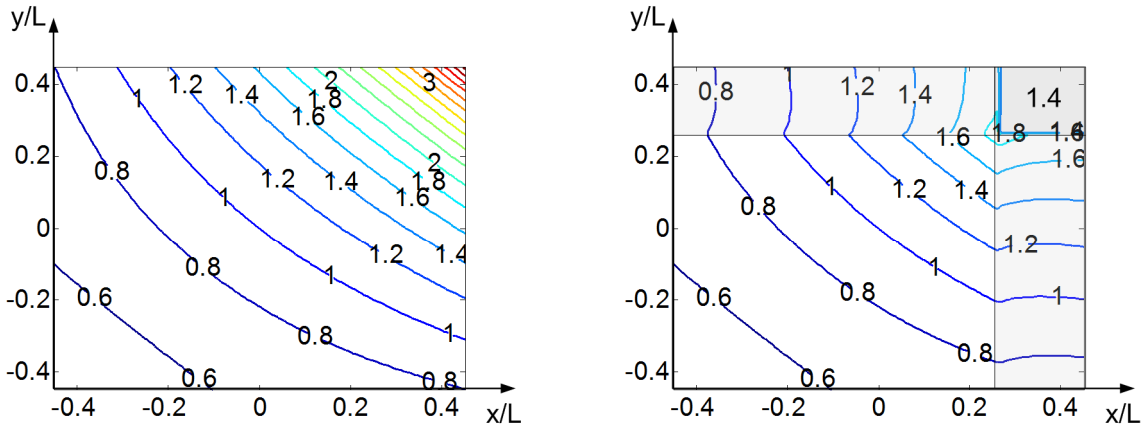

Figure 4.9 Compliance maps for cases of: (a) manipulator without preloading; (b) manipulator with preloaded nonlinear springs ($K_\vartheta = 0.05\, K_\theta\, L^2$ and $\vartheta_0 = \pi/12$)

Table 4.1 Manipulator stiffness for different linear preloading

Stiffness in preloaded joints	$K_\vartheta = 0$	$0.01\, K_\theta\, L^2$	$0.05\, K_\theta\, L^2$	$0.1\, K_\theta\, L^2$
Point Q0 :(isotropic point)				
Actuating joint coordinates ρ	L	L	L	L
Manipulator stiffness $\mathbf{K}_C$	K_θ	$1.01 K_\theta$	$1.05 K_\theta$	$1.10 K_\theta$
Point Q1 (neighborhood of "bar" singularity)				
Actuating joint coordinates ρ	0.437 L	0.433 L	0.419 L	0.402 L
Manipulator stiffness $\mathbf{K}_C$	$2.276 K_\theta$	$2.286 K_\theta$	$2.329 K_\theta$	$2.382 K_\theta$
Point Q2 : (neighborhood of "flat" singularity)				
Actuating joint coordinates ρ	1.345 L	1.356 L	1.399 L	1.453 L
Manipulator stiffness $\mathbf{K}_C$	$0.24 K_\theta$	$0.27 K_\theta$	$0.39 K_\theta$	$0.55 K_\theta$
Critical force $\mathbf{F}_{cr}$	$0.020 K_\theta L$	$0.027 K_\theta L$	---	---

The most efficient solution that eliminates this problem is to use the non-linear springs with mechanical stop-limit that are activated while approaching Q_2. For instance, as it follows from the dedicated study, the preloading with the parameters $K_\vartheta = 0.05 \cdot K_\theta \cdot L^2$, $\vartheta_0 = \pi/12$ provides almost the same improvements in Q_2 as the linear spring while preserving usual control strategies if the preloading is not activated. The efficiency of this approach is illustrated by the compliance maps presented in Figure 4.9.

Thus, in Section 4.5, the stiffness model aggregation technique for parallel manipulators was extended for the loaded mode. Compared to the related results presented in Sections 3.4 and 3.5, it allows us to obtain a non-linear force-deflection (or deflection-force) relation and to compute corresponding Cartesian stiffness matrix that depends on the loading magnitude and direction. In practice, this technique can be applied for two purposes: (i) evaluating the external loading impact on the positioning errors and (ii) compensating the compliance errors by proper adjustment of actuated coordinates. The last issue is the focus for the next Section.

4.6 COMPENSATION OF COMPLIANCE ERRORS IN PARALLEL MANIPULATORS IN LOADED MODE

In many robotic applications such as machining, grinding, trimming etc., the interaction between the workpiece and technological tool causes essential deflections that significantly decrease the processing accuracy and quality of the final product. To overcome this difficulty, it is possible to modify either the control algorithm or the prescribed trajectory, which is used as the reference input for a control system. This section focuses on the second approach that is considered to be more realistic for the practice. In contrast to the previous works, the proposed technique is based on the non-linear stiffness model (developed in this Chapter) that is able to take into account external and internal loadings of high magnitude.

4.6.1 Inverse and direct kinetostatic problems for loaded manipulator

In industrial robotic controllers, the manipulator motions are usually generated using the inverse kinematic model that allows us to compute the input signals for actuators $\boldsymbol{\rho}_0$ corresponding to the desired end-effector location $\mathbf{t}_0$, which is assigned assuming that the compliance errors are negligible. However, if the external loading is essential, the kinematic control becomes non-applicable because of changes in the end-platform location. It can be computed from the non-linear compliance model as

$$\mathbf{t}_{\mathrm{F}} = f^{-1}\left(\mathbf{F} \mid \mathbf{t}_0\right) \tag{4.73}$$

where the subscript 'F' refers to the loaded mode.

To compensate this undeterred end-platform displacement from $\mathbf{t}_0$ to $\mathbf{t}_{\mathrm{F}}$, the target point should be modified in such way that, under the loading $\mathbf{F}$, the end-platform is located in the desired point $\mathbf{t}_0$. This requirement can be expressed using the stiffness model (4.63) in the following way

$$\mathbf{F} = f\left(\mathbf{t}_0 \mid \mathbf{t}_0^{(\mathrm{F})}\right) \tag{4.74}$$

where $\mathbf{t}_0^{(\mathrm{F})}$ denotes the modified target location (which obviously is not attained because of the loading). Hence, the problem is reduced to the solution of the nonlinear equation (4.74) for $\mathbf{t}_0^{(\mathrm{F})}$, while $\mathbf{F}$ and $\mathbf{t}_0$ are assumed to be given. It is worth mentioning that this equation completely differs from the equation $\mathbf{F} = f(\mathbf{t} \mid \mathbf{t}_0)$ considered in sub-section 4.5.2, where the unknown variable is $\mathbf{t}$. It means that here the compliance model does not allow us to compute the modified target point $\mathbf{t}_0^{(\mathrm{F})}$ straightforwardly, while linear compensation technique directly operates with Cartesian compliance matrix [Seo 1998] [Gong 2000].

To solve equation (4.74) for $\mathbf{t}_0^{(\mathrm{F})}$, the Newton-Raphson technique can be applied similar to sub-section 4.5.2. It yields the following iterative scheme

$$\mathbf{t}_0^{(\mathrm{F})\prime} = \mathbf{t}_0^{(\mathrm{F})} + \mathbf{K}_{\mathrm{t.p.}}^{-1}(\mathbf{t}_0 \mid \mathbf{t}_0^{(\mathrm{F})}) \cdot \left(\mathbf{F} - f(\mathbf{t}_0 \mid \mathbf{t}_0^{(\mathrm{F})})\right) \tag{4.75}$$

where the prime corresponds to the next iteration and $\mathbf{K}_{\mathrm{t.p.}}(\mathbf{t}_0 \mid \mathbf{t}_0^{(\mathrm{F})})$ is Cartesian stiffness matrix computed with respect to the second argument of the stiffness model (4.63)

$$\mathbf{K}_{\mathrm{t.p.}}(\mathbf{t} \mid \mathbf{t}_0) = \frac{\partial f(\mathbf{t} \mid \mathbf{t}_0)}{\partial \mathbf{t}_0}, \tag{4.76}$$

which can be interpreted is the target point. Here, the location $\mathbf{t}_0$ can be also used as the initial value of $\mathbf{t}_0^{(\mathrm{F})}$. The stopping criterion can be also expressed as

$$\left\| \mathbf{F} - f\left(\mathbf{t}_0 \mid \mathbf{t}_0^{(\mathrm{F})}\right) \right\| < \varepsilon_{\mathrm{F}} \tag{4.77}$$

where ε_{F} is the desired accuracy.

To overcome computational difficulties related to the evaluation of the matrix $\mathbf{K}_{\mathrm{t.p.}}(\mathbf{t}_0 \mid \mathbf{t}_0^{(\mathrm{F})})$, it is possible to use its simple approximation that does not changes from iteration to iteration. In particular, assuming that $\mathbf{t}$ and $\mathbf{t}_0$ are closed enough and the stiffness properties do not vary substantially in their neighborhood, the stiffness model can be approximated by a linear expression $\mathbf{F} = \mathbf{K}_{\mathrm{C}} \cdot (\mathbf{t} - \mathbf{t}_0)$, which gives $\mathbf{K}_{\mathrm{t.p.}} = -\mathbf{K}_{\mathrm{C}}$. Hence, the iterative scheme (4.75) can be modified as

$$\mathbf{t}_0^{(\mathrm{F})\prime} = \mathbf{t}_0^{(\mathrm{F})} - \alpha \cdot \mathbf{K}_{\mathrm{C}}^{-1}(\mathbf{t}_0 \,|\, \mathbf{t}_0^{(\mathrm{F})}) \cdot \left(\mathbf{F} - f(\mathbf{t}_0 \,|\, \mathbf{t}_0^{(\mathrm{F})})\right) \tag{4.78}$$

where $\alpha \in (0,1)$ is the scalar parameter insuring convergence. Using non-linear compliance model (4.73), this idea can be also implemented in iterative algorithm

$$\mathbf{t}_0^{(\mathrm{F})\prime} = \mathbf{t}_0^{(\mathrm{F})} + \alpha \cdot \left(\mathbf{t}_0 - f^{-1}(\mathbf{F} \,|\, \mathbf{t}_0^{(\mathrm{F})})\right) \tag{4.79}$$

which does not include stiffness matrices $\mathbf{K}_{\mathrm{C}}$ or $\mathbf{K}_{\mathrm{t.p.}}$ (see Figure 4.10 for details). Obviously, this is the most computationally convenient and it will be used in the next sub-section.

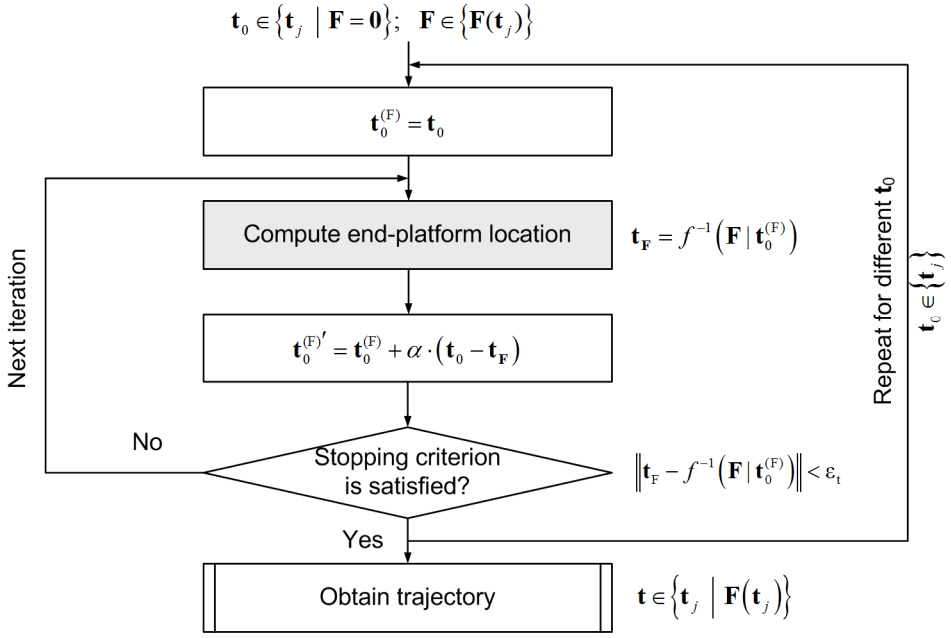

Figure 4.10 Procedure for compensation of compliance errors in parallel manipulator

Hence, using the computational techniques proposed in this sub-section, it is possible to compensate the compliance errors by proper adjustment of the reference trajectory that is used as an input for robotic controllers. In this case, the control is based on the inverse kinetostatic model (instead of kinematic one) that takes into account both the manipulator geometry and elastic properties of its links and joints. Efficiency of this technique is confirmed by an example presented below.

4.6.2 Application example: kinetostatic control of Orthoglide in milling application

Let us illustrate now the compliance errors compensation technique by an example of the circle groove milling of the radius $r = 50\,mm$ with Orthoglide manipulator for the different workpiece locations in the manipulator workspace. It is assumed that the manipulator has assembling errors in actuator angular locations of about 1° (around the corresponding actuated axis). More detailed description of these assumptions is given in sub-section 3.5.2 that focuses on the assembling errors influence on the manipulator accuracy (using linear stiffness modeling technique and assuming that $\mathbf{F} = \mathbf{0}$). In contrast, there are two sources of inaccuracy here

(i) the assembling errors in the kinematic chains causing internal forces and relevant deflections in joints and links (similar to sub-section 3.5.1);

(ii) the external loading $\mathbf{F} \neq \mathbf{0}$ which generates essential compliance deflections causing non-desirable end-platform displacement.

It is worth mentioning that non-linear stiffness modelling technique, which has been developed in this Chapter, allows to compensate for the influence of both the factors above.

For the considered process (groove milling), the magnitude and direction of the external loading $\mathbf{F}$ can be found from the cutting technology models. According to [Majou 2007] such a technological process causes the loading

$$\mathbf{F} = (F_x, F_y, F_z, -F_y \cdot h, F_x \cdot h, 0) \tag{4.80}$$

where F_x and F_y depend on the machining tool orientation angle φ (Figure 4.11 a, b) as

$$F_x = F_r \cos\varphi + F_t \sin\varphi; \qquad F_y = F_r \sin\varphi + F_t \cos\varphi \tag{4.81}$$

and $F_r = 215\,N$; $F_t = -10\,N$; $F_z = -25\,N$; $h = 100\,mm$

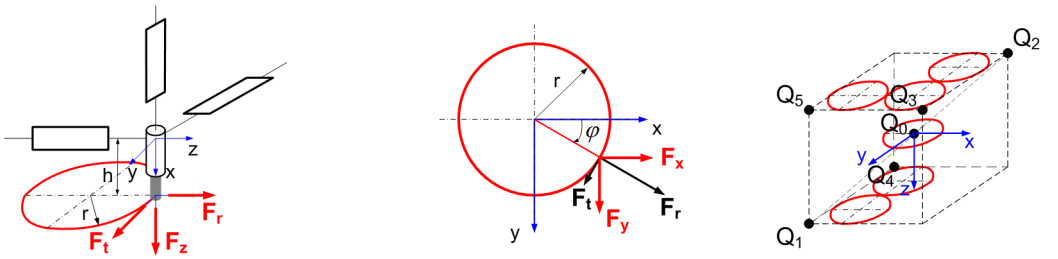

(a) groove milling with Orthoglide (b) milling forces (c) milling workpiece location

Figure 4.11 Milling forces and trajectory location for groove milling using Orthoglide manipulator

The milling process was studied for six typical locations of the desired circular trajectory (see Figure 4.11c):

(1) in the neighborhood of the isotropic point Q_0, (which coincides with the circle center), where the manipulator configuration is the best from kinematic point of view;

(2,3) in the opposite corners of the cubic workspace Q_1 and Q_2 corresponding to the symmetrical manipulator configurations;

(4,5,6) in the area of the workspace corners Q_3, Q_4 and Q_5 that correspond to the non-symmetrical configurations of the manipulator.

For each of these locations, the milling trajectory was oriented in xy-plane as shown in Figure 4.11.

For such process parameters, without compensation, the compliance errors can exceed 1.2 mm, which is too high for the considered application. In particular, for the best location Q_0, the cutting forces provoke the end-effector deflection of 0.35 mm. And for the worst location Q_3, the end-effector deflection is about 1.25 mm. Hence, the application of the developed compliance errors compensation technique is reasonable here.

After compensation, the above mentioned errors are reduced to zero (it is obvious that in practice, the compensation level is limited by the accuracy of the stiffness model parameters). This compensation is achieved due to the modification of the actuator coordinates $\boldsymbol{\rho}$ along machining trajectory. Compared to relevant values computed via the inverse kinematics (as in common-used industrial controllers), the actuator coordinates differ up to 0.6 mm for location Q_0, and up to 1.9 mm for location Q_3. Corresponding forces in actuators can reach 300 N. A more detailed result describing the compliance errors compensation are presented in Table 4.2, which includes a number of plots giving modification of the actuator coordinates $\Delta\boldsymbol{\rho}$, values of compensated end-effector displacement $\Delta\mathbf{t}$ and the torques in actuators τ.

It is worth mentioning, that the shape of the compensation curve $\Delta\boldsymbol{\rho}(\varphi)$ highly depends on the location of the milling trajectory (i.e. the function $\Delta\boldsymbol{\rho}(\varphi)$ cannot be normalized by scaling and shifting) and the compensation procedure requires intensive computing. However, it can be implemented off-line and the robot model motion program can be properly modified.

Table 4.2 Compliance error compensation for Orthoglide milling application with cutting force (215 N, -10 N, -25 N, 1 N·m, 21.5 N·m, 0) for different location of the workpiece

Location	Compensation in actuators	Compensated error (end-effector)	Forces in actuators
Location Q_0 (0, 0, 0)	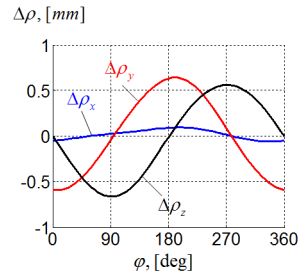	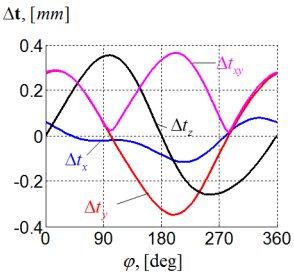	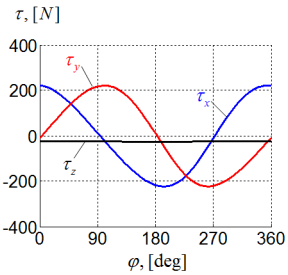
Location Q_1 (126.35, 126.35, 126.35)	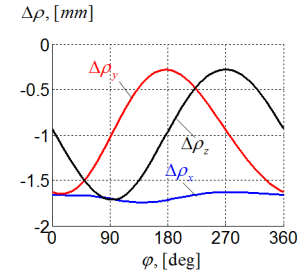	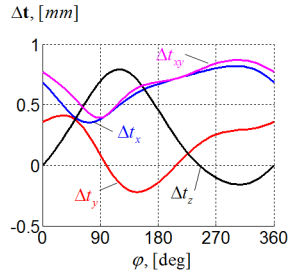	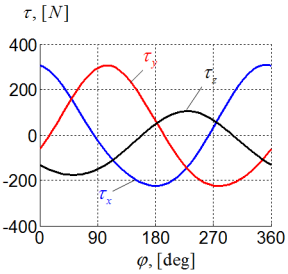
Location Q_2 (-73.65, -73.65, -73.65)	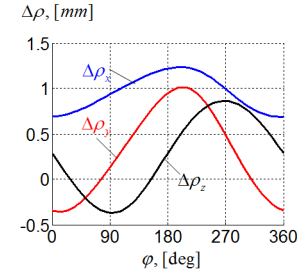	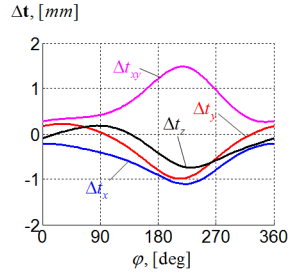	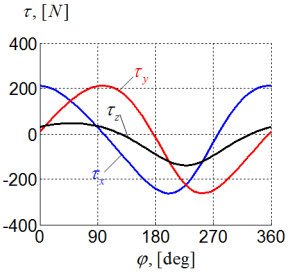
Location Q_3 (126.35, 126.35, -73.65)	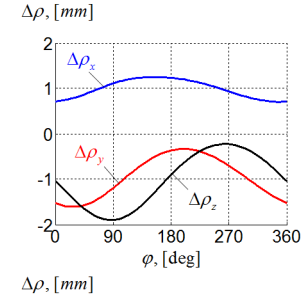	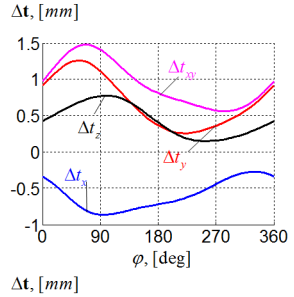	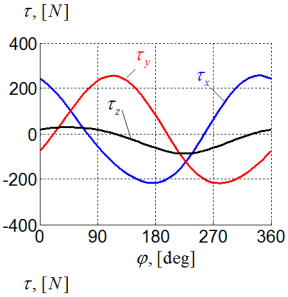
Location Q_4 (-73.65, -73.65, 126.35)	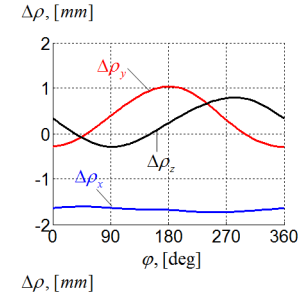	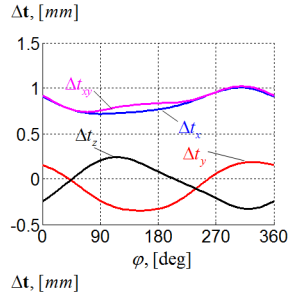	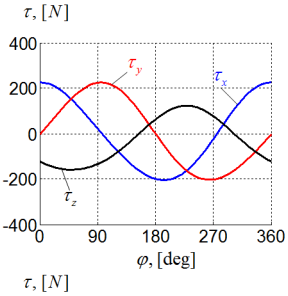
Location Q_5 (-73.65, 126.35, -73.65)	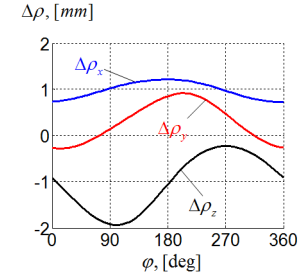	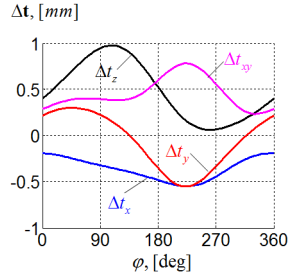	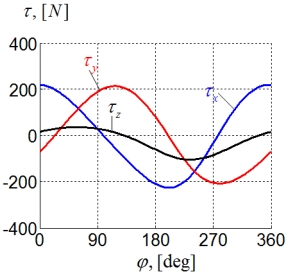

Hence, as follows from the presented results, the developed algorithm demonstrates good convergence, it is able to compensate the compliance errors caused by different types of loadings and it can be efficient both for off-line trajectory planning and for on-line errors compensation.

4.7 SUMMARY

The chapter is devoted to the non-linear stiffness modeling of serial and parallel manipulators in the loaded mode (i.e. under assumption of large deformations). The main contributions are in the area of the VJM modeling approach that was generalized for the case of large deflections caused by internal and external loadings applied to the end-point or/and to the intermediate nodes of the kinematic chains. In contrast to the other works, the developed technique includes computing of the static equilibrium configuration corresponding to the given loading. In addition, it allows us to check the "internal stability" of the relevant chain configuration. Similar to Chapter 3, the stiffness modeling of parallel manipulators starts from kinematic chains, but it yields a non-linear function describing force-deflection relation. Besides, for each kinematic chain, this technique is also able to obtain *both non-singular and singular stiffness matrices*. Relevant aggregation procedure allows us to obtain a non-linear force-deflection (or deflection-force) relation for the parallel manipulator and to compute the *aggregated Cartesian stiffness matrix*, as well as to evaluate the *internal forces/torques* and *end-platform deflections* caused by loadings and geometrical errors in the kinematic chains. In addition, this model is used for compensation of the compliance errors caused by the internal and external loadings. Similar to the previous chapter, the developed method combines advantages of the FEA and the VJM modeling approaches (accuracy and computational efficiency respectively).

In more details, new results and contributions of Chapter 4 can be formulated as

(i) Non-linear stiffness modeling technique for serial kinematic chain under external and internal loadings (applied to end-point, to the intermediate nodes, preloading in the joints) which includes: computing the static equilibrium configuration in the loaded mode, obtaining full-scale force-deflections relation and computing of the stiffness matrix for the loaded mode

(ii) Stability analysis technique and related matrix stability criterion for kinematic chain configuration under loading in the case of single and multiple equilibriums, which takes into account the second derivatives of the chain potential energy.

(iii) Enhanced stiffness model aggregation technique for over-constrained parallel manipulators under internal and external loadings, which takes into account shifting of the equilibrium due to the loadings and allows to evaluate internal deflections and forces/torques in joints, as well as deflections of the reference point, caused by geometrical errors in kinematic chains.

(iv) Numerical technique for on-line and off-line compensation of the compliance errors caused by external loadings in parallel manipulators (including over-constrained ones) with perfect and non-perfect serial chains. In contrast to previous works this technique is based on non-liner stiffness model that gives essential advantages for robotic-based machining, where the elastic deflections can be essential.

Concerning limitations of these results, it is worth mentioning that they are generally destined for the case of a parallel manipulator with strictly parallel architecture, as in Section 3. However, for some architectures (incorporating kinematic parallelograms, for instance) the developed method can be efficiently applied sequentially as shown in the author's publications [Klimchik 2010b], [Klimchik 2011d]. In addition, the developed modeling technique is able to detect some important non-linear effects in the manipulator stiffness behavior, which are considered in the next Chapter.

The main results of Chapter 4 are published in the following works: [Klimchik 2009a], [Klimchik 2009c], [Klimchik 2010a], [Klimchik 2010b], [Klimchik 2010c], [Klimchik 2011a], [Klimchik 2011b], [Klimchik 2011e].

CHAPTER 5

NON-LINEAR EFFECTS IN MANIPULATOR STIFFNESS BEHAVIOR UNDER LOADINGS

The chapter is devoted to the application of the developed modeling technique for the non-linear stiffness analysis of the manipulators with passive joints in the loaded mode. It focuses on detecting non-linear effects in the manipulator stiffness behavior under loading and determining potentially dangerous configurations and critical forces that may provoke undesired buckling phenomena (i.e. sudden change of current configuration of the loaded manipulator). The stiffness analysis is carryied out for serial and parallel manipulators with different assumptions on their flexibility and type of loading. Particular attention is paid to multiple equilibriums, stability of the kinematic chain configuration and kinetostatic singularities in loaded manipulators.

5.1 INTRODUCTION

To demonstrate advantages of the stiffness analysis technique developed in previous chapters, let us consider several case studies assuming that the loading is essential and causes significant deflections in elastic elements of the manipulators. In contrast to previous works, it allows us to investigate potential non-linear phenomena in stiffness behavior of manipulators that were not detectable in the frame of linear models. It is worth mentioning that for robotics this problem is fairly new, but in structural mechanics, there are a number of interesting results that provide a useful analogy.

As known from mechanics, in a general case the stiffness behavior of a structure (or a mechanism) may be essentially non-linear as it is illustrated by the force-deflection curves in Figure 5.1 [Jones 2006], [Timoshenko 1970]. In particular, in the simplest case, a corresponding curve is smooth, monotonically increasing but with its inclination progressively reduces while the force is increasing (see Figure 5.1a). Such a non-linear shape yields the stiffness coefficient, which depends on the applied loading and monotonically reduces. The second example (see Figure 5.1b) shows the force-deflection curve that is also monotonically

increasing but contains a salient point that corresponds to a sudden reduction of the stiffness coefficient (buckling). And finally, the third example (see Figure 5.1c) presents a non-monotonic (but smooth) force-deflection curve with local maximum and minimum. In this case, the curve includes a region with negative inclination (i.e. negative stiffness coefficient) and the system behavior under the loading is highly non-linear. Here, deflection is increasing continuously at the beginning, but then it changes abruptly, while the loading achieves its critical value (it is also called buckling). Analyzing these examples, we can conclude that in robotic systems, similar phenomena may exist.

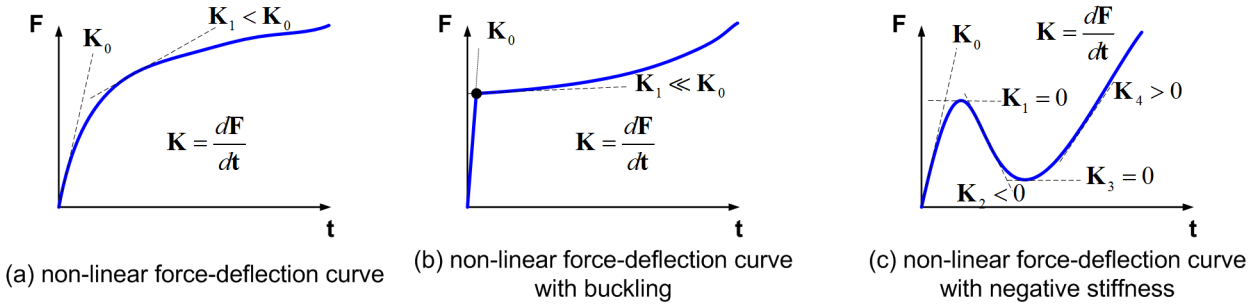

(a) non-linear force-deflection curve

(b) non-linear force-deflection curve with buckling

(c) non-linear force-deflection curve with negative stiffness

Figure 5.1 Examples of non-linear force-deflection curves

In the following sections, we will pay special attention to the buckling phenomena since they are considered as potentially very dangerous for mechanical structures and mechanisms, and may provoke failures. In general theory of elasticity, several types of buckling are usually distinguished:

local buckling of a structural element (rod, beam, etc.), observed as a sudden change of the element shape and significant reducion of its stiffness;

geometrical buckling of a mechanism or structure (arches, shells, etc.), observed as a sudden change of mechanism/structure geometrical configuration;

contact buckling associated with boundary conditions for the mechanism/structure elements that can be observed similar to either local or geometrical buckling.

Below, it will be shown that similar buckling phenomena also exist in robotic systems, but have never been studied in details.

For the local buckling, a classical example is usually related to the *axially compressed column* [Jones 2006], which is also referred to as "Euler buckling". As shown in Figure 5.2, depending on end-point constrains, the loading may provoke different changes in the column shape that appear after achieving a critical value for the compressing force. Besides, here the column end-point can abruptly be moved either in axial or lateral direction. It is obvious that in application to the robotic manipulator, similar behavior may be observed both for a separate link and for a serial chain of links. However, it is unlikely that the VJM model can detect the local buckling for a separate link due to its simplified approximation (rigid rod and virtual spring at the end).

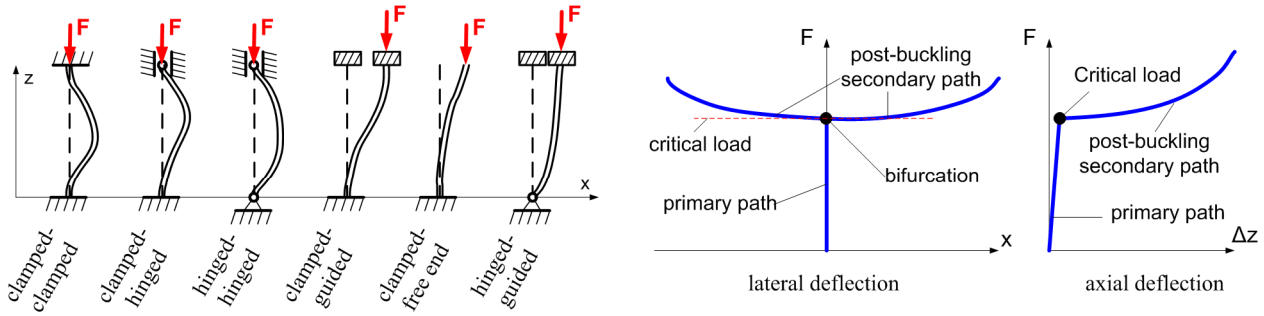

(a) end-points constrains

(b) force-deflection relations

Figure 5.2 Local buckling in axially compressed column

For the geometrical buckling, a representative example is *two-rod arch* with vertical loading presented in Figure 5.3. Here, when the loading exceeds its critical value, the elastostatic equilibrium becomes unstable and the system suddenly changes its configuration. Making the analogy with robotic manipulators, it is clear that similar behavior can be observed in parallel architectures with end-point loading and in serial chains with auxiliary loading applied in the intermediate nodes.

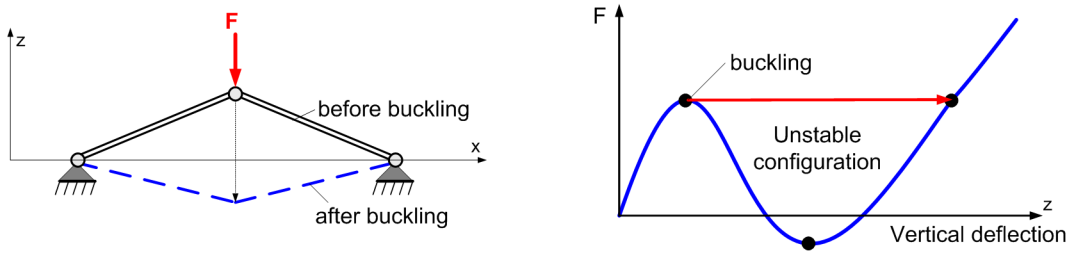

(a) geometrical model (b) force-deflection curve

Figure 5.3 Geometrical buckling in vertically loaded arch

It is worth mentioning that in previous works devoted to the manipulator stiffness analysis, much attention has not been paid to the buckling phenomena. The authors mainly concentrated on computing of the stiffness matrices implicitly assuming that the force-deflection relation is monotonic and its second order approximation is good enough. Obviously, this approach does not allow us to detect salient points or local maximums/minimums that are essential for full-scale non-linear force-deflection analysis. To our knowledge, the only works that contain some comprehensive results on non-linear stiffness analysis are [Hines 1998], [Carricato 2002] where several case studies have been considered using the catastrophe theory. But it is unlikely that such technique can be applied in a general case.

Hence, the goal of this Chapter is an application of the developed technique to the analysis of non-linear effects in manipulator stiffness behavior under loadings and determining the potentially dangerous configurations and critical forces that may provoke an undesired buckling phenomena, i.e. sudden change of current configuration. To achieve this goal, the remainder of this chapter is organized as follows. Section 5.2 deals with detecting buckling phenomena and determining potential dangerous configurations for serial chains under end-point loading and different assumptions of flexibility. Section 5.3 considers stiffness analysis of kinematic chains under auxiliary loadings. Section 5.4 focuses on the stiffness modeling of parallel manipulators in the loaded mode. And finally, Section 5.5 summarizes main results and contributions of this Chapter.

5.2 BUCKLING PHENOMENA IN SERIAL CHAIN UNDER END-POINT LOADING

Let us consider first a serial kinematic chain consisting of three similar links, which are separated by two similar rotating actuated joints. It is assumed that the chain is a part of a parallel manipulator and it is connected to the robot base via a universal passive joint, and the end-platform connection is achieved via a spherical passive joint. For each of these configurations, let us investigate three types of the virtual springs corresponding to different physical assumptions concerning the stiffness properties of the actuators/links. They cover the cases, in which the main flexibility is caused by the torsion in the actuators, by the link bending, and by the combination of elementary deformations of the links.

5.2.1 Kinetostatic model of serial kinematic chain and its parameterization

To apply the developed technique, first it is required to derive the models that describe geometry of the considered serial chain and stiffness properties of its elements. For all sub-cases, similar parameterization will be used that allows us to present results in a comparable form.

Geometric model. The geometry of the examined kinematic chain (Figure 5.4) can be defined as $U_pR_aR_aS_p$ where R, U and S denote respectively the rotational, universal and spherical joints, and the

subscripts '*p*' and '*a*' refer to the passive and active joints respectively. Using the homogeneous matrix transformations, it can be described by the equation

$$\mathbf{T} = \mathbf{R}_{\mathrm{u}}(\mathbf{q}_0)\cdot\mathbf{T}_{\mathrm{x}}(L)\cdot\mathbf{T}_{\mathrm{s}}(\boldsymbol{\theta}_1)\cdot\mathbf{R}_{\mathrm{z}}(q_{\mathrm{a1}})\cdot\mathbf{T}_{x}(L)\cdot\mathbf{T}_{\mathrm{s}}(\boldsymbol{\theta}_2)\cdot\mathbf{R}_{\mathrm{z}}(q_{\mathrm{a2}})\cdot\mathbf{T}_{\mathrm{x}}(L)\cdot\mathbf{T}_{\mathrm{s}}(\boldsymbol{\theta}_3)\cdot\mathbf{R}_{\mathrm{s}}(\mathbf{q}_{\mathrm{t}}) \tag{5.1}$$

where $\mathbf{R}_{\mathrm{z}}(...)$ and $\mathbf{T}_{\mathrm{x}}(...)$ are the elementary rotation/translation matrices around/along the *z*- and *x*-axes, $\mathbf{R}_{\mathrm{u}}(...)$ is the homogeneous rotation matrix of the universal joint (incorporating two elementary rotations), $\mathbf{R}_{\mathrm{s}}(...)$ is the homogeneous rotation matrix of the universal joint (incorporating three elementary rotations), $q_{\mathrm{a1}}, q_{\mathrm{a2}}$ are the coordinates of the actuated joints, L is the length of the links, $\mathbf{q}_0$ is the coordinate vector of the universal passive joint located at the robot base, $\mathbf{q}_t$ is the coordinate vector corresponding to the passive spherical joint at the end-platform, $\mathbf{T}_{\mathrm{s}}(...)$ is the homogenous matrix-function describing elastic deformations in the links and actuators (they are represented by the virtual coordinates incorporated in the vectors $\boldsymbol{\theta}_1, \boldsymbol{\theta}_2, \boldsymbol{\theta}_3$). It is obvious that this model can be easily transformed into the form $\mathbf{t} = \mathbf{g}(\mathbf{q}, \boldsymbol{\theta})$ used in the frame of the developed technique.

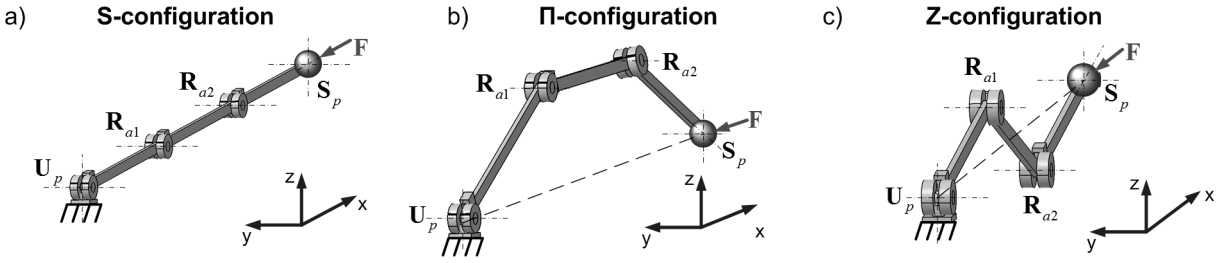

Figure 5.4 Examined kinematical chain and its typical configurations
(U_p – passive universal joint, R_{a1}, R_{a2} – actuated rotating joints, S_p – passive spherical joint)

To investigate particularities of this kinematic chain with respect to the external loading, let us also consider three typical postures that differ in values of the actuated coordinates:

S-configuration: the links are located along the straight line (Figure 5.4a),
the actuated coordinates are $q_{\mathrm{a1}} = q_{\mathrm{q2}} = 0$

П-configuration: the chain takes a trapezoid shape (Figure 5.4b),
the actuated coordinates are $q_{\mathrm{a1}} = q_{\mathrm{q2}} = -30^{\circ}$

Z-configuration: the chain takes a zig-zag shape (Figure 5.4c),
the actuated coordinates are $q_{\mathrm{a1}} = -q_{\mathrm{a2}} = 30^{\circ}$

For presentation convenience, let us also assume that the coordinates $\mathbf{q}_0$ of the universal passive joint are computed to ensure location of the end-effector on the Cartesian axis *x*.

Stiffness models. In order to investigate possible non-linear effects in the stiffness behavior of this chain, let us consider several cases that differ in stiffness models of the links and actuated joints:

Case of 1D-springs (Model A): the flexible elements are localized in the actuating drives while the links are considered as strictly rigid. It allows without loss of generality to reduce the original $U_pR_aR_aS_p$ model down to $R_pR_aR_aR_p$ and define a single stiffness parameter K_θ (similar for both actuators) that will be used as a reference value for further analysis. Besides, it is possible to ignore the end-effector orientation and consider a single passive joint coordinate q (at the base) and two virtual joint coordinates θ_1, θ_2 (at actuators).

Case of 2D springs (Model B): the actuators do not include flexible components but the manipulator links are subject to non-negligible elastic deformations in Cartesian xy-plane (bending and compression). Correspondingly, the link flexibility is defined by a 3×3 matrix that includes elements describing deformation in x- and y- directions and rotational deformation with respect to the z-axis.

Case of 3D springs (Model C): the actuators are strictly rigid but the link flexibility is described by a full-scale 3D model that incorporates all deflections along and around x-,y-,z-axes of the three-dimensional Cartesian space. Relevant stiffness matrix of the links has the dimension 6×6. The kinematics of this model corresponds to the general expression $U_pR_aR_aS_p$, it includes two passive joints $(\mathbf{q}, \mathbf{q}_t)$ incorporating in total five passive coordinates and three virtual-springs with 18 virtual coordinates totally (six for each link).

Parameterization of stiffness models for serial kinematic chains. In order to simplify comparison of numerical values derived from the stiffness analysis of examined serial kinematic chains, the compliance matrices corresponding to all considered case studies have been parameterized similarly. Relevant expressions are presented below.

In the *case of 1D-springs (Model A),* it is assumed that all flexible elements are localized in the actuating drives while the links are considered as strictly rigid. It allows to define a single stiffness coefficient K_θ (similar for both actuators) that is used as a reference value for other case studies.

In the *case of 2D springs (Model B),* it is assumed that the actuators do not include flexible components but the manipulator links are subject to elastic deformations in Cartesian xy-plane (bending and compression). Correspondingly, the link flexibility is defined by a 3×3 matrix that includes elements describing linear deformation in x- and y- directions and rotational deformation with respect to z-axis. Relevant stiffness matrix may be written as [Connor 1976]

$$\mathbf{K} = \frac{E}{L^3} \cdot \begin{bmatrix} A \cdot L^2 & 0 & 0 \\ 0 & 12 \cdot I & -6 \cdot I \cdot L \\ 0 & -6 \cdot I \cdot L & 4 \cdot I \cdot L^2 \end{bmatrix} \tag{5.2}$$

where L is the length of the links, I and A are respectively its second moment and area of the cross-section, E is the Young module. To ensure comparability with model A, the element $k_{3,3}$ (corresponding to z-rotation) of the compliant matrix $\mathbf{k} = \mathbf{K}^{-1}$ was denoted as $1/K_\theta$. It allows to eliminate the Young module and present the desired matrix as

$$\mathbf{K} = K_\theta \cdot \begin{bmatrix} I/A & 0 & 0 \\ 0 & L^2/3 & L/2 \\ 0 & L/2 & 1 \end{bmatrix}^{-1} \tag{5.3}$$

where, for the rectangular cross-section $a \times b$, the remaining parameters are expressed as $A = ab$ and $I = ab^3/12$.

In the *case of 3D springs (Model C),* the actuators are strictly rigid but the link flexibility is described by a full-scale 3D model that incorporates all deflections along and around x-,y-,z-axes of the three-dimensional Cartesian space. Relevant stiffness matrix of the links has the dimension 6×6 and may be expressed as [Connor 1976]

$$\mathbf{K} = \frac{E}{L^3} \cdot \begin{bmatrix} A \cdot L^2 & 0 & 0 & 0 & 0 & 0 \\ 0 & 12 \cdot I_z & 0 & 0 & 0 & -6 \cdot I_z \cdot L \\ 0 & 0 & 12 \cdot I_y & 0 & 6 \cdot I_y \cdot L & 0 \\ 0 & 0 & 0 & G \cdot J \cdot L^2 / E & 0 & 0 \\ 0 & 0 & 6 \cdot I_y \cdot L & 0 & 4 \cdot I_y \cdot L^2 & 0 \\ 0 & -6 \cdot I_z \cdot L & 0 & 0 & 0 & 4 \cdot I_z \cdot L^2 \end{bmatrix} \tag{5.4}$$

where A, I_y, I_z are the area and the second moments of the link cross-section, J is the polar moment, E and G are the Young and Coulomb modules of the material. For the rectangular cross-section $a \times b$, the required parameters may be computed as $A = ab$ and $I_y = a^3 b/12$, $I_z = ab^3/12$ .Similar to the previous case, the parameterization is performed by defining the compliance with respect to the z-axis as $1/K_\theta$ (here, it is element $k_{6,6}$ of the compliant matrix $\mathbf{k} = \mathbf{K}^{-1}$). This leads to the expression:

$$\mathbf{K} = K_\theta \cdot \begin{bmatrix} I_z / A & 0 & 0 & 0 & 0 & 0 \\ 0 & L^2/3 & 0 & 0 & 0 & L/2 \\ 0 & 0 & k_I \cdot L^2/3 & 0 & k_I \cdot L/2 & 0 \\ 0 & 0 & 0 & k_J \cdot I_z / \left(2 \cdot L \cdot (1+\nu)\right) & 0 & 0 \\ 0 & 0 & k_I \cdot L/2 & 0 & k_I & 0 \\ 0 & L/2 & 0 & 0 & 0 & 1 \end{bmatrix}^{-1} \tag{5.5}$$

where the coefficient k_J depends on the cross-section shape, $k_I = I_y / I_z$, and ν is the Poisson ratio coefficient.

Let us use these parameterizations of flexible elements sequentially and compare the stiffness analysis results for S, Π and Z configurations of the kinematic chain.

5.2.2 Stiffness analysis for serial chain with 1D-springs

In this case, the model includes a minimum number of flexible elements (two 1D virtual springs in the actuated joints) and may be tackled analytically. However, in spite of its simplicity, it is potentially capable to detect the buckling phenomena at least for S-configuration, because of evident mechanical analogy to straight columns behavior under axial compression. It is also useful to evaluate other initial configurations with respect to the multiple loaded equilibriums, their stability and to compare with numerical results provided by the developed technique.

In the frame of this model, the end-effector motions are restricted to Cartesian *xy*-plane and the geometry is defined by equations

$$\begin{aligned} x &= L \cdot \cos q + L \cdot \cos q_{12} + L \cdot \cos q_{13}, \\ y &= L \cdot \sin q + L \cdot \sin q_{12} + L \cdot \sin q_{13} \end{aligned} \tag{5.6}$$

where L is the length of links, q is the passive joint coordinate, θ_1, θ_2 are the virtual spring coordinates, $q_{12} = q + \theta_1$ and $q_{13} = q + \theta_1 + \theta_2$. It is obvious that this model includes exactly one redundant variable. Without loss of generality, one can assume that the redundant variable is the passive joint coordinate q while the manipulator end-effector is initially located at the point $(x, y) = (3L - \delta, 0)$, where δ is a linear displacement along the x-axis.

Then, assuming that the initial values of the actuating coordinates (i.e. before the loading) are denoted as θ_1^0, θ_2^0, the potential energy stored in the virtual springs may be expressed as the following function of the redundant variable

$$E(q) = \frac{1}{2} K_\theta \cdot \left(\theta_1(q) - \theta_1^0\right)^2 + \frac{1}{2} K_\theta \cdot \left(\theta_2(q) - \theta_2^0\right)^2 \tag{5.7}$$

where K_θ is the stiffness coefficient, and θ_1, θ_2 are computed via the inverse kinematics. Using these equations, the desired equilibriums may be computed from the extremum of $E(q)$. In particular, stable equilibriums correspond to minima of this function, and unstable ones correspond to maxima.

To illustrate this approach, Figure 5.5 presents a case study for the initial S-configuration. It allows comparing 12 different shapes of the deformated chain and selecting the best /worst cases with respect to the energy. As it follows from these results, here there are two symmetrical maximal and two minimal, i.e. two stable and two unstable equilibriums. Besides, the stable equilibriums correspond to Π-shaped deformated postures, and the unstable ones correspond to Z-shaped postures, as it is shown in Figure 5.6. A more detailed analysis allows deriving analytical expressions for the force and energy for small values of δ:

stable equilibrium: $E_{\min} \approx \delta \cdot K_\theta / L$; $F_S \approx K_\theta / L$

unstable equilibrium: $E_{\max} \approx \delta \cdot 3K_\theta / L$; $F_N \approx 3K_\theta / L$

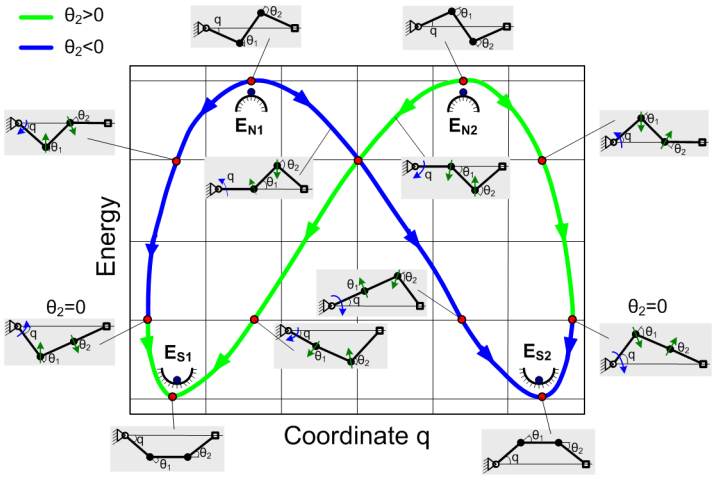

Figure 5.5 Potential energy $E(q)$ and geometric postures for different values of q (Model A, case of initial S-configuration, $\delta = L/10$)

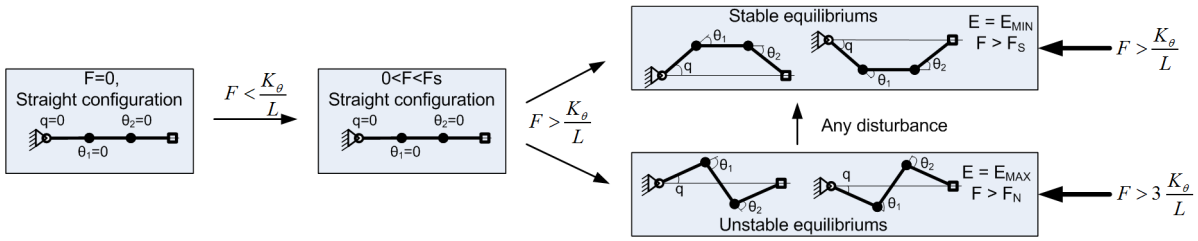

Figure 5.6 Evolution of the S-configuration under external loading

Hence, the external force $F \le K_\theta / L$ cannot change the manipulator shape, similar to small compressing of straight columns that cannot cause lateral deflections. Consequently, in this case the straight configuration is stable. Further, for $K_\theta / L < F \le 3K_\theta / L$, the straight configuration may be hypothetically restored but becomes unstable, so any small disturbance will cause sudden reshaping in the direction of the stable trapezoid-type posture. And finally, for $F > 3K_\theta / L$, there may exist two types of unstable equilibriums: the trivial straight-type and a more complicated zig-zag one.

If the assumption concerning small values of δ is released, analytical solutions for the non-trivial equilibriums may be still derived. In particular, for the stable equilibrium, one can get

$$F_S(\Delta) = \frac{K_\theta}{L} \cdot \frac{\varphi}{\sin\varphi} \tag{5.8}$$

where $\varphi = \pm\arccos(1 - \Delta/2)$. For the unstable equilibrium a similar equation may be written as

$$F_N(\Delta) = \frac{K_\theta}{L} \cdot \frac{\cos(q+\theta) + 2\cdot\cos q}{\sin\theta} \cdot \theta \tag{5.9}$$

where

$$q = \pm\arccos\left(\frac{12 - 6\Delta + \Delta^2}{12 - 4\Delta}\right);$$
$$\theta = \mp\arccos\left(1 - \frac{3\Delta}{2} + \frac{\Delta^2}{4}\right) \tag{5.10}$$

Corresponding plots are presented in Figure 5.7 where there are also shown the bifurcation. The interpretation of this plot is similar to the axial compression of a straight column, which is a classical example in the strength of materials. It should be noted, that the developed numerical algorithm exactly produces the curve corresponding to the stable equilibrium.

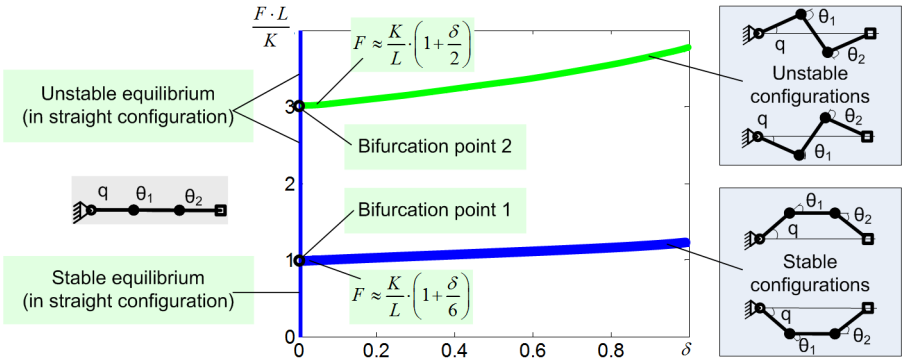

Figure 5.7 Model A: Force-deflection relations and bifurcations for the initial S-configuration

For other initial shapes (Π-type and Z-type), the results essentially differ from the above ones (see Table 5.1). In particular, for small deflections, both Π- and Z-configuration demonstrate a rather linear behavior. Moreover, in most of the cases there exist a single stable and a single unstable equilibrium, so the kinematic chain cannot suddenly change its shape due to external loading. The only exception is the case of the initial Π-configuration where there are two stable and two unstable equilibriums, and here there exists a bifurcation of the stable equilibriums corresponding to the cuspidal point of the function $F(\Delta)$ where the stiffness reduces sharply. Another conclusion concerns the profile of the force-deflection plots that are highly nonlinear in all cases.

A more detailed analysis shows that Π-configuration demonstrates good analogy with axially compressed imperfect column where the deflection starts from the beginning of the loading and there is no sudden buckling, but the stiffness essentially reduces while the loading increases. In particular, for the examined kinematic chain the stiffness coefficient is about $1.78\, K_\theta / L^2$ at the beginning and $0.43\, K_\theta / L^2$ at the end of the curve $F(\Delta)$.

However, for Z-configuration that corresponds to the unloaded zig-zag shape, the stiffness behavior demonstrates the buckling that leads to sudden transformation from a symmetrical to a non-symmetrical posture as shown in Figure 5.8. Here, there exist two stable equilibriums that differ in the values of the potential energy, so the stiffness coefficient reduces from $16.7\, K_\theta / L^2$ at the beginning to $0.39\, K_\theta / L^2$ at the end of the curve $F(\Delta)$ (see Table 5.2).

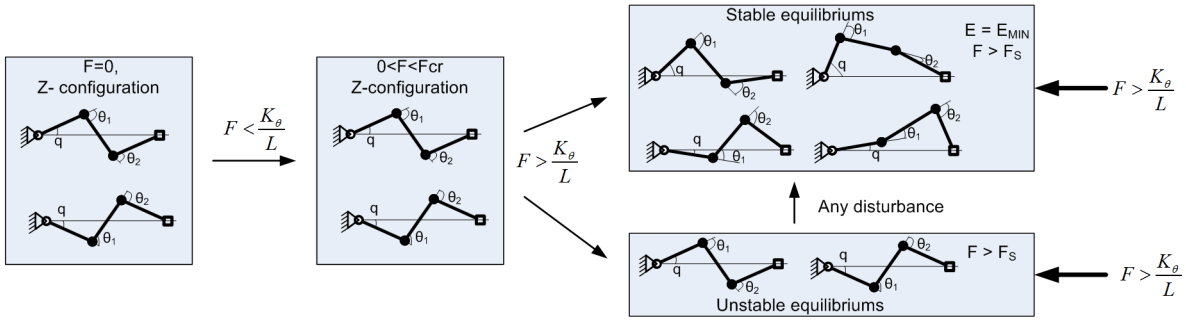

Figure 5.8 Evolution of the Z-configuration under external loading

Table 5.1 Force-deflection relations for different elasticity models of serial chain with passive joints

Elasticity models	S-configuration	Π-configuration	Z-configuration
	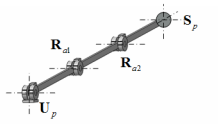	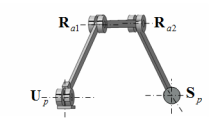	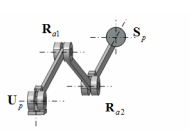
	$\theta_1^0 = \theta_2^0 = 0$	$\theta_1^0 = \theta_2^0 = -30^\circ$	$\theta_1^0 = -30^\circ,\ \theta_2^0 = 30^\circ$
Model A: 1D-springs	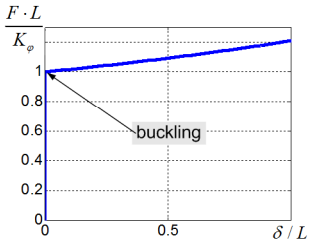	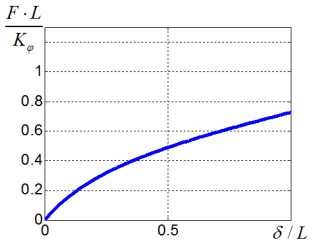	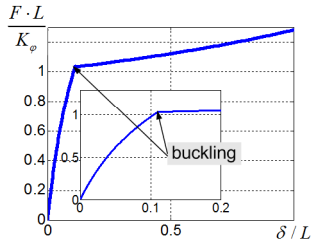
Model B: 2D-springs	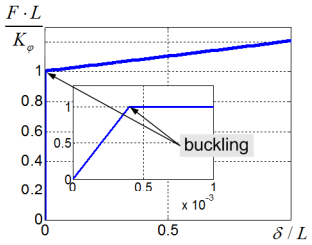	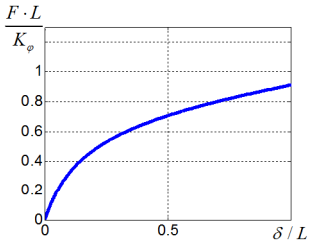	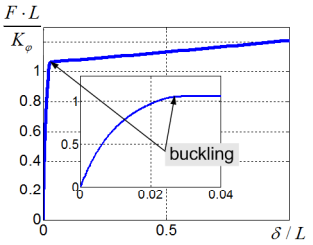
Model C: 3D-springs	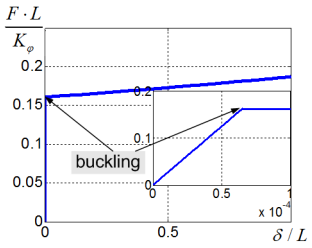	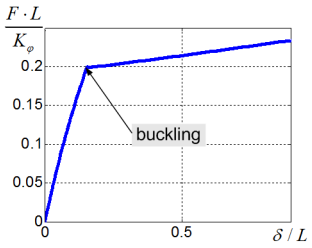	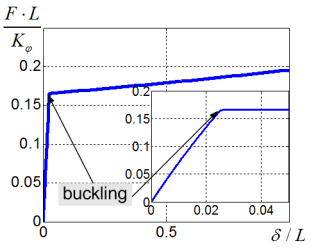

Table 5.2 Summary of stiffness analysis for serial chain with passive joints and 1D-springs

Configuration	Critical force	Stiffness for unloaded mode	Stiffness around the buckling		Stiffness for large deformations ($\delta \approx L$)
			$F < F_{cr}$	$F > F_{cr}$	
S-configuration	$\frac{K_\theta}{L}$	∞	∞	$0.20\,\frac{K_\theta}{L}$	$0.22\,\frac{K_\theta}{L}$
Π-configuration	---	$1.78\,\frac{K_\theta}{L}$	---	---	$0.43\,\frac{K_\theta}{L}$
Z-configuration	$1.03\,\frac{K_\theta}{L}$	$16.7\,\frac{K_\theta}{L}$	$5.50\,\frac{K_\theta}{L}$	$0.20\,\frac{K_\theta}{L}$	$0.39\,\frac{K_\theta}{L}$

Hence, in the case of model A, the developed numerical technique provides results that correspond to the stable loaded equilibriums and coincide with relevant analytical solutions. Besides, a more general class of manipulator postures that are dangerous with respect to buckling was detected. They include all configurations possessing by an axial symmetry with respect to the direction of the external force (S- and Z-configurations, for instance).

5.2.3 Stiffness analysis for serial chain with 2D-springs

In this case, the manipulator stiffness is caused by elasticity in the links while the actuating joints are assumed to be rigid. The elastic deflections (bending and compression) are still restricted by the Cartesian xy-plane but each link includes three virtual joints. Totally, the stiffness model has 11 variables, so it was studied numerically (using the developed technique). The stiffness parameters of the elements (5.3) were evaluated assuming that the links are rectangular beams of the length L and the cross-section $a \times b$, where $a = 0.02L$ and $b = 0.05L$. For comparison purposes, corresponding stiffness matrices were scaled with respect to the bending coefficient $1/K_\theta$ to keep similarity with model A. The stiffness analysis was performed for the above defined S-, Π- and Z-configurations, assuming that the external force is directed along the x-axis. A summary of the modeling results are presented in Table 5.1 and Table 5.3 and are briefly described below.

For *S-configuration*, here there is still a very strong analogy with the compression of the straight column. In particular, at the beginning of the loading, the links are subject to the axial compression and the stiffness is very high (about $2500\,K_\theta / L^2$, for the assumed link proportions). Then, after the buckling, the manipulator changes its shape to become non-symmetrical and the stiffness falls down to $0.20\,K_\theta / L^2$. The critical force may be also computed using the previous results, as $F_0 = K_\theta / L$.

For *Π-configuration*, the stiffness properties are also qualitatively equivalent to the case of Model A but the stiffness coefficient is slightly lower (in the frame of the adopted parameterization); it varies from $5.31\,K_\theta / L^2$ to $0.34\,K_\theta / L^2$. For *Z-configuration*, it also detected the buckling that occurs if the loading approaches the critical value $F_0 = 1.07\,K_\theta / L$. At this point, the stiffness falls down from $100 \cdot K_\theta / L^2$ to $0.13 \cdot K_\theta / L^2$, which essentially differs from model A.

Table 5.3 Summary of stiffness analysis for serial chain with passive joints and 2D-springs

Configuration	Critical force	Stiffness for unloaded mode	Stiffness around the buckling		Stiffness for large deformations ($\delta \approx L$)
			$F < F_{cr}$	$F > F_{cr}$	
S-configuration	$\frac{K_\theta}{L}$	$2500\,\frac{K_\theta}{L^2}$	$2500\,\frac{K_\theta}{L^2}$	$0.20\,\frac{K_\theta}{L^2}$	$0.22\,\frac{K_\theta}{L^2}$
Π-configuration	---	$5.31\frac{K_\theta}{L^2}$	---	---	$0.34\,\frac{K_\theta}{L^2}$
Z-configuration	$1.07\,\frac{K_\theta}{L}$	$100\,\frac{K_\theta}{L^2}$	$0.13\frac{K_\theta}{L^2}$	$0.13\,\frac{K_\theta}{L^2}$	$0.16\,\frac{K_\theta}{L^2}$

Hence, stiffness analysis of Model B demonstrates qualitative similarity but some quantitative difference compared to Model A. The latter is caused by different arrangement of the elastic elements in the virtual joints that corresponds to other physical assumptions.

5.2.4 Stiffness analysis for serial chain with 3D-springs

Finally, for model C, the link elasticity is described in 3D space and corresponding stiffness matrices have dimension 6×6 (5.5) (the actuating joints are assumed perfect and rigid, similar to model B). It is also assumed that the links are rectangular beams of the length L with the cross-section $a \times b$, where $a = 0.02L$, $b = 0.05L$ and the smaller value a corresponds to z-direction, which was not studied above. To ensure comparability of all examined cases, the link stiffness matrices were parameterized with respect to the bending coefficient of the z-axis K_θ. In total, the stiffness model includes 23 variables (five for passive joints and 18 for the virtual springs of three links) and it was studied numerically. The stiffness analysis was performed for the same initial configurations (S-, Π- and Z-type) and for the same direction of the external

force as for the models A and B. Summary of the modeling results are presented in Table 5.1 and Table 5.4 and are briefly described below.

For *S-configuration*, the results are qualitatively similar to ones obtained for model B. Besides, numerical value of the stiffness for the non-loaded case is the same, $2500\,K_\theta / L^2$. However, here the buckling occurs for an essentially lower critical force, $0.16\,K_\theta / L$, that corresponds to sudden lateral deflection in z-direction. For comparison, according to the Euler formula, the local buckling of the links occurs for a compressing force of $0.40\,K_\theta / L$, which is 2.5 times higher than the loading that provokes the geometric buckling of the examined mechanism. Then, after the buckling, the stiffness falls down to $0.20\,K_\theta / L^2$. It is worth mentioning that the axial deflection corresponding to the critical force is very low, it is equal to $7 \cdot 10^{-5} \cdot \delta / L$.

In contrast, for *Π-configuration* buckling which does not exist in models A and B was detected. In particular, if the external force exceeds the critical value $0.20\,K_\theta / L$ the stiffness suddenly reduces from $1.03\,K_\theta / L^2$ to $0.04\,K_\theta / L^2$ (for comparison, the stiffness coefficient for unloaded mode is $1.70\,K_\theta / L^2$). Physically it is also explained by sudden deflection in z-direction, which was beyond capabilities of previous models. It is also worth mentioning that, in this case study, the stiffness of manipulator links in z-direction is essentially lower than in y-direction. Another interpretation of this buckling phenomenon may be presented as sudden loss of symmetry with respect to xy-plane.

For *Z-configuration*, the results remain qualitatively the same as above, but corresponding numerical values are changed. Thus, manipulator stiffness for the unloaded mode is $7.52\,K_\theta / L$, then it gradually reduces to $5.88\,K_\theta / L$ and, after buckling, falls down to $0.03\,K_\theta / L$. Corresponding value of the critical force is $0.17\,K_\theta / L$ and it also corresponds to the z- deflection.

Table 5.4 Summary of stiffness analysis for serial chain with passive joints and 3D-springs

Configuration	Critical force	Stiffness for unloaded mode	Stiffness around the buckling		Stiffness for large deformations ($\delta \approx L$)
			$F < F_{cr}$	$F > F_{cr}$	
S-configuration	$0.16\,\frac{K_\theta}{L}$	$2500\,\frac{K_\theta}{L^2}$	$2500\,\frac{K_\theta}{L^2}$	$0.023\,\frac{K_\theta}{L^2}$	$0.029\,\frac{K_\theta}{L^2}$
Π-configuration	$0.20\,\frac{K_\theta}{L}$	$1.70\,\frac{K_\theta}{L^2}$	$1.03\,\frac{K_\theta}{L^2}$	$0.043\,\frac{K_\theta}{L^2}$	$0.13\,\frac{K_\theta}{L^2}$
Z-configuration	$0.17\,\frac{K_\theta}{L}$	$7.52\,\frac{K_\theta}{L^2}$	$5.88\,\frac{K_\theta}{L^2}$	$0.027\,\frac{K_\theta}{L^2}$	$0.035\,\frac{K_\theta}{L^2}$

Summarized results concerning all models A, B, C are presented in Table 5.1, Table 5.2, Table 5.3 and Table 5.4. As it follows from them, a full-scale 3D stiffness analysis yields essentially lower values of critical force compared to models A and B. Besides, for model C, all examined postures demonstrated buckling related to sudden deflections in the z- direction. This presents another source of potential structural instability of kinematic chains that posses the symmetry with respect to a plane.

5.3 BUCKLING PHENOMENA IN SERIAL CHAIN WITH AUXILIARY LOADING

Let us now focus on the non-linear stiffness analysis of a serial chain under auxiliary loadings applied to an intermediate node. It is assumed that the considered chain consists of two links (either rigid or flexible) separated by a flexible joint. Relevant analysis includes evaluating stiffness variation due to the loading, detecting of buckling and computing corresponding critical forces, as well as analysis of the auxiliary spring influence on the chain stiffness.

5.3.1 Serial chain with torsional springs

Let us consider first a 2-link manipulator with a compliant actuator between the links and two passive joints at both ends. It is assumed that the left passive join is fixed, while the right one can be moved along x direction (Figure 5.9a). Besides, here both rigid links have the same length L and the actuator stiffness is K_θ. The positions of the end-effector and the actuator for such a manipulator are defined as

$$\begin{aligned} x_e &= 2L\cdot\cos\alpha; \qquad & x_a &= L\cdot\cos\alpha \\ y_e &= 0; & y_a &= L\cdot\sin\alpha \end{aligned} \tag{5.11}$$

where α is the angle between the first link and x-direction, and indices 'e' and 'a' correspond to the end-effector and actuator positions respectively.

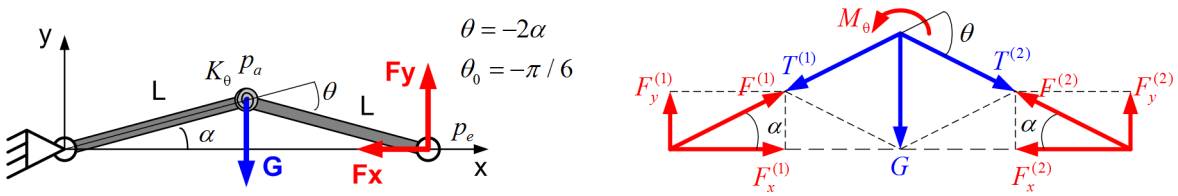

(a) kinematic chain (b) static forces/torques

Figure 5.9 Kinematic chain with compliant actuator between two links and its static forces/torques

Let us assume that the initial configuration (i.e. for $M_\theta = 0$) of the manipulator corresponds to $\theta_0 = -\pi/6$, where $\theta = -2\cdot\alpha$ is the coordinate of the actuated joint. It is also assumed that the external loading G is applied to the intermediate node (Figure 5.9a) and it is required to apply the external loading (F_x, F_y) at the end-point to compensate the auxiliary loading G. Since this example is quite simple, it is possible to obtain the force-deflection relation and the stiffness coefficient both analytically and numerically.

Let us start from the analytical stiffness analysis taking into account static forces/torques presented in Figure 5.9b. The static equilibrium equation of this system can be written as

$$M_\theta + M_{\mathrm{Fx}} + M_{\mathrm{Fy}} = 0 \tag{5.12}$$

where

$$M_\theta = K_\theta\cdot(\theta - \theta_0), \qquad M_{\mathrm{Fx}} = -F_x\cdot L\cdot\sin\alpha, \qquad M_{\mathrm{Fy}} = F_y\cdot L\cdot\cos\alpha \tag{5.13}$$

Taking into account that $\theta = -2\alpha$, $\theta_0 = -2\alpha_0$ and $F_y = -G/2$, the force-displacement relation can be expressed in a parametric form as

$$\begin{gathered} F_x = -\frac{G}{2}\cdot\frac{\cos\alpha}{\sin\alpha} - 2\cdot\frac{K_\theta}{L}\cdot\frac{\alpha-\alpha_0}{\sin\alpha}; \qquad F_y = -\frac{G}{2}; \\ x = 2\cdot L\cdot\cos\alpha; \qquad y = 0 \end{gathered} \tag{5.14}$$

and stiffness of the manipulator can be presented in a parametric form as

$$K_x = -\frac{G}{4L}\cdot\frac{1}{\sin^3\alpha} - \frac{K_\theta}{L^2}\cdot\frac{(\alpha-\alpha_0)\cdot\cos\alpha - \sin\alpha}{\sin^3\alpha}; \qquad K_y = 0 \tag{5.15}$$

where $\alpha \in (-\pi/2;\ \pi/2)$ is treated as a parameter.

As it follows from expression (5.15), the stiffness coefficient K_x essentially depends on the auxiliary loading G. In particular, for the initial configuration (when $M_\theta = 0$), the coefficient K_x can be both positive and negative or even equal to zero when the auxiliary loading is equal to its critical value

$G^* = 4K_\theta / L \cdot \sin\alpha_0$. It is evident that the case $G > G^*$ is very dangerous from a practical point of view, since the chain configuration is unstable.

Summarized results for this case study are presented in Figure 5.10 and in Table 5.5 that contain the force-deflection relations and values of translational stiffness K_x respectively. They show that the auxiliary loading G significantly reduces the stiffness of the serial chain. For example, in an initial configuration ($\Delta x = 0$), for $G = 0$ the stiffness is $14.9 \cdot K_\theta / L^2$, while for $G = 0.5 \cdot G^*$ it reduces to $8.67 \cdot K_\theta / L^2$. Further increasment of the auxiliary loading up to $G = 1.5 \cdot G^*$ leads to the unstable configuration with negative stiffness $-7.46 \cdot K_\theta / L^2$. Moreover, in the neighborhood of the critical value of $G \approx G^*$ (Figure 5.11), the force-deflection curves have extremum points which may provoke buckling.

For this case study, similar analysis has also been performed using the developed numerical technique presented in Section 4.3. Some details concerning functions and matrices used in relevant expressions are presented in Table 5.6, where L_1 and L_2 denote the manipulator link lengths, q_1 and q_2 are the passive joint coordinates, θ is the virtual spring coordinate and θ_0 is the actuator coordinate. It is worth mentioning that the numerical technique yielded the same results as the analytical one, which confirms validity of the developed approach.

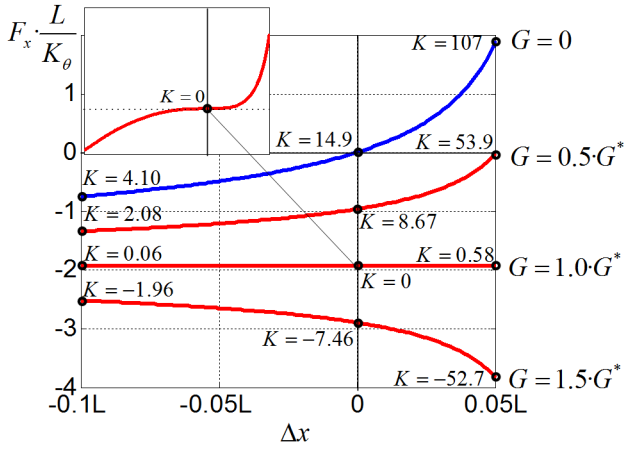

Figure 5.10 Force-deflections relations for different values of auxiliary loading G: chain with torsional spring ($G^* = 4K_\theta / L \cdot \sin\alpha_0$, $K_x = K \cdot K_\theta / L^2$)

Table 5.5 Translational stiffness K_x for different values of auxiliary loading G and different displacements Δx ($G^* = 4K_\theta / L \cdot \sin\alpha_0$)

Auxiliary loading G	Translational stiffness K_x			
	$\Delta x = -0.1L$  $\alpha = 24^\circ$	$\Delta x = -0.05L$  $\alpha = 20^\circ$	$\Delta x = 0$  $\alpha = 15^\circ$	$\Delta x = 0.05L$  $\alpha = 7.7^\circ$
0	$4.10 \cdot \frac{K_\theta}{L^2}$	$6.69 \cdot \frac{K_\theta}{L^2}$	$14.9 \cdot \frac{K_\theta}{L^2}$	$107 \cdot \frac{K_\theta}{L^2}$
$0.5 \cdot G^*$	$2.08 \cdot \frac{K_\theta}{L^2}$	$3.36 \cdot \frac{K_\theta}{L^2}$	$8.67 \cdot \frac{K_\theta}{L^2}$	$53.9 \cdot \frac{K_\theta}{L^2}$
$1.0 \cdot G^*$	$0.06 \cdot \frac{K_\theta}{L^2}$	$0.03 \cdot \frac{K_\theta}{L^2}$	0	$0.58 \cdot \frac{K_\theta}{L^2}$
$1.5 \cdot G^*$	$-1.96 \cdot \frac{K_\theta}{L^2}$	$-3.31 \cdot \frac{K_\theta}{L^2}$	$-7.46 \cdot \frac{K_\theta}{L^2}$	$-52.7 \cdot \frac{K_\theta}{L^2}$

Table 5.6 Functions and matrices used in numerical stiffness analysis of two-link manipulator with auxiliary loading (case of rigid links and compliant intermediate joint)

		Intermediate point p_a	End-effector p_e
Position		$\mathbf{g}_a = \begin{bmatrix} L_1 \cdot \cos q_1 \\ L_1 \cdot \sin q_1 \\ q_1 \end{bmatrix}$	$\mathbf{g} = \begin{bmatrix} x_e \\ y_e \\ \varphi_e \end{bmatrix} = \begin{bmatrix} L_1 \cdot \cos q_1 + L_2 \cdot \cos(q_1 + \theta) \\ L_1 \cdot \sin q_1 + L_2 \cdot \sin(q_1 + \theta) \\ q_1 + \theta + q_2 \end{bmatrix}$
Jacobians	$\mathbf{J}_\theta$	$\mathbf{J}_\theta^{(G)} = \begin{pmatrix} 0 \\ 0 \\ 1 \end{pmatrix}$	$\mathbf{J}_\theta^{(F)} = \begin{pmatrix} -L_2 \cdot \sin(q_1 + \theta) \\ -L_2 \cdot \cos(q_1 + \theta) \\ 1 \end{pmatrix}$
	$\mathbf{J}_q$	$\mathbf{J}_q^{(G)} = \begin{pmatrix} -L_1 \cdot \sin q_1 & 0 \\ L_1 \cdot \cos q_1 & 0 \\ 1 & 1 \end{pmatrix}$	$\mathbf{J}_q^{(F)} = \begin{pmatrix} -L_1 \cdot \sin q_1 - L_2 \cdot \sin(q_1 + \theta) & 0 \\ L_1 \cdot \cos q_1 + L_2 \cdot \cos(q_1 + \theta) & 0 \\ 1 & 1 \end{pmatrix}$
Hessians	$\mathbf{H}_{\theta\theta}$	$\mathbf{H}_{\theta\theta}^{(G)} = [0]$	$\mathbf{H}_{\theta\theta}^{(F)} = [h_2]$
	$\mathbf{H}_{\theta q}$	$\mathbf{H}_{\theta q}^{(G)} = [0 \quad 0]$	$\mathbf{H}_{\theta q}^{(F)} = [h_2 \quad 0]$
	$\mathbf{H}_{q\theta}$	$\mathbf{H}_{q\theta}^{(G)} = [0 \quad 0]^T$	$\mathbf{H}_{q\theta}^{(F)} = [h_2 \quad 0]^T$
	$\mathbf{H}_{qq}$	$\mathbf{H}_{qq}^{(G)} = \begin{bmatrix} h_1 & 0 \\ 0 & 0 \end{bmatrix}$	$\mathbf{H}_{qq}^{(F)} = \begin{bmatrix} h_3 & 0 \\ 0 & 0 \end{bmatrix}$
$h_1 = -L_1 \cdot \sin q_1 \cdot G_y$, $h_2 = -L_2 \cdot \cos(q_1 + \theta) \cdot F_x - L_2 \cdot \sin(q_1 + \theta) \cdot F_y$, $h_3 = -(L_1 \cdot \cos q_1 + L_2 \cdot \cos(q_1 + \theta)) \cdot F_x - (L_1 \cdot \sin q_1 + L_2 \cdot \sin(q_1 + \theta)) \cdot F_y$			

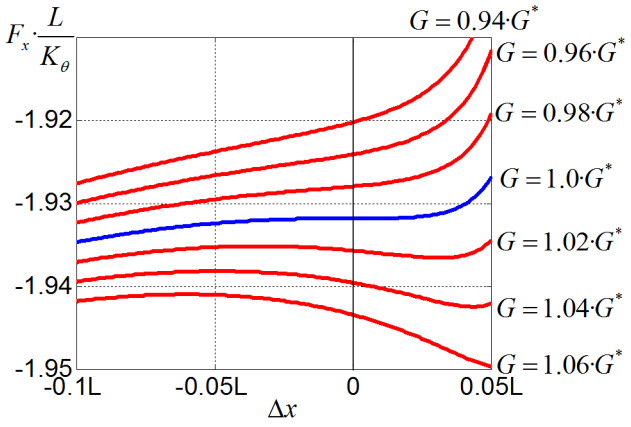

Figure 5.11 Force-deflections relations for different values of auxiliary loading G in the neighborhood of critical value $G = G^*$:

Hence, the presented case study demonstrates rather interesting features of stiffness behavior for kinematic chains under auxiliary loading that where not studied previously (negative stiffness, non-monotonic force-deflection curves, etc.). This motivates the consideration of more sophisticated examples, with more complicated compliant elements.

5.3.2 Serial chains with torsional and translational springs

In the second example, it is assumed that there are three compliant elements: an actuated joint with torsional stiffness parameter K_θ and two non-rigid links with translational stiffness K_L. Intuitively, it is expected that such systems should demonstrate more complicated stiffness behavior under the loadings compared to the previous one.

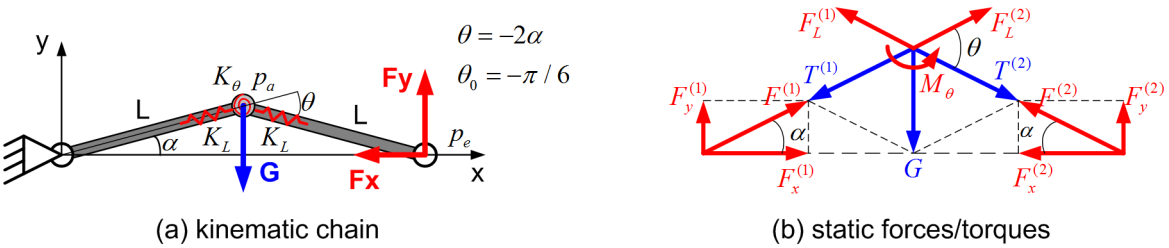

(a) kinematic chain (b) static forces/torques

Figure 5.12 Kinematic chain with compliant links and actuator and its static forces/torques

Under such assumptions, the chain geometry (Figure 5.12a) is described by equations

$$\begin{aligned} x_e &= 2(L-\Delta L)\cdot\cos\alpha; & x_a &= (L-\Delta L)\cdot\cos\alpha \\ y_e &= 0; & y_a &= (L-\Delta L)\cdot\sin\alpha \end{aligned} \tag{5.16}$$

where ΔL is the axial deformation of the links (assumed to be similar to both of them) and the remaining notation corresponds to subsection 5.3.1. The static equilibrium of this system is defined by the balance of forces

$$F_x\cdot\cos\alpha + F_y\cdot\sin\alpha = -K_L\cdot\Delta L \tag{5.17}$$

and the balance of torques (5.12) where L is replaced by $(L-\Delta L)$. Furthermore, applying a similar methodology as above, the force-displacement relation can be expressed in a parametric form as

$$F_x = -\frac{G}{2}\cdot\frac{\cos\alpha}{\sin\alpha} - \frac{8K_L\cdot K_\theta\cdot(\alpha-\alpha_0)}{2\cdot L\cdot K_L\cdot\sin\alpha - G + \sqrt{(G-2\cdot K_L\cdot L\cdot\sin\alpha)^2 - 32\cdot K_L\cdot K_\theta\cdot(\alpha-\alpha_0)\cdot\sin\alpha}} \tag{5.18}$$

$$x = \frac{8K_L\cdot\sin\alpha\cdot\cos\alpha}{2\cdot L\cdot K_L\cdot\sin\alpha - G + \sqrt{(G-2\cdot K_L\cdot L\cdot\sin\alpha)^2 - 32\cdot K_L\cdot K_\theta\cdot(\alpha-\alpha_0)\cdot\sin\alpha}} \tag{5.19}$$

where

$$\Delta L = \left(\frac{G}{4K_L}\cdot\frac{1}{sin\alpha} + \frac{L}{2}\right) - \sqrt{\left(\frac{G}{4K_L}\cdot\frac{1}{sin\alpha} - \frac{L}{2}\right)^2 - 2\cdot\frac{K_\theta}{K_L}\cdot\frac{\alpha-\alpha_0}{\sin\alpha}} \tag{5.20}$$

This expression also allows us to compute stiffness coefficient K_x (via the parametric differentiation), but it is not presented here due to its cumbersome form.

The force-deflection relations corresponding to expressions (5.18) are presented in Figure 5.13. Compared to the previous case, here for $G = 0...G^*$ there is only a quantitative difference (i.e. the shape of the examined curves remains almost the same). However, for $G > G^*$ the chain may not only be unstable with respect to end-effector loading F_x, but also the chain configuration may become unstable. Geometrically, the qualitative difference of the latter is observed similar to buckling in a vertically loaded

arch (see Section 5.1). Summary of different chain configurations and their stiffness behavior is presented in Figure 5.14.

Similar results have also been obtained numerically using the expression presented in Table 5.7, which corresponds to a more general case, where the link lengths are not assumed to be the same and the auxiliary loading can be oriented arbitrary and includes the torque component. This, more general, model can be useful for stiffness analysis of serial manipulators with auxiliary loading caused by gravity compensators where G is not oriented strictly vertically.

Summarizing Section 5.3, it should be concluded that auxiliary loading essentially influences on the stiffness behavior of robotic manipulators. This may reduce the stiffness coefficient and also provoke undesirable phenomena (such as buckling) that must be taken into account by designers. This justifies results of Section 4.3 and gives perspectives for practical applications.

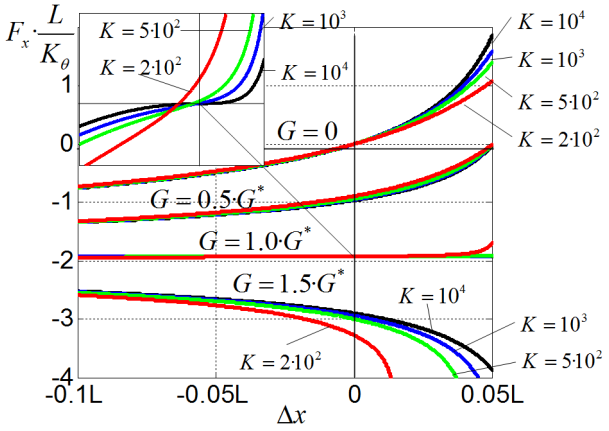

Figure 5.13 Force-deflections relations for different values of auxiliary loading G: chain with torsional and translational springs ($G^* = 4K_\theta / L{\cdot}\sin\alpha_0$, $K_L = K{\cdot}K_\theta / L^2$)

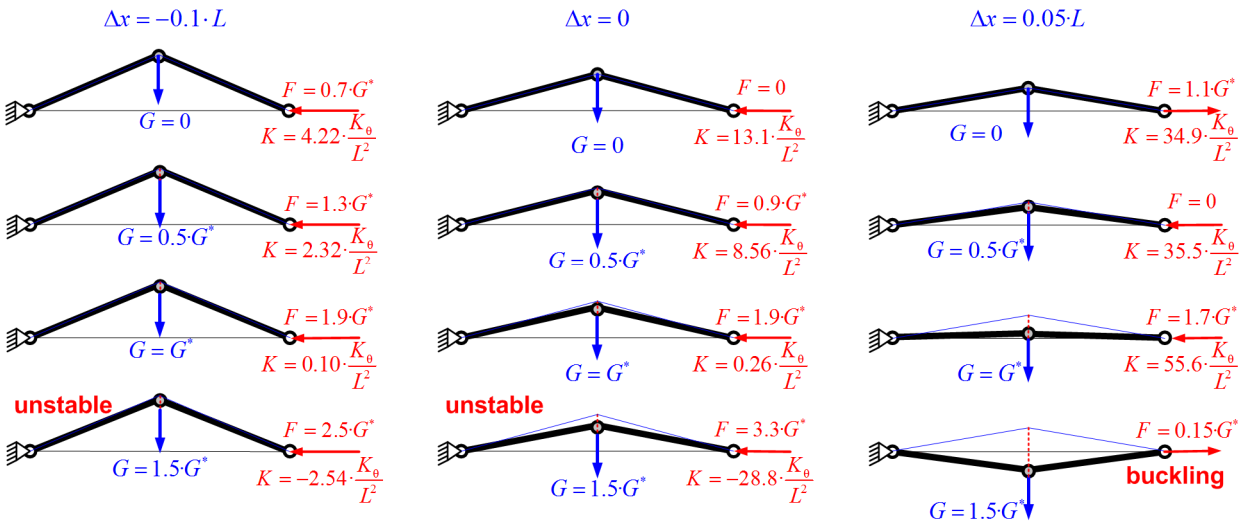

Figure 5.14 Configuration of kinematic chain with auxiliary loading: case of torsional and translational springs ($G^* = 4K_\theta / L{\cdot}\sin\alpha_0$, $K_L = 2{\cdot}10^2{\cdot}K_\theta / L^2$)

Table 5.7 Functions and matrices used in numerical stiffness analysis of two-link manipulator with auxiliary loading (case of compliant links and compliant intermediate joint)

		Internal point p_a	End-effector p_e
Position		$x_a = (L_1+\theta_1)\cdot\cos q_1$ $y_a = (L_1+\theta_1)\cdot\sin q_1$ $\varphi_a = q_1$	$\mathbf{g} = \begin{bmatrix} (L_1+\theta_1)\cdot\cos q_1 + (L_2+\theta_3)\cdot\cos(q_1+\theta_2) \\ (L_1+\theta_1)\cdot\sin q_1 + (L_2+\theta_3)\cdot\sin(q_1+\theta_2) \\ q_1+\theta_2+q_2 \end{bmatrix}$
Jacobians	$\mathbf{J}_\theta$	$\mathbf{J}_\theta^{(F)} = \begin{pmatrix} j_1 & 0 & 0 \\ j_2 & 0 & 0 \\ 0 & 0 & 0 \end{pmatrix}$	$\mathbf{J}_\theta^{(F)} = \begin{pmatrix} j_1 & j_5 & j_7 \\ j_2 & j_6 & j_8 \\ 0 & 1 & 0 \end{pmatrix}$
	$\mathbf{J}_q$	$\mathbf{J}_q^{(G)} = \begin{pmatrix} j_3 & 0 \\ j_4 & 0 \\ 1 & 1 \end{pmatrix}$	$\mathbf{J}_q^{(F)} = \begin{pmatrix} j_3+j_5 & 0 \\ j_4+j_6 & 0 \\ 1 & 1 \end{pmatrix}$
Hessians	$\mathbf{H}_{\theta\theta}$	$\mathbf{H}_{\theta\theta}^{(G)} = \begin{bmatrix} 0 & 0 & 0 \\ 0 & 0 & 0 \\ 0 & 0 & 0 \end{bmatrix}$	$\mathbf{H}_{\theta\theta}^{(F)} = \begin{bmatrix} 0 & 0 & 0 \\ 0 & h_3 & h_4 \\ 0 & h_4 & 0 \end{bmatrix}$
	$\mathbf{H}_{\theta q}$	$\mathbf{H}_{\theta q}^{(G)} = \begin{bmatrix} h_1 & 0 \\ 0 & 0 \\ 0 & 0 \end{bmatrix}$	$\mathbf{H}_{\theta q}^{(F)} = \begin{bmatrix} h_5 & 0 \\ h_3 & 0 \\ h_4 & 0 \end{bmatrix}$
	$\mathbf{H}_{q\theta}$	$\mathbf{H}_{q\theta}^{(G)} = \begin{bmatrix} h_1 & 0 & 0 \\ 0 & 0 & 0 \end{bmatrix}$	$\mathbf{H}_{q\theta}^{(F)} = \begin{bmatrix} h_5 & h_3 & h_4 \\ 0 & 0 & 0 \end{bmatrix}$
	$\mathbf{H}_{qq}$	$\mathbf{H}_{qq}^{(G)} = \begin{bmatrix} h_2 & 0 \\ 0 & 0 \end{bmatrix}$	$\mathbf{H}_{qq}^{(F)} = \begin{bmatrix} h_6 & 0 \\ 0 & 0 \end{bmatrix}$

$j_1 = \cos q_1$, $j_2 = \sin q_1$, $j_3 = -(L_1+\theta_1)\cdot\sin q_1$, $j_4 = (L_1+\theta_1)\cdot\cos q_1$, $j_5 = -(L_2+\theta_3)\cdot\sin(q_1+\theta_2)$,
$j_6 = (L_2+\theta_3)\cdot\cos(q_1+\theta_2)$, $j_7 = \cos(q_1+\theta_2)$, $j_8 = \sin(q_1+\theta_2)$

$h_1 = -\sin q_1\cdot G_x + \cos q_1\cdot G_y$, $h_2 = -(L_1+\theta_1)\cdot\cos q_1\cdot G_x - (L_1+\theta_1)\cdot\sin q_1\cdot G_y$,
$h_3 = -(L_2+\theta_3)\cdot\cos(q_1+\theta_2)\cdot F_x - (L_2+\theta_3)\cdot\sin(q_1+\theta)\cdot F_y$, $h_4 = -\sin(q_1+\theta_2)\cdot F_x + \cos(q_1+\theta)\cdot F_y$
$h_5 = -\sin q_1\cdot F_x + \cos q_1\cdot F_y$, $h_6 = h_3 - (L_1+\theta_1)\cdot\cos q_1\cdot F_x - (L_1+\theta_1)\cdot\sin q_1\cdot F_y$

5.4 BUCKLING PHENOMENA IN TRANSLATIONAL PARALLEL MANIPULATORS

Let us now consider several examples that deal with the stiffness analysis of 3-d.o.f. translational manipulators of the Orthoglide family and their kinematic chains that include parallelogram-based linkages. Each of these manipulators consists of three identical kinematic chains actuated by mutually orthogonal linear drives, which are arranged in a special way to ensure almost isotropic workspace kinematic properties and to restrict the end-effector motions in translation only. This architecture ensures the velocity transmission factors close to 1.0 (similar to the conventional Cartesian-type machines) and provides high stiffness in the unloaded mode [Chablat 2003] [Pashkevich 2010]. However, nonlinear stiffness properties of such manipulators and potential buckling phenomena have not been studied in previous works yet.

5.4.1 Kinetostatic models of translational parallel manipulators under study

For the Orthoglide manipulator, each kinematic chain includes a foot, a kinematic parallelogram with two axes and two bars, and an end-effector (Figure 5.15). To convert this architecture into a set of strictly serial chains two types of approximations were used:

3-PUU model, where the legs are comprised of equivalent limbs with U-joints at the ends (here, the limb stiffness is described a 6-dof virtual spring corresponding to the parallelogram bars with doubled cross-section area);

3-PU_cU_c model, where there is an explicit kinematic constraint describing parallelism of the parallelogram axes (in this case, the limb stiffness is described by equivalent 5-d.o.f. virtual spring).

More details concerning these approximations can be found in [Pashkevich 2010].

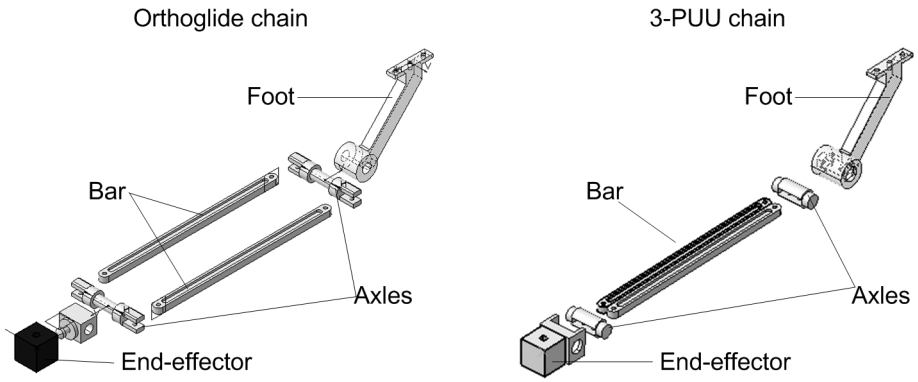

Figure 5.15 Kinematic chains of the Orthoglide manipulator and its 3-PUU counterpart

Under these assumptions, the kinematic model of the PUU-chain is expressed as

$$\mathbf{T} = \mathbf{T}_{\text{base}} \cdot \mathbf{T}_x(\theta_{\text{a}}) \cdot \mathbf{V}(\boldsymbol{\theta}_{\text{Foot}}) \cdot \mathbf{R}_y(q_1) \cdot \mathbf{R}_z(q_2) \cdot \mathbf{T}_x(L) \cdot \mathbf{V}(\boldsymbol{\theta}_{\text{Link}}) \cdot \mathbf{R}_z(q_3) \cdot \mathbf{R}_y(q_4) \cdot \mathbf{T}_{\text{Tool}} \tag{5.21}$$

where $\mathbf{T}_{\text{base}}, \mathbf{T}_{\text{Tool}}$ are the constant transformations matrices (the matrix $\mathbf{T}_{\text{base}}$ includes also the "foot" transformation); $\theta_{\text{a}}, \boldsymbol{\theta}_{\text{Foot}}, \boldsymbol{\theta}_{\text{Link}}$ are the virtual joint coordinates of the actuator, the "foot" and the "link" respectively; $\mathbf{V}(...)$ is the homogeneous matrix-function of the virtual springs, and $\mathbf{T}_x, \mathbf{T}_y, \mathbf{T}_z, \mathbf{R}_x, \mathbf{R}_y, \mathbf{R}_z$ are elementary homogeneous transformation matrices. In the case of PU_cU_c-chain, the third passive joint is eliminated by adding the kinematic constraint $q_3+q_2=0$). It is also assumed that for the PUU-chain the matrix $\mathbf{V}(...)$ is expressed via the multiplication of six elementary transformations:

$$\mathbf{V}(\theta_x, \theta_y, \theta_z, \theta_{\varphi x}, \theta_{\varphi y}, \theta_{\varphi z}) = \mathbf{T}_x(\theta_x) \cdot \mathbf{T}_y(\theta_y) \cdot \mathbf{T}_z(\theta_z) \cdot \mathbf{R}_x(\theta_{\varphi x}) \cdot \mathbf{R}_y(\theta_{\varphi y}) \cdot \mathbf{R}_z(\theta_{\varphi z}) \tag{5.22}$$

These presentations allow computing the Jacobians and Hessians semi-analytically, via the straightforward differentiation of relevant products of homogenous matrices.

The elasticity of the manipulator elements has been evaluated using the FEA-based methodology and special accuracy improvement tools proposed in Chapter 2. As it follows from our study, the rigidity of the parallelogram axes is high compared to the bar and the foot. For the remaining components, the compliance matrices were presented in Chapter 2.

In the case of PU_cU_c chain, the parallelogram stiffness matrix depends on the joint variable q_2 and is computed from the analytical expression [Pashkevich 2010].

$$\mathbf{K}_{\text{plg}}(q_2) = 2 \cdot \begin{bmatrix} K_{11} & 0 & 0 & 0 & 0 & 0 \\ 0 & K_{22} & 0 & 0 & 0 & K_{26} \\ 0 & 0 & 0 & 0 & 0 & 0 \\ 0 & 0 & 0 & K_{44} + \dfrac{d^2 \cos^2 q_2 K_{22}}{4} & 0 & \dfrac{d^2 \sin 2q_2 K_{22}}{8} \\ 0 & 0 & 0 & 0 & \dfrac{d^2 \cos^2 q_2 K_{11}}{4} & 0 \\ 0 & K_{26} & 0 & K_{44} + \dfrac{d^2 \sin 2q_2 K_{22}}{8} & 0 & K_{66} + \dfrac{d^2 \sin^2 q_2 K_{22}}{4} \end{bmatrix} \tag{5.23}$$

where K_{ij} are the elements of $\mathbf{K}_{bar}$.

5.4.2 Stiffness analysis of parallelogram-based chains

The most complex element from the point of view of the stiffness analysis in Orthoglide manipulator is a kinematic parallelogram. It is usually approximated by linear model (5.23) or even by a bar element with the double stiffness. To evaluate accuracy and validity of both approximations, first let us obtain the stiffness matrices for both of the models and then apply them for the parallel manipulator. For the purposes of comparison, the VJM-based approach developed in this work will be complemented by FEA-based analysis. The latter allows us to determine accuracy of the proposed technique and to detect critical forces that may provoke buckling phenomena.

The considered manipulators include three parallelogram-type linkage where the main flexibility source is concentrated in the bar elements of length 310 mm. The stiffness matrix of the bar element was evaluated in Chapter 2. This bar-element has also been evaluated with respect to the structural stability under compression, and the FEA-modeling produced three possible buckling configurations presented in Figure 5.16. It is obvious that these configurations (in different combinations, for two bar elements) are potentially dangerous for the compressed parallelogram. However, the parallelogram may also produce some other types of buckling because of the presence of the passive joints.

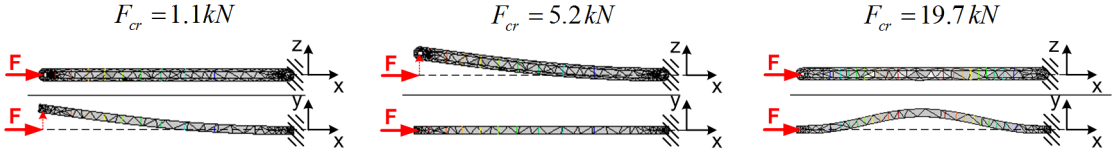

Figure 5.16 Critical forces and buckling configurations of a bar element employed in the parallelograms of Orthoglide obtained by FEA

For the parallelogram-base linkage incorporating the above bar elements, expression (5.23) yields the following stiffness matrix

$$\mathbf{K}_{p\lg} = 2\cdot\left[\begin{array}{ccc|ccc} 2.20\cdot10^{4} & 0 & 0 & 0 & 0 & 0 \\ 0 & 1.81\cdot10^{1} & 0 & 0 & 0 & -2.84\cdot10^{3} \\ 0 & 0 & 0 & 0 & 0 & 0 \\ \hline 0 & 0 & 0 & 5.64\cdot10^{4} & 0 & 1.25\cdot10^{4} \\ 0 & 0 & 0 & 0 & 2.64\cdot10^{7} & 0 \\ 0 & -2.84\cdot10^{3} & 0 & 1.25\cdot10^{4} & 0 & 5.92\cdot10^{5} \end{array}\right] \tag{5.24}$$

corresponding to the straight configuration of the linkage (i.e. to $q = 0$). Being in good agreement with physical sense, this matrix is rank deficient and incorporates exactly one zero row/column corresponding to the z-translation, where the parallelogram is completely non-resistant due to the specific arrangement of passive joints. Also, as it follows from comparison with doubled stiffness matrix of a bar element (see Chapter 2) that may be used as a reference, the parallelogram demonstrates essentially higher rotational stiffness that mainly depends on the translational stiffness parameters of the bar (moreover, the rotational stiffness parameter K_{55} of the bar is completely eliminated by the passive joints). The most significant here is the parallelogram width d that was explicitly presented in the rotational sub-block of $\mathbf{K}_{p\lg}$.

To investigate applicability range of the linear model based on the stiffness matrix (5.23), a non-linear "force-deflection" relation corresponding to the parallelogram compression in the x-direction was computed. This computation has been performed using an iterative algorithm presented in Chapter 4. As it follows from the obtained results, the matrix (5.23) ensures a rather accurate description of the parallelogram stiffness in small-deflection area. However, for large deflections, the corresponding VJM-model detects a geometrical buckling that limits the applicability of the matrix (5.23).

Similar analysis was performed using the FEA-technique, which yielded almost the same "force-deflection" plot for the small deflections but detected several types of the buckling, with critical forces may be both lower and higher than in the VJM-modeling. Corresponding numerical values and parallelogram configurations are presented in Figure 5.17.

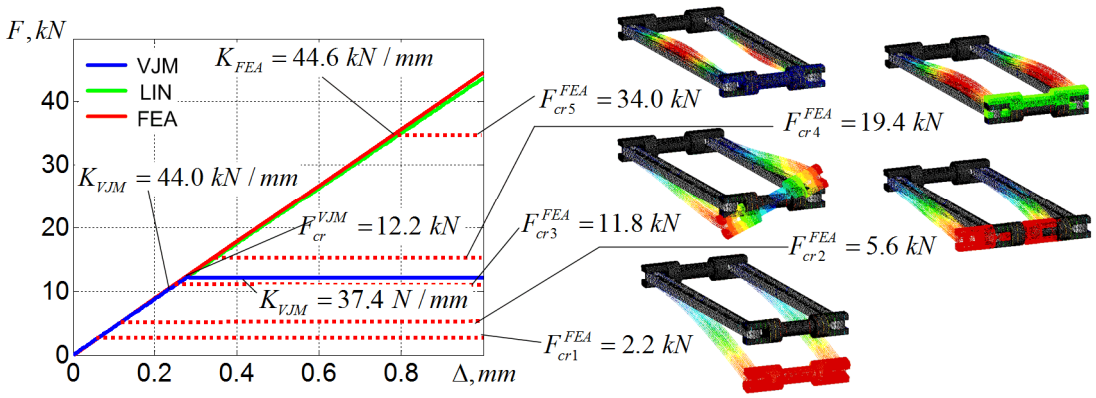

Figure 5.17 Force-deflection relations and buckling configurations for parallelogram compression (modeling methods : VJM, FEA, and LIN – linear model with proposed stiffness matrix).

Table 5.8 Critical forces corresponding to different types of buckling for two configurations of the parallelogram-based linkage

Critical force	Straight configuration (q=0)	Inclined configuration (q=30°)
F_{cr1}	2.2 kN	2.3 kN
F_{cr2}	5.6 kN	10.2 kN
F_{cr3}	11.8 kN	12.7 kN
F_{cr4}	19.4 kN	19.7 kN
F_{cr5}	34.0 kN	35.0 kN

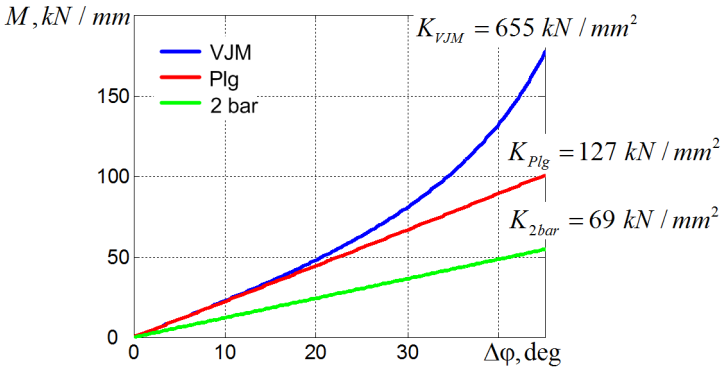

Figure 5.18 Torque-rotation relations for parallelogram twisting.

It is worth mentioning that a particular type of buckling that may appear in the manipulator highly depends on the type of joints that precede and succeed the parallelogram. This statement is confirmed by a separate stiffness modeling of the entire manipulators with parallelogram-based linkage. Besides, critical forces essentially depend on parallelogram joint variable q defining its non-loaded configuration (Table 5.8). Hence, with respect to translational deflections, the linearity zone where matrix (5.23) may be used without caution is defined by the value ±0.1 mm, which is in the frame of reasonable technical specifications for this case study.

A similar analysis has also been performed for the rotational displacement around the x-axis (Figure 5.18). The obtained results confirmed both validity of the linear model with the derived stiffness matrix (for very large linearity range, deflections up to 15°), and essential advantages of the parallelograms compared to equivalent bar-type links with doubled cross-section area. In particular, for the width parameter d=80 mm, this type of linkage ensures at least twice better rotational stiffness than a bar-type one. It is obvious that increasing of this parameter leads to further improvement of the rotational stiffness but there exists some physical limit that is beyond the presented model (in this case, increasing of parameter d will introduce some additional sources of flexibility).

Table 5.9 Stiffness coefficients of the Orthoglide manipulator for different assumptions concerning parallelogram linkage

Model of linkage	VJM-model		FEA-model	
	K_{tran} [N/mm]	K_{rot} [N/rad]	K_{tran} [N/mm]	K_{rot} [N/rad]
2x-Bar linkage	$3.35 \cdot 10^3$	$0.13 \cdot 10^6$	---	---
Parallelogram linkage (solid axis)	$3.23 \cdot 10^3$	$4.33 \cdot 10^6$	$3.33 \cdot 10^3$	$4.10 \cdot 10^6$
Parallelogram linkage (flexible axis)	$3.08 \cdot 10^3$	$4.06 \cdot 10^6$	$3.31 \cdot 10^3$	$4.07 \cdot 10^6$

Finally, the developed VJM-model of parallelogram has been verified in the frame of the stiffness modeling of the entire manipulator. Relevant results are presented in Table 5.9. They confirm the advantages of the parallelogram-based architectures with respect to the translational stiffness and perfectly match to the values obtained from FEA-method. However, releasing some assumptions concerning the stiffness properties of the remaining parallelogram elements (other than bars) modifies the values of the translational and rotational stiffness. The latter gives a new prospective research direction that targeted at more general stiffness model of the parallelogram.

5.4.3 Kinetostatic singularity in the neighborhood of the flat configuration

It is evident that the lowest stiffness of the considered translational manipulators corresponds to the near-flat configuration, where the parallel is approaching to geometrical singularity (flat configuration corresponds to geometrical singularity when all kinematic chains are laying in the single plane). Thus, to evaluate specificity of the near-flat configuration, let us consider this case in details. In order to provide comparability of all case studies which correspond to translational parallel manipulators, let us keep the same assumption concerning the force orientation (parallel to the coordinate frame bisector) but consider both of two possible directions, i.e. towards inside and outside of the cubic workspace.

The simulation results for this manipulator posture are presented in Figure 5.19 and Table 5.10 where d_0 denotes initial distance from the flat singularity, K_0 is the translational stiffness for the unloaded mode, $(\Delta_{cr}^{+}, F_{cr}^{+})$ and $(\Delta_{cr}^{-}, F_{cr}^{-})$ are respectively the critical deflection and the critical force for the opposite directions of the displacement. As it follows from these results, in the neighborhood of the flat singularity the stiffness properties are essentially non-symmetrical with respect to the force direction. This conclusion is valid for both of the examined models (3-PUU and 3-PU_cU_c), which demonstrate almost similar behaviors. In particular, for the inside-direction of the loading, the force increases non-linearly but monotonically while the deflection augments. However, for the outside-direction, initially the manipulator reacts to external loading in the same way: increasing of the deflection leads to increasing of the resisting elastic force. But after achieving the critical value, the reacting force begins to decrease, the configuration becomes unstable and the manipulator abruptly changes its posture to the symmetrical ones (in kinematics, it is treated as an alternative assembling mode). After that, the manipulator demonstrates stable behavior with respect to the loading.

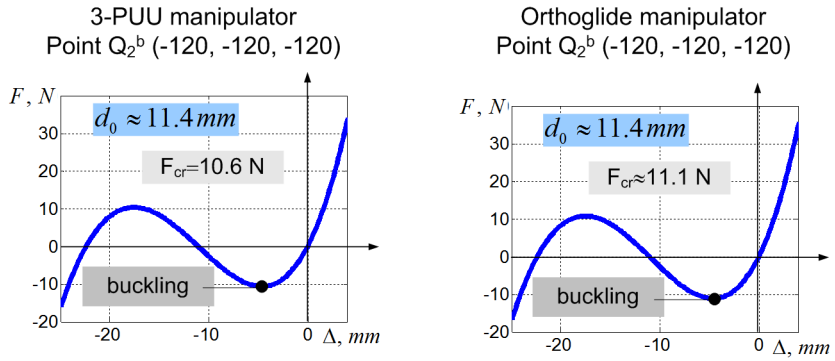

Figure 5.19 Force-displacement relations for both of the examined manipulators (neighborhood of the flat singularity; distance to the singularity is 11.4 mm)

Table 5.10 Summary of stiffness analysis in the neighborhood of the flat singularity

Configuration	d_0, [mm]	Stiffness for unloaded mode, [kN/mm]	F_{cr}^{-}, [kN]	Δ_{cr}^{-}, [mm]	F_{cr}^{+}, [kN]	Δ_{cr}^{+}, [mm]
Model A: 3-PUU manipulator						
Point Q_2	91.7	0.402	-3.61	-12.6	4.80	9.8
Point Q_2^a	46.0	0.090	-0.67	-16.8	3.20	18.6
Point Q_2^b	11.4	0.005	-0.01	-4.6	2.50	36.6
Model B: Orthoglide manipulator						
Point Q_2	91.7	0.418	-2.06	-5.7	2.20	4.9
Point Q_2^a	46.0	0.095	-0.70	-17.1	1.45	11
Point Q_2^b	11.4	0.006	-0.01	-4.6	0.92	24
Q_2 = (-76.35, -76.35, -76.35); Q_2^a = (-100, -100, -100); Q_2^b = (-120, -120, -120)						

The simplest model that explains the above described phenomenon is presented in Figure 5.20. It is derived via generalization of the "toggle-frame" construction known from the structural mechanics, with relevant modifications motivated by the Orthoglide architecture and relative stiffness properties of its elements. Here, the elasticity is concentrated at the basis of the manipulator legs and it is presented by linear springs with the parameter K_θ. It is assumed that initial distance between the end-point and the singularity-plane is $d_0 = L\sin\varphi_0$, where φ_0 is the corresponding angle between the leg and the plane. The derived expressions

$$F = 3K_\theta L_0\left(1-\cos\varphi_0/\cos\varphi\right)\sin\varphi; \qquad \Delta d = L_0\left(\sin\varphi_0-\sin\varphi\right) \tag{5.25}$$

perfectly describe the shape of the force-deflection curves obtained from the complete stiffness models.

Besides, a more detailed analysis shows extremely fast reduction of the stiffness while approaching this singularity. Corresponding expressions derived for small value of φ_0 yield a linear relation for the critical deflection $\Delta_{cr} \approx 0.42 d_0$ and cubic relation for the critical force $F_{cr} \approx K_\theta / \sqrt{3L^2 \cdot d_0^3}$. Hence, this simplified model is in perfect agreement with the simulation results and justifies conventional kinematic design objectives (velocity transmission factors, condition number, etc.) that preserve the manipulator from approaching the flat posture. In addition, it proves the common notion of the "distance-to-singularity" that is used in kinematics must be revised in kinetostatics taking into account the fact that loading essentially reduces the margin of the manipulator structural stability.

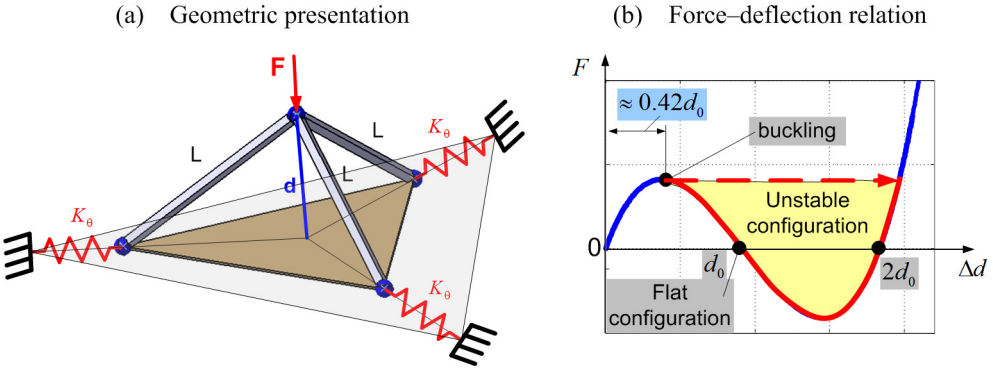

Figure 5.20 Simplified stiffness model of Orthoglide-type manipulators for near-flat configuration

5.4.4 Stiffness analysis of 3-PUU parallel manipulator

For a 3-PUU model, the stiffness analysis was performed for vertices $Q_1 \ldots Q_4$ of the dexterous cubical workspace 200×200×200 mm^3 corresponding to the Orthoglide design specification with the range of the velocity transmission factors [0.5, 2.0]. Besides, a similar study has been done for the isotropic point Q_0 where the transmission factors are equal to 1.0, similar to a conventional Cartesian machine [Ceccarelli 2002], [Pashkevich 2010]. For all of these points, there were computed non-linear curves of the force-deflection relations assuming that the displacement is directed along the bisecting line of the coordinate system.

As it follows from the obtained results (Figure 5.21, Table 5.11), for all considered points $Q_0 \ldots Q_4$, the force-deflection relations are essentially non-linear and include the buckling points where the stiffness reduces radically. Corresponding critical force varies from 4.8 kN for the point Q_2 to 15.0 kN for the point Q_1, while the critical deflections are within the range 2.1…9.8 mm. The isotropic point Q_0 that is usually used for the benchmarks of such manipulators possesses intermediate values of these indices (critical force 9.4 kN and critical deflection 2.7 mm). For all cases, the translational stiffness coefficient in the pre-buckling mode is almost constant, but it essentially varies throughout the workspace. In particular, the highest value 7.1 kN/mm is achieved at the Point Q_1 and the lowest one 0.4 kN/mm corresponds to the point Q_2. However, after the buckling, the stiffness abruptly reduces down to 0.05…0.09 kN/mm. Hence, the traditional linear stiffness analysis (which ignores the influence of external loading) provides rather reasonable indicators for the pre-buckling mode but it does not allow us to evaluate the range of the loading for which the deflections may be treated as ‘small’ ones and the buckling phenomena do not appear yet.

Table 5.11 Summary of stiffness analysis for 3-PUU manipulator in different workpoints along the bisecting line of the coordinate system

Configuration	Stiffness for unloaded mode, [kN/mm]	Critical force, [kN]	Critical deflection , [mm]	Stiffness around the buckling. [kN/mm]		Stiffness for large deformations, [kN/mm]
				$F < F_{cr}$	$F > F_{cr}$	
Point Q_0	3.35	9.35	2.68	3.63	0.05	0.05
Point Q_1	7.10	15.05	2.09	7.17	0.18	0.07
Point Q_2	0.40	4.83	9.80	0.58	0.12	0.05
Point Q_3	6.26	9.77	1.48	7.00	0.10	0.05
Point Q_4	1.55	9.78	6.40	1.62	0.40	0.09

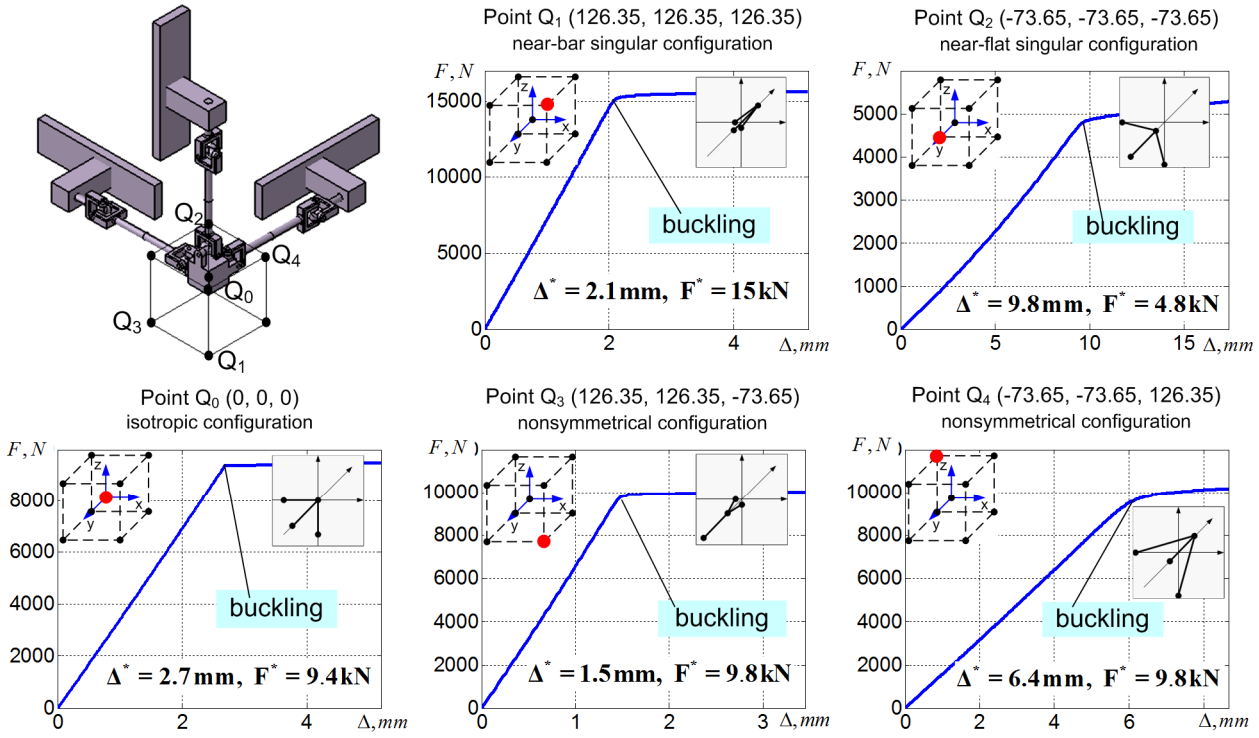

Figure 5.21 Stiffness of the 3-PUU manipulator in critical points of the cubic workspace

It is also worth mentioning that for the points $Q_0 \ldots Q_3$, the physical nature of the buckling is perfectly explained by the results from the previous subsection. In these cases, the buckling is caused by sudden change of the configuration of one of the serial chains (from S- or Z- to Π-configuration, for instance). For the point Q_2 that is close to the parallel singularity of the 'flat' type an additional analysis has been presented in Section 5.4.3.

5.4.5 Stiffness analysis of Orthoglide parallel manipulator

For 3-PU_cU_c model, the stiffness analysis has been performed for the same set of the workspace points $Q_0 \ldots Q_4$ where both of the considered manipulators are equivalent with respect to the kinematic performances. Similarly, for all of these points, the force-deflection relations have been computed and the critical values defining the buckling conditions were evaluated.

The obtained results (Figure 5.22, Table 5.12) are qualitatively analogous to the previous ones; in particular, the translational stiffness of the unloaded manipulator varies from 16.6 kN/mm for the point Q_2 to 0.4 kN/mm for the point Q_1. However, in this case, the numerical values of the critical forces are apparently lower, which slightly reduces advantages of the parallelogram-based architecture demonstrated in [Pashkevich 2010], where a comparison was done on the basis of the unloaded stiffness analysis. Thus, in the point Q_0, the translational stiffness coefficient is almost the same as for 3-PUU case (3.2 kN/mm) but the critical force and deflection are almost twice lower. Similar conclusions are also valid for the remaining points $Q_1 \ldots Q_4$. Therefore, the parallelogram-based architecture is less robust with respect to the buckling associated to the translational deflections but, as it follows from supplementary study, its rigidity is essentially higher with respect to the rotational deformations.

The physical nature of the buckling detected for most of the cases (points $Q_0 \ldots Q_3$) can also be explained using results for the serial kinematic chains presented in Section 5.2. However, the parallelograms introduce some particularities that lead to additional bifurcations and salient points on the force-deflection

curves. For the area of flat singularity (point Q_2) a complimentary analysis has been performed in Section 5.4.3.

Table 5.12 Summary of stiffness analysis for Orthoglide manipulator in different workpoints along the bisecting line of the coordinate system

Configuration	Stiffness for unloaded mode, [kN/mm]	Critical force, [kN]	Critical deflection , [mm]	Stiffness around the buckling. [kN/mm]		Stiffness for large deformations, [kN/mm]
				$F < F_{cr}$	$F > F_{cr}$	
Point Q_0	3.23	4.65	1.41	3.36	0.03	0.03
Point Q_1	16.60	7.85	0.48	16.40	0.42	0.31
Point Q_2	0.42	2.24	4.85	0.48	0.06	0.03
Point Q_3	9.95	4.75	0.48	9.60	0.84	0.11
Point Q_4	5.41	2.78	0.52	5.09	0.65	0.06

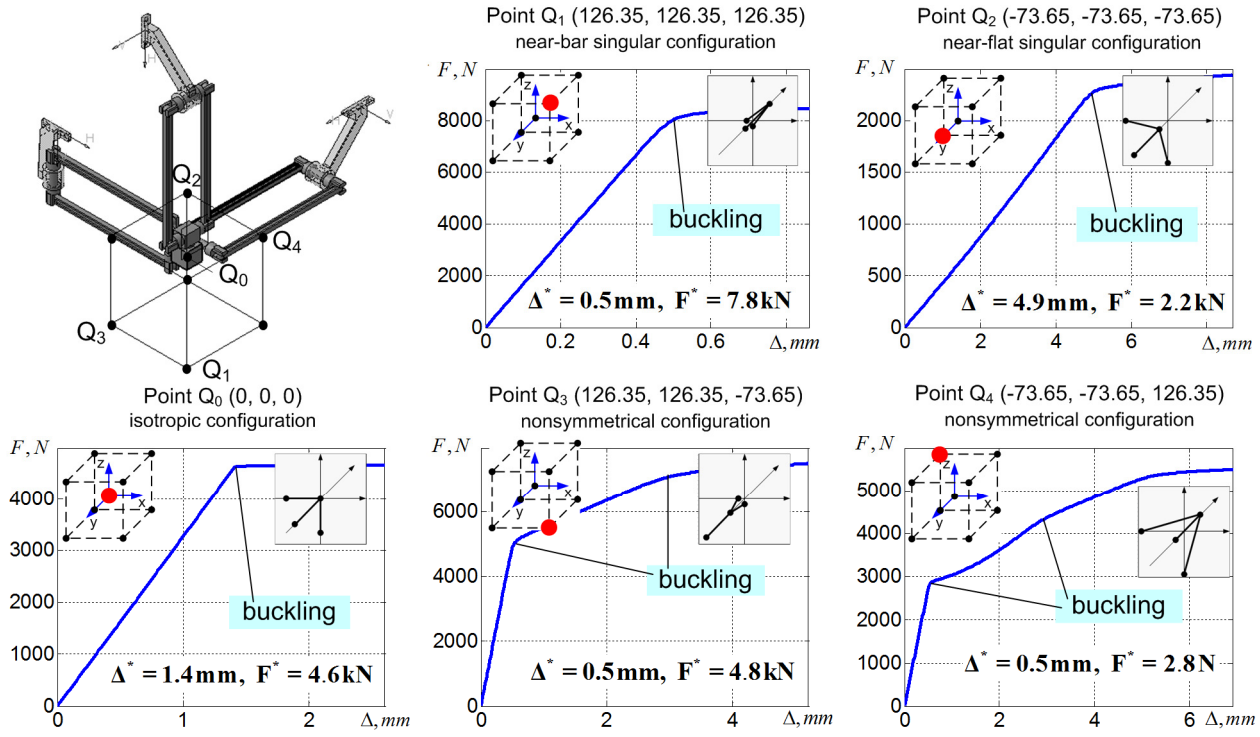

Figure 5.22 Stiffness of the 3-PU_cU_c manipulator in critical points of the cubic workspace

Summarizing Section 5.4 it should be noted that the stiffness of 3-PUU and Orthoglide translational parallel manipulators are dependent upon the end-effector location and external loading, force-deflection relations are rather non-linear and have bifurcation points, which are correspond to buckling. Besides, it was first discovered that in robotic manipulators, along with geometrical singularities, kinetostatic ones may appear.

5.5 SUMMARY

The chapter is devoted to the application of the developed stiffness modeling technique for the non-linear stiffness analysis of serial and parallel manipulators under different types of loadings The main contributions are in the area of detecting non-linear effects in the manipulator stiffness behavior and determining the potentially dangerous configurations and critical forces that may provoke undesired buckling phenomena in typical robotic architectures. In contrast to other works, it was first showed that in externally/internally loaded manipulators some kinematic chains may be unstable and/or there may exist kinetostatic singularities (in addition to ordinary geometrical ones), for which even small disturbances may lead to sudden change of current configuration. From practical point of view, these results are useful for pre-design stage, they allow a designer to evaluate an admissible range of the loading that does-not create undesirable effects in the manipulator behavior.

In more details, Chapter 5 includes the following results:

(i) Non-linear stiffness analysis of *three-link serial chains under end-point loading* with different assumptions on compliant elements. It is proved that, in such chains, the stiffness essentially depends on the loading and the chain can loose its stability if the loading is too high. Expressions allowing us to compute the stiffness coefficient critical loading for typical configurations were obtained.

(ii) Non-linear stiffness analysis of *two-link serial chains under auxiliary loadings* (applied in an intermediate node) with flexible/rigid links and compliant actuator. It was clearly demonstrated that the auxiliary loading may essentially reduce the stiffness of the chain or even to provoke a buckling. Relevant results are normalized with respect to designed parameters and are convenient in engineering form.

(iii) Non-linear stiffness analysis of Orthoglide parallel manipulators and its 3-PUU approximation. It has been discovered that, in the unloaded mode, the stiffness of Orthoglide is essentially higher than its 3-PUU counterpart. However, the critical forces (provoking buckling) for Orthoglide are about twice lower than for 3-PUU. Another essential result here is related to the notion of kinetostatic singularity that completely differs from the classical geometrical one.

Application study presented in this chapter has also demonstrated some limitations of the developed technique. In particular, only geometrical buckling can be detected in the frames of the adopted VJM approximation of the links. However, it is acceptable in practice since another types of buckling are usually observed for essentially higher loading that is not admissible in the normal operation mode. On the other hand, this limitation can be reduced by applying more sophisticated VJM-presentation of the links (i.e. dividing them by several rigid segments separated by virtual springs).

The main results of Chapter 5 are published in the following works: [Klimchik 2009a], [Klimchik 2009c], [Klimchik 2010a], [Klimchik 2010b], [Klimchik 2010c], [Klimchik 2011a], [Klimchik 2011b], [Klimchik 2011d], [Klimchik 2011e].

CONCLUSIONS AND PERSPECTIVES

CONTRIBUTIONS OF THE THESIS.

This thesis is devoted to the enhancement of stiffness modeling technique for serial and parallel manipulators in order to increase the accuracy and efficiency of robotic-based machining of high performance materials by means of compensation of the compliance errors (in on-line and/or off-line mode). To achieve this goal, four main problems were considered that are presented in Chapters 2-5 respectively.

Chapter 2 focuses on the accuracy improvement of the manipulator link elastostatic model parameters. It proposes a computationally efficient identification procedure which is based on the FEA-modeling and allowed us to obtain the stiffness matrix taking into account complex shape of the link, couplings between rotational and translational deflections and joints particularities. The developed method provides higher accuracy and good integration with existing CAD-based systems, comparing to existing ones (about 0.1% for the stiffness matrix element). In more detail, the results and contributions of Chapter 2 include:

- FEA-based methodology for stiffness matrix identification, to evaluate the stiffness matrix from the deflection field produced by virtual experiments in a CAD environment, taking into account the link shape, coupling between rotational/translational deflections and joint particularities
- Numerical technique to compute the stiffness matrix from the deflection field extracted from FEA-based virtual experiments; a comperative study of several versions (SVD-based, LIN-based etc.) with respect to computational efficiency and speed.
- Analytical expressions for accuracy evaluation of the developed identification technique, to determine the optimal settings for the FEA-based experiments and to improve the identification accuracy
- Technique for statistical processing of the experimental data, to minimize the identification errors by eliminating outliers, to determine the confidence intervals and to detect "zero" elements of the stiffness matrix.
- Application of the developed technique to case studies (Orthoglide links) and comparison with previous methods (based on approximated models), which confirmed advantages of the developed method: reduction of errors in significant elements of the stiffness matrix from 20-50% to 0.1%

Obtained results are also useful to the MSA-based modeling that operates with matrices of the size 12×12. The required transformation is performed using the derived analytical expressions that are applicable in general cases.

Chapter 3 deals with the stiffness modeling of serial and parallel manipulators in the unloaded mode (i.e. under assumption of small deformations). The main contributions are in the area of the VJM modeling approach that was enhanced for serial and parallel manipulators with arbitrary location of passive joints. In contrast to other works, the developed technique starts from stiffness modeling of all kinematic chains *separately* and then *aggregates* them in a unique model. Besides, for each kinematic chain, this technique is able to obtain *both non-singular and singular stiffness matrices* that take into account passive joints or the kinematic singularities. Relevant assembling procedure allowed us to compute the *aggregated Cartesian stiffness matrix* of the parallel manipulator and also to evaluate the *internal forces/torques* and *end-platform deflections* caused by geometrical errors in the kinematic chains of over-constrained mechanisms. The developed method combines advantages of the FEA and the VJM modeling approaches (accuracy and computational efficiency respectively) and allows us to obtain the stiffness matrices either in numerical or in analytical form. More precisely, the results and contributions of Chapter 3 include:

- Enhanced VJM-based stiffness modeling technique for serial kinematic chains with arbitrary location of passive joints, which allows us to take into account passive joints in an explicit form and to compute the stiffness matrix for any configuration (even for singular ones). Also, it evaluates internal deflections (and corresponding forces/torques) for kinematic chains with arbitrary number of passive and actuated joints. In contrast to previous results, the developed technique is more computationally efficient, includes low-order matrix inversion, and it is able to obtain even rank-deficient stiffness matrices caused by the presence of passive joints or singular configuration of the kinematic chain.
- Analytical expression for stiffness matrix modification induced by passive joints, which extends the classical stiffness mapping notion for serial manipulators, and related recursive procedure for stiffness matrix elements computing, which allows us to include passive joints sequentially (one-by-one). For typical industrial architectures, which include trivial passive joints (where axes are collinear with Cartesian ones), simple and practically convenient rules for stiffness matrix modification have been proposed. These results significantly simplify computation of the desired stiffness matrix and reduce them to elementary algebraic transformations.
- Stiffness model assembling technique that allows us to aggregate elastostatic models of separate kinematic chains in the stiffness model of the parallel manipulator. It also allows us to evaluate internal deflections and forces/torques in joints, as well as deflections of the reference frame, caused by geometrical errors in kinematic chains. This issue has never been studied in robotic applications before and has essential practical significance for evaluating desired tolerances in links/joints geometry and corresponding internal stresses in over-constrained mechanisms.

Chapter 4 deals with the non-linear stiffness modeling of serial and parallel manipulators in the loaded mode (i.e. under assumption of large deformations). The main contributions are in the area of the VJM modeling approach that was generalized for the case of large deflections caused by internal and external loadings applied to the end-point and/or to the intermediate nodes of the kinematic chains. In contrast to other works, the developed technique includes computing of the static equilibrium configuration corresponding to the given loading. In addition, it allows us to check the "internal stability" of relevant chain configuration. Similar to Chapter 3, the stiffness modeling of parallel manipulators starts from kinematic chains, but it yields a non-linear function describing force-deflection relation. Besides, for each kinematic chain, this technique is also able to obtain *both non-singular and singular stiffness matrices*. Relevant aggregation procedure allows us to obtain a non-linear force-deflection (or deflection-force) relation for the parallel manipulator and to compute the *aggregated Cartesian stiffness matrix*, as well as to evaluate the *internal forces/torques* and *end-platform deflections* caused by loadings and geometrical errors in the kinematic chains. Also, this model was used for the compensation of the compliance errors caused by the internal and external loadings. Similar to the previous chapter, the developed method combines advantages of the FEA and the VJM modeling approaches (accuracy and computational efficiency respectively). In more details, the results and contributions of Chapter 4 include

- Non-linear stiffness modeling technique for serial kinematic chains under external and internal loadings (applied to end-point, to the intermediate nodes, preloading in the joints) which includes: computing the static equilibrium configuration in the loaded mode, obtaining full-scale force-deflections relation and computing of the stiffness matrix for the loaded mode
- Stability analysis technique and related matrix stability criterion for kinematic chain configuration under loading in the case of single and multiple equilibriums, which takes into account the second derivatives of the kinematic chain potential energy.
- Enhanced stiffness model aggregation technique for over-constrained parallel manipulators under internal and external loadings, which takes into account shifting of the equilibrium due to loadings and allows to evaluate internal deflections and forces/torques in joints, as well as deflections of the reference point, caused by geometrical errors in kinematic chains.

- Numerical technique for on-line and off-line compensation of the compliance errors caused by external loadings in parallel manipulators (including over-constrained ones) with perfect and non-perfect serial kinematic chains. In contrast to previous works this technique is based on a non-linear stiffness model that gives essential advantages for robotic-based machining, where elastic deflections can be essential.

Chapter 5 demonstrates the application of the developed stiffness modeling technique for the non-linear stiffness analysis of serial and parallel manipulators under different types of loadings. The main contributions are in the area of detecting non-linear effects in the manipulator stiffness behavior and determining the potentially dangerous configurations and critical forces that may provoke undesired buckling phenomena in typical robotic architectures. In contrast to previous works, it was firstly showed that in externally/internally loaded manipulators, some kinematic chains may be unstable and/or there may exist elastostatic singularities, for which even small disturbances may lead to sudden change of current configuration. From practical point of view, these results are useful for pre-design stage. They allow the designer to evaluate an admissible range of the loading that does not create undesirable effects in the manipulator behavior. More precisely, the results and contributions of Chapter 5 include

- Non-linear stiffness analysis of *three-link serial chains under end-point loading* with different assumptions on compliant elements. It is proved that, in such kinematic chains, the stiffness essentially depends on the loading and the kinematic chain can lose its stability if the loading is too high. Expressions allowing us to compute the stiffness coefficient critical loading for typical configurations were obtained.
- Non-linear stiffness analysis of *two-link serial chains under auxiliary loadings* (applied in an intermediate node) with flexible/rigid links and compliant actuator. It was clearly demonstrated that the auxiliary loading may essentially reduce the stiffness of the kinematic chain or even to provoke a buckling phenomenon. Relevant results are normalized with respect designed parameters and are convenient in engineering form.
- Non-linear stiffness analysis of Orthoglide parallel manipulators and its 3-PUU approximation. It has been discovered that, in the unloaded mode, the stiffness of Orthoglide is essentially higher than its 3-PUU counterpart. However, the critical forces (provoking buckling) for Orthoglide are about twice lower than for 3-PUU. Another essential result here is related to the notion of elastostatic singularity that completely differs from the classical kinematic one.

In general, the obtained results contribute to the area of non-linear stiffness modeling of serial and parallel manipulators and give a robotic designer a useful tool allowing to estimate reasonable limits in minimization of link geometry (cross-section, in particular) in order to avoid potentially dangerous phenomena in the manipulator stiffness behavior under external and internal loadings.

LIMITATIONS OF OBTAINED RESULTS

In spite of numerous essential advantages, the developed stiffness modeling technique still has several limitations that are related to the stiffness modeling assumptions. The most significant of them are presented below

(i) Manipulator structure is assumed to be serial or strictly parallel (i.e. composition of serial chains assembled in end-point or at end-platform, except simple kinematic parallelograms). It is desirable to generalize the method to handle more complex structures that cannot be presented as composition of serial and parallel sub-chains (i.e. with cross-linkage) connected to the mobile platform with complex shape.

(ii) Some types of buckling cannot be detected. Due to limitations of links stiffness models (a pseudo-rigid body with multidimensional lumped virtual spring at the end) only geometrical buckling are detectible. To increase the method ability and allow us to detect buckling in a body (sudden change of link shape), the links should be described more precisely: as serial connections of several rigid bodies separated by the virtual springs.

(iii) Limitations of the model accuracy (contradiction between distributed nature of the links and their lamped models). The VJM approach explicitly assumes that the forces are applied at the points corresponding to the locations of the virtual springs and this presentation is sufficient to describe the links stiffness properties. For this reason, the accuracy of the VJM-based model can not exceed 1-2% compared to FEA-modeling.

However, these limitations are not critical for the most of industrial manipulators and the developed technique can be applied straightforwardly. Nevertheless some of these limitations will be in the focus of the future work.

FURTHER INVESTIGATIONS AND PERSPECTIVES

To generalize the obtained results and enlarge the application area, it is reasonable to continue research in the several directions and to concentrate on the following issues:

(i) To develop a modification of the proposed method that can be applied to the *parallel manipulators with internal loops*. Besides it is useful to consider the manipulators with several end-points (or end-effectors) and manipulators with non-rigid mobile platform. The main difficulty here (for both cases) is related to introducing additional geometrical constraints that are defined by another compliant mechanism. These allow us to generalize the developed stiffness modeling technique for any topology parallel manipulators. It is also desirable to extend the type of loadings that can be taken into account in the frame of the proposed method (by considering *distributed gravity forces* applied for the links, for instance).

(ii) To extend the developed method in order to insure its ability *to detect the local buckling of the manipulator links*. This extension can be achieved by decomposition of the manipulator links into several sequential parts with corresponding stiffness matrices (i.e. by presenting each link as a serial kinematic chain with virtual springs in the nodes). The main problem here is essential increasing of the number of virtual joint variables that may influence the algorithm convergence while computing the equilibrium configuration. Another problem is related to obtaining optimal discretization step for the link which is able to detect desired effects. It is also imperative to investigate discretization rule: should it be regular or may be it will be better to use special discretization which will provides good accuracy and ability to detect buckling with a less number of elements.

(iii) To evaluate *critical loadings for existing industrial robots* and to investigate the *risk to reach elastostatic singularity under the normal task load*. This type of singularity may exist in any manipulator, in addition to a conventional geometrical one, but this issue has never been studied. It is clear that this research may revise the dexterous work envelope of the industrial robots for the considered technological process.

(iv) To develop a *toolbox that generates the revised machining trajectory* for industrial robots using off-line compensation of the compliance errors caused by an interaction of the cutting tool and workpiece as well as by a gravity effect and a gravity compensation device. The main problem here is to evaluate the external loading caused by a technological process that depends on the type of the machining process, material properties, type of the tool, environmental factors, machining surface and other factors. Therefore, at first, it is reasonable to consider in details the technological process in order to obtain real models of cutting forces.

(v) To *optimize the workpiece location in the robot workspace* in order to minimize the compliance errors. These results should improve accuracy of the robotic-based machining process without essential changes in the workcell hardware and software. The most important issue here is to investigate influence of geometrical and elastostatic errors on the accuracy of serial and parallel manipulators, and to compare their impact in the unloaded and loaded modes. This analysis will also be useful for robot calibration and for optimal design of calibration experiments.

(vi) To extend capability of the developed stiffness model by taking into account the *properties of active and passive joints* (such as lubrication, temperature, bearing/velocity, clearance, friction and others). The main problem here is to obtain an adequate model for each factor and to investigate their influence on each other.

(vii) To develop an o*ptimal robot design procedure* which is based on the developed stiffness model and produces an optimal shape of robot links. The main focus has on the machining accuracy and balancing of different errors sources between all manipulator links.

(viii) To extend the proposed compliance errors compensation technique by adding to it the ability *to compensate the dynamic errors* (vibrations as well). The main problem which has to be solved here is related to the development of the adequate dynamic model of the robot-workpiece interaction, which produces forces/torques and state variables required for the compliance errors compensation.

(ix) To apply the developed technique to the *global stiffness modeling of the work-cell*, which takes into account the stiffness properties of both robotic manipulators and auxiliary work-cell components (robot base frame, workpiece fixtures, etc.).

(x) *Experimental validation* of the developed stiffness model that may also indicate some new directions for further enhancement of the proposed stiffness modeling technique.

(xi) *Integration of the obtained theoretical results in a software tool* such as SyMoRoT, which will be able to automate the stiffness analysis for the mechanisms with a complex structure.

The research results presented in this thesis were obtained in the frame of financial support provided by the project "Integrated design of parallel mechanisms and industrial robotic systems for automated processing of composite materials" (RoboComposite, region Pay de la Loire, France). Their practical implementation and further development will be performed in frame of the subsequent projects "Imageur Robotisé pour les Intervention Mini-Invasives" (IRIMI, FUI project) and "Modelling and control of robots for machining operations of large composite parts and friction stir welding." (COROSOO, ANR project) that have recently been started by robotic team of IRCCyN.

PUBLICATIONS

Journal papers.

[Klimchik 2009a] A. Pashkevich, **A. Klimchik**, D. Chablat, Ph. Wenger, Stiffness analysis of multichain parallel robotic systems with loading, Journal of Automation, Mobile Robotics & Intelligent Systems 3(3) (2009) 75-82

[Klimchik 2011a] A. Pashkevich, **A. Klimchik**, D. Chablat, Enhanced stiffness modeling of manipulators with passive joints, Mechanism and Machine Theory, Volume 46, Issue 5, May 2011, Pages 662-679

Book Chapters.

[Klimchik 2010a] A. Pashkevich, D. Chablat **A. Klimchik**, Enhanced stiffness modeling of serial manipulators with passive joints, In: Advances in Robot Manipulators, IN-TECH 2010, ISBN 978-953-307-070-4, April 2010 pp 331-360

International conference proceedings.

[Klimchik 2009b] A. Pashkevich, **A. Klimchik**, D. Chablat, Ph. Wenger, Accuracy Improvement for Stiffness Modeling of Parallel Manipulators, In: Proceedings of 42nd CIRP Conference on Manufacturing Systems, Grenoble, France, 2009, CD-proceedings (8 pages).

[Klimchik 2009c] A. Pashkevich, **A. Klimchik**; D. Chablat, Nonlinear effect in stiffness modeling of robotic manipulators, In: Proceedings of International Conference on Computer and Automation Technology (ICCAT 2009), Venice, Italy, 2009, World Academy of Science, Engineering and Technology 58 (2009) 168-173.

[Klimchik 2010b] A. Pashkevich, **A. Klimchik**, S. Caro, D. Chablat, Stiffness modelling of parallelogram-based parallel manipulators, 3-rd European Conference on Mechanism Science (EUCOMES 2010), Cluj-Napoca, Romania, Springer 2010 Mechanisms and Machine Science, 1, Volume 5, New Trends in Mechanism Science, Part 12, Pages 675-682

[Klimchik 2010c] A. Pashkevich, **A. Klimchik** and D. Chablat , Stiffness analysis of parallel manipulators with preloaded passive joints, In: 12th International Symposium Advances in Robot Kinematics 2010, June 27 - July 1, 2010, Piran-Portorož, Slovenia, Springer 2010, Advances in Robot Kinematics: Motion in Man and Machine, Part 7, Pages 465-474

[Klimchik 2011b] A. Pashkevich, **A. Klimchik**, S. Briot, D. Chablat, Performance evaluation of parallel manipulators for milling application, In: the 20th CIRP Design Conference 2010, Nantes. France, 2010, Global Product Development, 2011, Part 15, Pages 619-629

[Klimchik 2011c] A. Pashkevich, **A. Klimchik**, S. Caro, D. Chablat, Cartesian stiffness matrix of manipulators with passive joints: analytical approach, In: IEEE/RSJ International Conference on Intelligent Robots and Systems (IROS 2011), September 25-30, 2011, USA, San Francisco, California, Accepted

National conference proceedings.

[Klimchik 2011d] **Alexandr Klimchik**, Aggregation of stiffness matrix for parallel manipulators, 12e congres annuel de la ROADEF, Saint-Etienne, France, 2-4 Mars 2011, Volume II, pp 753-754

[Klimchik 2011e] **Alexandr Klimchik**, Stephane Caro, Anatol Pashkevich, Stiffness modeling of manipulators with auxiliary loadings, 12e congres annuel de la ROADEF, Saint-Etienne, France, 2-4 Mars 2011, Volume II, pp 765-766

REFERENCES

[Abele 2007] E. Abele, M. Weigold, S. Rothenbücher, Modeling and Identification of an Industrial Robot for Machining Applications, Annals of the CIRP Vol. 56/1/2007, 387-390

[Akin 2005] Akin, J. E., 2005, Finite Element Analysis With Error Estimators: An Introduction to the FEM and Adaptive Error Analysis for Engineering Students Elsevier, Amsterdam

[Alici 2005] G. Alici, B. Shirinzadeh, Enhanced stiffness modeling, identification and characterization for robot manipulators, Proceedings of IEEE Transactions on Robotics 21(4) (2005) 554–564.

[Angeles 2007] J. Angeles, Fundamentals of Robotic Mechanical Systems: Theory, Methods, and Algorithms, Springer, New York, 2007.

[Angeles 2008] J. Angeles, F. Park, Performance Evaluation and Design Criteria, in: B. Siciliano, O. Khatib, (Eds.), Handbook of robotics, Springer, Berlin, 2008, pp. 229-243.

[Arumugan 2004] H.K. Arumugam, R.M. Voyles, S. Bapat, Stiffness analysis of a class of parallel mechanisms for micro-positioning applications, in: Proceedings of IEEE/ RSJ International Conference on Intelligent Robots and Systems (IROS), 2004, vol. 2, pp. 1826–1831.

[Beitz 1994] Dubbel handbook of mechanical engineering, Ed. W. Beitz and K.-H. Kuttner, Springer-Verlag London Limited, Great Britain 1994

[Benamar 2010] F. Benamar, P. Bidaud, F. Le Menn, Generic differential kinematic modeling of articulated mobile robots, Mechanism and Machine Theory, Volume 45, Issue 7, 2010, Pages 997-1012

[Bennett 1991] D.J. Bennett, J.M. Hollerbach, D. Geiger, Autonomous robot calibration for hand-eye coordination, International Journal of Robotics Research, 10, 1991, pp. 550-559.

[Bera 2011] T.C. Bera, K.A. Desai, P.V.M. Rao, Error compensation in flexible end milling of tubular geometries, Journal of Materials Processing Technology, Volume 211, Issue 1, 1 January 2011, Pages 24-34

[Bernhardt 1994] R. Bernhardt, S. Albright (Eds.), Robot Calibration, Springer 1994, 328 p.

[Bogdan 2009] I.C. Bogdan, G. Abba: Identification of the servomechanism used for micro-displacement. IROS 2009: 1986-1991

[Bouzgarrou 2004] B.C. Bouzgarrou, J.C. Fauroux, G. Gogu, and Y. Heerah, Rigidity analysis of T3R1 parallel robot with uncoupled kinematics, Proc. Of the 35th International Symposium on Robotics, Paris, France, March 2004.

[Brogardh 2007] T. Brogardh, Present and future robot control development—An industrial perspective, Annual Reviews in Control 31 (2007) 69–79

[Budak 2006] E. Budak, Analytical models for high performance milling. Part I: Cutting forces, structural deformations and tolerance integrity, International Journal of Machine Tools and Manufacture, Volume 46, Issues 12-13, October 2006, Pages 1478-1488

[Carricato 2002] M. Carricato, J. Duffy, V. Parenti-Castelli, Catastrophe analysis of a planar system with flexural pivots, Mechanism and Machine Theory 37 (2002) 693–716

[Castelino 2003] K. Castelino R. D'Souza and P.K. Wright, Tool-path Optimization for Minimizing Airtime during Machining, Journal of Manufacturing Systems Vol. 22/No, 3 2003, 173-180

[Chablat 2003] D. Chablat, P. Wenger, Architecture Optimization of a 3-DOF Parallel Mechanism for Machining Applications, the Orthoglide, IEEE Transactions On Robotics and Automation 19(3) (2003) 403-410.

[Chakarov 1999] D. Chakarov, Study of passive compliance of parallel manipulators, Mechanism and Machine Theory 34 (1999) 373–389.

[Chakarov 2004] D. Chakarov, Study of antagonistic stiffness of parallel manipulators with actuation redundancy, Mechanism and Machine Theory 39 (2004) 583–601.

[Cheboxarov 2000] V. V. Cheboxarov, V. F. Filaretov, M. Vukobratoviimage, Raising the stiffness of manipulators with lightweight links, Mechanism and Machine Theory, Volume 35, Issue 1, January 2000, Pages 1-13

[Chen 1999] S.-F. Chen and I. Kao, Conservative congruence transformation of stiffness control in robotic grasping and manipulation, in the 9th International Symposium on Robotics Research, Snowbird, Utah, USA, 1999, pp. 7-14.

[Chen 2000a] S. Chen and I. Kao, Conservative Congruence Transformation for Joint and Cartesian Stiffness Matrices of Robotic Hands and Fingers, The International Journal of Robotics Research, 19(9) , 2000, pp. 835–847.

[Chen 2000b] S. Chen, I. Kao: Simulation of Conservative Congruence Transformation: Conservative Properties in the Joint and Cartesian Spaces. ICRA 2000: 1283-1288

[Chen 2002] Sh.-F. Chen, I. Kao, Geometrical Approach to The Conservative Congruence Transformation (CCT) for Robotic Stiffness Control, In: Proceedings of the 2002 IEEE lntemational Conference on Robotics and Automation (ICRA) Washington, DC, 2002, pp 544-549.

[Chen 2008] J. Chen, F. Lan, Instantaneous stiffness analysis and simulation for hexapod machines, Simulation Modelling Practice and Theory 16 (2008) 419–428

[Ciblak 1994] N. Ciblak, H. Lipkin, Asymmetric Cartesian stiffness for the modeling of compliant robotic systems. In: Proc. 23rd Biennial ASME Mechanisms Conference, Minneapolis, MN (1994)

[Ciblak 1998] N. Ciblak, and H. Lipkin, Synthesis of stiffness by springs, In: Proceedings of DETC'98, 1998 ASME Design Engineering Technical Conferences, Atlanta, Georgia, 1998.

[Ciblak 1999] N. Ciblak, H. Lipkin, Synthesis of Cartesian Stiffness for Robotic Applications, In: IEEE International Conference on Robotics and Automation (ICRA), 1999(3), pp. 2147–2152.

[Clavel 1988] R. Clavel (1988). DELTA, a fast robot with parallel geometry, *Proceedings, of the 18th International Symposium of Robotic Manipulators*, IFR Publication, pp. 91–100.

[Company 2002] O. Company, S. Krut, F. Pierrot, Modelling and preliminary design issues of a 4-axis parallel machine for heavy parts handling, Journal of Multibody Dynamics 216 (2002) 1–11.

[Company 2005] O. Company, F. Pierrot, J.-C. Fauroux, A Method for Modeling Analytical Stiffness of a Lower Mobility Parallel Manipulator, in: Proceedings of IEEE International Conference on Robotics and Automation (ICRA), 2005, pp. 3232 - 3237

[Connor 1976] J. Connor, Analysis of Structural Member Systems, Ronald Press, 1976.

[Corradini 2002] M. Ceccarelli, G. Carbone, A stiffness analysis for CaPaMan (Cassino Parallel Manipulator), Mechanism and Machine Theory 37 (5) (2002) 427–439.

[Corradini 2004] C. Corradini, J.C. Fauroux, S. Krut, and O. Company, "Evaluation of a 4 degree of freedom parallel manipulator stiffness," Proc of the 11th World Cong. in Mechanism & Machine Science, IFTOMM'2004, Tianjin, China, April 1-4 2004.

[Cui 2006] Hongliang Cui and Zhenqi Zhu, Error Modeling and Accuracy of Parallel Industrial Robots, Source: Industrial-Robotics-Theory-Modelling-Control, ISBN 3-86611-285-8, pp. 964, ARS/plV, Germany, December 2006, Edited by: Sam Cubero pp 573-646

[Dadfarnia 2004] M. Dadfarnia, N. Jalili, Z. Liu, D.M. Dawson, An observer-based piezoelectric control of flexible Cartesian robot arms: theory and experiment, Control Engineering Practice, Volume 12, Issue 8, August 2004, Pages 1041-1053

[Daney 2006] D. Daney, N. Andreff, G. Chabert, Y. Papegay, Interval method for calibration of parallel robots: Vision-based experiments, Mechanism and Machine Theory, Volume 41, Issue 8, August 2006, Pages 929-944

[Das 2005] M. Taylan Das, L. Canan Dülger, Mathematical modelling, simulation and experimental verification of a scara robot, Simulation Modelling Practice and Theory, Volume 13, Issue 3, April 2005, Pages 257-271

[Deblaise 2006a] D. Deblaise, X. Hernot and P.Maurine, A systematic analytical method for PKM stiffness matrix calculation, Proceedings of the 2006 IEEE International Conference on Robotics and Automation, pp. 4213-4219, May 2006, Orlando, Florida.

[Deblaise 2006b] D. Deblaise, 2006, Contribution à la modélisation et à l'étalonnage élasto-géométriques des manipulateurs à structure parallèle, Ph.D. thesis, Devant l'Institut National des Sciences Appliquées de Rennes, Rennes, France.

[Depince 2006] Ph. Dépincé, J.-Y. Hascoët, Active integration of tool deflection effects in end milling. Part 2. Compensation of tool deflection, International Journal of Machine Tools and Manufacture, Volume 46, Issue 9, July 2006, Pages 945-956

[Dolinsky 2007] J.U. Dolinsky, I.D. Jenkinson, G.J. Colquhoun, Application of genetic programming to the calibration of industrial robots, Computers in Industry, Volume 58, Issue 3, April 2007, Pages 255-264

[Dow 2004] T.A. Dow, E.L. Miller, K. Garrard, Tool force and deflection compensation for small milling tools, Precision Engineering, Volume 28, Issue 1, January 2004, Pages 31-45

[Drouet 1998] P. Drouet, S. Dubowsky and C. Mavroidis, Compensation of Geometric and Elastic Deflection Errors in Large Manipulators Based on Experimental Measurements: Application to a High Accuracy Medical Manipulator", submitted to the 6th International Symposium on Advances in Robot Kinematics, 1998,Austria.,

[Dumas 2010] C. Dumas, S. Caro, M. Cherif, S. Garnier and B. Furet, A Methodology for Joint Stiffness Identification of Serial Robots, Intelligent Robots and Systems (IROS), 2010 IEEE/RSJ International Conference on, pp. 464 - 469

[Duffy 1996] J. Duffy, Statics and Kinematics with Applications to Robotics, Cambridge University Press, New York, 1996.

[El-Khasawneh 1999] B.S. El-Khasawneh, P.M. Ferreira, Computation of stiffness and stiffness bounds for parallel link manipulators, International Journal of Machine Tools and Manufacture 39 (2) (1999) 321–342.

[Elatta 2004] A.Y. Elatta, Li Pei Gen, Fan Liang Zhi, Yu Daoyuan and Luo Fei, An Overview of Robot Calibration, Information Technology Journal 3 (1): 74-78, 2004

[Fassi 2000] Irene Fassi, Gloria J. Wiens,Multiaxis Machining: PKMs and Traditional Machining Centers, Journal of Manufacturing Processes, Volume 2, Issue 1, 2000, Pages 1-14

[Gantmacher 1959] F. Gantmacher, Theory of matrices, AMS Chelsea publishing, 1959

[Garant 2010] Garant machining manual, http://www.hoffmann-group.com/download/en/zerspanungshandbuch/en-zerspanungshandbuch.pdf

[Geldart 2003] M. Geldart, P. Webb, H. Larsson, M. Backstrom, N. Gindy, K. Rask, A direct comparison of the machining performance of a variax 5 axis parallel kinetic machining centre with conventional 3 and 5 axis machine tools, International Journal of Machine Tools and Manufacture, Volume 43, Issue 11, September 2003, Pages 1107-1116

[Gong 2000] C. Gong, J. Yuan and J. Ni, Nongeometric error identification and compensation for robotic system by inverse calibration, International Journal of Machine Tools & Manufacture 40 (2000) 2119–2137

[Gosselin 1990] C. Gosselin, Stiffness mapping for parallel manipulators, IEEE Transactions on Robotics and Automation 6 (3) : 377–382, 1990.

[Gosselin 2002] C.M. Gosselin, and D. Zhang, "Stiffness analysis of parallel mechanisms using a lumped model," Int. J. of Robotics and Automation, vol. 17, pp 17-27, 2002.

[Goto 1985] Goto, J, Okuma Krauss-Maffei Injection Moulding Machine--OSP KM-5000 With Computerized Numerical Control, Jpn. Plast. Age. Vol. 23, no. 205, pp. 35-38. Sept.-Oct. 1985

[Gower 2004] J.C. Gower, G.B. Dijksterhuis, 2004, Procrustes Problems, Oxford University Press, USA

[Grote 2009] Springer handbook of mechanical engineering, Ed. K-H Grote and E. Antonsson, Springer, New York 2009

[Hines 1998] R. Hines, D. Marsh, J. Duffy, Catastrophe analysis of the planar two-spring mechanism, International Journal of Robotics Research 17 (1) (1998) 89–101.

[Hjelmstad 1997] K.D. Hjelmstad, Fundamentals of Structural Mechanics, Prentice-Hall, New York, 1997.

[Hollerbach 2008] J. Hollerbach, W. Khalil, M. Gautier, Springer Handbook of robotics, Springer, 2008, Chap. Model identification, pp. 321-344.

[Howard 1998] S. Howard, M. Zefran, V. Kumar, On the 6x6 Cartesian stiffness matrix for three-dimensional motions. Mech. Mach. Theory **33**(4), 389–408 (1998)

[Huang 2002] C. Huang, W. H. Hung, I. Kao, New Conservative Stiffness Mapping for the Stewart-Gough Platform, Proceedings of the 2002 IEEE International Conference on Robotics & Automation, pages 823–828, Washington, DC. May, 2002

[Jones 2006] Buckling of Bars, Plates, and Shells by Jones, Robert M 2006

[Kanaan 2009] Daniel Kanaan, Philippe Wenger, Damien Chablat, Kinematic analysis of a serial–parallel machine tool: The VERNE machine, Mechanism and Machine Theory, Volume 44, Issue 2, February 2009, Pages 487-498

[Kao 1999] Kao, I. and Ngo, C., Properties of grasp stiffness matrix and conservative control strategy, The International Journal of Robotics Research, 18 (2):159 -167, 1999

[Kaya 2011] B. Kaya, C. Oysu, H.M. Ertunc, Force-torque based on-line tool wear estimation system for CNC milling of Inconel 718 using neural networks, Advances in Engineering Software 42 (2011) 76–84

[Kevin 2000] Kevin L. Conrad, Panayiotis S. Shiakolas, T. C. Yih, Robotic calibration issues: accuracy, repeatability and calibration. 2000

[Khalil 2002] W. Khalil, S. Besnard, Geometric Calibration of Robots with Flexible Joints and Links, Journal of Intelligent and Robotic Systems 34: 357–379, 2002. Kluwer Academic Publishers. Netherlands.

[Khalil 2004] W Khalil, E Dombre, Geometric calibration of robots, Modeling, Identification and Control of Robots, 2004, Pages 257-289

[Kim 1997] Kim, J., Park, C., Kim, J. and Park F.C., 1997, "Performance Analysis of Parallel Manipulator Architectures for CNC Machining Applications," Proc. IMECE Symp. On Machine Tools, Dallas.

[Koseki 2000] Koseki, Y., Tanikawa, T., Koyachi, N., Arai, T., 2000, Kinematic Analysis of Translational 3-DOF Micro Parallel Mechanism Using Matrix Method, Proc. of IROS 2000, W-AIV-7/1:786-792

[Kövecses 2007] J. Kövecses, J. Angeles, The stiffness matrix in elastically articulated rigid-body systems, Multibody System Dynamics 18(2) (2007) 169–184.

[Krause 1984] Krause, P.C., Analysis of Electrical Machinery, New Work, McGraw-Hill (1984)

[Lamikiz 2004] A. Lamikiz, L.N. Lorpez de Lacalle, J.A. Sarnchez, M.A. Salgado, Cutting force estimation in sculptured surface milling, International Journal of Machine Tools & Manufacture 44 (2004) 1511–1526

[Larsson 2006] Soren Larsson, J.A.P. Kjellander, Motion control and data capturing for laser scanning with an industrial robot, Robotics and Autonomous Systems 54 (2006) 453–460

[Li 2001] Yanmei Li and Imin Kao, On the Stiffness Control and Congruence Transformation Using the Conservative Congruence Transformation (CCT), Proceedings 2001 ICRA. IEEE International Conference on Robotics and Automation, 2001, vol.4, pp. 3937 - 3942

[Li 2002a] Y. Li 1, Sh.-F. Chen, and I. Kao, Stiffness Control and Transformation for Robotic Systems With Coordinate and Non-Coordinate Bases, In: Proceedings of the 2002 IEEE lntemational Conference on Robotics 8 Automation (ICRA), Washington, DC, 2002, pp 550-555.

[Li 2002b] Y.W. Li, J.S. Wang, L.P. Wang (2002). Stiffness analysis of a Stewart platform-based parallel kinematic machine, In: Proceedings of IEEE International Conference on Robotics and Automation (ICRA), Washington, US, 2002(4), pp. 3672–3677

[Li 2008] Li Y. & Xu Q. (2008). Stiffness analysis for a 3-PUU parallel kinematic machine, *Mechanism and Machine Theory*, vol. 43, no. 2, pp. 186-200.

[Lin 2009] Lin Lin, Chao Yang, Jianfeng Lu, Lexing Ying, Weinan E, A Fast Parallel Algorithm for Selected Inversion of Structured Sparse, Matrices with Application to 2D Electronic Structure Calculations, Lawrence Berkeley National Laboratory, October 19, 2009, http://escholarship.org/uc/item/46q6w084

[Lin 2011] Shih-Wei Lin, Zne-Jung Lee, Kuo-Ching Ying, Chung-Cheng Lu, Minimization of maximum lateness on parallel machines with sequence-dependent setup times and job release dates, Computers & Operations Research38(2011)809–815

[Lo 2000] Chih-Ching Lo, CNC machine tool surface interpolator for ball-end milling of free-form surfaces, International Journal of Machine Tools & Manufacture 40 (2000) 307–326

[Long 2003] C.S. Long, J.A. Snyman, A.A. Groenwold, Optimal structural design of a planar parallel platform for machining, Applied Mathematical Modelling 27 (8) (2003) 581–609.

[Lu 1997] Tien-Fu Lu, Grier C. I. Lin, Juan R. He, Neural-network-based 3D force/torque sensor calibration for robot applications, Engineering Applications of Artificial Intelligence, Volume 10, Issue 1, February 1997, Pages 87-97

[Luca 2008] A. De Luca, W. Book, Robots with Flexible Elements, in: B. Siciliano, O. Khatib, (Eds.), Handbook of robotics, Springer, Berlin, 2008, pp. 287-319.

[Majou 2004] F. Majou, Kinetostatic analysis of translational parallel kinematic machines, Ph.D. thesis, Universite Laval, Quebec, Canada and Ecole Centrale Nantes, France, September 2004.

[Majou 2007] F. Majou, C. Gosselin, P. Wenger, D. Chablat, "Parametric stiffness analysis of the Orthoglide," Mechanism and Machine Theory, vol. 42, pp. 296-311. 2007.

[Martin 1996] Martin H. C. (1966). Introduction to matrix methods of structural analysis, McGraw-Hill Book Company

[Matsuoka 1999] Shin-ichi Matsuoka, Kazunori Shimizu, Nobuyuki Yamazaki, Yoshinari Oki, High-speed end milling of an articulated robot and its characteristics, Journal of Materials Processing Technology, Volume 95, Issues 1-3, 15 October 1999, Pages 83-89

[Meggiolaro 1998] M.A. Meggiolaro, C. Mavroidis, S. Dubowsky, Identification and compensation of geometric and elastic errors in large manipulators: application to a high accuracy medical robot, Proceedings of DETC1998: 1998 ASME Design Engineering Technical Conference September 13-16, 1998, Atlanta, GA pp 1-7

[Meggiolaro 2004] Meggiolaro, M.A., S. Dubowsky, C. Mavroidis, Error identification and compensation in large manipulators with application in cancer proton therapy, Revista Controle & Automação/Vol.15 no.1/Jan., Fev. e Março 2004 pp 71-77

[Meggiolaro 2005] M A. Meggiolaro, S Dubowsky, C Mavroidis, Geometric and elastic error calibration of a high accuracy patient positioning system, Mechanism and Machine Theory 40 (2005) 415–427

[Merlet 2006] J.-P. Merlet, Parallel Robots, Kluwer Academic Publishers, Dordrecht, 2006.

[Merlet 2008] J.-P. Merlet, C. Gosselin, Parallel mechanisms and robots, In B. Siciliano, O. Khatib, (Eds.), Handbook of robotics, Springer, Berlin, 2008, pp. 269-285.

[Mirman 1992] Mirman, C.R. and K.C. Gupta, 1992. Compensation of robot joint variables using special Jacobian Matrices. J. Robotic System, 9: 133-137.

[Nagai 2008] Kiyoshi Nagai and Zhengyong Liu, A Systematic Approach to Stiffness Analysis of Parallel Mechanisms, 2008 IEEE International Conference on Robotics and Automation Pasadena, CA, USA, May 19-23, 2008

[Nektarios 2010] A. Nektarios, N.A. Aspragathos, Optimal location of a general position and orientation end-effector's path relative to manipulator's base, considering velocity performance, Robotics and Computer-Integrated Manufacturing, Volume 26, Issue 2, April 2010, Pages 162-173

[Neugebauer 1998] Neugebauer, R., Wieland, F., Schwaar, M., Karczewski, Z., Hochmuth, C., Erfahrungen mit dem Mikromat Hexapod 6X (1998), Internationales Parallelkinematik-Kolloquium 1998. Zürich: IWF ETH-Zürich, 1998, pp. 65-79

[Neumann 1988] K.E. Neumann, 1988, “Robot,” United State Patent no. 4,732,625.

[Newmana 2008] S.T. Newmana, A. Nassehi, X.W. Xu, R.S.U. Rosso Jr, L. Wang, Y. Yusof, L. Ali, R. Liu, L.Y. Zheng, S. Kumar, P. Vichare, V. Dhokia, Strategic advantages of interoperability for global manufacturing using CNC technology, Robotics and Computer-Integrated Manufacturing 24 (2008) 699– 708

[Nof 1999] Sh. Y. Nof, (Ed.), Handbook of industrial robotics, John Wiley, New York, 1999.

[Olabi 2010] Adel Olabi, Richard Béarée, Olivier Gibaru, Mohamed Damak, Feedrate planning for machining with industrial six-axis robots, Control Engineering Practice, Volume 18, Issue 5, May 2010, Pages 471-482

[Oysu 2009] Cuneyt Oysu, Zafer Bingu, Application of heuristic and hybrid-GAS Aalgorithms to tool-path optimizati on problem for minimizing airtime during machining, Engineering Applications of Artificial Intelligence 22 (2009) 389–396

[Ozgur 1995] C. O. Ozgur, J. R. Brown, A two-stage traveling salesman procedure for the single machine sequence-dependent scheduling problem, Omega, Volume 23, Issue 2, April 1995, Pages 205-219

[Paris 2007] H. Paris, D. Brissaud, A. Gouskov, A More Realistic Cutting Force Model at Uncut Chip Thickness Close to Zero, Annals of the CIRP, 56:415-418, 2007

[Park 2008] J. Park, B. Kim, J. Song, H. Kim, Safe link mechanism based on nonlinear stiffness for collision safety. Mechanism and Machine Theory 43(10) (2008) 1332-1348.

[Pashkevich 2005] A. Pashkevich, P. Wenger, D. Chablat, Design strategies for the geometric synthesis of Orthoglide-type mechanisms, Volume 40, Issue 8, August 2005, Pages 907-930

[Pashkevich 2008] Pashkevich A., Chablat D. & Wenger P. (2008 a). Stiffness analysis of 3-d.o.f. overconstrained translational parallel manipulators, Proceedings of IEEE International Conference on Robotics and Automation, pp. 1562-1567

[Pashkevich 2010] Pashkevich A., Chablat D. & Wenger P., 2008. Stiffness analysis of overconstrained parallel manipulators, Mechanism and Machine Theory, vol. 44, pp. 966-982.

[Paziani 2009] Fabricio Tadeu Paziani, Benedito Di Giacomo, Roberto Hideaki Tsunaki, Robot measuring form, Robotics and Computer-Integrated Manufacturing, Volume 25, Issue 1, February 2009, Pages 168-177

[Pierrot 1991] Pierrot, F., Dauchez, P., Fournier, A., HEXA: a fast six-DOF fully-parallel robot, Fifth International Conference on Advanced Robotics, 1991. 'Robots in Unstructured Environments', 91 ICAR., , vol. 2 pp. 1158 - 1163

[Pierrot 1999] F. Pierrot and T. Shibukawa, From Hexa to previous termHexaM.next term In: C.R. Boër, L. Molinari-Tosatti and K.S. Smith, Editors, Parallel kinematic previous termmachines:next term theoretical aspects and industrial requirements, Springer-Verlag (1999), pp. 357–364.

[Pierrot 2009] Francois Pierrot, Vincent Nabat, Olivier Company, Sebastien Krut, Optimal Design of a 4-DOF Parallel Manipulator, From Academia to Industry, IEEE Transactions on Robotics, vol. 25, no. 2, 2009 pp 213-224

[Pigoski 1998] Pigoski, T., Griffis, M., Duffy, J.: Stiffness mappings employing different frames of reference. Mech Mach. Theory 33(6), 825–838 (1998)

[Przemieniecki 1968] J. S. Przemieniecki, Theory of Matrix Structural Analysis : McGraw-Hill 1968.

[Quennouelle 2008a] Quennouelle C. & Gosselin C. M. (2008 a). Stiffness Matrix of Compliant Parallel Mechanisms, In Springer Advances in Robot Kinematics: Analysis and Design, pp. 331-341..

[Quennouelle 2008b] Quennouelle, C., and Gosselin, C., 2008, Stiffness Matrix of Compliant Parallel Mechanisms, Proceedings of the ASME Mechanisms and Robotics Conference.

[Quennouelle 2008c] C. Quennouelle, C. M.Gosselin, Instantaneous Kinemato-Static Model of Planar Compliant Parallel Mechanisms, In: Proceedings of ASME International Design Engineering Technical Conferences, Brooklyn, NY, USA, 2008.

[Quennouelle 2009a] Quennouelle, C., 2009, Modrelisation greomretrico-statique des mrecanismes paralleles compliants, Ph.D. thesis, Universite Laval, Quebec, QC, Canada.

[Ramesh 2000] R. Ramesh, M. A. Mannan, A. N. Poo, Error compensation in machine tools — a review: Part I: geometric, cutting-force induced and fixture-dependent errors, International Journal of Machine Tools and Manufacture, Volume 40, Issue 9, July 2000, Pages 1235-1256

[Rehsteiner 1999] Rehsteiner, F., Neugebauer, R., Spiewak, S. and Wieland, F., 1999, “Putting Parallel Kinematics Machines (PKM) to Productive Work,” Annals of the CIRP, Vol. 48:1, pp. 345–350.

[Renault 1999] Renault Automation Magazine, n° 21, may 1999

[Rizk 2006] R. Rizk, J.C. Fauroux, M. Mumteanu, G. Gogu, A comparative stiffness analysis of a reconfigurable parallel machine with three or four degrees of mobility, Journal of Machine Engineering 6 (2) (2006) 45–55.

[Rizk 2007] R. Rizk, N. Andreff, J.C. Fauroux, J.M. Lavest and G. Gogu, Precision Study of a Decoupled Four Degrees of Freedom Parallel Robot Including Manufacturing and Assembling Errors, Advances in Integrated Design and Manufacturing in Mechanical, S. Tichkiewitch et al. (eds.), Springer 2007, Engineering II, 111–127.

[Rocco 1997] P. Rocco, G. Ferretti, G. Magnani, Implicit force control for industrial robots in contact with stiff surfaces, Automatica, Volume 33, Issue 11, November 1997, Pages 2041-2047

[Rolland 2003] L. Rolland, Outils algébriques pour la résolution de problèmes géométriques et l'analyse de trajectoire de robots parallèles prévus pour des applications à haute cadence et grande précision, PhD Thesis, Université Henri Poincaré (2003).

[Roth 1987] Roth, Z., Mooring, B., Ravani, B., An overview of robot calibration, IEEE Journal of Robotics and Automation, vol. ra-3, no. 5, October 1987

[Salisbury 1980] J. Salisbury, 1980, Active Stiffness Control of a Manipulator in Cartesian Coordinates, 19*th IEEE Conference on Decision and Control*, pp. 87–97.

[Seo 1998] Seo T.E., Intégration des effets de déformation d'outil en génération de trajectoires d'usinage, 1998, Thèse de doctorat, IRCCyN - Ecole Centrale de Nantes.

[Sharma 2001] Sharma I. R. (2001). Latest Trends in machining 209 pages. Http: //www. drishtikona.com/books /latest-trends-in-machining/ch-all.pdf (21 OCT 2009).

[Son 2009] Seungkil Son, Taejung Kim, Sanjay E. Sarma, Alexander Slocum, A hybrid 5-axis CNC milling machine, Precision Engineering, Volume 33, Issue 4, October 2009, Pages 430-446

[Strang 1998] G. Strang, Introduction to Linear Algebra, Wellesley, MA, Wellesley Cambridge Press, 1998

[Su 2006] Su H.-J., McCartny J.Mc.: A Polynomial Homotopy Formulation of the Inverse Static Analysis of Planar Compliant Mechanisms. Transactions of the ASME 128, 776-786 (2006)

[Sulzer 2010] J. Sulzer, I. Kovač, Enhancement of positioning accuracy of industrial robots with a reconfigurable fine-positioning module, Precision Engineering, 34(2) 2010, pp. 201-217

[Surdilovic 1996] D. Surdilovic, M. Vukobratovi, Deflection compensation for large flexible manipulators, Mech. Mach. Theory Vol. 3l, No. 3, pp. 317-329, 1996

[Svinin 2001] M.M. Svinin, S. Nosoe, M. Uchiyama, On the stiffness and stability of Gough-Stewart platforms, in: Proceedings of IEEE International Conference on Robotics and Automation (ICRA), 2001, pp. 3268–3273

[Taghvaeipour 2010] Afshin Taghvaeipour, Jorge Angeles, Larry Lessard, Online computation of the stiffness matrix in robotic structures using finite elements analysis, Report TR-CIM-10-05 Department of mechanical engineering and center for intelligent machines, McGill University, September 2010.

[Terrier 2004] Myriam Terrier, Arnaud Dugas, Jean-Yves Hascoet, Qualification of parallel kinematics machines in high-speed milling on free form surfaces, International Journal of Machine Tools & Manufacture 44 (2004) 865–877.

[Timoshenko 1970] S. Timoshenko, J.N. Goodier, Theory of Elasticity, 3d ed.McGraw-Hill, New York, 1970.

[Tlusty 1999] Tlusty, J., Ziegert, J, and Ridgeway, S., 1999, "Fundamental Comparison of the Use of Serial and Parallel Kinematics for Machine Tools," Annals of the CIRP, Vol. 48:1, pp. 351–356.

[Toyama 1998] Toyama, T. et al, 1998, "Machine Tool Having Parallel Structure," United State Patent no. 5,715,729.

[Tsai 2000] Tsai, L.W. and Joshi, S., 2000, "Kinematics and Optimization of a Spatial 3-UPU Parallel Manipulator," ASME Journal of Mechanical Design, Vol. 122, pp. 439–446.

[Tsai 2001] C.-L. Tsai, Y.-S. Liao, Prediction of cutting forces in ball-end milling by means of geometric analysis, journal of materials processing technology 205 (2008) 24–33

[Tyapin 2009] I. Tyapin, G. Hovland, Kinematic and elastostatic design optimization of the 3-DOF Gantry-Tau parallel kinamatic manipulator, Modelling, Identification and Control, 30(2) (2009) 39-56

[Veitchegger 1986] Veitchegger, W.K. and C.H. Wu, 1986. Robot accuracy analysis based on kinematics. IEEE J. Robotics and Automation, 2: 171-179.

[Veeramani 1998] Veeramani,D.,Gau,Y.S.,1998.Model for tool-path plan optimization in patch-by-patch machining. International Journal of Production Research 36(6), 1633–1651.

[Vertechy 2007] R. Vertechy, V. Parenti-Castelli, Static and stiffness analysis of a class of over-constrained parallel manipulators with legs of type US and UPS, in: Proceedings of IEEE International Conference on Robotics and Automation (ICRA), 2007, pp. 561–567.

[Wan 2009] Min Wan, Wei-Hong Zhang, Systematic study on cutting force modelling methods for peripheral milling, International Journal of Machine Tools & Manufacture 49 (2009) 424–432

[Wang 2009] J.Wang, H. Zhang, T. Fuhlbrigge, Improving machining accuracy with robot deformation compensation, the 2009 IEEE/RSJ international conference on intelligent robots and systems, October 11-15, 2009 St. Louis, USA, 3826-3831

[Watanabe 2006] A. Watanabe, S. Sakakibara, K. Ban, M. Yamada, G. Shen, T. Arai. A Kinematic Calibration Method for Industrial Robots Using Autonomous Visual Measurement, CIRP Annals - Manufacturing Technology, Volume 55, Issue 1, 2006, Pages 1-6

[Wei 2010] W. Wei, N. Simaan, Design of planar parallel robots with preloaded flexures for guaranteed backlash prevention, Journal of Mechanisms and Robotics 2(1) (2010) 10 pages.

[Wenger 1999] Wenger, P., Gosselin, C. and Maille, B., 1999, "A Comparative Study of Serial and Parallel Mechanism Topologies for Machine Tools," Proc. PKM'99, Milano, pp. 23–32.

[Wenger 2001] Wenger, P., Gosselin, C. and Chablat, D., 2001, "A Comparative Study of Parallel Kinematic Architectures for Machining Applications," Proc. Workshop on Computational Kinematics, Seoul, Korea, pp. 249–258.

[Werner 2000] A. Werner, Z. Lechniak, K. Skalski, K. KeÎdzior, Design and manufacture of anatomical hip joint end prostheses using CAD/CAM systems, Journal of Materials Processing Technology 107 (2000) 181±186

[Wiegand 1996] Wiegand, A., Hebsacker, M., Honegger, M., Parallele Kanematik und Lineamotoren: Hexaglide - ein neues, hochdynamisches Werkzeugmaschinenkonzept, Technische Rundschau Transfer Nr. 25, 1996.

[Xi 2004] F. Xi, D. Zhang, Ch. M. Mechefske, Sh. Y. T. Lang, Global kinetostatic modelling of tripod-based parallel kinematic machine, Mechanism and Machine Theory 39 (2004) 357–377.

[Xu 2006] X.W. Xu, S.T. Newman, Making CNC machine tools more open, interoperable and intelligent—a review of the technologies, Computers in Industry 57 (2006) 141–152

[Xu 2007] Min Xu, R. B. Jerard and B. K. Fussell, Energy Based Cutting Force Model Calibration for Milling, Computer-Aided Design & Applications, Vol. 4, Nos. 1-4, 2007, pp 341-351

[Yi 1992] B.-J. Yi, R.A. Freeman, Synthesis of actively adjustable springs by antagonistic redundant actuation, Journal of Dynamic Systems, Measurements and Control, 114 (1992) 454-461.

[Yi 1993] B.-J. Yi, R.A. Freeman, Geometric analysis antagonistic stiffness redundantly actuated parallel mechanism, Journal of Robotic Systems 10(5) (1993) 581-603.

[Zamani 2005] N. Zamani, CATIA V5 FEA Tutorials release 14, University of Windsor, SDC Publication, Windsor Ontario (2005).

[Zefran 1996] M. Žefran and V. Kumar, Coordinate-Free Formulation of the Cartesian Stiffness Matrix. 5th International Symposium on Advances in Robot Kinematics, Portoroz, Slovenia, pp. 119-128, 1996

[Zefran 2002] M. Zefran, R. V. Kumar**,** A Geometric Approach to the Study of the Cartesian Stiffness Matrix, *Journal of Mechanical Design*, Volume 124, Issue 1, March 2002, pages 30-38

[Zhang 2000] Zhang, D., 2000, Kinetostatic Analysis and Optimization of Parallel and Hybrid Architectures for Machine Tools, Ph.D. thesis, Universitre Laval, Qurebec, QC, Canada.

[Zhang 2002] D. Zhang, C.M. Gosselin, Kinetostatic modeling of parallel mechanisms with a passive constraining leg and revolute actuators, Mechanism and Machine Theory 37 (2002) 599–617.

[Zhang 2004] D. Zhang, F. Xi, C.M. Mechefske, S.Y.T. Lang, Analysis of parallel kinematic machine with kinetostatic modeling method, Robotics and Computer-Integrated Manufacturing 20 (2) (2004) 151–165.

[Zhang 2005] Dan Zhang, Lihui Wang, Conceptual development of an enhanced tripod mechanism for machine tool, Robotics and Computer-Integrated Manufacturing, Volume 21, Issues 4-5, August-October 2005, Pages 318-327

[Zhong 1996] Xiaolin Zhong, John Lewis, Francis L. N-Nagy, Inverse robot calibration using artificial neural networks, Engineering Applications of Artificial Intelligence, Volume 9, Issue 1, February 1996, Pages 83-93

[www civildb] http://www.civildb.com/buckling-analysis-of-tubular-beam-columns

[www highline] http://engineering.highline.edu/class/engr225/Bridge%20Competition/T09_photos.htm

[www robotmatrix] http://www.robotmatrix.org/default.htm